ADSORPTION OF SULPHUR COMPOUNDS ON NICKEL CATALYSTS: POISONING AND REGENERATION STUDIES

A Thesis Submitted for the Degree of
Doctor of Philosophy
of The University of London and
for the Diploma of Imperial College

by

Tomas Viveros-Garcia

Department of Chemical Engineering and Chemical Technology
Imperial College of Science and Technology

February 1985

A Carmen

Juan Fernando y Margarita

ACKNOWLEDGEMENTS

I wish to express my gratitude to my supervisor Dr. L. Kershenbaum for his guidance and friendship throughout the course of this work. I must also thank Dr. D. Chadwick for his suggestions and interest in the project.

I would also like to thank the personnel of the mechanical workshop and especially Messrs. T. Stephenson and A. Lucas for the construction of the high pressure reactor and their technical advice. The constant colaboration of Messrs. C. Smith and K. Grose of the glass workshop is also acknowledged. Thanks are also due to Mr. I. Drummond for his help in many aspects of the experimental work.

Patient reading of and advice on the manuscript by Dr. K. Senkiw are fully appreciated.

This work would not have been possible without the financial support of the Universidad Nacional Autonoma de Mexico (UNAM) and an ORS grant from the CVCP which are gratefully acknowledged.

I wish to thank Lesley Smith for the difficult task of dealing with the manuscript.

ABSTRACT

This work describes studies on the poisoning of alumina-supported nickel catalysts by sulphur compounds (H_2S and thiophene). The objective was to shed some light into the kinetics, thermodynamics and mechanism of adsorption as well as the regeneration of poisoned catalysts.

The studies carried out involved the adsorption of thiophene on both the catalyst and the support at concentrations of 100ppm and 1000ppm and temperatures between 298 and 773K. Thiophene was chosen to observe the behaviour of the sulphur adsorption in the presence of carbon in the compound. The regeneration was effected by H_2 treatment at 873K and atmospheric pressure; the effectiveness of the regeneration was evaluated by adsorption of CO and re-adsorption of thiophene. A high pressure system suitable for working under methanation or steam reforming conditions (1100K, $3x10^6$ Pa) and under the vacuum necessary for in situ area measurements ($1.3x10^{-2}$ Pa) was also built and tested.

The experiments were performed in a gravimetric system and the variation in weight was recorded as a function of time. After the poisoning process catalysts were analyzed by elemental microanalysis and electron microscopy.

The results showed that thiophene is dissociatively adsorbed on clean nickel catalysts, the adsorption apparently being composed of both modes: coplanar and perpendicular to the surface. At low temperatures thiophene polymerises on the catalyst surface and as the temperature is increased it decomposes producing gaseous hydrocarbons and a sulphided surface with some residual carbon.

During regeneration carbon was removed but most of the sulphur remained adsorbed and the regenerated catalysts could re-adsorb thiophene. CO however cannot be used to determine free nickel area of poisoned catalysts because sulphur catalyses nickel tetracarbonyl formation.

C O N T E N T S

		PAGE
CHAPTER 1	INTRODUCTION	11
CHAPTER 2	SULPHUR-NICKEL INTERACTIONS	15
2.1	Effect of Sulphur on Nickel Catalysts Performance and Carbon Formation.	16
2.2	The Chemistry of the Sulphur-Nickel Bond	23
2.2.1	Bulk Sulphides	23
2.2.2	Adsorbed Sulphur	25
2.3	Thermodynamics of the Sulphur-Nickel Bond.	32
2.3.1	Thermodynamics of Bulk Sulphides	32
2.3.2	Thermodynamics of Adsorbed Sulphur.	34
2.4	Mechanism of the Sulphur Adsorption and Adsorption Stoichiometry.	37
2.4.1	Mechanism of Adsorption	37
2.4.2	Adsorption Stoichiometry.	39
2.5	Adsorption of Thiophene and Sulphur-containing Compounds.	42
2.5.1	Mechanism and Kinetics of Thiophene Adsorption on Ni	42
2.5.2	Mechanism and Kinetics of Thiophene Adsorption on other metals. HDS reactions.	49
2.5.2.1	Thiophene Adsorption on Precious Metals	49
2.5.2.2	Hydrodesulphurization (HDS) Reactions.	50
2.5.3	Adsorption and Reaction of other Sulphur Compounds on Nickel.	53

		PAGE
2.6	Effect of Total Pressure on the Adsorption of Sulphur Compounds.	54
2.7	Regeneration of Sulphided Ni Catalysts.	56
2.7.1	Regenerating Agent.	56
2.7.2	Effect of Temperature and Pressure.	61
2.8	Adsorption of sulphur on the support.	63
2.9	Summary.	66
CHAPTER 3	CHARACTERISATION OF CATALYSTS.	68
3.1	Experimental Methods	69
3.1.1	Volumetric Method.	69
3.1.2	Gravimetric Method.	71
3.1.3	Dynamic Method.	76
3.2	Total surface area and pore size distribution.	79
3.2.1	Determination of Surface Area.	81
3.2.2	Pore Size Distribution (PSD).	86
3.3	Measurement of Ni Area.	94
3.3.1	Chemisorptive Agent.	95
3.3.2	Effect of Temperature.	103
3.3.3	Adsorption on the Support.	106
3.3.4	Monolayer Determination.	107
3.3.5	Effect of Sulphur on the Adsorption of H_2 and CO.	109
3.4	Summary.	114

			PAGE
CHAPTER 4		EXPERIMENTAL	116
	4.1	Apparatus	116
	4.1.1	Atmospheric Pressure System.	116
	4.1.2	High Pressure (HP) System.	119
	4.2	Catalyst Preparation.	123
	4.3	Materials.	125
	4.4	Procedure.	126
	4.4.1	Reduction	126
	4.4.2	Total (BET) Area and PSD Measurements.	126
	4.4.3	Ni Area Measurements.	128
	4.4.4	Reactivation	129
	4.4.5	Sulphur Compound Adsorption	129
	4.4.6	Regeneration	130
	4.4.7	Re-poisoning.	130
	4.5	Running the High Pressure (HP) System	130
	4.6	Elemental analysis	131
	4.7	Electron Microscopy	132
CHAPTER 5		CATALYST CHARACTERISATION. RESULTS AND DISCUSSION.	134
	5.1	Total Surface Area	134
	5.1.1	BET Method	134
	5.1.2	n* Method	137
	5.2	Pore Size Distribution (PSD)	141
	5.3	Metal Area Determination	156

PAGE

	5.3.1	Effect of Pressure	156
	5.3.2	Effect of Temperature	159
	5.3.3	Adsorption on the Support	166
	5.3.4	Method of Saturation Coverage Determination.	169
	5.3.5	Effect of Sulphur	175
	5.3.6	Discussion	187
CHAPTER 6		ADSORPTION AND REGENERATION STUDIES	197
	6.1	Adsorption of Thiophene on Ni/Al_2O_3 Samples	197
	6.1.1	Short Term Adsorption. Effect of Temperature and Concentration.	198
	6.1.2	Long Term Adsorption. Effect of Temperature and Concentration.	202
	6.2	Adsorption of Thiophene on the Support	211
	6.2.1	Short Term Behaviour. Effect of Temperature and Concentration.	211
	6.2.2	Long Term Behaviour. Effect of Temperature and Concentration.	214
	6.3	Adsorption of H_2S on Ni/Al_2O_3	219
	6.4	Regeneration of Catalysts	222
	6.4.1	Removal of Adsorbed Thiophene	222
	6.4.2	CO Chemisorption on Regenerated Catalysts	225
	6.4.3	Adsorption on Regenerated Catalysts	228

PAGE

	6.4.3.1	Short Term Behaviour. Effect of Temperature and Concentration	228
	6.4.3.2	Long Term Behaviour. Effect of Temperature and Concentration.	235
6.5		Kinetic Results	246
	6.5.1	Short Term Determinations	247
	6.5.2	Long Term Determinations	252
	6.5.3	Tests of Interparticle and Intraparticle Transport Limitations	257
6.6		Elemental Analysis Results	264
6.7		Electron Microscopy Results	271
6.8		Discussion	274
CHAPTER 7		CONCLUSIONS AND RECOMENDATIONS	292
7.1		Conclusions	292
7.2		Suggestions for Further Work	296
REFERENCES			298
APPENDICES	A.1	High Pressure Reactor Design	308
	A.2	Test of High Pressure System	313
	A.3	Comments on the Microbalance Operation	315
	B.1	N_2 Adsorption Raw Data	318
	B.2	PSD Calculations	320
	B.3	CO and N_2O Adsorption Data	329
	C.1	Thiophene Adsorption Data	334

CHAPTER 1

INTRODUCTION

The increased interest during the last decade in the study of the poisoning of metallic catalysts by sulphur compounds has been motivated by the need of more tolerant catalysts for use in the production of fuels by hydrogenation of CO and the production of synthesis gas by steam reforming (1).

Sulphur is a severe poison and is generally acknowledged that it deactivates most metal catalysts.

Based on the studies of sulphur poisoning up to 1950 Maxted (2) suggested that the toxicity of a compound depended on the electronic configuration of the potentially toxic element in the molecule in question, molecular size and length of stay of the adsorbed molecule on the surface. Unshielded structures such as H_2S and organic thiols are more toxic than shielded structures such as SO_4^{2-} and sulphonic acid for poisoning a catalyst. This is due to the presence of unshared electron pairs or unused valency orbitals in the unshielded structure, by which a chemisorptive bonding is possible. Therefore the toxicity of sulphur compounds diminishes with increasing oxidation state.

As for the molecular size it was demonstrated that the toxicity increased in the order of $H_2S < CS_2 <$ thiophene $<$ cysteine.

These generalisations were drawn from experiments performed at low temperatures (290K - 450K) and it would be expected that at higher

temperatures some of these compounds would decompose on the metal surfaces and toxicity would be independent of the starting compound under more severe conditions (3). Using this last premise most of the studies that have been carried out have employed H_2S as the poisoning agent.

With the development of new techniques such as ESCA, AES, SIMS and others by which the condition of the catalytic surface can be studied the advances in the field have been enormous. A great amount of fundamental information exists for well defined single crystal materials but such information is scant for supported metals.

The excellent review of the literature on sulphur poisoning carried out by Bartholomew et al (3) showed that:

. very small concentrations of H_2S (< 100ppb) are sufficient to deactivate metallic catalysts;

. H_2S and several other sulphur compounds adsorb dissociatively on metal surfaces over a wide range of temperatures;

. the strength of the adsorbed metal-sulphur bond is higher than metal-sulphur bonds in bulk sulphides;

. sulphur may deactivate metallic catalysts by geometric blockage of active sites;

. it is very difficult to regenerate catalysts poisoned by sulphur compounds because of the high stability of the metal-sulphur bond.

Despite the advances, the process is still far from being fully understood and the need to continue its study is apparent.

Among the aspects that merit considertion and research are: the study of adsorption and poisoning effects of sulphur compounds which

could be present in actual feed streams; the effect of sulphur on the adsorption of other compounds; studies at conditions more relevant to industrial situations; thorough investigation into the possible regeneration of poisoned catalysts.

This work was undertaken to study the adsorption of sulphur compounds such as thiophene and H_2S on nickel catalysts supported on alumina, the study of the regeneration of the poisoned catalysts and the design and development of a system capable of withstanding high pressures and temperatures similar to those found at reaction conditions.

In Chapter two the literature available on the sulphur-nickel interactions is presented. It includes the effect of sulphur on the performance of metallic catalysts under reaction conditions; the mechanism and kinetics of the adsorption of H_2S and sulphur compounds and the stability of bonds formed and the data available on the regeneration of sulphur poisoned catalysts.

Chapter three gives a view of how to characterise a catalyst by means of surface area and pore size distribution. It discusses the use of chemisorptive agents such as H_2, CO and N_2O for the metal area determination and the effect of sulphur on the adsorption of these compounds in a range of conditions.

The materials, apparatus and procedures used to carry out the experiments are described in Chapter four.

The results of the characterisation of the nickel catalysts are given and discussed in Chapter five. They include the total area measurements, the pore size distribution and the nickel area

determinations. The nature of the CO chemisorption is complicated further by the presence of sulphur and such results obtained on sulphur-poisoned catalysts are given. A comparison of the use of N_2O and CO for the evaluation of Ni metal areas is given.

In Chapter six the results of the adsorption of thiophene and H_2S are shown. The effect of temperature and concentration is discussed and the regeneration is assessed. Together with the results obtained by electron microscopy and elemental analysis they provide an insight into the mechanism of adsorption.

Chapter seven provides the conclusions obtained from this work and outlines the recommendations for future work.

CHAPTER 2

SULPHUR-NICKEL INTERACTIONS

In the last few years the number of investigations dealing with the sulphur-nickel interactions have increased; they have provided a better understanding of the sulphur poisoning process.

Fundamental aspects of the way the sulphur adsorbs onto nickel surfaces, the rate at which the adsorption takes place, the strength of the resultant sulphur-nickel bond have received considerable attention and almost definitive answers have been obtained. Other aspects such as the effect of sulphur during methanation, steam reforming and Fischer-Tropsch reactions have been dealt with; however the literature here is less abundant and some questions related to the effect on carbon deposition, selectivity of catalysts, effect of pressure on the adsorption of sulphur compounds are still under discussion and more work is needed to clarify them.

Regeneration of poisoned nickel catalysts has had very little attention indeed, perhaps due to the assumption that it is very difficult to carry it out at moderate conditions without affecting the catalyst, knowing the high stability of the surface sulphide compounds.

In this Chapter a bibliographical survey of the research dealing with all these aspects is provided. Most of the published works have used H_2S, and only a few of them have dealt with other sulphur-containing compounds as poisoning agents; the available literature on this subject as well as on the adsorption on catalyst supports has been

included.

2.1 Effect of Sulphur on Nickel Catalysts Performance and Carbon Formation

The presence of sulphur in a reactant stream poisons the catalyst, reduces activity, may change selectivity and introduces changes in the carbon formation. The use of nickel catalysts in steam reforming and methanation reactions, and the high sensitivity of the catalyst towards sulphur poisoning has motivated many research groups to study these processes in detail.

Studying the methanation reaction over several supported metals Dalla Betta et. al. (4) found that the presence of 1 ppm H_2S reduced the activity by a factor of 70; increasing the sulphur content to 5ppm resulted in only a further 1.3 fold decrease; a further increase to 10 ppm H_2S had no effect on the activity.

The presence of H_2S altered the product distribution increasing the relative content of heavier hydrocarbons. Moreover catalysts which in absence of sulphur did not produce any hydrocarbons larger than methane began to produce measurable amounts upon the addition of sulphur. The latter catalysts were also the most susceptible to sulphur poisoning. They stated: sulphur poisons the ability of the surface to hydrogenate the carbon atom much more severely than the ability to form carbon-carbon bonds.

Rostrup-Nielsen et.al. (5-7) studying the methanation and Boudouart reactions:

$$CO + 3H_2 \rightleftharpoons CH_4 + H_2O$$

$$2CO \rightleftharpoons C + CO_2$$

in a thermogravimetric system and a differential fixed-bed reactor found that both reactions are strongly poisoned by sulphur; with 1ppm H_2S only a small decrease in activity was observed, but the addition of 2ppm H_2S reduced the activity by a factor of 20; nevertheless the selectivity remained constant, supporting the assumption that both reactions have the same intermediate presumably adsorbed carbon atoms. Increasing the CO/H_2 pressure increased the selectivity of the Boudouart reaction in both sulphur-free and sulphur poisoned tests. The methanation activation energy determined from fixed-bed results was found to be independent of the sulphur coverage, a strong indication that sulphur poisoning is due to geometric rather than electronic effects.

The sulphur effects just mentioned have been confirmed in studies carried out by Bartholomew and co-workers (8-11), Wise and co-workers (12,13), Katzer and co-workers (14,15), and Goodman and Kiskinova (187).

Bartholomew and co-workers using different experimental apparatuses and conditions have confirmed that the presence of 10ppm of H_2S reduces methanation activity in 2-3 orders of magnitude (8,9), although the activation energy is not affected by sulphur coverage (11). Furthermore, they reported that for H_2S concentration values between 6.6 and 0.2 ppm the deactivation rate constant increased as the H_2S concentration was decreased, apparently due to progressively fewer nickel surface sites being deactivated per adsorbing H_2S molecule. Sulphur decreased the rate of carbon formation in methanation at temperatures below 650K but increased its rate of formation at high temperatures ($>$ 650K), this was explained by the tendency of sulphur to

poison the dissociative adsorption of H_2 to a much greater degree than the dissociative adsorption of CO (10). Indeed experiments at 300K on Ni/Al_2O_3 showed that the amount of dissociatively adsorbed CO decreased only by a factor of 2 after poisoning with sulphur whereas the fraction of active carbon (material that reacts with H_2 and can be removed) on the surface decreased from 0.78 to 0.19 and the fraction of inactive carbon (not removable) increased from 0.22 to 0.81 (10). Sulphur prevented the hydrogenation of surface carbon.

The results of Wentceck et al. (12,13) using temperature programmed desorption (TPD) and temperature programmed surface reaction (TPSR) agreed with the results of Bartholomew and co-workers; that is the adsorption of sulphur species caused a transformation of reactive surface carbon to the less reactive carbon form. Increasing amounts of H_2S progressively reduced the conversion of the surface carbon to methane. They concluded that sulphur poisoning of the nickel catalyst was the result of two concurrent effects:

i) preemption of surface sites needed for CO dissociation,

ii) conversion of surface carbon species to a relatively non-reactive form.

The presence of sulphur adspecies appears to favour the growth of islands of carbon with the formation of carbon to carbon bonds and the production of amorphous or graphitic carbon (13).

Goodman and Kiskinova (187) found that for Ni(100) at temperatures below 600K the reaction rate plots for the sulphided surface paralleled that for the clean surface, therefore no fundamental change had occurred in the reaction mechanism. The poisoning effect of sulphur on nickel for the methanation reaction was observed to be non-linear. At

low sulphur coverages ($\theta_s < 0.1$) the catalytic activity dropped steeply, leveling off later and no further reduction in reaction rate was observed at sulphur levels exceeding $\theta_s = 0.2$. They concluded that at low coverages one sulphur atom blocks about ten equivalent nickel sites, therefore long range electronic effects are important at low sulphur coverages.

In what are regarded as the best kinetic data available on the sulphur poisoning of nickel catalysts Katzer and co-workers (14,15) found that very low concentrations of H_2S can reduce the methanation activity by a factor of 10^3. A concentration of 13ppb H_2S reduced the steady state methanation activity of Ni/Al_2O_3 about 200-fold at 660K; with 100 ppb H_2S the activity was reduced 5000 fold, at this poison concentration levels though the sulphur adsorption was reversible since the activity was recovered as the H_2S concentration was reduced. A truly dynamic equilibrium existed at this conditions between the gas phase sulphur and the catalyst surface. In agreement with previous work the activation energy remained unchanged with sulphur poisoning. AES analysis of the catalysts showed that no carbon was present either on the surface or in the subsurface regions for poisoned catalysts, in contrast similar analysis of catalysts in sulphur-free tests demonstrated the presence of graphitic carbon which was easily regenerable in a H_2 stream at 660K for 6-15 hours (14).

It can be noticed then that sulphur poisoning:

i) strongly reduces the catalytic activity of Ni samples,

ii) changes the selectivity towards higher hydrocarbons (C_{2+}),

iii) does not change the methanation activation energy, suggesting blocking of nickel sites,

iv) promotes the formation of inactive carbon at high enough H_2S concentration and temperature (>0.2ppm, > 650K), although at 660K and H_2S concentration below 100ppb sulphur prevented carbon deposition.

A possible mechanism has been proposed (5, 16) for the carbon formation:

$$CO = CO(a) \qquad \text{(quasi equilibrium)}$$

$$CO(a) \rightarrow C_\alpha(a) + O(a)$$

$$C_\alpha(a) \xrightarrow{H_2} CH_4$$

$$\rightarrow (C, Ni) \rightarrow C \text{ (WHISKER)}$$

$$\rightarrow Ni_3C$$

$$\rightarrow C_\beta \rightarrow \text{ENCAPSULATION}$$

Carbon formed during methanation and Boudouart reactions observed in sulphur-free experiments is of the "Whisker-like" type (10,17), but no information is available for sulphur-poisoned samples.

Sulphur poisons nickel reforming catalysts effectively (7, 18-21). The high temperature used in steam reforming increases the reversibility of sulphur adsorption and therefore the tolerance of the catalysts. Conventional reforming feedstocks such as natural gas and naphta contain organic sulphides at levels of 300-500ppm and higher, in these circumstances desulphurization of the feed is essential before

reforming (3,20). However organic sulphur compounds are still present in the feed after desulphurization although at lower concentrations.

Morita et al. (18, 19) demonstrated that the poisoning by sulphur compounds is reversible. Experiments performed at typical steam reforming temperatures (1073K - 1173K) using methane over 3 different nickel catalysts showed that upon addition of 130mgS/m^3 (1mgS/m^3 STP=0.7ppm v/v) the activity decreased, but it was recovered after sulphur addition was stopped. The reaction temperature had a strong effect: the activity decreased from 100% to 32% at 1073K whereas only to 97% at 1173K for a 26% Ni catalyst. They reported that there was a threshold concentration below which no detectable poisoning was observed. Bartholomew et al. (3) collected the sulphur threshold levels for different catalysts available in the literature and compared them with the concentrations predicted by thermodynamic data for a sulphur coverage of 0.5, finding a good agreement between them suggesting that the reversibility of sulphur poisoning during reforming is a predictable consequence of equilibrium adsorption of H_2S (3). A coverage of 0.5 was used because it corresponds to the point at which saturation of a nickel surface at high temperature occurs as it is shown later in this Chapter.

Table 2.1 Sulphur Threshold[a] levels in steam reforming (3)

Catalyst	Catalyst exit temp. (K) 1073	1123	1173	Ref	Comments
14-25% Ni(ICI)	0.7	3.5	18	20	Full scale reforming
4.4% Ni	-	1.4	-	18,19	Isothermal bed
26% Ni	3	11	-	Ib	
Various Ni catalysts	7	14	21	156	Experimental concentrations based on equilibrium gas composition for $CO + 3H_2 = CH_4 + H_2O$
	3	7	16	3	P_{H_2S}/P_{H_2} based on extrapolation of equilibrium adsorption data at $\theta_s=0.5$

a) Threshold concentrations below which there is no measurable loss of activity at the temperature shown, in ppm.

Rostrup-Nielsen (7) reported that during steam reforming of ethane at 773K the deactivation appeared to be linear with sulphur coverage after an initial drop in activity. Nevertheless the specific activity based on the remaining nickel surface area remained constant over a wide range of sulphur coverage. At complete coverage, $\theta_s=1$, the catalyst was completely deactivated. Results also indicated the existence of a threshold content of sulphur below which rapid carbon formation occurs (6), however during steam reforming of ethane at 773K carbon was not formed on a sulphur poisoned catalyst.

No studies are available on the effects of products distribution neither on the kinetics of poisoning above threshold concentrations nor the effects of catalysts and gas compositions on the tolerance level and rate of deactivation (3).

It can be noticed though that steam reforming is less sensitive to sulphur than methanation or Boudouart reactions. The typical high temperatures at which steam reforming is performed increase the sulphur tolerance level of the catalysts, however the lower deactivation effect is remarkable even at 773K; it may be possible that steam plays a relevant role in preventing deactivation and could be used as a regenerating agent for poisoned catalysts.

2.2 The Chemistry of the Sulphur-Nickel Bond

2.2.1 Bulk Sulphides

Metal sulphides are in general of non ionic nature, this characteristic favours formation of non-stoichiometric compounds. Rosenqvist (22) studied the Ni-S system under controlled conditions so that gas-solid - liquid equilibrium was monitored. He showed that different nickel sulphide compounds exist, each compound is present over a limited range of H_2S pressure and temperature. A thermodynamic phase diagram was obtained from the results and it is given in Figure 2.1. This diagram shows the phases present at each temperature in equilibrium with a gas mixture of H_2S/H_2. It can be noticed that at temperatures of catalytic interest (400^0C-500^0C) nickel forms the most stable bulk nickel-sulphide Ni_3S_2, at pressure ratios P_{H_2S}/P_{H_2} above 10^{-3}-10^{-4}; below these values the sulphur is held in an adsorbed state. For low sulphur processing feeds in the ppm range bulk sulphides are

not formed, but the sulphur is adsorbed on the surface of the metal. In this case information about adsorption and the adsorbed state of sulphur on Nickel are needed.

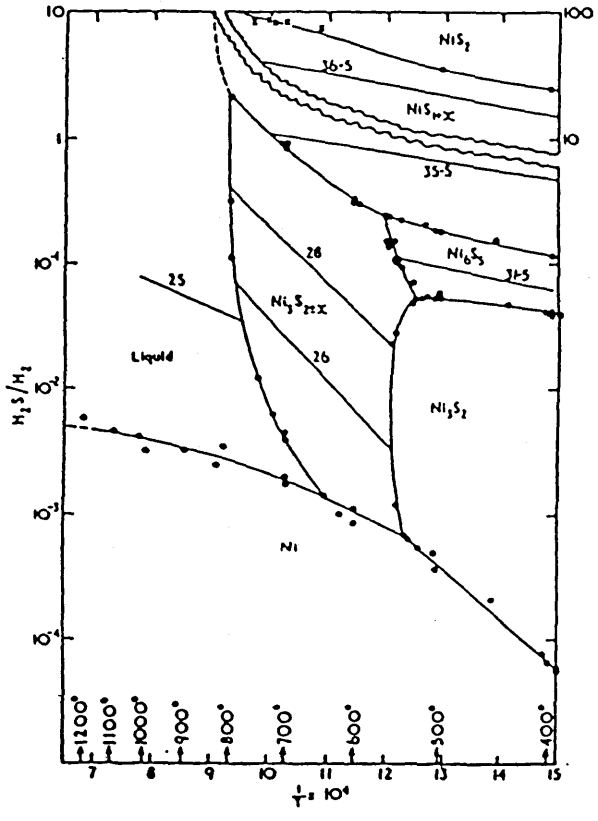

Figure 2.1 - Plot of H_2S/H_2 vs. 1/T for the system Nickel-Sulphur (Compositions of alloys are in Wt% of Sulphur) (from reference 22)

2.2.2 Adsorbed Sulphur

Information about the structure of adsorbed sulphur layers has been obtained by LEED (Low Energy Electron Diffraction), AES (Auger Electron Spectroscopy), UPS (Ultraviolet Photoemissions Spectroscopy), INS (Ion Neutralization Spectroscopy) and some other ultrahigh vacuum techniques. A summary of the work published up to 1982 appeared in the excellent review by Bartholomew et al. (3). Most of the information has been obtained by means of LEED. The studies have been performed basically on the low index planes of nickel [(100), (110), (111)] using H_2S as the adsorbate, however some studies have been done with other sulphur compounds.

Perdereau and Oudar (23) reported the work done on the (100), (110), (111) faces of Ni using LEED.

The adsorption of H_2S was performed at room temperature at a pressure of $1x10^{-8}$torr. Diffraction patterns were taken as a function of time. Upon saturation the temperature was raised to determine its effect on the structure obtained at ambient temperature.

They stated that there appeared to exist a common mechanism of adsorption. First, the H_2S is dissociated on the metal surface. On a second stage the surface is reconstructed. This reconstruction gives place to the formation of a S–Ni layer which can be considered as a bidimensional surface compound. In a third and final stage the units of bidimensional sulphides coalesce laterally. Figure 2.2 shows diagramatically this process.

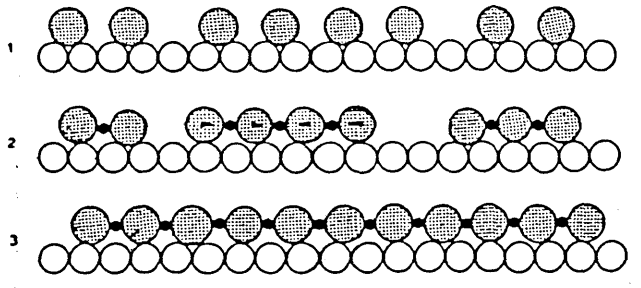

Figure 2.2 Adsorption Mechanism: 1- Initial stage; 2- Reconstruction, Nucleation of the bidimensional compound; 3- lateral coalescence of the bidimensional compound (from reference 23).

On the (100) plane they observed first a structure P(2x2), then for longer times of reaction a structure C(2x2). These two states correspond to square symmetries and can be considered as reconstructed states which appear directly on the surface.

For the (111) face they reported a succession of preliminary states at room temperature. First a structure P(2x2) was observed, which was followed by the structure $\sqrt{3}x\sqrt{3}$ $R30^0$. Further adsorption produced a 3rd state which corresponded to a compact arrangement of sulphur atoms with a coincidence lattice P(5x5). These states are shown in Figure 2.3. Upon heating the surfaces were reconstructed giving the arrangments shown in Figure 2.4. The sulphur atoms which were disposed in a hexagonal arrangement in the preliminary states were reorganized into square structures.

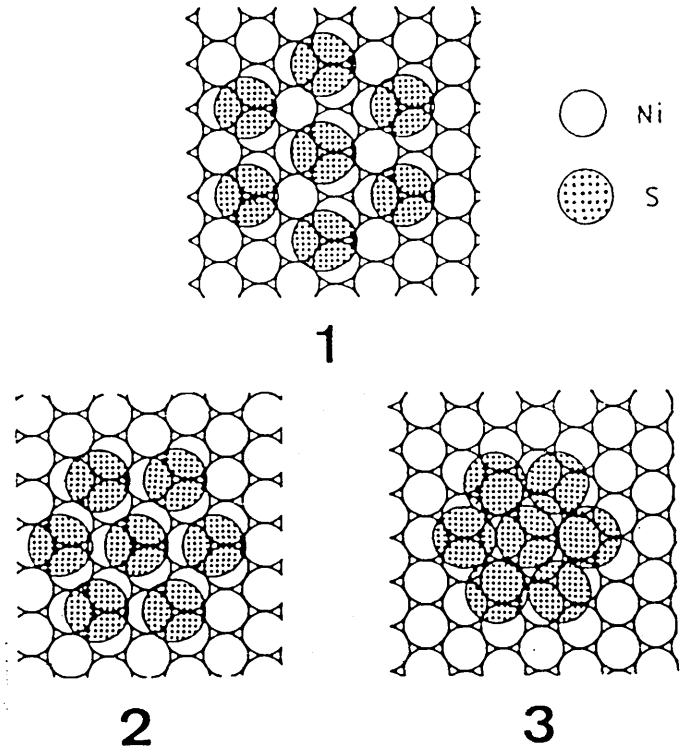

Figure 2.3 Preliminary States on Face (111). 1: P(2x2); 2: $\sqrt{3}x\sqrt{3}$ R30^0; 3: P(5x5). (As in reference 24)

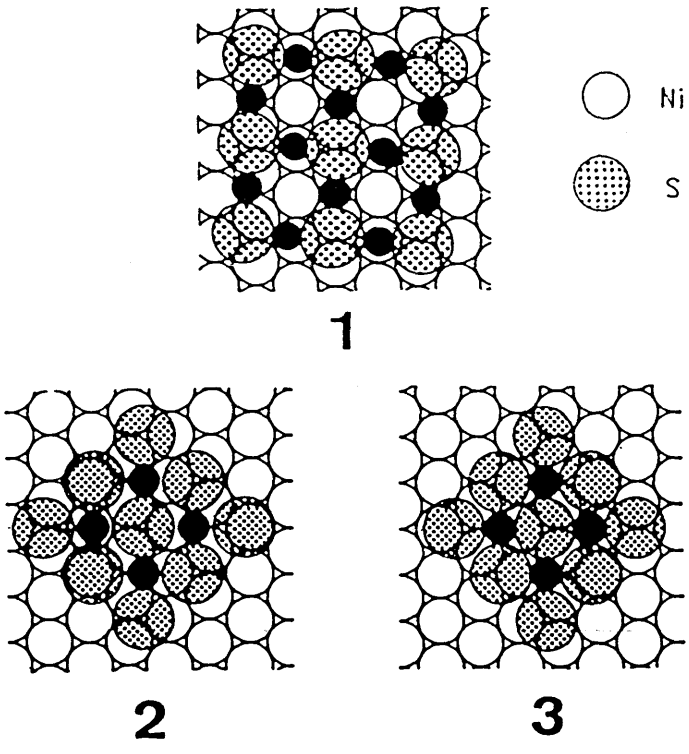

Figure 2.4 Reconstructed states on face (111)

(As in reference 24)

The preliminary structures show that the sulphur atoms follow hexagonal arrangements whereas in the reconstructed states the surface is characterised by square structures.

A situation similar to the one on the plane (111) was found for the plane (110); that is, the initial structure found corresponded to a C(2x2) after an exposure of 2 minutes. This structure was transformed with further exposure to H_2S to a saturation structure at room temperature corresponding to a lattice P(3x2). This structure was reorganized upon heating at 473K to a stable P(4xl) lattice.

That the adsorption of sulphur on the (110) and (111) faces of Ni is more complicated than on the (100) face as found by Perdereau and Oudar (23) has been confirmed by other authors (25-28).

Edmonds and co-workers (25,26) reported the adsorption of sulphur compounds (H_2S, n-propyl mercaptan, dimethylsulphide) on the (100), (111) faces of nickel studies by LEED at temperatures up to 700K. For the (100) face only two patterns were observed; they were assigned the unit meshes Ni(100) (2x2)S [p(2x2)] and Ni(100) C(2x2) S [C(2x2)]. For the (111) plane however a sequence of patterns were observed and grouped in 3 categories:

(i) Simple patterns formed during initial stages of reaction such as Ni(111) (2x2) S, Ni(111) ($\sqrt{3}$x$\sqrt{3}$) R30^0-S, and a pseudo $\sqrt{3}$ pattern which had a hexagonal unit mesh;

(ii) Complex patterns whose unit meshes could not be related to known nickel sulphide structures nor to coincidence nets between them and the Ni(111) plane;

(iii) Complex patterns whose unit meshes were hexagonal and could be described by the coincidence with the (111) plane of surface

structures, which were recognized as planes of known sulphides and had bulk sulphide dimensions.

The results described were similar to those reported by Perdereau and Oudar (23) but the interpretation of the complex structures of the category (ii) was different. They postulated that the complex patterns obtained: ($\sqrt{39}$x$\sqrt{39}$), (5$\sqrt{3}$x2), (8$\sqrt{3}$x2) and ($\sqrt{21}$x$\sqrt{84}$) arise from the reorientation of the (111) face of nickel to a (100) layer in the presence of sulphur. The presence of sulphur atoms on the nickel surface could weaken the bonding between the surface and next lower nickel layers and permit the arrangement suggested. They stated that all sulphur compounds used showed the same coincidence patterns.

Later Erley and Wagner (28) obtained LEED results from the adsorption of H_2S on Ni(111) and revised the surface reconstruction theory previously proposed (23).

They reported that with increasing H_2S exposure at room temperature the following sequence of patterns was observed: P(2x2) , ($\sqrt{3}$x$\sqrt{3}$) R30^0 and a more complex pattern. The ($\sqrt{3}$x$\sqrt{3}$) R30^0 structure was unstable even at room temperature. Above 370K the P(2x2) pattern disappeared but on cooling below 370K it reappeared again. Temperature had no effect on this structure. The complex sulphur structures observed by Perdereau and Oudar (23) after heat treatment could not be reproduced. They concluded that the complex pattern corresponds to a high S coverage without a surface reconstruction process; instead they proposed a structural arrangement of sulphur atoms on top of the Ni(111) plane which formed a coincidence mesh described by a C(20x2) structure. This pattern is shown below.

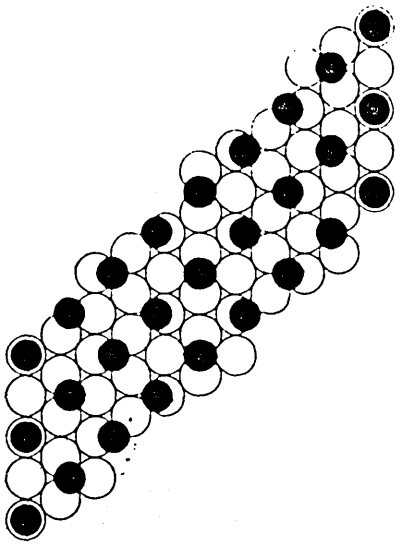

Figure 2.5 Model for C(20x2) structure

(•) S atoms, (0) Ni atoms (Ref. 28)

The results have shown that the adsorbed structures change with increasing sulphur coverage. For the case of Ni(100) the two ordered structures correspond to surface coverages of 0.25 for p(2x2) and 0.50 for C(2x2); a schematic diagram of these bondings was given by Fisher (29) showing that for the p(2x2) structure the sulphur is bonded to four Ni atoms, whereas it is bonded to 2 Ni atoms in the case of the C(2x2), as it is seen in Figure 2.6

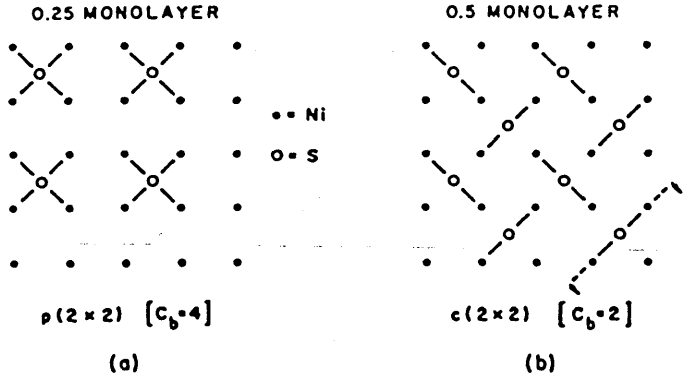

Figure 2.6 Schematic Top View of a Ni(100) surface with Sulphur in a Fourfold side. Cb: coordination bond (ref. 29)

Demuth et al. (27) reported a structural analysis of the chemisorbed sulphur layers on (100), (110) and (111) nickel surfaces. Their data are considered to be the most reliable and are shown in Figure 2.7 and table 2.2. For all the surfaces the determined Ni-S bond lengths are smaller than stable bulk compound lengths which are 2.28, 2.34 and 2.38Å for Ni_3S_2, NiS_2 and αNiS respectively. The metastable γ phase of NiS (millerite) has a bond length of ~2.18Å.

Table 2.2 - Summary of bond distances (in Å) (Ref. 27)

Ni-S	(110)	(100)	(111)
$d_\perp$	0.93 ± 0.1	1.30 ± 0.1	1.40 ± 0.1
d_{nn}	2.17 ± 0.1 (1)	2.18 ± 0.06 (4)	2.02 ± 0.06 (3)
d_{nnn}	2.35 ± 0.04 (4)	3.06 ± 0.1 (1)	2.93 ± 0.04 (3)

$d_\perp$: displacement of the centre of the adsorbed sulphur atom from the surface plane of Ni.

d_{nn}; d_{nnn}: nearest and next-nearest-neighbour Ni-S bond distances.

The number of nearest and next-nearest-Ni neighbours is given in parenthesis.

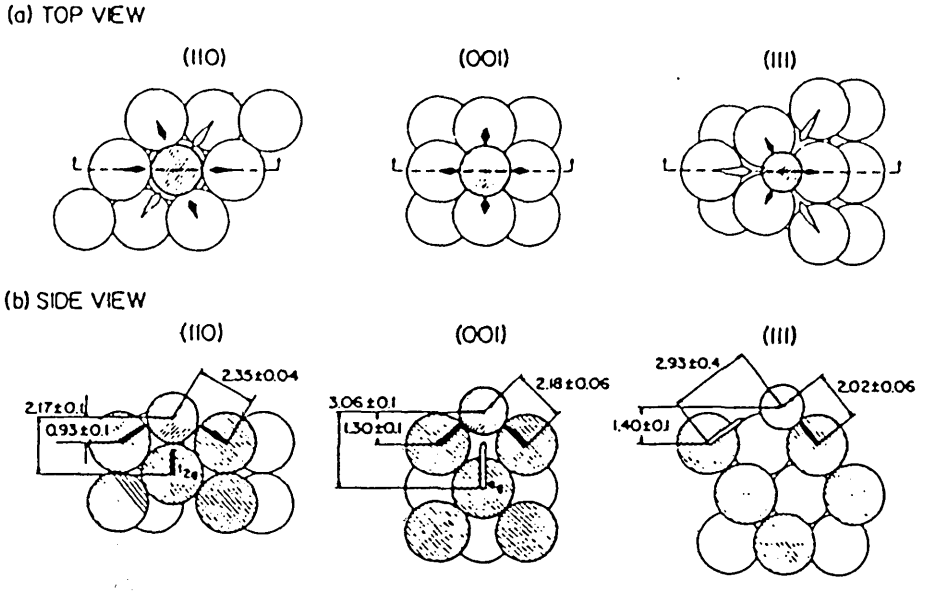

Figure 2.7 Diagram of the Atomic Bonding Sites of the Sulphur Atoms in the C(2x2), C(2x2), and p(2x2) structures on the (110), (100) and (111) nickel surfaces. (from ref. 27)

Demuth's data together with the low electron transfer between metal and sulphur deduced from work function measurements (30) provide evidence that the Ni-S bonding is mainly covalent.

With these results in consideration it may be possible to observe "electronic" as well as "geometric" effects in catalytic systems in which sulphur poisoning is involved (3).

2.3 Thermodynamics of the Sulphur Nickel Bond

The results from Demuth et al. (27) that the Ni-S bond lengths found on Ni surfaces are smaller than those in stable Ni-S bulk compounds suggest that adsorbed sulphur is bonded more strongly to Ni than sulphur in a bulk Nickel sulphide. Data available in the literature for both types of compounds are reported below.

2.3.1 Thermodynamics of bulk sulphides

The thermodynamic properties of bulk nickel sulphides were reported by Rosenqvist (22). Table 2.3 gives the thermodyanmic

properties for Ni sulphides. The values are per sulphur atom and based on the stoichiometry:

$$(x/y)M + H_2S \rightleftharpoons (1/y)\ M_xS_y + H_2 \qquad (2.1)$$

and ΔG^0 is defined by:

$$\Delta G^0 = RT\ \ln\ (P_{H_2S}/P_{H_2}) \qquad (2.2)$$

Table 2.3 - Molar free energies, entropies and heats of formation of Nickel sulphides at 1000K (727^{0}C)[a] (Ref. 22)

Compound	ΔG^0 (kJ)[b]	ΔS^0(J/K)	ΔH(kJ)[b]	S_{1000K}(J/K)[c]
Ni_3S_2 (low temperature form)	-43.3	-32.2	-75.5	156
Ni_3S_2 (high temperature form)	-48	-5.2	-53.0	183
Ni_6S_5	-38.6	-24.2	-62.8	143
NiS	-33.5	-22.6	-56.1	131
NiS_2	+1.2	-39.8	-38.5	80

[a] Reference states: solid metals, hydrogen sulphide and hydrogen at 1 atm.

[b] To obtain the free energy and heat of formation from S_2(gas), - 40.9 and -90.3KJ respectively must be added for each atom of sulphur in the compound.

[c] The entropies of the reference states at 1000K have been calculated from their entropies at 298K, and their specific heats between 298 and 1000K as given by Kubaschewski et al. (31).

For typical temperature range for catalytic reactions (300-600K) Bartholomew et al (3) calculated the free energy of formation of bulk metal sulphides based on the data by Rosenqvist (22), as shown below:

Table 2.4 Free energy of formation of metal sulphides[a]

Compound	ΔG^0 (kJ/g atom)	
	300K	600K
Ni_3S_2	-65.7	-56.1
Ni_6S_5	-55.7	-48.6
Ni_3S_{2-x}	-54.0	-58.2

[a] Based on one mole of H_2S.

2.3.2 Thermodynamics of adsorbed sulphur

The qualitative assessment of the strength of the adsorbed Ni-S bond that has been mentioned prompted several authors to determine the heat of H_2S chemisorption on Ni.

Oliphant et al. (32) determined from desorption isotherms for supported nickel catalysts that the heat of H_2S adsorption on nickel was estimated to be $-160 kJmol^{-1}$ of chemisorbed sulphur.

McCarty and Wise (33) measured sulphur chemisorption isosteres for nickel powder and alumina-supported nickel. From these measurements

they calculated a heat of formation of chemisorbed sulphur which was $-158 kJmol^{-1}$, more negative than the heat of formation of Ni_3S_2. It was also found that the heat of adsorption varies with sulphur coverage as can be seen in figure 2.8. The heat of adsorption of sulphur was shown to be energetically more stable than the formation of Ni_3S_2 of sulphur disolved in nickel, this is reported in figure 2.9.

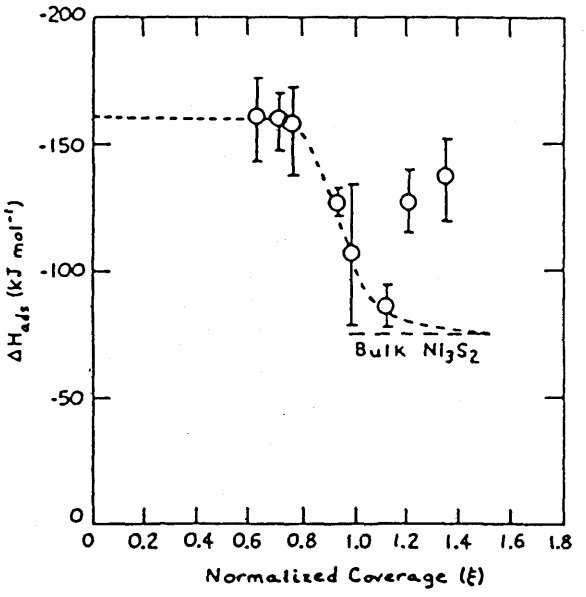

Figure 2.8 Heat of adsorption of sulphur via H_2S/H_2 on $Ni/\alpha\ Al_2O_3$ vs. coverage (ξ) normalized to CO uptake at 300K (ref. 33)

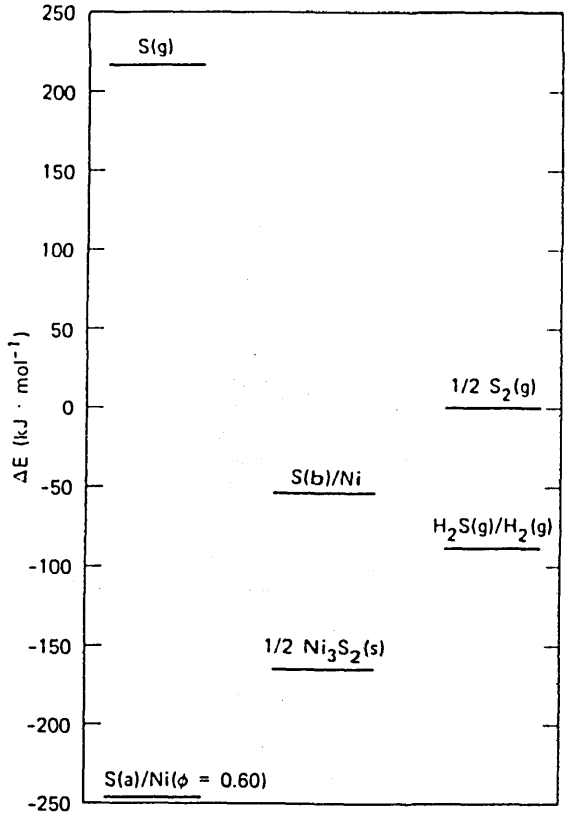

Figure 2.9 Energetics of sulphur interaction with nickel at 800K S(a): adsorbed sulphur with 0.60 fractional saturation coverage (ϕ); $Ni_3S_2(s)$: bulk nickel sulphide; S(b): sulphur dissolved in the bulk metal; S(g): gaseous monatomic sulphur. The reference states are $H_2(g)$, $S_2(g)$, and Ni(s) at 800 K. (ref. 33)

The coverage dependence for the heat of adsorption was corroborated by Alstrup et al. (34) who measured adsorption isobars for the adsorption of H_2S on $Ni/MgAl_2O_4$ catalysts. The heat of adsorption of sulphur followed the equation:

$$\Delta H = \Delta H_o^0 \ (1-0.69\theta) \quad kJmol^{-1}$$

Where $\Delta H_o^0 = -289$ $kJmol^{-1}$, $\theta = \frac{S}{So}$: sulphur coverage, S and So are

actual and saturation amounts of adsorbed sulphur respectively. This expression reproduced with good accuracy the data from McCarty and Wise especially at $0.6 < \theta < 0.8$.

The quantitative data available were collected by Bartholomew et al. (3,35) and produced a figure showing the remarkable consistency of them all. It was obvious that all the data predicted a more stable Ni-S bond in the adsorbed state than in the bulk phase Ni_3S_2.

2.4 Mechanism of the Sulphur Adsorption and Adsorption Stoichiometry

2.4.1 Mechanism of adsorption

Several techniques have been used to determine the way sulphur is attached to the metal surface. The majority of the studies have employed H_2S, although other sulphur-containing compounds such as carbon disulphide and mercaptans have also been used. The results point to the fact that the adsorption is dissociative but not all agree in the number of nickel sites occupied by a sulphur atom.

From adsorption experiments performed in a volumetric apparatus Saleh et al. (36) concluded that in the range 193K - 373K H_2S occupies 3 nickel atoms:

$$H_2S + Ni\text{-}Ni\text{-}Ni \rightarrow \overset{H}{|}Ni\text{-}\overset{S}{|}Ni\text{-}\overset{H}{|}Ni$$

Den Besten and Selwood (37) found that the adsorption of H_2S favours a four-site mechanism as follows:

$$H_2S + Ni\text{-}Ni\text{-}Ni\text{-}Ni \rightarrow \overset{H}{|}Ni\text{-}Ni\text{-}\overset{S}{\diagup\diagdown}Ni\text{-}\overset{H}{|}Ni$$

This conclusion was reached through magnetisation measurements and

confirmed by H_2-D_2 exchange.

Magnetisation measurements were also used by Ng and Martin (38), who also suggested that the H_2S forms four bonds with the Ni surface.

Attempts have been made to fit results to adsorption isotherms. Rostrup-Nielsen (39) studied the adsorption of H_2S on Ni supported on magnesium aluminum spinel in the temperature range 823K - 918K. The adsorption data were fitted to an equation of the form:

$$\theta s = \frac{a(P_{H_2S}/P_{H_2})^n}{1 + b(P_{H_2S}/P_{H_2})^n} \qquad (2.3)$$

and obtained n = 1.1; from which he suggested a one-site mechanism. Following the same treatment, Oliphant et al. (32) adjusted desorption data to a Langmuir-type equation (eqn. 2.3) and obtained exponents of 2.94 for nickel powder, and 2.72 for a 3% Ni/Al_2O_3 at 725K. These exponents suggest a 3-site mechanism for the H_2S adsorption. More recently Alstrup et al (34) measured sulphur chemisorption isobars for a $Ni/MgAl_2O_4$ catalyst in the range 773 - 1023K and fitted the data to a Temkin-like adsorption isotherm of the form:

$$\frac{P_{H_2S}}{P_{H_2}} = \exp\left[\Delta H_o^0(1 - \alpha\theta)/RT - \Delta S^0/R\right] \qquad (2.4)$$

with $\Delta H_o^0 = -289 kJmol^{-1}$, $\Delta S^0 = -19 JK^{-1}mol^{-1}$, $\alpha = 0.69$.

The data from Oliphant et al. (32) as well as those from McCarty and Wise (33) and Rostrup-Nielsen (39) were very well reproduced by

this equation.

The linear decrease of the heat of adsorption with increasing coverage can arise either on a uniform surface from repulsive forces or from surface heterogeneity (40). The constant entropy resembled gas-solid solution equilibrium and suggested subsurface sulphur uptake (34) at high temperature as was found by Weeks and Plummer (41) in their angle-resolved photo-emission studies on Ni (100) surfaces.

The adsorption and dissociation of H_2S on Ni seems to have SH species as intermediates (36, 37, 42). The adsorption experiments and D_2 exchange results from Saleh et al. (36) supported the suggestion that HS radicals were involved in an intermediate stage in the adsorption of H_2S since two types of Hydrogen atoms were found on the surface. Desorption and D_2 exchange experiments by Den Besten and Selwood (37) and thermal desorption results from Rudajevova et al. (42) also suggested the presence of SH as intermediate in the dissociation of H_2S.

The adsorption of sulphur-containing compounds, other than H_2S, on Ni has also been studied (37,43-52). The mechanism seems more complicated than with H_2S and strongly dependent on temperature. It will be described later in Section 2.5.

2.4.2 Adsorption Stoichiometry

Perdereau and Oudar (23) obtained the sulphur saturation coverage values for single crystal faces and polycrystalline samples of Nickel. These values are listed in Table 2.5 below. It shows that the amount of sulphur adsorbed at saturation is independent of the crystal orientation. However the sulphur coverage θ_s ranges from 0.48 to 1.09; variations that seem to arise from the differences in Ni atom

concentration on the various surface planes.

Table 2.5 Sulphur Saturation Coverages for Crystal Faces of Nickel (Ref.23)

Crystal Face	Sulphur Concentration at saturation ($g\ S/m^2$)	Number of Sulphur atoms per m^2 ($\times 10^{19}$)	Number of Ni atoms per m^2 ($\times 10^{19}$)	S atoms per surface Ni atom
(111)	$(47\pm1) \times 10^{-5}$	0.86	1.8	0.48
(100)	$(43\pm1) \times 10^{-5}$	0.80	1.6	0.50
(110)	$(44.5\pm1) \times 10^{-5}$	0.82	1.1	0.74
(210)	$(42\pm1) \times 10^{-5}$	0.78	0.72	1.09
Polycrystalline	$(44.5\pm1) \times 10^{-5}$			

Experimental Conditions: $P_{H_2S}/P_{H_2} = 8\times10^{-4}$; T = 873K.

Bartholomew et al. (3) suggested that if reconstruction occurs a better way to evaluate θ_s would be to consider the structure of the surface Ni layer at saturation rather than the structure of the clean Ni surface before adsorption of any sulphur. Thus, assuming that all Ni faces reorient to a (100) configuration at saturation coverage the values of θ_s in table 2.5 would be 0.54, 0.50, 0.51, 0.49 and 0.51 for Ni(111), Ni(100), Ni(110), Ni(210) and polycrystalline faces respectively. Therefore a value of θ_s of 0.50 appeared to be universal.

For polycrystalline unsupported and supported Ni catalysts the saturation coverage varies with temperature and H_2S partial pressure.

The adsorption of H_2S at room temperature and high pressures ($P_{H_2S} > 5x10^{-2}$ torr) has produced sulphur coverages of 0.25 - 0.33 for Ni films (36), Ni supported on Kieselguhr (37) and on silica (38). At higher temperatures the sulphur coverage tends to be higher. It was found to be 0.74 on $Ni/MgAl_2O_4$ at temperatures of 823 - 918K and P_{H_2S}/P_{H_2} = 2-8 ppm (39); 1.14 for Nickel powder and 1.08 for 3% Ni/Al_2O_3 at 723K and 25ppm, and 0.86 for 3% Ni/Al_2O_3 at 723K and 8ppm (32), the coverage values θ_s are based on a H/Ni_s ratio of 1. Fitzharris et al. (15) obtained θ_s = 0.50 for a α-Al_2O_3 supported Ni catalyst at 661K and 13ppb H_2S. These results suggest:

i) That at low temperature the hydrogen occupies Ni sites so that the θ_s obtained are low, whereas at high temperature hydrogen is desorbed allowing sulphur atoms to cover the Nickel sites; and thus obtain higher S/Ni_s ratios.

ii) Very low concentration of H_2S is needed to saturate unsupported and supported Ni surfaces; the values of sulphur coverage obtained at these concentrations ($<$ 100ppb) agree well with the saturation values of well defined simple crystal faces; and

iii) The near unity values of θ_s obtained at high concentrations (10ppm-25ppm) are explained by surface reconstruction of the Nickel faces to a Ni surface sulphide layer (2-dimensional Ni sulphide compound).

2.5 Adsorption of Thiophene and Sulphur-Containing Compounds

2.5.1 Mechanism and kinetics of thiophene adsorption on Ni

The adsorption of thiophene on nickel catalysts has received little attention, and few studies exist. Lyubarskii et al (45) studied the poisoning of supported nickel catalysts by thiophene in the temperature range 293K-393K. They found that for low sulphur coverage the benzene hydrogenation activity decreased linearly as the thiophene increased; the activation energy for the benzene hydrogenation remained constant for both fresh and partially poisoned catalysts. These results agree with a geometric effect of the poisoning rather than an electronic effect. They reported that at room temperature an adsorbed thiophene molecule occupied on average 5 nickel atoms, thus the area of the thiophene molecule could be taken as approximately $33Å^2$, and suggested the following mechanism:

at room temperature the thiophene molecule lies flat on the nickel surface binding five atoms; as the temperature is increased hydrogenation of thiophene to thiophane occurs, although the thiophane molecule is held only through the sulphur atom. With further temperature increase (573K-623K) butane is produced leaving sulphur strongly adsorbed on the nickel sites. This process is shown in Figure 2.10.

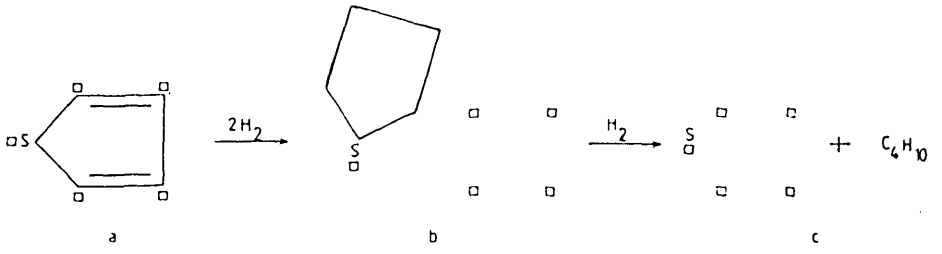

Figure 2.10 Mechanism of Thiophene Poisoning of Nickel

a) adsorbed thiophene; b) adsorbed thiophane; c) surface sulphide and butane product.

Bourne et al (46) showed the effect of temperature on the sulphidation of Ni catalysts. Over the range 303K-423K the S/Ni ratio increased from 0.03 to 0.09 (S/Ni is the ratio of total sulphur atoms to total nickel atoms in the catalyst). Above 423K the S/Ni ratio increased rapidly as can be seen in figure 2.11; there was evidence of sulphiding in depth at temperatures above 473K. The results of sulphidation at 373K showed that only 25% of the surface nickel sites were occupied by sulphur; and based on the results of Lyubarskii et al. (45) they suggested that maximum surface coverage by sulphur occurred when 19% of sites on Ni (100), 38% on Ni (110) and 24% on Ni(111) have been covered.

During high temperature sulphiding (above 423K) they postulated that thiophene reacts with nickel in two ways:

i) direct reaction to give butane and leave sulphur attached to the nickel,

ii) decomposition to give H_2S.

The first accounts for the maintained selectivity, the second for the sulphiding in depth. No H_2S, however, was found at temperatures below 523K.

They suggested that the rate controlling step was the decomposition of the thiophene.

The results reported by Richardson (51) agree with the mechanism of adsorption, decomposition and sulphiding mentioned above. The data were obtained in a fixed-bed reactor using nickel - Kieselguhr at temperatures between 473K and 673K. He suggested that in this temperature region the controlling mechanism may be the adsorption of the thiophene.

During liquid-phase hydrogenation of octines at 303K Koppova et al. (49) showed that the activity of the nickel/kieselguhr catalyst decreased with increasing amounts of thiophene although the selectivity was similar to that on unpoisoned catalyst. They assumed that at this temperature the thiophene was adsorbed coplanar to the surface and employing the molecular area given by Lyubarskii et al. (45) they calculated an area which was in good agreement to that determined by H_2 chemisorption.

Thiophene was found to poison a maximum of 75% of the sites available on Ni boride and Raney Nickel catalysts during the hydrogenation of 1-octene at 295K (50) even at high poison concentrations; a result which is in agreement with the estimate given by Bourne et al. (46). The thiophene poisoning curves showed characteristics of a strongly adsorbed poison which produces "pore-mouth" poisoning. The results suggested that the geometric requirements for thiophene adsorption restricted its easy access to a portion of the catalyst, especially the small pores. Therefore diffusional limitations may be present during the poisoning of porous nickel catalysts by thiophene.

Poisoning kinetics data measured in a differential reactor at thiophene partial pressures of 5-25 Pa and temperatures of 333K to 453K were fitted to a power law equation consistent with a one-site mechanism by Weng et al. (52). The correlation of poisoning kinetics was not able to predict the propagation of the zone of activity (hot spot) on poisoning of an integral fixed bed reactor during hydrogenation of benzene. A semi-empirical two site deactivation model was developed to solve the discrepancy. In this model they considered the sites active for thiophene chemisorption to be the sum of those active for hydrogenation and those active for chemisorption alone.

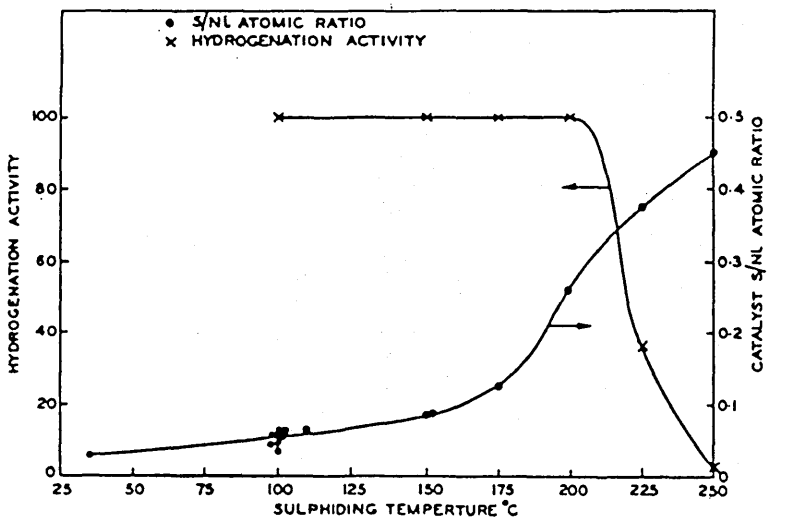

Figure 2.11 Effect of Sulphiding temperature on S/Ni ratio and catalytic activity (thiophene treatment). (Ref. 46)

Infrared studies on the adsorption of thiophene on supported Ni catalysts have been carried out (43, 48, 53). Blyholder and Bowen (43) observed frequency bands when thiophene was adsorbed onto silica-supported nickel at 2940cm^{-1}, 2885(shoulder), 1610(weak) and 1460cm^{-1} which were assigned to CH_2(2940cm^{-1}), CH_2 and CH(2885cm^{-1}) and CH_2 or CH_3(1460cm^{-1}). They proposed that thiophene was chemisorbed

with the double bonds opened to form carbon-nickel bonds with the surface; and suggested that at room temperature carbon metal bonds rather than sulphur metal bonds were responsible for the strong chemisorption, at higher temperatures the poisoning process might be envisioned as starting first with adsorption of the sulphur compound by carbon-metal bond formation and then dissociation to sulphide the catalyst surface.

IR spectra determined by Rochester and Terrell (48) for the adsorption of thiophene on silica-supported nickel were similar to those recorded by Blyholder and Bowen. However spectra obtained from the interaction between thiophene and silica support alone were the same as those found on the supported Ni samples, therefore species adsorbed specifically on the metal could not be distinguished in the presence of bands due to species on the surface of the oxide support. It was questionable, thus, to attribute IR bands entirely to adsorption on the metal surface.

Klostermann and Hobert (53) reported the appearance of C-H stretching vibrations characteristic of aliphatic hydrocarbons resulting from the interaction between thiophene an freshly reduced silica-supported nickel, addition of H_2 increased the intensity of the respective absorption bands, and concluded that thiophene is dissociatively adsorbed on Ni/SiO_2. Thermodesorption experiments from room temperature to 1100K showed that the main product was C_6H_6, but C_4H_8, $C_6H_5CH_3$, $C_6H_5C_2H_5$, H_2, CH_4 and CO were also detected. The sulphur remained on the sample whereas the carbon and hydrogen contained were removed (53).

The adsorption of thiophene has been reported to be slow as found

in the IR studies (48) at room temperature. Bourne et al. (46) suggested that the adsorption-decomposition of thiophene to be the rate controlling step; the results of Richardson (51) were in agreement with this suggestion. From Richardson's data for thiophene adsorption rate constants an activation energy of sulphidation can be calculated. The value obtained between 473K and 673K is:

$$E_d = 10776 \text{ J/moleK} = 2575 \text{ Cal/moleK}$$

Weng et al (52) obtained a rate equation for poisoning of nickel/kieselguhr catalysts by thiophene linear in concentration of poison and availability of active sites:

$$-r_d = k_d^0 \, e^{-E_d/RT} \, P x_T \, \theta_A \qquad (2.5)$$

where: k_d^0: pre-exponential factor , $(\text{torr-sec})^{-1}$

E_d: activation energy of poisoning

P: total pressure, torr

x_T: thiophene mole fraction

θ_A: ratio of the number of present active sites to initial active sites

k_d^0 and E_d were determined in the region 338K-448K and are given below:

Parameters for thiophene poisoning kinetics

E_d = 4518 J/mole

k_d^0 = 2.40 x 10^{-2} $(torr\text{-}sec)^{-1}$

Equation (2.5) was proved to be unsatisfactory to predict integral fixed-bed dynamics of benzene hydrogenation and was modified to a two-site mechanism rate equation:

$$-r_T = Px_T M_T k_d^0 \exp(-E_d/RT) \{\gamma\theta_A + f(1-\gamma)\ \theta_A^f\} \qquad (2.6)$$

in this case:

M_T : catalyst adsorption capacity of thiophene (kmol/kg)

γ : ratio of hydrogenation-active sites to total sites measu- red by M_T

f : ratio of pre-exponential factors for poisoning of inert (for hydrogenation) to active sites.

γ, and f were found to be: 0.35 and 0.015 respectively. The γ value indicates that there were somewhat fewer hydrogenation-active sites than inactive sites, and the f value indicates that thiophene chemisorption on the sites inactive for hydrogenation is slow compared to that on active sites.

The activation energy for poisoning reported by Weng is more than

twice the value calculated from Richardson's data. The disagreement may lie in the different temperature regions in which they were obtained. It is possible that different processes may be occurring in the two temperature regions as was pointed out by Lyubarskii et al. (45) and Bourne et al. (46), thus the two activation energies represent different chemical processes.

2.5.2 Mechanism and kinetics of thiophene adsorption on other metals . HDS reactions

This part includes studies on the adsorption of thiophene on metals other than nickel, which are relevant since they might provide essential features shared by all of them, and the possible reaction scheme for the hydrodesulphurization of thiophene described below could be applied to any metallic catalyst as was pointed out by Zdrazil (63).

2.5.2.1 Thiophene adsorption on precious metals

The effect of thiophene poisoning on Pt, Rh, Pt-Re catalysts has been reported (54-58). Menon and Prasad (54) reported that surface sulphidation of Pt/Al_2O_3 and $Pt-Re/Al_2O_3$ affected only marginally their activities for dehydrogenation, dehydroisomerization, dehydrocyclization and hydrocracking, however further sulphidation leads to poisoning of the two catalysts. The results by Coughlin et al. (56) agree with those of Menon and Prasad (54), they found that at low thiophene concentration, up to about 25ppm, the effect on the performance of Pt and Pt-Re catalysts was minor, however higher concentrations of thiophene (75ppm) caused severe poisoning of Pt-Re catalytic activity but caused little further change in the activity of Pt catalysts. Sulphur seemed to be preferentially adsorbed on Re

sites.

González-Tejuca et al. (57) found that at temperatures below 373K thiophene was not a very effective poison for platinum on alumina and is readily desorbed from the surface. At 323K the thiophene is competitively adsorbed in both the metal and the support as was concluded by Barbier et al. (58) on Pt/Al_2O_3. The adsorption being structure sensitive. On Rh supported on silica and alumina the poisoning by thiophene was also found to be structure sensitive, with an activation energy of 33.5KJ/mole in the temperature region 325K-355K (55).

2.5.2.2 Hydrodesulphurization (HDS) reactions

Thiophene has been used with particular interest as model compound in residual oil and coal hydrodesulphurization (HDS). Several reviews of the process exist, they include discussion of the mechanisms and kinetis (59-64) of HDS reactions. The usual industrial catalyst for HDS consists of MoO_3 (~14%) promoted with CoO (~4%) and supported on γ-Al_2O_3. Some catalysts contain Ni instead of Co, and some contain W instead of Mo (60,62). The transition metal oxides in HDS operations become reduced and partially or completely converted to sulphides. At conditions typical of laboratory HDS reactions (500K - 673K, latm) a possible reaction scheme has been proposed to be:

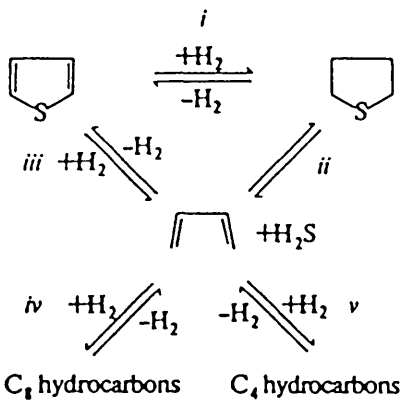

Figure 2.12 HDS Reaction Scheme (63,65)

Mitchell (61) and Zdrazil (63) have pointed out that there is increasing evidence that the HDS reaction proceeds via steps (i) and (ii), that is: the hydrogenation-elimination (hydrocracking) sequence. A partial saturation of the ring seems to be needed in the first step, leading to a change in the type of sulphur bonding from the aromatic to sulphidic one. Elimination of H_2S gives butadiene as the primary product which is subsequently hydrogenated and/or oligomerized to C_4, C_8 and higher hydrocarbons. The oligomerization of dienes could play an important role in the catalyst deactivation (61). The direct hydrogenolysis of the ring (step iii) states that HDS starts by C-S bond splitting with the direct participation of hydrogen, it is the most frequent alternative to the previous pathway. Zdrazil (63) has criticized this scheme on the basis that not even single C-S bonds in sulphides and thiols are supposed to be cleaved via the substitution attack of hydrogen on sulphur or carbon but rather by a two-step elimination-hydrogenation mechanism, besides it has no analogy in the general chemistry of sulphur aromatics.

The way in which thiophene binds to the catalyst surface has continued to attract interest. Mitchell (61) has noted that a consensus seems to be developing in favour of a structure in which the thiophene molecule sits parallel to the catalyst surface (four point adsorption), having an interaction with the surface through the ring π-system in a way similar to that of benzene (65).

In the temperature region 278K-300K the thiophene molecule seems to be physcially adsorbed only as was determined by Dollimore et al. (66) from adsorption-desorption measurements. Furthermore, they suggested that part of the catalyst surface was inaccessible to thiophene due to its size, as the observed maxima of the pore size distributions decreased, and the monolayer capacity increased as the temperature decreased, suggesting that the effective volume of the thiophene was smaller at lower temperatures.

Kinetic expressions for thiophene hydrodesulphurization have been obtained based on Langmuir-Hinshelwood rate equations. The currently most favoured equation is that reported by Satterfield and Roberts (67):

$$r_{HDS} = k \frac{P_T P_H}{(1+K_T P_T+K_s P_s)^2} \qquad (2.7)$$

where: k: rate constant

P: pressure

K: adsorption coefficient

H: hydrogen ; T: thiophene ; S: H_2S

This expression implies a two point thiophene adsorption in competition with H_2S on one type of site and hydrogen adsorption on a

second type of site. However the rate equation can not always be unequivocally established as found by Massoth (68) and Hernández (69), good data correlation could be obtained with more than one kinetic expressions. Claiming absence of mass transfer influence Satterfield and Roberts (67) reported an activation energy of HDS of 15.5kJ mol^{-1}, a value which seems to indicate the opposite, other values reported are in the region 67-92 kJ mol^{-1} (see ref. 64, 70,71). In general regarding the kinetics it can be said that:

i) the kinetics are consistent with the assumption that the slow step of the reaction is a surface reaction between adsorbed thiophene and adsorbed hydrogen

ii) hydrodesulphurization is strongly inhibited by hydrogen sulphide

iii) the surface reaction involves a dual site mechanism: one site on which thiophene and H_2S competitively adsorb and another site on which hydrogen is adsorbed.

2.5.3 Adsorption and reaction of other sulphur compounds on nickel

Studies on the adsorption of other sulphur containing compounds have been carried out. Methyl mercaptan was dissociatively adsorbed with methane production at 193K-423K and formation of dimethyl sulphide at temperatures above 313K (44). Dimethyl sulphide adsorbed associatively at room temperature, dissociatively at 393K and yielded methane and ethane at temperatures above 500K (37). The Ni sulphidation by t-butyl mercaptan at 373K produced isobutane firstly, shifting to isobutene after the Ni surface had been sulphided to about a sulphur to nickel ratio of 0.2 (46).

IR studies on the adsorption of sulphur on Nickel demonstrated

that dimethylsulphide was dissociatively adsorbed (48); mercaptans with longer chain groups such as ethyl, n-propyl, isopropyl, n-butyl, isobutyl and tert-butyl mercaptans were adsorbed as mercaptide structures R-S-Ni at room temperature (43,47,48,72); with heating at 353K the adsorbed mercaptans underwent decomposition forming olefins and a sulphided surface (47).

The results of Klosterman and Hobert (53) favour the dissociatively chemisorption of sulphur compounds on silica-supported nickel. Dissociation of C-S, S-H, S-S, C-H, C-C bonds occurred at room temperature and the extent of dissociation decreased in the order C-S, S-H S-S, C-H C-C. Thermodesorption experiments revealed that the dissociation reactions of C-H and C-C bonds are favoured at higher temperatures. H_2-containing carbon species were detected up to 600K, only carbon and sulphur remained above 600K. Between 800K and 1100 K carbon reacted with surface oxygen giving CO, whereas most of the sulphur remained on the silica supported nickel. The main products of the thermodesorption of mercaptans, sulphides, disulphides, thiophene, thiophane and CS_2 were alkanes, olefins and aromatics, although dimers and cyclic compounds were also observed (53).

2.6 Effect of Total Pressure on the Adsorption of Sulphur-Compounds

The very high rates at which hydrogen sulphide and sulphur-containing compounds adsorb on metal surfaces and the high stability of the sulphur-metal bond may be the reasons why the adsorption process has only been studied at or below atmospheric pressures. The studies available on the effect of pressures higher than atmospheric have been performed under reaction conditions during activity tests (8,21,46).

Fixed bed results for methanation at 2500 kPa, and temperatures between 723K-773K were reported by Fowler and Bartholomew (8). The catalysts were presulphided at 723K and 130kPa with a gas mixture of 10 ppm H_2S in H_2 in a fluidized bed. The CO conversion at 773K decreased from 97% for a fresh Ni catalyst to 95.8% for the same catalyst presulphided; for a Mo catalyst the conversion on a presulphided catalyst was slightly higher than on a fresh sample (76.5% compared to 74%). Higher decrease was observed for Ni-Co (from 99% to 89%) and Ni-Cu-Mo (from 97% to 68%). The CO conversions and methane yields were very near the predicted equilibrium values on the fresh catalysts, and the same behaviour was still in evidence on the presulphided Ni catalysts. The effects of H_2S poisoning were less in the high pressure, high temperature tests than in the atmospheric pressure, low temperature tests (see section 2.1). The difference was suggested to result mainly from the presence of very high reaction rates and heat and mass transport limitations under the high pressure conditions and the absence of these limitations at low temperature and pressures. Apparently under high pressure conditions only a portion of the bed was needed to reach near equilibrium conditions, thus presulphiding 50% of the sites had little effect on the catalyst performance.

Rostrup-Nielsen (21) found that the activity of a steam reforming catalyst decreased after a few hours at 773K and 3140 kPa (31 atm), whereas the activity was maintained at atmospheric pressure, and other conditions similar over the same period; days were needed to observe gradual deactivation. The feedstream contained less than 0.05ppm S. Sulphur poisoning was assumed to cause the deactivation, being faster at high pressures due to quick accumulation of sulphur at the very high

throughputs. However mass and heat transfer limitations are suspected to be present at high pressures since the experiments developed axial and radial temperature gradients higher than experiments at atmospheric pressure which were considered to be isothermal.

During the hydrogenation of isoprene at 373K and 1380kPa the activity of the nickel/silica catalyst remained constant at 100% even after 50h under a stream containing between 0.01 and 0.5 wt% of thiophene. Olefin selectivity increased with the amount of sulphur retained by the catalyst. The olefin selectivity was higher at atmospheric pressure. However no further comparisons can be made since the results reported for both sets of tests were obtained at different experimental conditions (46).

Results obtained at high pressure have involved heat and mass transfer limitations which mask the effect of sulphur on the activity and selectivity of catalysts.

2.7 Regeneration of Sulphided Ni Catalysts

2.7.1 Regenerating agent

Few studies exist on the regeneration of sulphided nickel catalysts. H_2 (8,9,44,51,73), O_2/air (9,47,74-77), and steam (78) have been used. Attempts to regenerate sulphided catalysts with H_2 to restore their catalytic activity have normally failed. Richardson (51) could restore the magnetic properties of H_2S sulphided Ni beds but were inactive for benzene hydrogenation. Regenerated samples could be resulphided by H_2S but not by thiophene, a behaviour expected since thiophene had to be adsorbed by Nickel and decomposed before sulphiding could occur.

Bartholomew and co-workers reported that H_2 treatment for 24h at

725K allowed a 5% recovery of the surface area (assessed by H_2 chemisorption) but failed to restore methanation activity (9); and at 773K all samples lost whatever residual activity they may have retained up to that point (8). The latter fact was tried to be explained either as a restructuring of the surface to an inactive metal sulphide at the higher temperature or metal support interactions with adsorbed sulphur to form sulphospinels as suggested by Dalla Betta et al. (4). Chemical analysis of the catalysts before and after regeneration tests showed that only 5-10% of the sulphur was removed from the catalysts. Elution curves obtained by flowing H_2 over H_2S sulphided catalysts over a period of 2-3 days indicated that only 5-10% could be removed at 725K. Dobashi (73) reported that Ni/Al_2O_3 poisoned with sulphur could be regenerated to about 15-60% in the temperature region 700K-1100K but no sulphur was removed during the treatment. Bartholomew and co-workers (3) questioned the results since it is difficult to regenerate a catalyst without sulphur removal.

Regeneration with steam at 973K removed up to 80% of the sulphur adsorbed on Ni steam reforming catalysts promoted with Mg and Ca (78). Rostrup Nielsen (78) detected sulphur dioxide and hydrogen sulphide in the effluent gas and proposed the following reaction pattern for the regeneration process:

$$Ni\text{-}S + H_2O \rightleftharpoons NiO + H_2S$$

and

$$H_2S + 2H_2O \rightleftharpoons SO_2 + 3H_2$$

This reaction pattern requires total oxidation of the catalyst.

From catalysts promoted with Na and K sulphur was not removed; presumably due to sulphate formation.

Treatment with O_2 of sulphided Ni catalysts has had partial success. Bartholomew et al. (9) reported that up to 12% methanation activity was restored after the catalyst was treated in O_2 followed by H_2 reduction at 525K.

IR spectra obtained after mercaptan-poisoned nickel samples were exposed to oxygen at 353K were similar to those observed after the addition of SO_2 to fresh nickel (47). It was suggested that when oxygen was added the sulphur was oxidized with sulphate formation on the surface, however the exact nature of the species was difficult to discern because the spectral bands were weak.

Holloway and Hudson (74) reported that the exposure to oxygen of surface sulphur on Ni (111) at room temperature resulted in the removal of sulphur as SO_2 and coverage of the surface with oxygen. The rate of reaction was proportional to the gas phase oxygen pressure which led them to propose that the rate controlling process was the reaction:

$$O_2(a) + S(a) \rightarrow SO_2(a)$$

Where (a) means adsorbed species. The oxygen was weakly adsorbed. The mechanism devised consists of: First, adsorption of oxygen on defect sites on the surface; second, reaction between oxygen and sulphur on these defect sites; third, growth of holes in the surface structure around these initial sites with the reaction taking place only at the perimeter of the holes. The holes are filled by adsorption of oxygen resulting in formation of islands of oxygen.

The interaction of oxygen with a surface nickel sulphide formed on polycrystalline nickel was studied by Windawi and Katzer (75) using AES. At room temperature SO_2 was formed, and the Auger peak shapes and heights were consistent with a three-layer nickel oxide, and no sulphur present. Upon heating to 673K in vacuum (10^{-10} Torr) approximately 62% of the oxygen signal was lost while the sulphur signal increased to about 55% of the original level. Further treatment with H_2 at 673K reduced the sulphur signal intensity to ~65% of the corresponding to preoxidation level. Thus oxidation at room temperature at ~10^{-6} Torr resulted in the removal of ~1/3 of the sulphur present initially. The observation of an increase in the oxygen signal and a decrease of sulphur signal does not prove effective sulphur removal because the surface sulphur may just be buried by the metal oxide over it. Oxidation at 673K of a sulphided sample at an oxygen pressure of ~$1-5\times10^{-7}$ Torr produced SO_2 and formed multilayer oxide; upon Ar^+ ion sputtering the oxide thickness was found to be 10-20 layers; no sulphur burial was observed.

The last finding is in contrast to the results reported by Colby (77). He attempted to remove sulphur from polycrystalline nickel surface by oxidation at temperatures from 300K to 800K and atmospheric pressure, (P_{O_2} =10-760 Torr). He found that nickel oxide layers were formed on top of the sulphur layer. Subsequent treatment with H_2 at 700K reduced the nickel oxide to the metal, and the sulphur layer was observed again on the surface. He explained the results in terms of two competing processes on the surface; (1) oxidation of the sulphur to SO_2, and (2) oxidation of the nickel to nickel oxide. At low oxygen

pressures sulphur is oxidized to SO_2 and removed, with formation of a monolayer of nickel oxide at a slow rate. At higher oxygen pressures formation of nickel oxide is faster, and the rapid growth of nickel oxide buries the sulphide. Sulphur removal by SO_2 conversion does not occur.

Using properties of bulk compounds Chughtal and Riter (76) modelled the oxidation with O_2 and reduction with H_2 of sulphur poisoned nickel catalysts. The heterogeneous phase and chemical equilbria were determined at atmospheric pressure and temperatures between 300K-1100K. The results for the oxidation of Ni_3S_2 showed that for oxygen rich gas phase all the Ni_3S_2 is converted to $NiSO_4$ and NiO; for oxygen poor gas phase the Ni is oxidized to NiO first, leaving the Ni_3S_2 unchanged; after all the Ni had been oxidized then O_2 attacked Ni_3S_2. H_2 treatment after oxidation reduces NiO to Ni but $NiSO_4$ only to Ni_3S_2 until a large excess of H_2 is present. That is the Ni_3S_2 compound at all temperatures was more stable to oxidation with O_2 than was metallic nickel and more stable to reduction with H_2 than NiO. They also found that direct reduction of Ni_3S_2 by H_2 was thermodynamically possible; and concluded that the combination oxidation/reduction was slightly wasteful because of the necessity of carrying the unsulphided nickel through all the treatment with loss of surface area.

The methanation reaction mixture CO/H_2 has been tried as a regenerative agent (4,8,9). Dalla Betta et al. (4) could recover up to 12% of the methanation activity after H_2S (10ppm) was removed from a CO/H_2 reaction mixture at 673K. However at 523K the catalyst lost all of its remaining activity after the poison was removed. Bartholomew

and co-workers (8,9) did not have any success. Indeed upon increasing the temperature from 525K to 695K after the H_2S had been removed the rate of deactivation increased rapidly and complete loss of activity was obtained within a few minutes, caused probably by a restructuring of the surface at the higher temperature as in the case of hydrogen explained before.

2.7.2 Effect of temperature and pressure

Using H_2 to regenerate sulphided beds Richardson (51) reported that as the temperature is increased the "regeneration" rate increases. At 650K the regeneration, measured by magnetic methods as the percentage of nickel reduced, was very slow, whereas at 1033K complete reduction could be obtained in about 20 hours. However the regenerated catalyst bed could only be used for guard chamber applications since no catalytic activity was recovered.

Oxygen treatment of sulphided Ni catalysts has been proved to be pressure and temperature dependent. At low oxygen pressures typical of high vacuum systems ($\sim 10^{-6}$ - 10^{-7} torr) and room temperature sulphur was removed from Ni surfaces as SO_2 leaving a surface layer of nickel oxide which grows over the remnant sulphur and buried it (74,75); at higher temperatures, 673K, no sulphur burial was observed. At higher oxygen pressures, near atmospheric, the growth of nickel oxide over sulphur was observed at room temperature up to 800K (77). This result agrees with the thermodynamic modelling of oxygen regeneration of bulk sulphides in that the nickel oxide formation is favoured over the sulphur oxidation at atmospheric pressure and temperatures in the region 300K-1100K (76).

The results of Rostrup-Nielsen (78) for regeneration with steam

show that the process is affected by temperature and steam partial pressure. Sulphur removal increased from about 40% at 773K to ~90% at 973K-1073K. At 973K it was shown that below a H_2O/H_2 ratio of 200-250 regeneration was constant at ~35%, above that H_2O/H_2 ratio the sulphur removal increased sharply to about 85% at a value of H_2O/H_2 = 400. At those high temperatures (~1000K) however the treatment with steam is expected to promote sintering of the catalysts.

In summary, regeneration of sulphided catalysts is therefore a process influenced by temperature and partial pressure of the regenerative agent. H_2 has not proved to be suitable for regeneration since the catalytic activities are not recovered, and indeed could be lost completely. Regenerated Ni beds are suitable only for H_2S readsorption despite having the same magnetic properties as clean samples.

Oxidation of sulphided samples has to be performed carefully to be successful. Too low the oxygen pressure the sulphur removal is very slow, but high oxygen pressures may bring about oxidation of nickel without considerable sulphur oxidation. The regeneration is favoured by high temperatures (~700K), but too high could be damaging. The results until now have been modestly successful.

It seems that steam treatment of poisoned catalysts can remove large amounts of sulphur. The partial pressure of steam (H_2O/H ratio) has to be high and the temperature around 1000K, although, sintering may result at these conditions. Besides no results of catalytic activity after this treatment are available.

2.8 Adsorption of Sulphur on the Support

Few studies are available on the adsorption of sulphur compounds on support materials. It has normally been assumed that either the amount adsorbed is zero or negligible compared to the metallic component of the catalyst.

DeRosset et al. (79) studied the adsorption of H_2S on alumina at low coverages and temperatures of 533K - 833K. The alumina samples pretreated with H_2 at either 773K or 853K showed saturation coverages of 39-107μmol H_2S/gAl_2O_3 with an apparent decrease in saturation amount as the temperature was increased. Aluminas pretreated at 773K exhibited a heat of adsorption of -104kJ/mole over the coverage range θ between 0.3 and 0.7; whereas the 853K pretreated aluminas gave heats of adsorption of -125 to -158 kJ/mole which varied with coverage. Entropies of adsorption were around -109 J/moleK.

The results of Glass and Ross (80) compare resonably well with those of deRosset et al. Besides H_2S they studied the adsorption of other sulphur-containing compounds at 423K on γ-alumina. The adsorption capacity of γ-alumina for H_2S is small when compared to the adsorbed amounts of methanethiol, ethanethiol and dimethylsulphide (see Table 2.6 below). At low coverges the heat of adsorption decreased as the coverage increased reaching a constant value at high coverages ($\theta > 0.5$). Desorption experiments showed that H_2S could not be desorbed completely from the sample, whereas the adsorption was reversible with the other three gases.

Table 2.6 Adsorption Characteristics of Sulphur Compounds Adsorbed on γ-alumina at 423K. (80)

Adsorbate	'Limiting' heat[a] of adsorption, ΔH kJ mol^{-1}	Amount adsorbed at 20 kPa; μmol m^{-2}	Δ S[b] $Jmol^{-1}K$
H_2S	-67	0.37	41.8
Methanethiol	-69	1.20	72.4
Ethanethiol	-77	1.51	107.5
Dimethyl Sulphide	-86.6	1.72	123.4

[a] Measured at 1.40 μmol m^{-2}; at 0.41 μmol m^{-2} for H_2S

[b] Measured at 0.120 μmol m^{-2}; at 0.41 μmol m^{-2} for H_2S

The increase in the heat of adsorption with increasing methylation of the adsorbate was explained as an effect of the increasing base strengths of the compounds in the order

$$(CH_3)_2S > C_2H_5SH > CH_3SH > H_2S$$

which would increase the ability to form bonds with an electron acceptor.

The same trends were observed for silica gel (81), although the heats of adsorption are higher on γ-alumina. This feature might be explained by the greater acidity of the hydroxyl hydrogens on alumina which would give rise to stronger hydrogen bonds on association with

electron donor molecules (80). Rostrup-Nielsen (78) however reported that the sulphur uptake of magnesium aluminum spinel and α-alumina was increased with the addition of alkali and alkaline earth promoters (Na, K, Ca, Mg), which decreased the acidity of the supports.

The sulphur uptake on alumina represented about 4% of that adsorbed on 3% Ni/Al_2O_3 using H_2S concentrations of 25ppm at 723K (32); but it was negligible at 653K-663K in the H_2S range of 13-100ppb (15). At lower temperatures (500K) the amount of H_2S adsorbed on Al_2O_3 was found to be quite significant compared to that on the metal (11) at H_2S concentrations of 0.5-10ppm.

IR results (48) showed the existence of hydrogen bonding interactions between isolated hyroxyl groups on silica and adsorbed H_2S, n-propylmercaptan, dimethylsulphide and thiophene molecules. Chemisorption of n-propylmercaptan and dimethylsulphide involved primarily reaction of adsorbate molecules with strained siloxane bridges in the oxide surface:

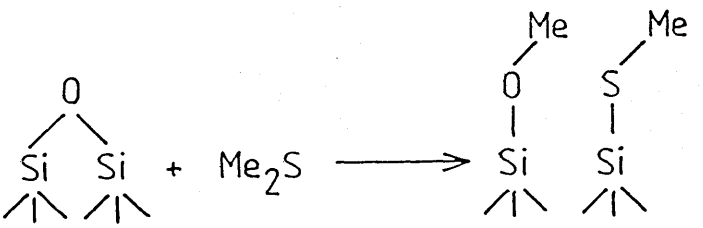

Thiophene was slowly chemisorbed to give surface species, the formation of which involved slow exchange of hydrogen atoms between thiophene molecules and surface hydroxyl groups. Thiophene was assumed to adsorb onto silica to form a polymer-like aggregate of thiophene molecules which are weakly bonded to the surface and to adjacent adsorbed molecules. These polymerization reactions have been detected on acid

catalysts including silica-alumina, and a trimer and pentamer have been characterized (48,82).

Upon evacuation of the IR cell mass spectroscopic analysis showed that thiophene was the major desorption product, but not all the thiophene was desorbed (48).

2.9 Summary

Some remarks can be drawn from available data on the poisoning effect of sulphur-containing compounds on Nickel catalysts:

i) Sulphur compounds adsorb dissociatively on nickel catalysts

ii) Concentrations as low as 13ppb H_2S are needed to saturate and poison nickel surfaces

iii) saturation coverages involve 2 nickel atoms per sulphur atom adsorbed ($\theta_s = 0.5$). Higher sulphur coverages may involve surface reconstruction.

iv) Surface sulphur-nickel compounds are more stable than bulk nickel sulphides.

v) At low temperatures thiophene seems to be adsorbed flat occupying five nickel sites, at higher temperatures it undergoes decomposition leaving sulphur adsorbed and gaseous products.

vi) Sulphur poisons effectively nickel catalysts reducing in 2-3 orders of magnitude the activity for methanation and changing the selectivity towards higher hydrocarbons.

vii) Catalyst supports adsorb H_2S, but at reaction temperatures above 400K the amount adsorbed represents only about 4% of the total.

viii) The few studies at high pressure have been performed with

heat and mass transfer limitations that have masked the results.

Notwithstanding the advances in the understanding of the poisoning effects of sulphur on nickel (and other metallic) catalysts there are still several points that need attention:

- the mechanism and kinetis of adsorption of sulphur-containing compounds such as mercaptans, sulphides, cyclic compounds; the effect of temperature and concentration over a wide range of conditions;
- the effect of sulphur on carbon deposition and the nature of that deposit;
- the extent of the pressure effects on the adsorption of sulphur on nickel, and on the activity and selectivity of catalysts under reaction conditions free of transport limitations;
- the regeneration of poisoned catalysts, conditions and regenerating agent to use, and mechanism and kinetics of the process.

Some of these points were studied in the course of this work and the conclusions provide some insight into the complex process of poisoning by sulphur.

C H A P T E R 3

CHARACTERIZATION OF CATALYSTS

The performance of a catalyst in a chemical process, the extent of the reaction involved, the life of the catalyst and changes in the reaction pattern are related to properties such as total surface area, the metal or active area, the size of the pores and its distribution. These properties are of major importance since catalytic rates of reaction depend on available active surface, whereas pore strucutre affects surface access, surface stability and resistance to poisoning and selectivity as well as heat transfer. In summary, the catalyst has to be characterised to gain information on its potential sorption sites, dispersion and porosity characteristics.

The importance of the characterisation of Ni/Al_2O_3 catalysts subject to poisoning by sulphur rests on the nature of the adsorption process. The low concentration needed to poison the catalysts and the high stability of the surface nickel bond may favour the progressive "core" or "pore mouth" poisoning; in these circumstances an evaluation of the internal mass transfer as the poisoning increases becomes necessary, and can be obtained knowing the mean pore radius and pore size distribution. The extent of the sulphur adsorption and the effectiveness of the regeneration can be evaluated through the measurement of the active metal area of the fresh and sulphur treated catalysts.

The surface area and pore size distribution are determined by

using physisoprtion measurements. The interpretation of physisorption data is not always straightforward, and a considerable amount of research has shown that its computation is justified only if certain conditions are fulfilled (10). Physisorption occurs whenever a gas is brought about into contact with an outgassed solid. The phenomenon is thus a general one, unlike chemisorption which is specific and which is used to determine the metal or active area of a catalyst. In this case an adsorption selectivity is required.

The principles of these techniques, the current practice and difficulties that may arise are described and briefly discussed in this Chapter.

3.1 Experimental Methods

For the determination of adsorption isotherms there are basically three types of methods: volumetric, gravimetric and dynamic methods. The most widely used being the volumetric method.

3.1.1 Volumetric method

In this method successive charges of gas from a volumetric measuring device are admitted to an adsorbent and the changes in equilibrium pressure in the dead space monitored. The amount of gas adsorbed is determined by taking the difference between the amount of gas dosed into the volume containing the sample and the amount retained in the dead space. The volume of the dead space must be known accurately, and is usually measured using helium (83,84). A simple design is shown in Figure 3.1

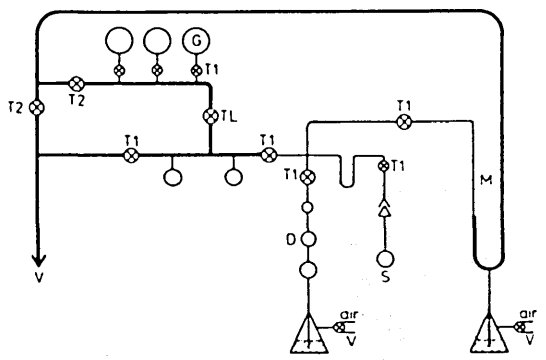

D: gas doser
G: glass bulb
M: manometer
S: sample
T1,T2: taps
TL: leak valve
V: vacuum

Figure 3.1 A Simple Apparatus for the Volumetric Determination of Adsorption of Gases (84)

In assessing the sources of error two points should be emphasised:

First, the errors in the measured doses are cumulative, and second, the amount remaining unadsorbed in the dead space becomes more and more important as the pressure increases.

The accuracy with which the gas uptake is measured deteriorates with decreasing sample surface area. For small area samples the problem is overcome by using an adsorbate gas which has a lower vapour pressure (P_o), reducing the equilibrium gas pressure over the sample. Xenon or Krypton are recommended for this purpose.

A number of improvements can be made to the simple volumetric apparatus for the determination of isotherms on solids of low area or of small samples of high area adsorbents; they can be found elsewhere (84,85).

Computer-controlled systems already exist to obtain higher speed and convenience in routine measurements, but they are of considerable instrumental complexity (86,87).

Simplified designs of volumetric apparatus for routinary fast measurements have been developed (88). Usually they are aimed at the determination of one or few points on the isotherms. Surface area values obtained by single point evaluations lie about 10% below the values obtained with multiple measurements and have a reproducibility of 1% (85).

3.1.2 Gravimetric method

In this method the sample is suspended on one sidearm of an ultransensitive microbalance, the uptake of gas is observed by following the change in weight of the sample. The cumbersome dead space calculation performed in the volumetric method is entirely avoided but a buoyancy correction is required. This method has the advantage over volumetric methods that the sensitivity is not diminished at high pressures.

There are two main types of adsorption balance: the coil spring balance and the beam-torsion balance.

In a beam-torsion (beam) balance a light rigid beam is centrally supported on a fibre of circular or ribbon cross-section. In the usual design the sample is suspended from one arm of the beam and a counterweight from the other. There are however commercial designs (from Mettler Co.) in which the suspended counterweight is eliminated (84,89).

Figure 3.2 shows a simple beam microbalance.

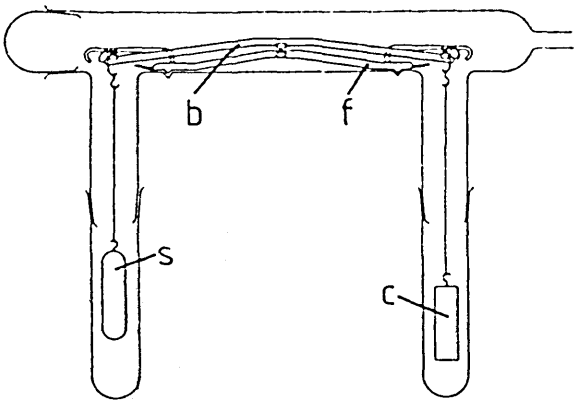

Figure 3.2 A Simple Microbalance (83)

s: sample, c: counterweight, b: beam, f: framework.

The microbalance may be used either in a deflection or null mode: the latter is usually achieved by using magnetic coupling; the magnitude of magnetic field applied being related to the weight change provides a means for recording. With the deflection operation the mass changes that can be monitored are limited to the free swing of the beam which restricts the range of the instrument. The null mode is thus preferred over the deflection one. The position of the beam may be detected by capacitance, inductive or photoelectric methods. Photoelectric method is preferred when the vacuum properties of the system are to be optimized (84,90). Calibration is normally effected by using standard weights.

The coil-spring balance consists of a helical spring, usually of fused silica, freely suspended from a hook inside a glass tube, with a bucket containing the sample attached to a hook at the lower end. The mass change is followed by measuring the extension of the spring by means of a good cathetometer. A typical arrangement for a spring balance is given below.

Spring balances suffer the disadvantage that their sensitivity is inversely proportional to their maximum load.

Another type of microbalance which should be mentioned is the quartz crystal resonator which can be used in adsorption work in certain circumstances. It has been developed as a result of recent trends in thin-film research. Despite an inherently high sensitivity for mass changes ($\sim 10^{-12}$g) the technique is fairly restricted in its applicability to evaporated metal films.

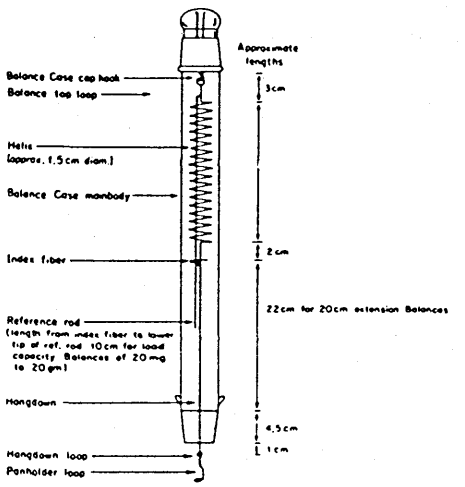

Figure 3.3 Typical Spring Balance (89)

Overall the beam balance is the most reliable of the gravimetric instruments. It is less susceptible to vibration than the spring balance, the sensitivity is less dependent on the load capacity, partial compensation for gas buoyancy is possible, and in a null mode the position of the sample is invariant, a feature which may be important if simultaneous examination of the specimen is being made.

The measurements in a microbalance can be affected by undesirable disturbances which produce spurious mass changes. Among them are: gas buoyancy, thermal transpiration and static electricity.

To correct gas buoyancy the usual procedure is to assess the effect directly and allow for it in the calculations of weight adsorbed (91).

In a beam balance compensation for gas buoyancy can be attempted by making the real volumes of the sample and counterweight equal, provided the real volume of the displaced gas is known.

Buoyancy corrections can not be made on measurements taken with coiled-spring balances, and are not usually necessary in the type of experiments that utilise these less sensitive instruments; however buoyancy effects can become significant at high pressures for the more sensitive spirals.

In Figure 3.4 the effect of buoyancy on the apparent weight of the sample in a beam balance is shown.

The effects of thermal transpiration and convection of the gas arise from temperature gradients in the suspension system. The importance of these effects is dependent on the pressure in the system.

Thermomolecular flow of gases cause spurious forces in the pressure range of 10^{-2} to 300Pa (92). These forces may be minimized by employing identical suspension fibres, hang down tubes, and temperature gradients about an identical sample and counterweight. In practice it is difficult to obtain ideal compensation, but if all variables remain the same, it is reproducible and may be corrected for.

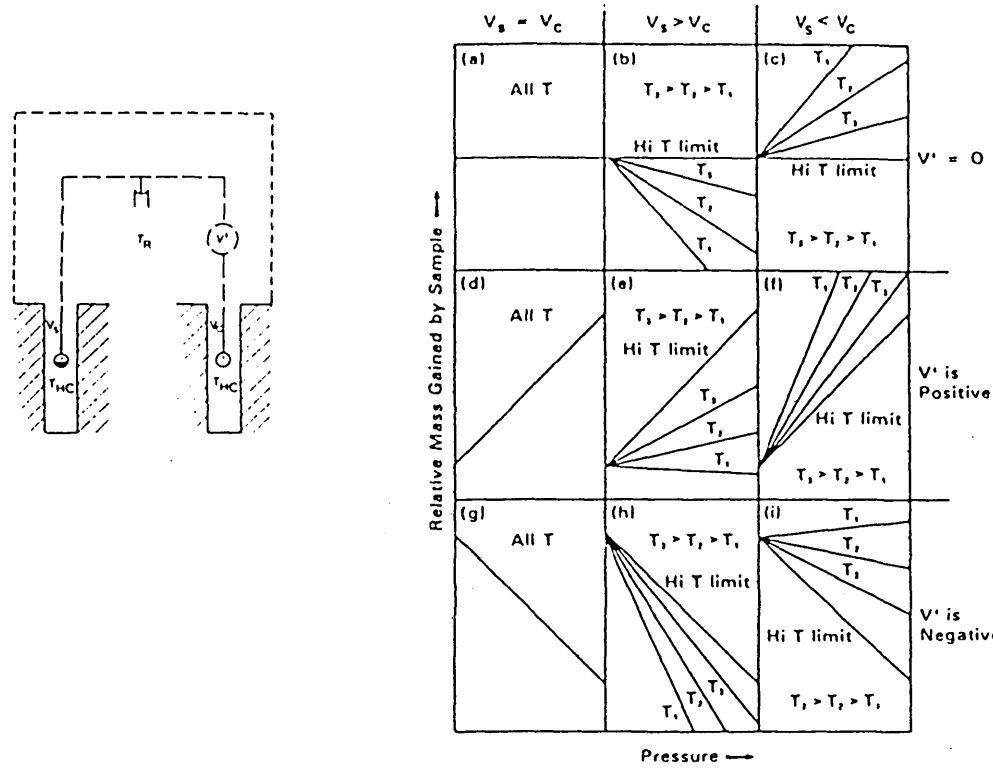

Figure 3.4 Effect of Buoyancy on the Apparent Mass Gained by Sample (After Czanderna (92))

Convection currents may become a serious problem at pressures exceeding 15 to 45 kPa, and produce continuous oscillations of an undamped balance. The use of baffles and damping become necessary to minimize the effect.

Disturbances that arise from static electricity may be avoided by using grounded conductive coatings on the balance housing and hang down tubes.

Table 3.1 gives some characteristics of the most common microbalances.

3.1.3 Dynamic methods

The adsorption of gases on solids can be studied making use of the advantages provided by the gas chromatographic methods. Techniques involving the continuous addition of adsorbate onto a solid adsorbate have been developed.

A widely used procedure, developed by Nelsen and Eggersten (93), is as follows: a known mixture of nitrogen and helium is passed through a bed of the solid sample, and the composition of the effluent is monitored by a thermal conductivity detector connected to a recorder (Figure 3.5). When the sample is cooled in liquid nitrogen, the adsorption of nitrogen is indicated by a peak on the recorder. After equilibrium is established at the particular partial pressure used, the recorder pen returns to its original position. The sample tube is allowed to warm by removing the liquid nitrogen bath, and the desorbed nitrogen produces another peak on the recorder. The area under each peak is proportional to the amount of nitrogen adsorbed or desorbed. Normally only the desorption peaks are used since they are relatively free of tailing which is sometimes observed during the adsorption stage. Figure 3.6 gives a schematic diagram of the response.

Table 3.1 Properties and Characteristics of Spring and Beam Microbalances (Adapted from Czanderna (92))

	Balance Type	
Consideration	SPRING	BEAM
Response to small Change in Mass	Stretching of a Spring	Rotation of beam at Primary Fulcrum
Capacity	Variable depending on helix size	Up to 25g
Range of Load to Precision Ratio (LPR)	10^4 to 10^6	$2x10^8$ or less
Typical Operation: manual automatic Usual calibration Method	Optical lever for vertical displacement P,T,C. Standard weights	Optical lever; torsion head P,T,C. Buoyancy Standard Weights
Range	Variable; limited by size of helix; 1 to 10mg	Deflection:0.01 to 1mg automatic:over 10mg
Virtues	Simple in design, operation and for incorporation into a vacuum system; readily outgassed	Large LPR; simple symmetrical design; versatile; adaptable to vacuum and ultra-high vacuum excellent sensibility over extended pressures and temperatures, can be operated using manual or automatic null techniques; large range, superior zero point stability
Disadvantages	Total load must be weighed to the full accuracy of the helix; limited LPR and range; susceptible to vibrations, especially in vacuum, must be thermostated to achieve-precision $\leq$ 1 μg; fragile	Thermostating may be needed; limited range on use as a deflection instrument; requires manual skills to build, costly jigs are almost essential, zero shifts may result from beam banging arrest or from lateral impacts on balance support stand

P: Photo electric; T: transducer; C: capacitance

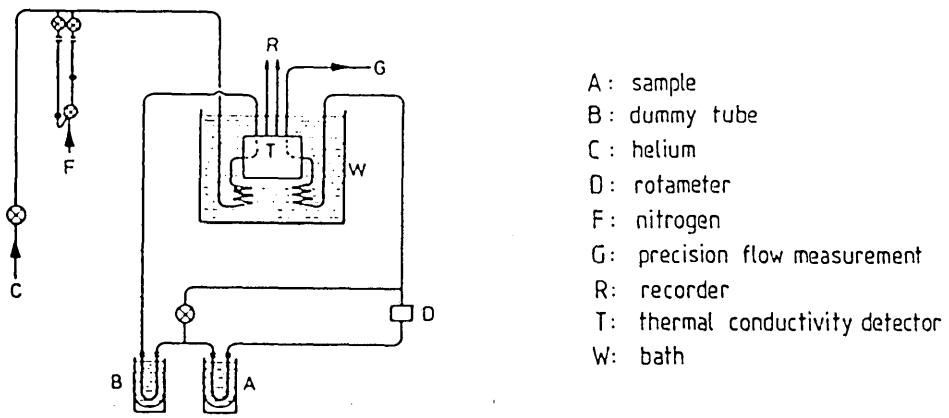

Figure 3.5 Flow Apparatus for the adsorption of N_2 from a N_2/He Stream (Ref. 93)

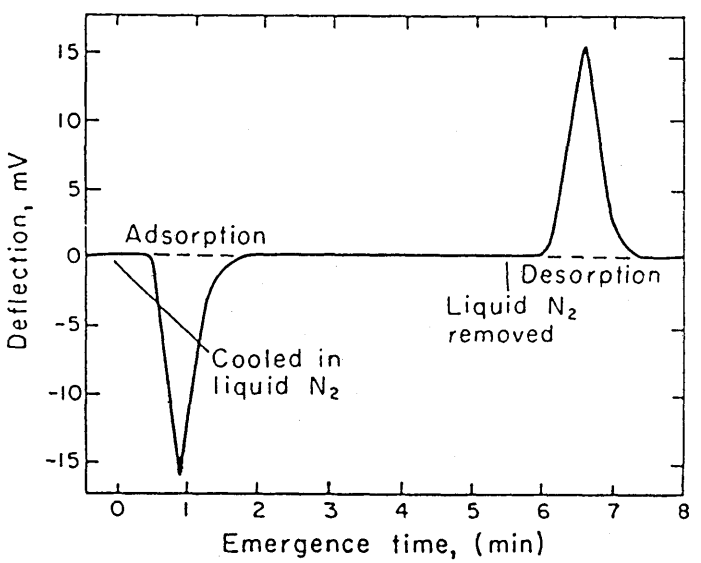

Figure 3.6 Adsorption-Desorption Peaks for N_2 Obtained with the Continuous Flow Method (83)

Values of the surface area are obtained within about 2% of those from conventional BET methods.

With small modifications the procedure can be adapted for the measurement of chemisorption of gases.

The advantages of the dynamic method include fast one point surface area analysis, small sample requirement, good reproducibility (~±2%) and rugged non-glass construction (85).

The sources of error including effects of ambient temperature and pressure changes, lack of completely linear response, changes in flow rate at high partial pressures, effects of H_2O vapour can be minimized with care.

The description of improvements and variations of this method can be found elsewhere (83,84,94).

In conclusion it can be stated that all three of the methods outlined above are able to give reliable determinations of adsorption-desorption isotherms. The selection of a particular method in preference to the others will depend finally upon the accuracy desired. For an accurate determination static methods are to be preferred, and in principle the gravimetric method is more accurate than the volumetric method (95).

3.2 Total Surface Area and Pore Size Distribution

The measurement of the total surface area of a sample is observed by measuring the non specific physical adsorption. This is the adsorption in which the forces involved between the adsorbent and the adsorbate are intermolecular forces of the van der Waals type. These are the same forces that are responsible for deviation from ideality of real gases and the condensation of vapours. The adsorption phenomenon is strongly dependent on the physical properties of the solid and in particular on its porous texture (95). The adsorbate must be as chemically inert as possible. The most commonly used adsorbates are nitrogen, argon and krypton.

The adsorption isotherm relates the amount of substance adsorbed

at equilibrium to adsorbate pressure in the gas phase, at constant temperature. The majority of physisorption isotherms may be grouped into the six types (96) shown in figure 3.7. The isotherms types I- V are those given in the original classification of Brunauer et al. (97) called Brunauer classification. Type I isotherms are characterisitc of microporous adsorbents, and are fitted by the Langmuir equation. Isotherms of types II and III are characteristic of unrestricted monolayer multilayer adorption on non-porous or macroporous solids. Type II isotherms occur frequently, but type III corresponding to very weak adsorbent-adsorbate interactions are not common. Type IV and V isotherms are obtained with mesoporous solids. Type IV in their initial part resemble type II isotherms, and are widespread. Type V are related to type III isotherms in that they represent weak adsorbent-adsorbate interaction and are seldom encountered.

Type VI isotherms occur as a result of stepwise multilayer adsorption on uniform surfaces. Lateral interactions between the adsorbed molecules contribute to the layer by layer process. These isotherms are comparatively rare.

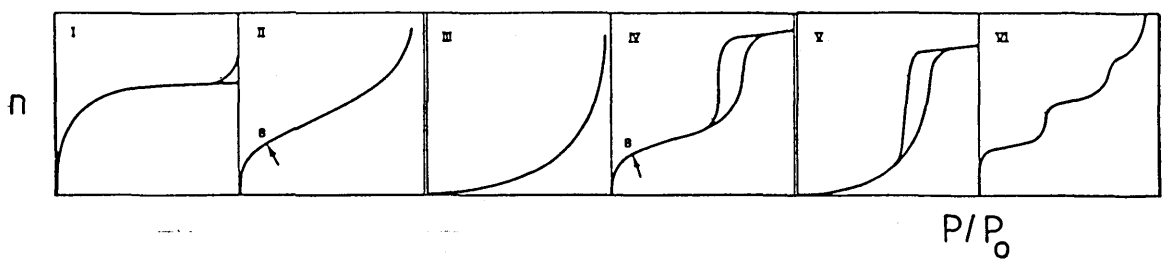

Figure 3.7 Types of Physisorption Isotherms (102)

3.2.1 Determination of surface area

In the analysis of isotherm data, two different methods of approach have been used:

1) application of mathematical relationships based on a simple model or obtained empirically, such as BET, Kelvin and DR equations; and
2) Comparison of the isotherms with standard isotherms obtained with selected non-porous reference materials.

The method most frequently used is the BET (Brunauer-Emmett-Teller) method. The BET theory extends the Langmuir model to multilayer adsorption.

The BET equation is:

$$n = \frac{n_m CP}{(P_o - P)\left[1+(C-1)P/P_o\right]} \qquad (3.1)$$

where:

n: amount of gas adsorbed at an equilibrium pressure p

P_o: vapour pressure of the adsorbate in the condensed state at the adsorption temperature

n_m: monolayer capacity

C: constant related to the heat of adsorption into the first layer

and may be re-written:

$$\frac{P}{n(P_o - p)} = \frac{1}{n_m C} + \frac{C-1}{n_m C}\ P/P_o \qquad (3.2)$$

which gives a linear relationship between $P/n(P_o-P)$ and P/P_o, and from which the values of C and n_m are obtained.

The constant C, characteristic of the intensity of the adsorbate-adsorbent interactions, determines the shape of the isotherm. The stronger the adsorbate-adsorbent interaction, the higher the C value, the more the isotherm tends towards type II; the lower the C value the more the isotherm tends towards type III, when the latter case occurs the validity of n_m is questionable.

For the calculation of the surface area one makes use of the relation:

$$A = a_m \, n_m \, N_a \qquad (3.3)$$

where:

a_m: effective area of the adsorbate molecule in the monolayer

N_a: Avogadro's number

In the case of nitrogen adsorption at liquid nitrogen temperature (77K), the most widely admitted value of a_m is 16.2×10^{-20} m^2.

It should be noted that a_m is often somewhat dependent on the nature of the adsorbent, and a range of possible values exists for each adsorptive (84).

In the application of the BET method one should work within the linear region of the isotherm, usually in the P/P_o range of 0.05-0.30. If the nitrogen C values are outside the approximate range 80-120, care should be taken in the interpretation of the BET area.

If point B is well defined it can be identified with the completion of the monolayer; and close agreement obtained between the value of n_m and the amount adsorbed at point B helps to confirm the validity of n_m.

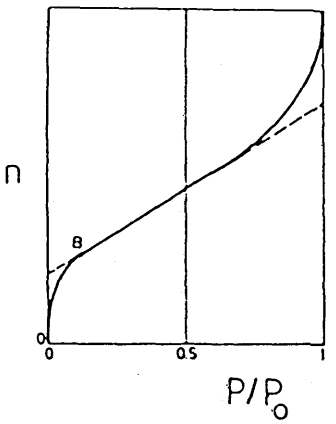

Figure 3.8 Location of Point B of an Isotherm

Comparison methods are based on the existence of a standard isotherm for non-porous materials with which the measured isotherm is compared. Because isotherm equations covering the whole range of relative pressure are not available, experimentally obtained averaged curves valid for a group of materials are used, and they are called standard isotherms. Discrepancies appear between the different versions of standard isotherms. These discrepancies may occur from the fact that the various solids are not necessarily free of pores, and that the strength of interaction of a given adsorbate with the adsorbent varies from one adsorbent to another.

In the t-method the adsorbed amount is transformed into the layer thickness t which is a function of the relative pressure

$$t = f(P/P_o)$$

According to de Boer (98), the thickness t is nearly independent of the nature of the adsorbent if the latter is non-porous. The method requires the comparison of the nitrogen adsorption isotherm obtained

for a given porous solid with a particular reduced form of a standard isotherm (the t curve) corresponding to a non-porous solid of the standard. The amount adsorbed on the sample at different pressures is plotted versus t determined at the same pressures on the standard. The plot gives a straight line if the two materials have a similar surface structure. The slope is a measure of the ratio of the surface area of the sample to that of the standard. The surface area of the sample is calculated by:

$$A(m^2) = 1.24 \frac{dn}{dt} \qquad (3.4)$$

when using nitrogen as adsorbate at 77K.n is given in mg. t in n_m.

The t method depends strongly on the BET method because the monolayer capacity from which the layer thickness is calculated is determined by the BET formalism. It depends strongly on the validity of the standard isotherm for a given temperature which can not be used for another group of materials or for another adsorbate. For such another system the reliable standard isotherm has to be chosen first (99).

Sing (100) modified the t method by replacing the thickness t by the ratio $\alpha_s = n/n_s$ where n_s is the amount adsorbed by a non-porous reference solid at a selected relative pressure. α_s could be set equal to unity at any convenient point on the standard isotherm. It is usually convenient to set $\alpha_s = 1$ at $P/P_o = 0.4$ since monolayer coverage and micropore filling occur at $P/P_o < 0.4$ whereas capillary condensation takes place at $P/P_o > 0.4$; besides at this relative pressure many isotherms coincide in a better way than if it is normalized at the BET monolayer capacity. The n-vs-α_s plot is constructed, with shape

essentially the same as those of the n-t plots. The α_s method also needs relevant standard isotherms normalized to a specific surface area determined by another method.

Another method based on the use of standard isotherms is the n* method proposed by Lecloux (95,101). He pointed out that the thickness of the adsorbed layer not only depends on the relative pressure, but also on the magnitude of the adsorbent-adsorbate interactions. A set of 5 standard isotherms belonging to 5 different ranges of C_{BET} was produced. These isotherms are n^*_1, for $C_{BET} > 300$; n^*_2 for $300 > C_{BET} > 100$ n^*_3 for $100 > C_{BET} > 40$; n^*_4 for $40 > C_{BET} > 30$; and n^*_5 for $30 > C_{BET} > 20$. Above $P/P_o = 0.4$ the standard isotherms have the same value. A plot of n-vs-n* is made using the appropriate standard isotherm from the value of C obtained by the BET equation. When the correct isotherm is used the plot gives a linear relationship at low relative pressures which should pass through the origin. The surface area is calculated with the slop of the linear part of the plot using:

$$A = 3.496 \frac{dn}{dn^*} \quad (m^2/g) \qquad (3.5)$$

where n is given in mg/g, and n* in nm.

The correct standard isotherm should be chosen to get the straight line to pass through the origin and to obtain the correct slope value; otherwise the straight line cuts the n axis at a positive or negative value according to whether the C_{BET} constant of the test isotherm has a higher or a lower value than the C_{BET} value of the standard isotherm used.

The use of standard isotherms to characterise solids is subject to the same limitations as the BET model, for all the methods have been

demonstrated to be directly or indirectly related to the BET theory.

3.2.2 Pore Size Distribution (PSD)

The transport processes that occur indside a catalyst pellet, and the effectiveness of the internal surface area depend upon the void volume and the size of the pores. It is desirable, thus, to assess the porous structure of a determined catalyst.

The pore systems of solids are of many different kinds. Individual pores vary greatly both in size and shape within a given solid, and between one solid and another. A convenient classification of pores according to their average width - the diameter of a cyclindrical pore - and adopted by IUPAC is given below (102):

Table 3.2 Classification of Pores According to their Width

	Width
Micropores	< 2nm
Mesopores	between 2nm and 50nm
Macropores	>50nm

The basis of the classification is that each of the size ranges corresponds to characteristic adsorption effects as manifested in the isotherm. In micropores the interaction potential is significantly higher than in wider pores owing to the proximity of the walls and the amount adsorbed is correspondingly enhanced. In mesopores capillary condensation, with its characteristic hysteresis loop, takes place. In the macropore range the pores are so wide that it is virtually

impossible to map out the isotherm in detail because the relative pressures are close to unity.

There are a number of experimental methods for studying pore structure, but the two most important are: gas physical adsorption isotherm data and mercury porosimetry.

The effect of the pore structure on multilayer adsorption is to convert an isotherm which would otherwise be BET type II into type IV, or a type III into type V. This occurs because the finite pore width places a limit on the extent of multilayer formation before the pore becomes filled with liquid-like condensate, and this will occur with the formation of a highly curved miniscus which results in a depression of the liquid vapour pressure below its normal value. Adsorption-desorption hysteresis also happens because pores are filled and emptied by different processes: emptying occurs by evaporation from the liquid miniscus which retreats down the pore in the process. The shape of the hysteresis loop contains information about pore shape. Loop shapes have been classified by deBoer (103) and are presented in figure 3.9 with a modification on the type B at the high pressure end by Gregg and Sing (102). The various pore shapes corresponding to the loop shapes are drawn below each graph.

In practice types C and D hardly ever occur.

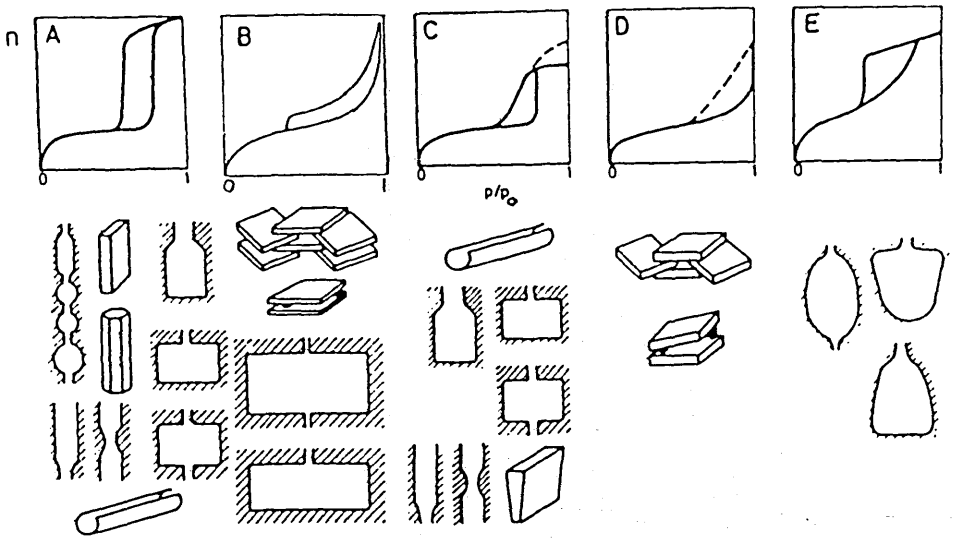

Figure 3.9 The Hysteresis Loops and the Associated Pore Shapes (99)

When using adsorption-desorption isotherms to calculate PSD one must remember that mesopore filling occurs by the process of capillary condensation. This process appears after the monolayer-multilayer coverage on the pore walls has happened. The region of the isotherm involved is the hysteresis loop.

The mesopore size is usually calculated with the aid of the Kelvin equation:

$$\ln(P/P_o) = - \frac{2V_L \gamma \cos \phi}{r_k R T} \qquad (3.6)$$

Where: P/P_o : relative pressure

r_k : radius of a hemispherical meniscus

γ : surface tension of the condensed liquid

V_L : molar volume of the condensed liquid

ϕ : contact angle between the condensate and the adsorbed film on the walls, normally taken equal to zero.

When this equation is applied to porous solids it is necessary to assume that r_k is dependent on the dimensions of the pore. For a simple cylindrical pore shape, the most widely used, the pore radius r_p is given by the relation:

$$r_p = r_k + t \qquad (3.7)$$

where t is the multilayer thickness.

Another simple model used is that of a cylindrical meniscus in a slit-shaped pore. If the slit is parallel-sided, its width dp is given by:

$$dp = \frac{-2\gamma V_L}{RTln(P/P_o)} + 2t \qquad (3.8)$$

Other pore shapes, like 'ink-bottle' or packed spheres may be postulated but it is strictly the meniscus shape and curvature which determines the P/P_o at which the capillary condensate is in equilibrium with the vapour.

A number of procedures have been developed for the calculation of PSD. All of them are tedious and require attention to detail, and at some stage involve the assumption of pore model.

The procedures are based on an imaginary emptying of the pores by the step-wise lowering of relative pressure, from the point at which the mesopore system is taken as being filled; a relative pressure of

$0.95P_o$ is frequently adopted as starting point.

It is more convenient to divide the desorption process into a number of standard steps in either P/P_o or pore radius, rather than the use of the consecutive points on the experimental isotherm.

Several methods have been devised for the calculation of the PSD and the incorporation of the correction due to thinning of the adsorbed film; a detailed description can be found elsewhere (102).

The calculation of PSD involves several assumptions on the model of pore, correction of the thickness and to whether the adsorption or desorption branch should be used. The pore models employed for the calculation of PSD's include: cylindrical, parallel slits, packed-spheres and "modelless".

The cylindrical model is the conventional and most widely used due to its simplicity; parallel-slits renders a simpler calculation method; the packed-spheres model attracts attention because of its relevance to actual solids as found by electron microscopy (104,105) but its implementation is highly complicated if all the possible processes involved are considered (105); "modelless" method of Brunauer, Mikhail and Bodor (106) which is a model that tries to eliminate the dependence on a physical model by using an hydraulic radius rather than the Kelvin radius, but in the end falls into any of the previous models during the conversion of the modelless core distribution curve to pore size distribution. The calculations involved in the last two methods are rather cumbersome and produce no advantage over the more conventional models. This was demonstrated by Dollimore and Heal (105) and Havard and Wilson (104). The pore size distribution curves given by the cylindrical model were hardly different from the most complicated packed sphere model (105) or the modelless method when corrected to

cylindrical geometry (104).

It can be concluded that the use of more complicated models, such as the packed-sphere or the modelless is not justified when the results obtained by simpler models are the same, and the calculations involved are more difficult and more time-consuming.

The effect of the method used for the evaluation of t on the PSD has been studied by Irving and Butt (107) and Dollimore and Heal (108). Irving and Butt questioned the use of the Halsey equation as proposed by Wheeler (109) on the basis that the resulting PSD's were shifted towards pores larger than those obtained using the experimental t values reported by Shull (110).

These conclusions were criticised by Dollimore and Heal (108) since they were arrived at after considering only one sample. A careful study using several samples showed that the best estimations of t, based on the agreement between A_{cum} and A_{BET}, are given by the de Boer's modification of the Halsey equation, and the Shull experimental values modified by the same de Boer's factor. When it comes to many calculations and the use of computerized procedures the modified Halsey equation is recommended. As Havard and Wilson (104) pointed out, it is difficult to justify the use of more complicated methods for calculating t when the approximate nature of the models for the calculation of PSD's is considered.

There has been some debate as to whether to use the adsorption or the desorption branches of the isotherm for the calculation of the PSD. Traditionally there appears to be a preference for the desorption curve on the grounds that it is more likely to represent conditions closer to equilibrium. However evidence is available to demonstrate that both adsorption and desorption branches are irreversible, therefore neither

branch can be used with confidence for the calculation of PSD.

Everett (111) pointed out that in systems where pore blocking can occur, as in hysteresis loops types B and E, PSD curves derived from the desorption branch are likely to give an erroneous picture of the pore structure, showing distributions much narrower than they actually are and strongly biased towards smaller pore sizes. In such cases the adsorption branch is to be preferred.

Mercury Porosimetry

Mercury porosimetry is a technique originally developed to determine pore sites in the mesopore range. Since the contact angle of mercury with solids is more than 90^0, an excess pressure ΔP is required to force liquid into the pores of a solid (102). The relation between the required pressure difference and the pore radius is given by the Washburn equation:

$$r_p = \frac{-2\gamma\cos\phi}{\Delta P} \qquad (3.9)$$

where: r_p : radius of pore assumed to be cylindrical

ΔP : $P_{Hg_l} - P_{Hg_g}$

The contact angle of mercury depends not only on whether the mercury is advancing over or receding from the solid surface, but also on the physical and chemical state of the surface itself. The values reported in the literature lie between 130^0 and 150^0; most workers assume $\phi = 140^0$ as valid for all solids. The uncertainty of the r_p calculated due to this is considerable.

The technique consists essentially measuring the extent of mercury

penetration into an evacuated solid as a function of the applied hydrostatic pressure. The volume v of mercury taken up by the solid is measured as the applied pressure is increased. The pore size distribution curve is obtained by differentiation of the curve of cumulative pore against r_p as in gas adsorption, giving a curve of dv_p/dr_p against r_p.

The total area of the surface of the solid covered by mercury is given by:

$$A = -\frac{1}{\gamma c \cos\phi} \int_o^{P_{max}} p dv \qquad (3.10)$$

Even if P_{max} value is very high, this equation generally leads to an erroneous estimation of the specific surface area of the solid, for the reversible pore filling assumed is rarely found in practice.

Hysteresis is a general feature of mercury porosimetry. The interpretation of this phenomenon is more complex than with capillary condensation, inasmuch as it can depend not only on the pore structure of the solid - presence of ink-bottle pore shape - but also on the magnitude of the applied pressure. Another cause of hysteresis is the change of the contact angle due to the chemical interaction of mercury with the surface to form an amalgam.

Among the possible sources of error in mercury porosimetry are:

a) the assumption of some constant, average value for the contact angle between the mercury and the solid surface. This can lead to errors of as much as 50% in the calculated pore size value if a difference of 20^0 between the chosen and the actual values exists (95).

b) The degree of purity of mercury, for it has an important effect on the surface tension. In extreme cases actual amalgamation can occur.

c) The presence of hysteresis complicates the interpretation of the data.

In spite of its shortcomings this technique constitutes a powerful tool in the assessment of pore structure, especially in the macropore range.

3.3 Measurement of Ni Area

In supported metal catalysts the principal reactive sites are considered to be on the surface of the metal phase. Specialized techniques are required to measure the metal surface areas.

The techniques fall in two categories: those which determine the effective metal particle size distribution such as electron microscopy, light microscopy and x-ray diffraction line broadening, from which the metal area can be calculated; and those which determine the metal surface area directly such as gas chemisorption.

The most frequent method applied to determine the active area of metal catalysts is gas chemisorption. The probe gas should be selectively adsorbed on the metal surface with very little (ideally zero) adsorption on the non-metallic components. Chemisorption unlike physisorption is a process mostly irreversible, with a high heat of adsorption of the order of heats of reaction, and may be activated. Chemisorption requires that the chemical composition of the surface be well defined so that adsorption stoichiometry be also well defined. Chemisorption stoichiometry may be defined as the average number of surface metal atoms associated with the adsorption of each adsorbate molecule, X_m (84).

The application of gas chemisorption for metal area determinations has seen the use of gases such as: H_2, CO, O_2, NO, N_2O, etc., at temperatures ranging from 77K to 770K.

Published results on the chemisorption of H_2 and CO on nikel catalysts have shown the dependence of the adsorption on temperature, pressure, catalyst preparation and pretreatment history. The majority of the works have been performed in static volumetric systems, but results from gravimetric, flow and pulse systems are also available.

3.3.1 Chemisorptive agent

In reviewing the literature on the measurements of Ni metal surface areas before 1975, Farrauto (112) observed that the gases used most often in chemisorption studies were hydrogen, carbon monoxide and oxygen.

Hydrogen is widely used as a quasi-standard component due to its simple interaction with metals.

The adsorption of H_2 on clean polycrystalline specimens of nickel to give saturation coverage is fast with a time scale of the order of a few seconds to a minute at conditions of temperature and pressure used normally for metal area measurements (84).

In a volumetric study on the adsorption of hydrogen on a high purity nickel powder, Pannell et al. (113) confirmed that the stoichiometry of the H-Ni bond is 1:1 irrespective of the temperature of adsorption by comparison of the hydrogen uptake with BET surface areas. The H_2 isotherms were slightly dependent on pressure.

Cremer and Huber (114) found no dependence on pressure when using evaporated nickel films for the adsorption of H_2 at 90K.

On supported specimens however there is always a substantial slow uptake component which has a time scale of the order of minutes to

several hours. This slow adsorption depends on the sample history, type of support and pretreatment. Thus the chemisorption uptake may have two components: the main intrinsic adsorption on the metal and the contribution from physical adsorption or adsorption on the support or both. The intrinsic adsorption on the metal is strong and often called irreversible adsorption whereas the second component is weak and also named reversible adsorption.

Brooks and Christopher (115) in a comparative study on the dispersion of supported Ni catalysts found that for H_2 adsorption the slow contribution to the uptake is appreciable for supported catalysts. On both nickel-alumina and nickel-zeolites the adsorption uptake showed appreciable pressure dependence. Metal areas determined by H_2 chemisorption agreed well with the estimates from x-ray cystallite size, evidence that hydrogen is dissociated on crystallites of sufficient size to afford adjacent adsorption sites, however the samples used were in a narrow range of low dispersion.

Freel et al (116) taking a stoichiometry of 1:1 from the results of Mars et al. (117) studied the chemisorption of H_2 on Raney Nickel, to determine the percentage of metal in terms of total BET area. This fraction of nickel surface decreased with increasing alumina content, from which it was deduced that it was possible for nickel to be blocked by alumina.

In their study of nickel-alumina catalysts Bartholomew and Farranto (118) calculated the catalytic surface area assuming a 1:1 stoichiometry for the H-Ni interaction. They also reported for their catalysts a small contribution from the support to the uptake, indicated by the almost zero slope of the isotherm.

All these assumptions and results for the hydrogen chemisorption

stoichiometry were confirmed in a thorough study by Bartholomew and Pannell (119) on alumina and silica supported nickel. Using nickel loadings varying from 0.5 to 23 wt% in the case of alumina-supported nickel; and 2.7% to 15wt% for silica-supported nickel they confirmed the H-Ni ratio of 1:1, as the good agreement among values of average crystallite diameter estimated from hydrogen chemisorption, x-ray line broadening and transmission electron microscopy indicated that the ratio was indeed unity. Nevertheless, due caution should be taken for loadings below 3% or catalysts on different supports on which the stoichiometry may change due to strong metal-support interactions. Indeed at very low loadings they reported unexpected low uptakes, making the behaviour of the Ni/Al_2O_3 catalysts similar to that observed for titania supported nickel (120).

Using a microbalance for the determination of silica-supported nickel surface area Lohrengel and Baerns (121) reported a strong dependence on pressure for the H_2 adsorption at 296K. This might be caused, they said, either by a change in adsorption stoichiometry, absorption of H_2 or interaction of H_2 with the support.

Following the long established method of using CO chemisorption to determine the area of iron catalysts, Emmett and co-workers (122,123) measured active nickel surface areas by adsorption of CO. Many studies have since tried to assess the chemisorption of carbon monoxide on metal catalysts. The adsorption of carbon monoxide is more complex than the hydrogen adsorption, with strong dependence on pressure, temperature, metal loading and dispersion of the metal.

For nickel powder the ratio between the irreversible adsorption uptakes of carbon monoxide and hydrogen was reported by Pannell et al.

(113) to be 1.16 at room temperature. No pressure dependence was observed. However at 195K the isotherm slope and adsorption uptakes vary considerably with pressure, suggesting that reversible chemisorption has an important role. The total (irreversible and reversible) CO adsorption uptake to H_2 ratio at room temperature of 2.09 suggests formation of nickel carbonyl $Ni(CO)_4$; the same ratio at 195K is 0.54.

For Raney nickel samples Freel et al. (116) determined that the average ratio of the adsorption volumes of carbon monoxide to hydrogen at 77K was about 1.7.

As was the case for hydrogen chemisorption the presence of a support complicates the adsorption process. Schuit and Van Reijen (124) found that the measurement of the maximum coverage of the metal by CO was more difficult than for H_2 on silica-supported nickel catalysts.

At lower temperatures there was considerable physical adsorption on the support, while at higher temperatures there was formation of nickel carbonyl. They implied that two processes were responsible for the observed adsorption: one observed as by very rapid uptake followed by a much slower that, they said, could not be taken as intrinsic adsorption on the metal. On alumina-supported nickel catalysts a negligible pressure dependence for the carbon monoxide adsorption was reported by Brooks and Christopher (115) whereas a strong pressure dependence was found on nickel zeolites at the adsorption temperature of 523K. The CO/H_2 mole ratio on the nickel-alumina catalysts lay within the range 1.6 to 3.6, whereas for the zeolite-supported catalysts the range was from 6.7 to 59. This last result led the authors to conclude that CO chemisorption provides the only estimate of total surface nickel, including the contribution of nickel in an

essentially atomic state of dispersion.

Below 100-200 torr Bartholomew and Pannell (119) determined that the CO uptake depended significantly on equilibration pressure but at 300-400 torr the equilibrium was approached more rapidly and could be obtained within 30-45 minutes. Assuming $H/Ni_s = 1$ the CO/Ni_s values for Ni/Al_2O_3 range from 1.9 for a particle diameter (d) of 4.4nm (3% Ni/Al_2O_3), to 0.8 for d = 6.3nm (23% Ni/Al_2O_3) to 0.55 for d = 2000 nm (100% Ni). However changes in CO/Ni_s stoichiometry may also be caused by metal-support interactions and not only by changes in metal crystallite size.

LEED and AES studies on the adsorption of CO on well defined Ni planes (100), (110) and (111) gave constant saturation coverage regardless of crystal orientation (125-128). The constant saturation was determined to be 1.10×10^{19} CO molecules/m^2 at 190K, which corresponded to a saturation coverage of 0.7 of a monolayer. This saturation coverage is equivalent to a stoichiometry of 1.40, or as calculated by Klier et al. (125) to an area of 9Å^2 occupied by a CO molecule.

Infrared (IR) studies have been carried out to study the CO-Ni interactions. Carbon monoxide adsorbed on the transition metals gives an intense absorption band in the region between 2100 and 1700cm^{-1}, a result analogous to that observed in the infrared spectra of metal carbonyls and arising from the stretching vibrations of the carbon oxygen bond of the CO. Eischens et al. (129) studied CO adsorbed on a silica supported nickel catalyst and reported that three absorption bands could be resolved at 2073, 1924 and 1870cm^{-1}. They attributed the absorption of the adsorbed CO to a bridged carbonyl type structure below 2000cm^{-1} and to linear monodentate carbonyl surface species above

this frequency. The studies of Yates and Garland (130) confirmed the previous results and they assigned the very strong absorption at 2035cm^{-1} to linear CO-Ni bond. Absorption at frequencies above this were found to be of a weaker strength.

At 1915cm^{-1} there was a very strong bridged bond between CO and Ni

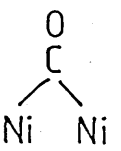

The adsorption was pressure dependent and at higher pressures it was proposed that CO was adsorbed as a bridged species between Ni atoms already having adsorbed linear CO species, but such bonds are weakly held.

They also found that at low loadings (1.5% Ni/Al_2O_3) CO was preferably adsorbed as a single linear species and at higher loadings (23% Ni/Al_2O_3) as bridged species.

Blyholder (131) however preferred to assign the low frequency bands to linear CO adsorption on edge or corner sites on the metal crystallites of the sample.

Primet et al. (132) in agreement with Eischens et al. (129) found that CO is adsorbed as linear and multicentered forms on Ni/SiO_2 catalysts.

The former in the range 2075 - 2045cm^{-1} and the latter in 1935 - 1800cm^{-1}.

Completely reduced samples gave a constant concentration ratio of

linear and multicentered species, whereas for partially reduced samples the relative abundance of multicentered species decreased. In the adsorption of CO on Ni/SiO_2 catalysts at room temperature Rochester and Terrel (133) indentified the infrared band at 2030 - 2050cm^{-1} at low surface coverages as arising from adsorption by isolated carbon monoxide molecules strongly bonded to single metal atoms, which at high pressures of the gas could be converted to subcarbonyl species. Summarizing these results Bartholomew and Pannell presented a table of the surface species of chemisorbed CO on supported nickel (Table 3.3).

Table 3.3 Surface CO Species Chemisorbed on Supported Ni (119)

Infrared frequency (cm^{-1})	Species	Site	Strength of adsorption
1960	Bridged 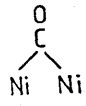	poorly dispersed, crystalline	very strong
2030-2050	Linear 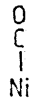	Moderately dispersed Ni	Strong
2065-2090	Subcarbonyl 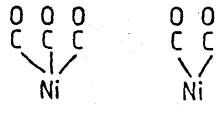	well dispersed Ni	Weak to fairly strong
2195	Ni^{2+} 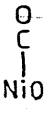	partially reduced catalysts	Weak

Oxygen has also been used as a titrant for nickel metal, and the determination of Ni surface areas (134-136). However its use is restricted by the complexity of the stoichiometry in both direct adsorption and titration of adsorbed H_2 (113,137) and bulk oxides formation. Muller (135) showed that at temperatures as low as 190K there was still considerable slow adsorption which accounts for subsurface nickel oxidation. This process was almost absent at 77K but the physical adsorption is considerable and the results were doubtful. With the O_2-H_2 titration of Ni powder Pannell et al. (113) obtained results in agreement with those of Muller, and concluded that oxygen adsorption was unreliable because of the multilayer oxidation.

Other gases have been used as adsorbates for nickel catalysts but their use has been isolated and limited in their success due basically to problems of stoichiometric uncertainty (124,39).

H_2, CO and O_2 are also the gases used for active area measurements of other metals. For copper and silver, however, the best titrant has been proved to be N_2O (138-140). The use of this gas avoids the problems presented by H_2 (activated adsorption hence low surface areas), O_2 (sublayer oxidation), CO (high physical adsorption). The nitrous oxide is decomposed on a copper surface, the oxygen atom is adsorbed on two metal atoms, and N_2 is liberated. The adsorption is strongly dependent on temperature giving best results at 363 - 373K.

3.3.2 Effect of temperature

In their study on silica-supported nickel catalysts Schuit and van Reijen (124) showed that the H_2 uptake at 13.3kPa decreases with temperature from 195K to 673K. The amount adsorbed of H_2 was reduced by a factor of 4. Adsorption temperatures of 523K (115) or higher may lead to low hydrogen uptakes and low surface areas due to the highly reversible character of the adsorption. Roberts and Sykes (141) reported the adsorption of H_2 on nickel powder. For very well reduced samples the adsorption uptakes of H_2 decreased as the temperature was increased from 90K to 578K; however if the surface was not very clean there was a slight increase in the uptake as the temperature changed from 90K to 293K.

Temperatures as low as 77K have been used for the study of hydrogen chemisorption on Raney nickel (116); the low nickel areas obtained led the authors to claim that the mild temperature (400K) used for outgassing the samples allowed some hydrogen to remain adsorbed on the surface.

Comparing the H_2 adsorption uptakes on unsupported nickel at 293K and 473K with the argon and nitrogen BET surface areas Pannell et al. (113) found the same stoichiometry at both temperatures $H/Ni_s = 1$, although they reported higher uptakes at the higher temperatures.

Wanke and Dougharty (142) measured a continuous decrease in the hydrogen adsorption uptakes on supported rhodium as the temperature was increased from 373K to 573K which they explained as the effect of

temperature on the equilbirium of an exothermic adsorption.

In the temperature range 187K to 298K the hydrogen uptake was nearly constant, leading to the conclusion that room temperature determinations of surface area were reliable. The use of liquid nitrogen temperature for the adsorption was not justified because the corrections for adsorption on the support were too high.

The chemisorption of CO has been used from 77K to 423K for the determination of nickel surface areas. The behaviour, however, is more complex than that of H_2. 77K has been used for unsupported nickel catalysts (122,123) and Raney nickel (116,117). At this temperature the corrections for physical adsorption were of the same order of magnitude than that of the total (physical and chemical) adsorption. As the temperature was increased to 190K - 195K the corrections were lower although still considerable and results for the chemisorption of CO at this temperature on unsupported (113) and supported (119,124) nickel catalysts have been reported. At room temperature Hughes et al. (143) and Bartholomew and co-workers (113,119) have found that Ni reacts with CO to form $Ni(CO)_4$. This was observed for both unsupported and supported nickel; however Brooks and Christopher (115) failed to detect it. Nickel tetracarbonyl could be formed even at 273K as was reported by Srinivasan and Krishnaswami (144).

Pannell et al. (113) reported that for unsupported nickel the ratio of irreversibly (chemical) adsorbed CO to surface Ni atoms was 0.54 at 190K whereas at 298K the value was 1.16. Considering the total adsorption uptake (irreversible and reversible) of CO the ratio of CO/Ni_s was 2.09 at 298K suggesting formation of nickel carbonyl. For

supported nickel catalysts the situation is less clear. For a 3wt% Ni/Al_2O_3 catalyst the irreversibly held CO/H ratio decreased from 2.4 at 195K to 1.8 at 273K and finally to 1.4 at 294K where $Ni(CO)_4$ was produced (119). But with a 2.3wt% Ni/Al_2O_3 the CO/H ratio was constant at about 2.0 in the range 190K - 273K for one sample batch, while for another batch the CO/H ratio increased from 1.6 to 3.8 as the temperature increased in the same range (145). For higher loadings the ratio at 190K was 1.1 for 9%, 0.95 for 14% and 0.8 for 23wt% Ni/Al_2O_3 samples (119). It seems therefore that the CO/Ni_s ratio has a strong dependence on the metal loading.

Bartholomew and Pannell (119) also pointed out that the magnitude of the correction for physical adsorption decreased significantly with increasing temperature. From their results they concluded that the optimum temperature for measuring CO adsorption on nickel was 273K.

For silica-supported Ni catalysts the magnetization measurements reported by Primet et al. (132) gave increasing bond numbers as temperature increased: from 1.3 at 190K to 1.85 at 293K irrespective of metal loading and dispersion; from 293K to 373K the values remained constant at 1.85. These bond numbers correspond to CO/Ni_s values of 0.77 at 190K and 0.54 at 293K.

Bourne et al. (46) determined the Ni metal areas of silica-supported catalysts measuring the adsorption of CO at 423K. No nickel carbonyl formation was reported.

Assuming an adsorption stoichiometry of one to one between CO and Ni, Lohrengel and Baerns (121) determined an active surface area 15% smaller than the surface area calculated by hydrogen adsorption. That percentage accounts for the proportion of bridged species besides the

linear bonded species present. The adsorption isotherms were determined at room temperature on 18wt% Ni/SiO_2 samples.

3.3.3 Adsorption on the support

Besides the effect that the metal-support interactions may have on the chemisorption process, as has been stated above, the support material can also adsorb the chemisorptive agent and hence influence the metal area determination. The support materials vary so much in their adsorption behaviour that the intrinsic adsorption always needs to be determined experimentally for each practical situation so that a proper correction can be applied to measurements made on the supported catalysts (84).

In their study on the adsorption of CO on metal catalysts Hughes et al. (143) determined the adsorption on the support. They reported that at room temperature reduced alumina adsorbs more CO than silica. It was suggested that this might be due to removal of oxygen from the alumina surface as water as the support is treated with H_2 at high temperature.

Adsorption of H_2, O_2 and CO on η-alumina and silica gel were reported by Wanke and Dougharty (142) in the temperature range 190K - 473K. The carbon monoxide uptake by both supports was much larger than that for oxygen or hydrogen; the latter gas showing the lowest levels of adsorption. The uptake decreased as the temperature was increased for all the adsorbents. For H_2 and O_2 the isotherms were linear above a few torr, whereas for carbon monoxide the isotherm on alumina was nonlinear below about 150torr (20kPa).

In agreement with these results are the data from Bartholomew and Pannell (119). They found negligible adsorption of H_2 and CO on

silica. For alumina the H_2 uptake was small, but the CO adsorption was significant.

3.3.4 Monolayer determination

The methods for the evaluation of the saturation coverage are essentially empirical. All depend on the assumption that the data have been taken into a pressure range where the uptake has become only a slowly varying function of pressure, and that this region corresponds to the close approach of monolayer formation (84). The term monolayer in this case is an operative rather than a strict term; it means the point at which all the surface metal particles have been saturated with the chemisorptive agent, it will be used likewise hereafter.

The methods can be summarised as follows:

a) If in the saturation region the uptake becomes almost independent of pressure, this is often taken as equal to n_m without further adjustment (114,119). Normally found in H_2 chemisorption on evaporated metal films.

b) When the isotherm is a slowly varying function of pressure, a condition may be chosen at which monolayer coverage is assumed. This condition has normally been set at a pressure of 100torr (13.3kPa) at 195K (124) or at room temperature (146,147).

c) If the data span over a usefully wide range, the monolayer uptake is evaluated by fitting to a Langmuir-type adsorption isotherm, as was done by Spenadel and Boudart (137) for the dissociative chemisorption of hydrogen using the equation:

$$n = \frac{n_m b p^{\frac{1}{2}}}{1 + b p^{\frac{1}{2}}} \qquad (3.11)$$

and by Lohrengel and Baerns (121) for the one-site adsorption of CO on nickel.

d) The method proposed by Benson and Boudart (148) consisted of measuring the uptakes over a range of pressure and extrapolate the linear part of the isotherm to zero pressure to get the net uptake. This is a widely used procedure (118,121,142,149).

e) If the adsorption isotherm shows a noticeable dependence on pressure this may be due to reversible adsorption or adsorption on the support. The monolayer is determined by subtracting the uptakes for the support from the supported-metal catalyst determined by either the method in b) or in d) described above. The former has been used for H_2 (116) and CO (115,123,149), the latter has been reported for H_2 CO, O_2 (142).

f) Yates and Sinfelt (147) determined the monolayer point in the CO adsorption of Rh/Al_2O_3 by measuring an isotherm at room temperature for the total uptake, then a correction isotherm was determined by evacuating the sample for 1 minute, removing the weakly adsorbed CO, and then redetermining the isotherm. The net adsorption is obtained by subtracting the 2nd isotherm from the first. The amount of gas adsorbed at 100 torr was taken as the monolayer point. They obtained the same result when determining the correction isotherm using the support alone.

A similar procedure was used by Wanke and Dougharty (142). They determined the monolayer by the extrapolation to zero pressure of the straight line region of the net uptake. This was obtained by the subtraction of the adsorption isotherm on the support from the adsorption isotherm on the catalyst.

The procedure was refined by Pannell and Bartholomew (119). The

irreversible adsorption of CO on the metallic constituent of the supported nickel catalyst was determined by measuring an isotherm after equilibration at 300-400torr (40-55kPa) for ½h. Then the sample was evacuated for ½h at the adsorption temperature and the procedure repeated. This isotherm was subtracted to the first one to obtain the chemically adsorbed CO. The result was corrected for chemisorption on the support which was obtained following the same procedure.

Clearly the last method represents the best way for the metal area determination especially when CO is used. However as Anderson has pointed out (84) when the nature of the data permits, the application of the linear back extrapolation to the total uptake data is highly convenient (method d). The uptake intercept at zero pressure gives as good an estimate of n_m as may be had by a two step process involving first correcting the isotherm of adsorption on the support followed by back extrapolation of the corrected isotherm.

3.3.5 Effect of sulphur on the adsorption of H_2 and CO

The effect of sulphur on the adsorption of H_2 and CO on metal surfaces has received some attention since the nickel area measurements are generally done by titration with these gases.

The H_2 adsorption has been shown to be lowered by the presence of adsorbed sulphur (3,38,113,145,150). The adsorption behaviour is the same for both unsupported and supported catalysts.

Studies on polycrystalline nickel surfaces (150) showed that the initial sticking coefficient of hydrogen decreased linearly with the sulphur content below a saturation coverage $\theta_s = 0.3$. Above $\theta_s = 0.3$ the slope decreases and deviates to higher coverages, see figure 3.10.

In a plot of the fractional H_2 uptake versus H_2S coverage in

molecules of H_2S per surface nickel atom Bartholomew and Pannell (145) showed that the H_2 uptake decreased linearly with increasing sulphur coverage for Ni powder and supported Ni catalysts. The intercept with

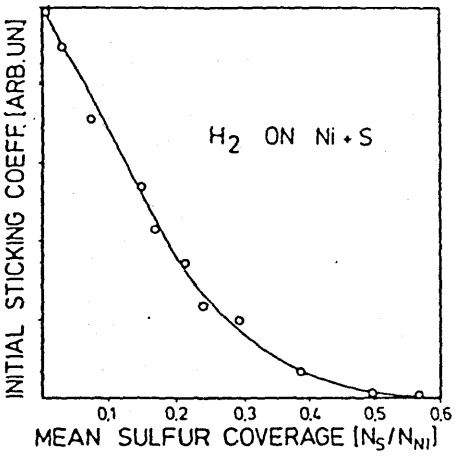

Figure 3.10 Variation of Initial Sticking Coefficient with Sulphur Coverage (Adap. from 150)

the abscisa gave a value of $H_2S/Ni_s = 0.75$ which is a measure of the sulphur to nickel stoichiometry at saturation coverage and in agreement with the stoichiometric values reported by Oliphant et al. (32).

Ng and Martin (38) found that the change in saturation magnetization was constant over a wide range of sulphur coverages, θ_s, while the H_2 uptake decreased linearly as the sulphur coverage increased. These results led them to state that H_2 is adsorbed on the nickel surface that remains free, and that the free nickel surface is not perturbed by the sites on which sulphur has been adsorbed. The adsorption temperature in both works (145,38) was 300K.

For the H_2 chemisorption at 475K, Pannell et al. (113) found that the amount of H_2 adsorbed on the presulphided nickel powder was lowered by a smaller percentage than the adsorption at room temperature. It

has been suggested that a possible explanation is H_2 being weakly adsorbed on the sulphided portion of the surface at high temperature (3).

The complexity of the adsorption of CO on clean nickel surfaces is incresed by the presence of sulphur.

At pressures typical of ultra high vacuum systems, sulphur appears to have a blocking effect. A SIMS study on single-crystal faces by Bordoli et al. (151) showed that for Ni(100) the concentration of bridged CO species decreased constantly with sulphur coverage, θ_s; whereas the linear species concentration remained constant over a wide range of sulphur coverage, and then decreased rapidly near saturation coverage. On Ni(111) the concentration of bridged species decreased to zero with increasing θ_s, but the number of linear species decreased only to a half of its initial concentration as the surface was saturated with sulphur.

The results of Erley and Wagner (28) showed that sulphur poisons the CO adsorption on Ni(111). CO flash desorption spectra showed that the amount of CO adsorbed decreased with increasing sulphur coverage. At $\theta_s < 0.1$ each sulphur atom blocked about nine potential CO adsorption sites, but the CO adsorption energy deduced was only slightly changed by the presence of coadsorbed S atoms. Above a sulphur coverage of $\theta_s = 0.33$ the adsorption of CO was completely blocked.

At moderate pressures of CO, typical of chemisorption for metal area determinations the results have shown a complicated behaviour. For unsupported nickel catalysts the irreversible adsorption of CO was decreased by the presence of sulphur at both 190K and 300K. At 300K,

however, the total (irreversible and reversible) adsorption of CO on a poisoned sample nearly doubled the CO uptake adsorbed on a clean sample, with the CO/H ratio being consistent with the formation of nickel tetracarbonyl (113). This means that the formation of nickel tetracarbonyl is catalized by the presence of sulphur, a fact that had been pointed out by Milliams et al. (152).

For supported catalysts the results are somewhat contradictory. At low pressures (less than 0.1kPa) CO adsorption was decreased with increasing sulphur adsorption as reported by Ng and Martin (38). At moderate pressures Bourne et al. (46) and Feng (153) reported a decrease of CO adsorption with sulphur at 423K and 195K respectively, whereas Bartholomew and Pannell (145) reported an increase in both total and irreversible adsorption of between 300 to 800% depending upon sulphur coverage and temperature. The CO/Ni_s values ranging from 7 to 20 were consistent with the formation of nickel carbonyl and subcarbonyl species, the lower values were obtained at lower (190K) temperatures.

IR studies (47,53,133,154,155) have shown that during the exposure of sulphided nickel samples to CO, subcarbonyl and tetracarbonyl species are formed. For samples increasingly sulphided with H_2S it was found that the number of bridged bonded CO molecules decreased while the number of linear bonded molecules at first increased but did decrease at larger sulphur coverage (155). The binding energy of the CO linear adspecies formed was quite low since a large fraction could be desorbed in H_2/He at room temperature. Garland (154) indicated that for samples that were sulphided by exposure to CS_2 the population of both types of CO adsorption states decreased continuously with increasing sulphur contamination. Heavily poisoned samples adsorbed CO

which was determined by a single band at 2084-2094cm^{-1} in the IR spectrum, band which was completely removed by evacuation of samples after 30 minutes at room temperature (133,154). The addition of CO to samples presulphided with mercaptans produced the appearance of bands at 2040 and 420 cm^{-1} which were attributed to nickel tetracarbonyl and which readily disappeared after evacuation (47).

Rochester and Terrell (133) found that of the five sulphur compounds studied thiophene apparently had the smallest catalytic effect on the uptake of carbon monoxide by nickel and carbonyl formation. The order of toxicity of the five sulphur compounds were: carbonyl sulphide> n-propyl mercaptan > hydrogen sulphide> dimethylsulphide>thiophene at low pressures. At higher pressures (0.05kPa) the order was similar except that n-propyl mercaptan became more toxic than carbonyl sulphide.

Klostermann and Hobert (53) found that thermodesorption results were in excellent agreement with those obtained by IR spectroscopy. That is the dissociative adsorption of CO decreased with increasing sulphur coverage on silica-supported nickel. The linearly bonded CO could be desorbed at lower temperatures as the sulphur coverage increased; however a weakly adsorbed CO layer was formed under complete sulphur coverage, it was assumed that this adsorption state was formed by coordination of CO molecules above a chemisorbed sulphur layer.

A summary of the interactions of CO adsorbed on presulphided Ni surfaces is given in Table 3.4 as discussed by Rochester and Terrell (133) and compiled by Bartholomew et al. (3).

Table 3.4 Effect of Sulphur Poisoning on the CO Adsorption (3,133)

Infrared Band cm^{-1}	Structural Assignment	Effect of Sulphur Poisoning
1960	Bridged or multicenter	Progressively, irreversibly poisoned with increasing sulphur coverage. Band not observed at high S coverages.
2030-2050	Linear	Progressively, irreversibly poisoned with increasing sulphur coverage with concomitant growth of band at 2056-2090cm^{-1}. The band is completely shifted at high sulphur coverages.
2050-2090	Subcarbonyl	Band increases in intensity with increasing amounts of sulphur at low coverages and subsequently decreases at high coverages. Can be removed by evacuation. Can be partly regenerated with O_2 treatment.

3.4 Summary

It has been shown in this Chapter that:

i) In surface area determination the gravimetric method is probably the most reliable, it has less drawbacks than the volumetric and is more accurate than the dynamic methods;

ii) the calculation of total surface areas can be done through the use of the BET equation or standard isotherms;

iii) for the evaluation of pore size distributions by gas adsorption the choice of the adsorption or desorption branch, and the

film thickness correction has to be considered carefully to obtain the correct distribution;

iv) the nickel metal areas can be evaluated by H_2, CO, O_2 chemisorption. H_2 seems the most reliable titrant due to the simple stoichiometry of the Hydrogen-metal bond, but may not be convenient when using microbalances because of its lightness. The use of CO is restricted, because of the possible $Ni(CO)_4$ formation, to temperatures below 273K; the CO-metal stoichiometry can vary with temperature and metal loading. Oxygen shows sublayer attack even at 77K;

v) In sulphur-poisoned nickel samples the measurement of free nickel areas is more complicated. H_2 appears to be the best adsorbent. The CO adsorption behaviour is more complex and the results available are contradictory.

The application of CO to measure nickel areas in sulphur-poisoned catalysts needs to be studied in the light of the results available, and the problems posed by the nickel tetracarbonyl formation. The possible use of other titrants such as NO or N_2O could also be investigated and developed since compounds heavier than H_2 are needed in gravimetric techniques.

CHAPTER 4

EXPERIMENTAL

The adsorption studies were performed in a thermogravimetric system operated at atmospheric pressure using alumina supported nickel catalysts. This system as well as the design and construction of the high-pressure rig are described in this chapter. Catalyst preparation, experimental procedure, elemental analysis and electron microscopy studies are also described.

4.1 Apparatus

4.1.1 Atmospheric pressure system

The central part of this system was a Cahn Instruments microbalance with a sensitivity of 10^{-6}g. It was coupled to a vacuum BET and a flow systems. Figure 4.1 shows a flow diagram of the arrangement.

The BET system could be operated at pressures down to 1.3×10^{-3} Pa (10^{-5} Torr) by using a rotary pump, an oil diffusion pump, and liquid nitrogen traps. The pressure was measured with a McLeod gauge and a mercury manometer. Gases used for the area measurements were stored in glass bulbs.

The flow system was employed for the H_2S and thiophene poisoning studies. Hydrogen passed through a saturator containing thiophene at a given temperature (236K-243K) and was mixed with a second hydrogen stream to obtain the desired concentration, the temperature of the saturator was controlled to ±0.1K. Flows were controlled by needle valves and measured with rotameters. A N_2 inert stream was fed to the

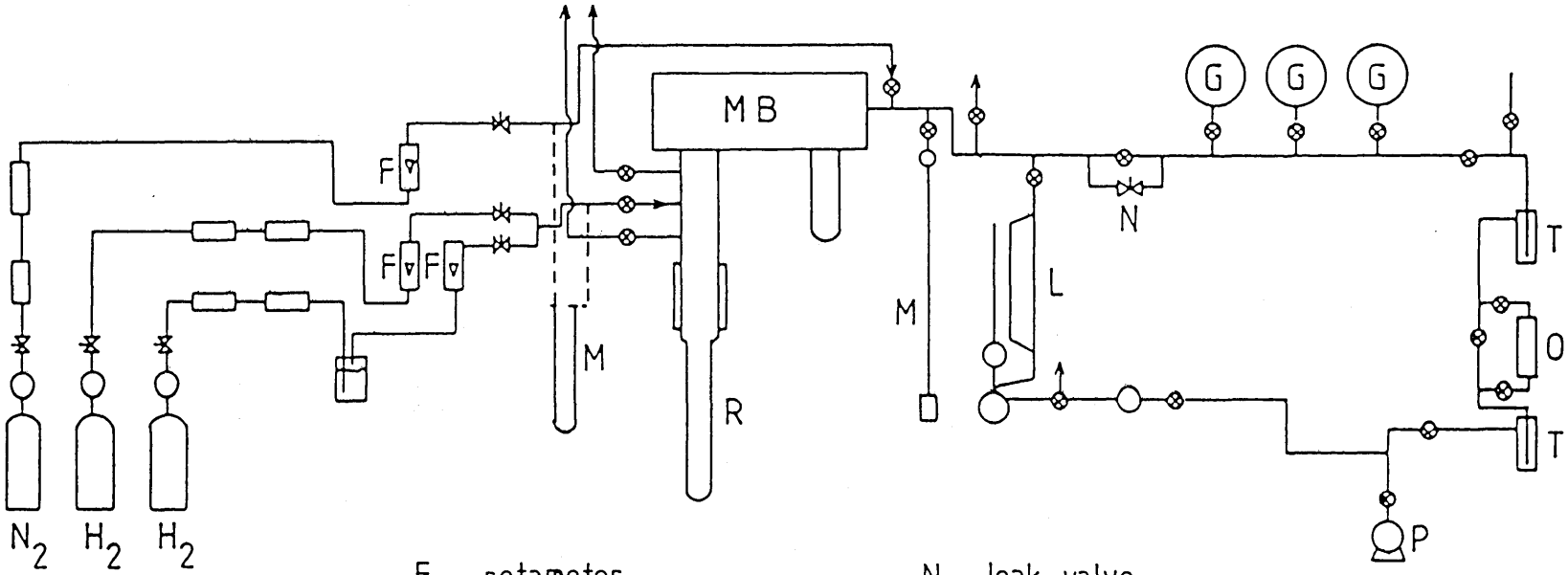

F rotameter
G glass bulb
L mc leod gauge
M manometer
MB microbalance
N leak valve
O diffusion pump
P rotary pump
R reactor
T cold trap

FIGURE 4.1

Diagram of Experimental System

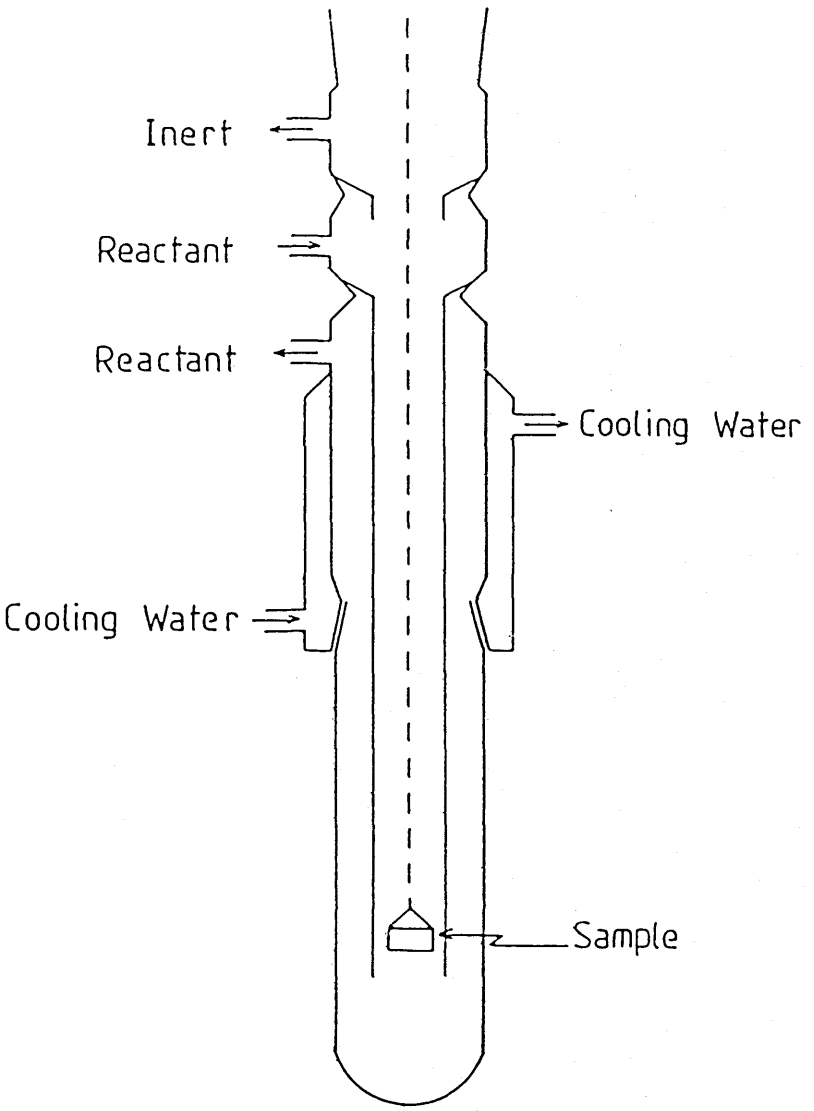

FIGURE 4.2

Sketch of the Atmospheric Pressure Reactor

microbalance head at a constant flow.

The reactor was attached to the left-hand side of the microbalance. The upper part was made of Pyrex, the lower of silica. A diagram is given in figure 4.2. The catalyst was placed in a 1cm diameter silica basket which hung at the end of a silica wire suspended from the left arm of the microbalance head. The counterweight was suspended from the right arm.

The output from the electrical control cabinet passed through a matching circuit to a chart recorder where the signal was recorded as a function of time.

The reactor was heated by a furnace capable of attaining 1100K; the temperature was controlled by an Eurotherm controller. A chromel-alumel thermocouple placed between the reactor and the furnace was used to monitor the temperature. Lobo (178) and Figueiredo (179) have demonstrated that the maximum temperature difference between the furnace and the inside of the reactor is about 5^0C at flow rates of about $400cm^3/min$.

The temperature given by the thermocouple was taken as the temperature of the experiment.

4.1.2 High pressure (HP) system

This system was built around a Sartorius microbalance model 4436 (sensitivity $10^{-7}g$). The arrangement was similar to the atmospheric pressure system in that it had an all-glass vacuum section capable of reaching a vacuum of $10^{-3}Pa$ (10^{-5} Torr) and a flow section to perform the adsorption studies.

The glass vacuum section was similar to the one described in 4.1.1, the only difference being that the vacuum was monitored by a Pirani gauge.

Stainless steel tubing was used for the flow system, valves and fittings in contact with the H_2S/H_2 mixture were also stainless steel. Due to the complex behaviour of the system under flow conditions the inert gas entering the microbalance head was mixed in the reactor with the poisoning stream. To avoid upward flow to the head the system was designed such that the pressure difference between the section above the reactor and the outlet stream was measured by a differential pressure transducer and controlled. This was a difficult task especially at the higher pressures ($P > 20$ bar). The total flow was measured in the outlet stream with a rotameter. The flows of the reactant and inert streams were measured through the position of the control metering valves which were calibrated at different pressures between 1 and 30 bar and the flow was recorded as a function of valve setting and pressure.

The reactor was connected to the right hand side of the balance. It was made of Incoloy 800 alloy; a high nickel content alloy capable of withstanding the maximum operating conditions. The design was carried out following the guidelines given in Brownell and Young (180) and data from ASM (181); the details are given in Appendix A. Figures 4.3 and 4.4 show the reactor and details of the flanges at the top of the reactor respectively. The reactor was in the form of two concentric tubes, the inner resting inside the outer by means of a tapered flange and an 8-hole ring at the bottom. Soft copper gaskets were used to seal the reactor which was held through the top flange by 8 stainless steel bolts.

The catalyst was placed inside a 1-cm diameter silica basket which was suspended from the microbalance using a 107cm long silica wire.

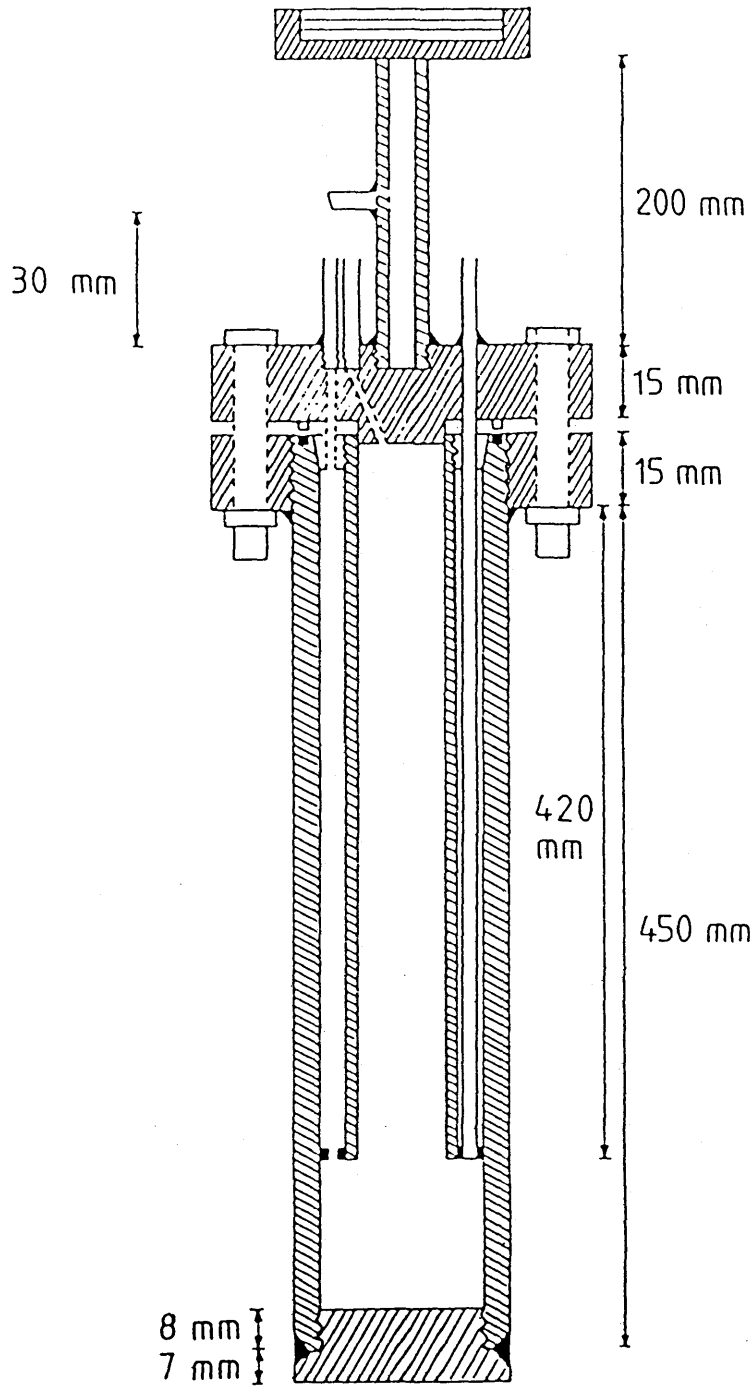

FIGURE 4.3

High Pressure Reactor

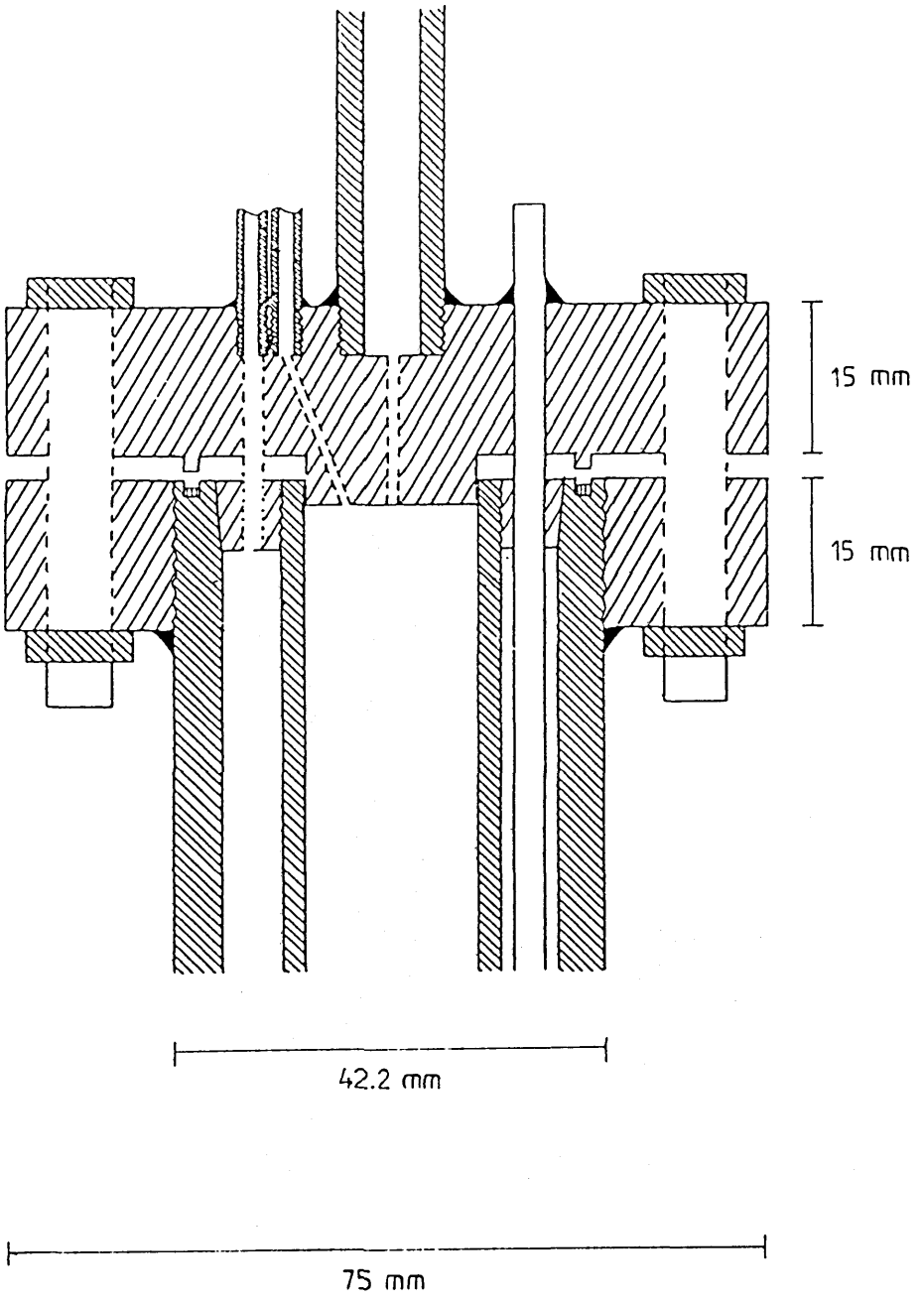

FIGURE 4.4

Details of the Flanges

The silica wire passed through a 3mm hole on the top flange.

The poisoning mixture was fed through a 1.5mm hole into the inner cylinder where it was mixed with the inert stream coming from the head of the balance through the 3mm hole in the top flange; this mixture left the reactor through a 1.5mm hole in the annulus between the inner and outer tubes at the top flange. The temperature was monitored by a chromel-alumel thermocouple placed in the annulus at the catalyst level, and was controlled manually by a variac connected to the furnace. This was determined to be the best way to control the temperature because of the great inertia showed by the furnace if the temperature was controlled automatically by a Eurotherm using the thermocouple signal.

An 8-baffle structure was added later to dampen convective currents arising from temperature gradients at high pressures ($P > 10$ bar) with heavy gases (N_2). This structure made of stainless steel was placed inside the inner tube and held by 2 small pins; it is shown in figure 4.5.

The baffled structure, the inner tube and the outer shell were placed and assembled once the catalyst sample was loaded. The assembly was found to be a very difficult and sensitive operation to do due to the fragility of the silica wire from which the catalyst basket was hanging and possible static charges being created if the assembly was carried out carelessly.

4.2 Catalyst Preparation

The catalyst was prepared by impregnation to incipient wetness (84,182,183). The alumina support extrudate was crushed and sieved to obtain particles between 30-50 mesh (300-500μm). The support was

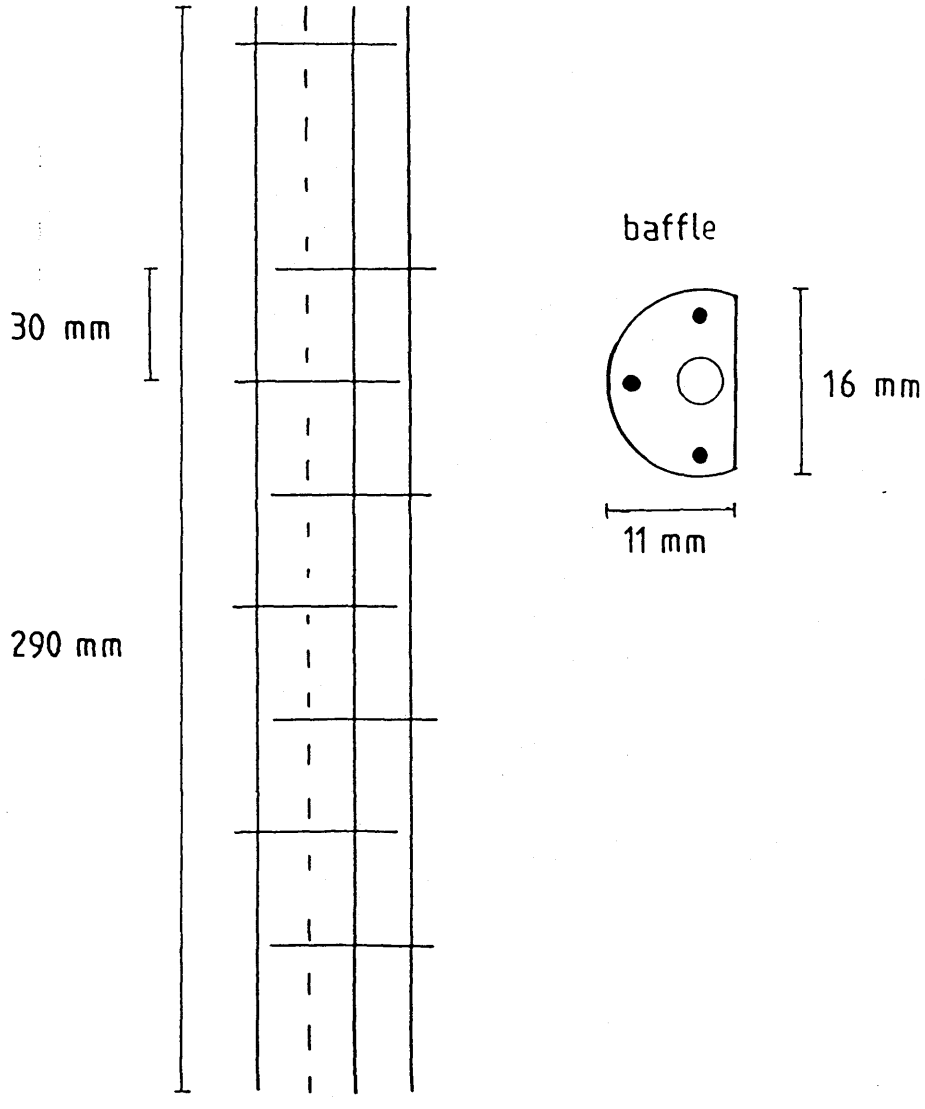

FIGURE 4.5

Baffled Structure

pretreated with air for 2 hours at 393K and for 18 hours at 673K. After cooling the water pore volume of the support was determined to be 0.44 ±0.05 cm^3g^{-1} using a pore filling technique (182,183).

A solution of $Ni(NO_3)_2.6H_2O$ of the required concentration to produce 20 wt% of Ni/Al_2O_3 was added dropwise to 50g of γ-Al_2O_3 (30-50 mesh) in a volume sufficient to fill the pores up to incipient wetness. The preparation was dried with 150cm^3/min of air at 393K for 3h and calcined for 16h at 673K. The catalyst was left to cool down in air and transferred to a flask kept in a desiccator. Several samples were prepared in this way. The catalyst used for the poisoning studies (NAT3) was prepared in sufficient amount to be used throughout the whole study and to avoid variations between samples.

4.3 Materials

A Norton SA6175 γ-Al_2O_3 extrudate was used as support.

$Ni(NO_3)_2.6H_2O$ AR grade and distilled water were employed for the catalyst preparation.

Hydrogen sulphide/hydrogen and hydrogen sulphide/nitrogen mixtures were obtained from BOC in spectroseal grade; while thiophene/hydrogen mixtures were produced by a thiophene bubbler/saturator kept at constant temperture in a Betta-Tech refrigeration unit. Thiophene GPR grade (99+%) was used as received. N_2 and H_2 gases supplied by BOC were passed through deoxo units and molecular sieve/silica gel dryers to remove oxygen and water respectively.

CO from BOC 99% purity was passed through molecular sieve before being stored in the glass bulbs of the BET system.

N_2O atomic absorption grade supplied by BOC was used as supplied.

4.4 Procedure

The experimental procedure employed for the adsorption-regeneration studies consisted of several steps which altogether took 7 days to perform. These steps are given in figure 4.6 with the approximate time taken for each, and are explained below.

4.4.1 Reduction

A sample of the calcined catalyst of approximately 0.13g was loaded into a silica basket which then was suspended from the microbalance. After setting the H_2 flow to 100ml/min the temperature was raised to 373K where it was kept for 1hr; the temperature was then raised to 473K and maintained for about 1hr after which it was considered that all the water had been removed (118); the temperature was then raised at a rate of ~10K/min to 873K. The sample was left at this temperature for 16h, sufficient for complete reduction of the NiO precursor. The reduction process adopted followed recommendations in the literature (118) and previous studies (153). Complete reduction is assured at 873K; and although the resulting metal area is lower due to sintering the nickel particles so obtained are highly stable.

γ-Al_2O_3 samples were subjected to the same treatment before CO chemisorption or thiophene adsorption studies.

4.4.2 Total (BET) area and PSD measurements

The determination of the total area and pore size distribution was done by N_2 adsorption-desorption at 78K.

The samples were outgassed for 2½h at 673K under a vacuum of 1.3×10^{-2}Pa (10^{-4} Torr), then kept at room temperature for about 15 min

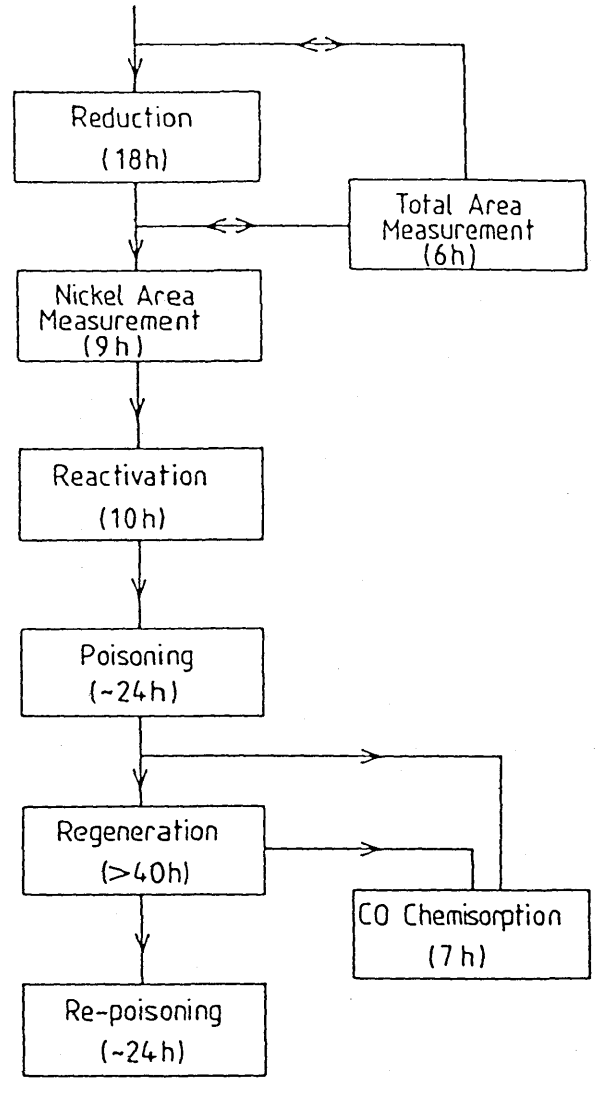

Total time: > 125 h

FIGURE 4.6

Steps in Experimental Procedure

followed by a cooling period of 45min at 78K. N_2 was slowly leaked through an Edwards high vacuum needle valve until the required pressure was obtained. The first adsorption point was normally determined at about 1.33kPa (10 torr) and took ca. 20 min to equilibrate but was measured after 30min. The subsequent points were determined at increasing pressure ratios of P/P_o = 0.05 every 10-15min up to P/P_o = 0.50.

If the adsorption-desorption isotherms were required the pressure was increased up to a relative pressure of 1.0. As the pressure increased the time for equilibration increased and in the region between P/P_o = 0.80 to P/P_o = 1.0 each point required approximately 2 to 2½h. For the desorption the system was evacuated through the high vacuum valve using the rotary pump; readings were taken every 6.6kPa.

4.4.3 Ni area measurements

After reduction the catalyst was outgassed following the same procedure used for the total area measurements. Several adsorption temperatures were employed: 78K (liquid nitrogen), 195K (CO_2/MeOH mixture), and 273K (ice bath). The first reading was taken at 1.33kPa (10Torr) after 40-45 min as recommended by Bartholomew et al. (113,119), time at which equilibrium was attained; longer times were demonstrated to be unnecessary and shorter times (~30min) were not enough. In the region 1.5-10kPa the adsorption points were taken every 2.7kPa, and every 5.3kPa in the pressure region 10kPa-30kPa, at time intervals of 20 min. Adsorption isotherms were normally carried out up to 20-25kPa. Higher pressures were tried but proved to be unneccessary and because of the latent possibility of $Ni(CO)_4$ formation they were avoided.

Once the last point in the adsorption isotherm reached equilibrium the system was evacuated for 20 minutes at the adsorption temperature using the rotary pump (0.13Pa); after which a second adsorption isotherm was determined. Points in the second isotherm were taken at the same pressures as in the first but required shorter times to reach equilibrium: 30 min for the first point and 15 min for the rest.

4.4.4 Reactivation

Adsorbed CO was removed by reaction with H_2 at 773K. The pressure in the reactor was increased from the last equilibrium point of the second adsorption isotherm to atmospheric pressure using H_2 at the adsorption temperature. At atmospheric pressure the H_2 flow was maintained at $100cm^3/min$ for about 30 min at the adsorption temperature, then the temperature was increased to 773K where was kept for 10h.

4.4.5 Sulphur compound adsorption

The sample was brought to the poisoning temperature under H_2 flow and kept there for about 2h to reach constant weight. During this period the thiophene/H_2 mixture of the desired concentration was produced by bubbling H_2 through a thiophene saturator in a refrigeration unit and regulating the flow with needle valves (Edwards High Vacuum Ltd.).

The thiophene/H_2 mixture (or H_2S/H_2, H_2S/N_2 mixtures) was fed to the reactor and the increase in weight was recorded as function of time.

A positive differential pressure (~30Pa) between the inert (N_2) stream and the poisoning stream was maintained throughout the

experiment to avoid poison flow to the microbalance head.

The experimental conditions used for posioning were as follows:

Temperature	298K-773K
Thiophene concentration	100ppm - 1000ppm
H_2S concentration	2ppm (H_2S/H_2) - 8ppm (H_2S/N_2)
Flow	150cm^3/min (291K, 1 bar)
Inert Flow	~250cm^3/min (291K, 1bar)
Mass of catalyst	~0.13g

4.4.6 Regeneration

The regeneration was carried out at 873K with a H_2 flow of 100cm^3/min. The temperature was increased from the adsorption temperature at 873K under H_2 flow. As the temperature increased the weight decreased due to two factors: loss of adsorbed material and buoyancy. The total weight loss was recorded, and separate experiments with a freshly reduced catalyst were carried out to quantify the buoyancy effect using the same procedure employed for the regeneration.

4.4.7 Re-poisoning

Some samples were repoisoned after regeneration. They were subjected to the same treatment as outlined in 4.4.5. The adsorption was carried out at the same temperature and concentration as in the first adsorption. Samples regenerated after poisoning with H_2S were repoisoned with 100ppm thiophene/H_2 mixtures at 373K and 773K only.

4.5 Running the High Pressure (HP) System

The operation of the high pressure system was more complex than the atmospheric pressure system. Changes in weight were observed due to convective currents especially at pressures higher than atmospheric;

this and other effects are explained in Appendix A. The procedure adopted for the poisoning experiments was as follows: Once the sample was loaded the reactor was assembled and tightened. The sample was reduced following the same procedure outlined in section 4.4.1. The heating rate was slower, ~3K/min. After reduction the sample was cooled to the adsorption temperature and the pressure increased to the adsorption pressure using H_2. The system was allowed to reach constant pressure and the flow was controlled by the Micromite needle valve (Hoke International Limited) in the outlet stream. A second H_2 (or N_2) stream was fed to the reactor through the reactants inlet at the top flange at the same pressure as the system. The differential pressure between the inert gas just above the reactor and the outlet stream was carefully monitored to maintain a positive value of ~20Pa (2mm H_2O). The stability of the system was measured by the constancy in weight. This was the critical step during the experiment since small variations in pressure had a strong effect on the weight.

Once the weight was constant the H_2S/H_2 (or H_2S/N_2) mixture was set at the same pressure as the system and switching a 3-way valve it was fed to the reactor substituting the second H_2 (or N_2) stream. The weight uptake was recorded as a function of time.

4.6 Elemental Analysis

Carbon and sulphur content of the poisoned catalysts were determined in a 'Carlo Erba Elemental Analyzer mod. 1102'. The instrument specifically designed for the determination of carbon, hydrogen, nitrogen (CHN) and oxygen was adapted for sulphur determination.

The general procedure was as follows:

The catalyst was grounded to very fine particles (~5-50μm). A sample of approximately 8mg was weighed into a tin continer. The container was loaded into an automatic sampler which dropped it into the oxidation tube where the organic components were pyrolized in an oxygen-rich atmosphere and the decomposition products were carried away by a constant stream of helium through part of the reactor to be converted to the desired state of oxydation (CO_2, SO_2). The gases were separated downstream in a chromatographic column and detected by a thermal conductivity cell. The signal was registered in a chart recorder. The carbon and sulphur percentages were determined by comparison with standards (cyclohexanone - 2,4-dinitro-phenylhydrazone OAS and Dibenzyldisulphide OAS). Figure 4.7 shows typical signals obtained in the recorder.

4.7 Electron Microscopy

Transmission electron microscopy (TEM) and scanning transmission electron microscopy (STEM) were used to characterise the catalysts and obtain information on the state of the carbon deposits. A JEOL 120cx TEMSCAN electron microscope was used. Samples were analysed at 100kv high resolution range. The samples were grounded to a very fine powder, and particles were suspended on carbon-coated copper grids (Gilder grids G200 Cu) by dipping the grids into the powder. With this method sufficiently thin platelets were produced for the analysis.

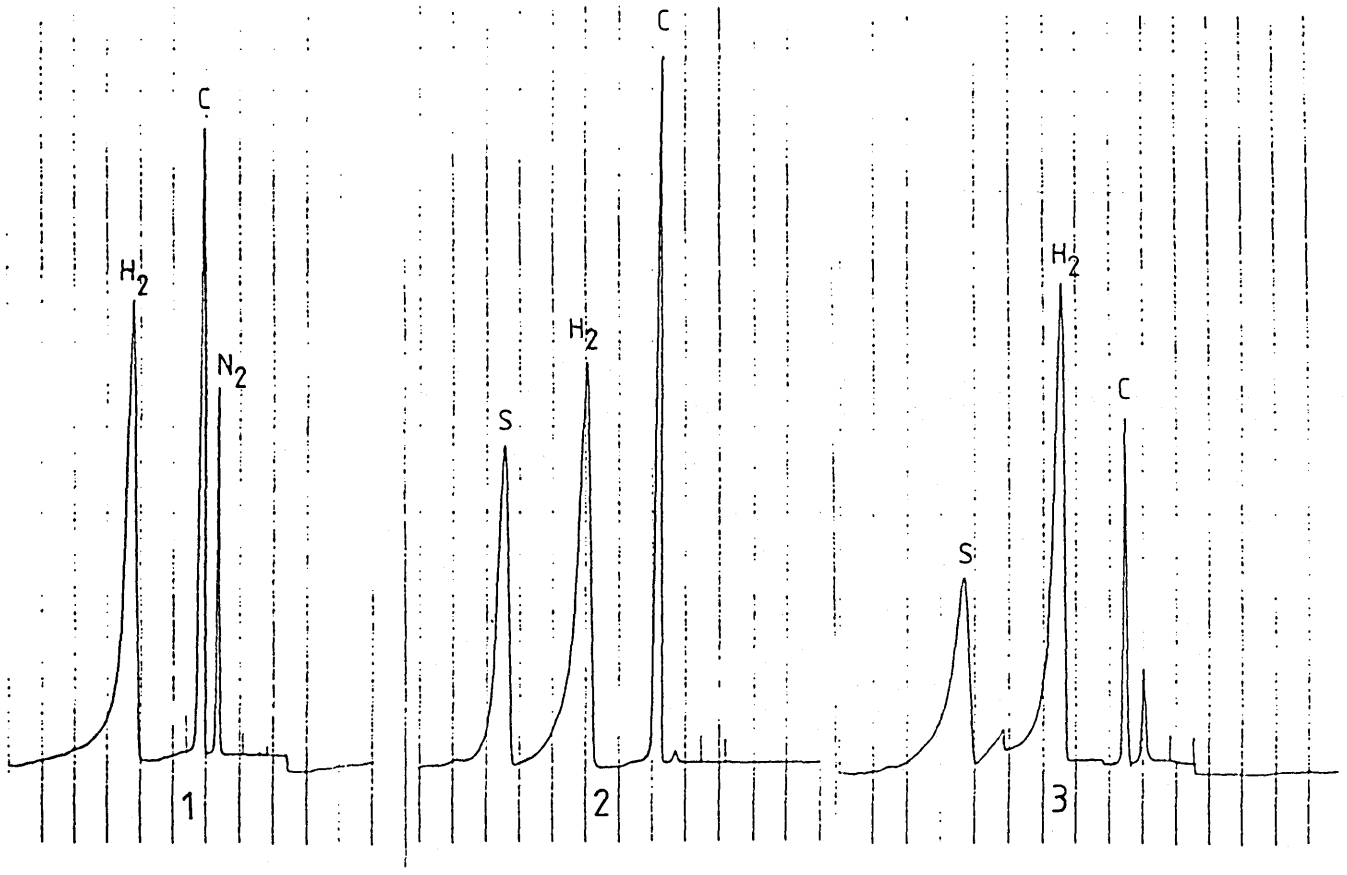

FIGURE 4.7

Typical Signals from the elemental analyzer.
1: CHN standard; 2: CHS standard; 3: Catalyst sample.

CHAPTER 5

CATALYST CHARACTERISATION. RESULTS AND DISCUSSION

In this Chapter the results of the characterisation of the Ni/Al_2O_3 catalysts are presented. The total surface area was determined using the BET method and the standard isotherms of Lecloux. The pore size distributions obtained by gas adsorption are discussed in section 5.2. The determination of nickel active areas of clean and sulphur-poisoned catalysts was carried out by CO chemisorption. The possible use of N_2O as nickel titrant is also described.

5.1 Total Surface Area

5.1.1 BET method

N_2 was used as adsorbent for the total surface area determination. Typical adsorption isotherms up to a relative pressure P/P_o of 0.5 are given in Figure 5.1. The isotherms in this figure represent the uptakes on fresh and reduced Ni/Al_2O_3 and γ-Al_2O_3 support samples. The BET equation in its linearized form was used to calculate the areas. The plots of $\frac{P/P_o}{n(1-P/P_o)}$ vs p/p_o for the monolayer uptake determination of the same samples are shown in Figure 5.2.

The BET surface areas were calculated employing adsorption values within the relative pressure limits of 0.05 and 0.35 as recommended (83,84,95,97). The N_2 molecule area used was 16.2×10^{-20} m^2 ($16.2 Å^2$). The results are given below

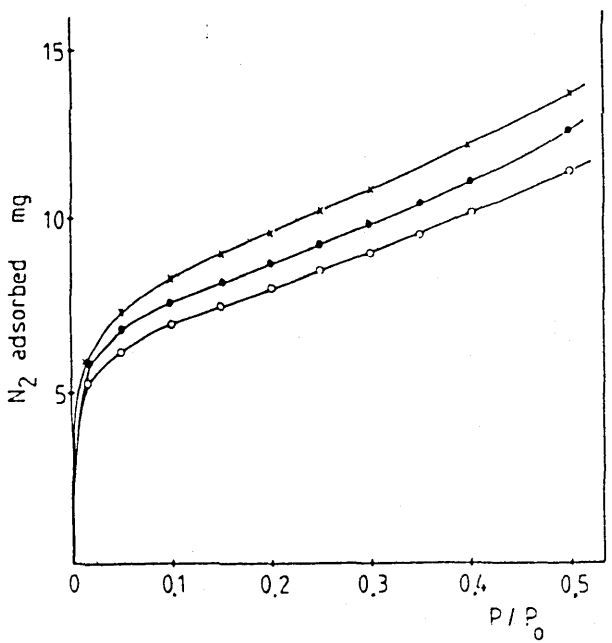

FIGURE 5.1

Adsorption of N_2 at 77K on Fresh Ni/Al_2O_3 (●), reduced Ni/Al_2O_3 (0), γ-Al_2O_3 (x).

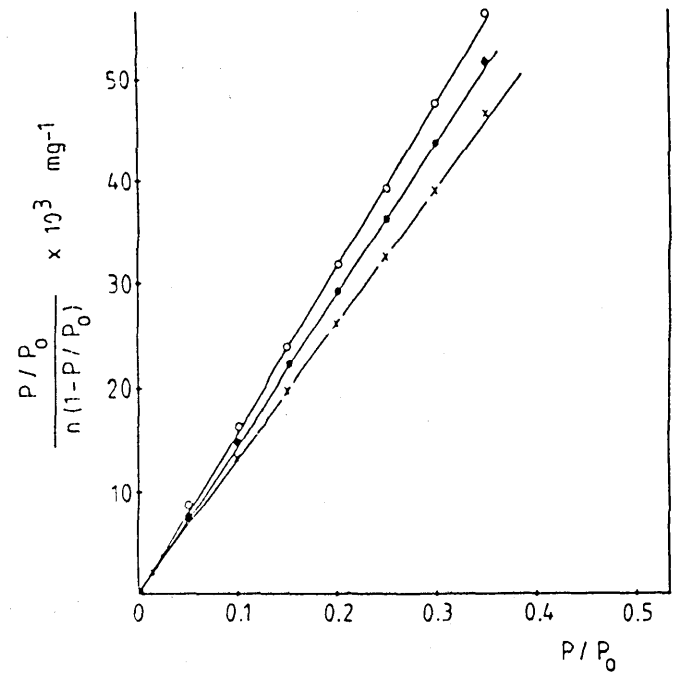

FIGURE 5.2

BET Plot of the Adsorption Values of N_2 at 77K on Fresh Ni/Al_2O_3 (●), reduced Ni/Al_2O_3 (0), γ-Al_2O_3 (x).

Table 5.1 Total BET Surface Areas for Ni/Al_2O_3 and γ-Al_2O_3

Sample	Area m^2/g	Area m^2/g
Ni/Al_2O_3 (fresh)	176 ± 4.6	185.6 ± 4.8
Ni/Al_2O_3 (reduced)	162 ± 3.2	171 ± 3.4
γ-Al_2O_3	199 ± 4.8	-

The values in the second column of table 5.1 were calculated using the weight of the sample as loaded to the microbalance. In the 3rd column the values are based on the weight after reduction of the NiO precursor in H_2 at high temperature.

It is noticeable that the surface areas of the reduced catalysts are lower than those of the fresh catalyst samples, a direct result of the reduction process at high temperatures which promotes sintering of the nickel metal particles. The larger crystals produced may be blocking certain pore sizes which in consequence are not available for adsorption.

The surface areas obtained after the standard reduction process were highly stable as was demonstrated. When the samples were subjected to further heating at the same reduction temperature (873K) but longer times ($>$18h), no significant difference was found in the surface area values.

The C_{BET} values obtained from the fitting of the adsorption data to the BET equation ranged from 130 to 500, with an average value of 220. In two determinations the value of C_{BET} went up to 1000 and 1100,

however the calculated surface areas were within the limits established in table 5.1.

It seems, then, that for the samples used in this work the value of C_{BET} has very little influence on the monolayer capacity determination. Any variation in C_{BET} from the average value has to be taken more as a fitting calculation error rather than a different behaviour of the adsorption isotherm.

The determination of the surface areas involved a standard pre-treatment consisting in the evacuation at 673K for 2 to 2½h at a vacuum of at least 10^{-4}torr. This pre-treatment produced consistent and reproducible results. Shorter evacuation times were tried; 1h at 673K was the minimum time needed to obtain the same results as with the standard treatment. Buoyancy corrections were unnecessary. The weight uptakes on the catalyst samples were high enough so that corrections due to buoyancy effects were negligible.

The results show that the total surface area of the samples used are well determined by the BET equation. The alumina support has the highest surface area as should be expected, followed by the fresh supported NiO precursor and finally the reduced Ni/Al_2O_3 catalyst.

The reduction in H_2 at 873 for 18h gives surface areas which have constant adsorption capacity. The values are not altered by reduction times longer than that used as standard during this investigation.

5.1.2 n* method

The n* method proposed by Lecloux (95,101) was employed to determine the surface area of some samples and test the validity of the average C_{BET} obtained in the previous section.

The standard isotherm chosen was n_2^* which corresponds to C_{BET}

values between 100 and 300. Figure 5.3 shows the plot of n-vs-n* for the 3 sample materials used in figure 5.1. It can be seen that in the low pressure region (low n values) and up to a pressure ratio of 0.35 (n* = 1.43) straight lines are obtained. The extrapolation of these lines pass through the origin, which according to Lecloux is an indication that the correct standard isotherm was used. The slope of the straight lines gives the surface area through the equation (3.5)

$$A = 3.496 \frac{dn}{dn^*} \quad (m^2/g)$$

Table 5.2 shows the value of the slopes and the areas obtained for the 3 sample materials: fresh and reduced Ni/Al_2O_3 and γ-Al_2O_3.

Table 5.2 Surface Areas Calculated from n_2^* Standard

Sample	Slope mg/gnm	Area m^2/g
Ni/Al_2O_3 (fresh)	53.55	187.2
Ni/Al_2O_3 (reduced)	48.86	171
γ-Al_2O_3	57.76	202

The agreement between the values of the areas obtained from this method and the BET equation is excellent. This is explained by the fact that the n* standard isotherm is directly related to the BET equation due to the use of the monolayer capacity in its definition:

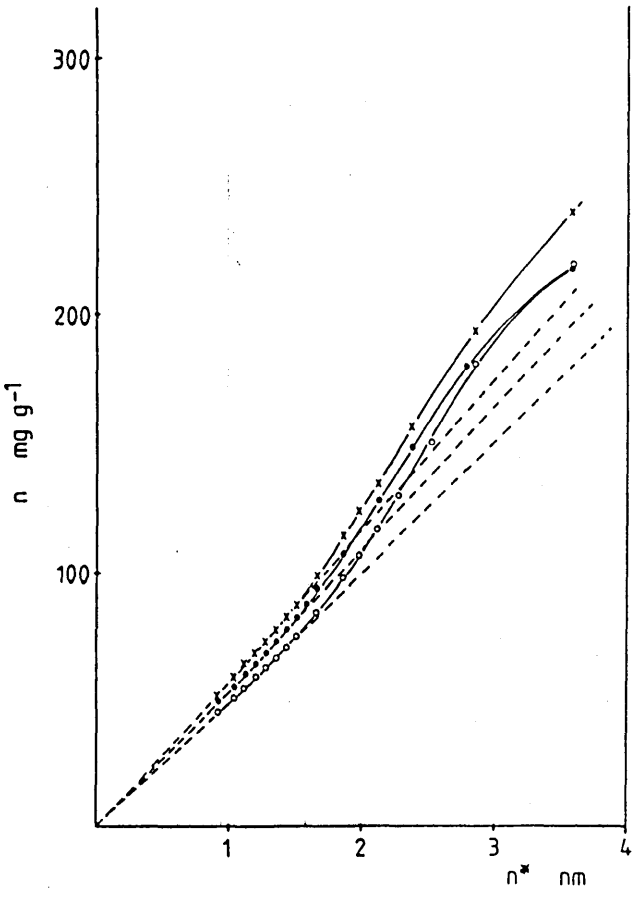

FIGURE 5.3

Plot of n vs n* using the standard isotherm for $300 \geqslant C_{BET} \geqslant 100$. Fresh Ni/Al_2O_3 (●), reduced Ni/Al_2O_3 (O), γ-Al_2O_3 (x).

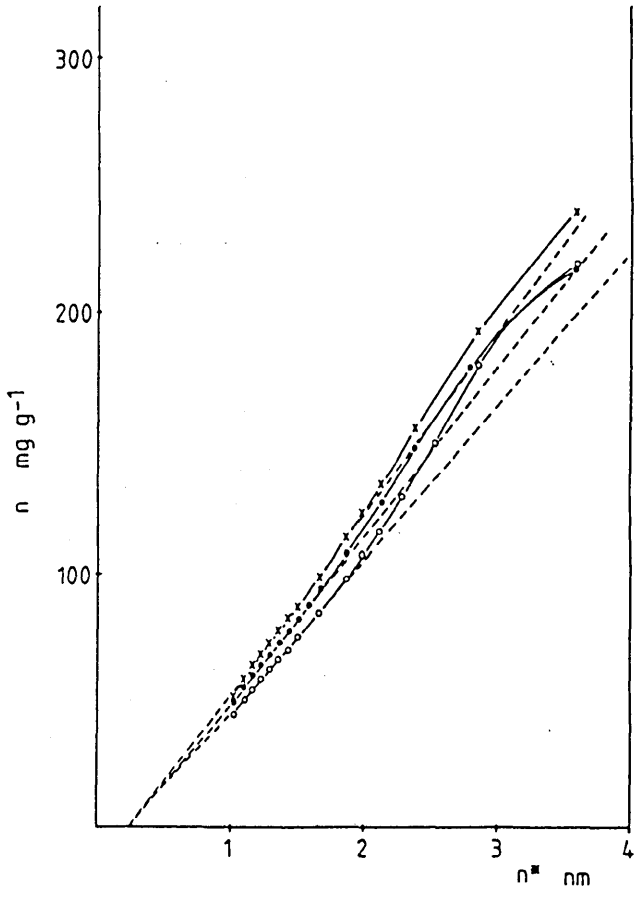

FIGURE 5.4

Plot n vs n* using the standard isotherm for $C_{BET} \geqslant 300$. Fresh Ni/Al_2O_3 (●), reduced Ni/Al_2O_3 (O), γ-Al_2O_3 (x).

$$n^* = \frac{v}{v_m} \qquad (5.1)$$

Since some C_{BET} values determined before were above 300, the standard isotherm corresponding to C_{BET} values greater than 300, n_1^*, was used to test the sensitivity of this method.

The results are shown in figure 5.4. The two Ni/Al_2O_3 samples plotted correspond to the samples having $C_{BET} \gg 1000$.

The plots of the three samples give straight lines at low relative pressures, but the intercepts with the ordinate have negative values. Therefore the reference isotherm used was not appropriate, and a standard isotherm with a lower C_{BET} value should have been used, as was done in figure 5.3.

These results support the view that the high values for C_{BET} found in some samples represent either variations in the fitting of the data to the BET equation or that very small experimental errors which have very little effect on the monolayer capacity have a strong effect on the C_{BET}.

The C_{BET} has to be calculated based on several determinations of N_2 adsorption on different samples of the same material to avoid wrong conclusions about the adsorbate-adsorbent interactions.

The n* method is very useful and complementary to the BET method. Using the appropriate standard isotherm the surface areas determined by this method should be in good agreement with the ones determined by the BET equation. It provides information as to the correct range of the C_{BET} values. It gives an assessment of the porosity of the sample

explaining the deviations from linearity at high relative pressures ($P/P_o > 0.4$) in the same way as the t and α_s methods; this subject is treated in the following section.

5.2 Pore size distribution (PSD)

The pore size distribution of a porous solid can be calculated from the capillary condensation region of its isotherm. Information about the pores can be obtained from the comparison of the N_2 adsorption with a reference isotherm and plotted in the way it is given in figure 5.3. The resultant n-vs-n* plot shows deviations from linearity which can be explained in the same way as the deviations from linearity shown when the t and α_s isotherms are used.

Figure 5.3 shows that three isotherms present upward deviations indicating the presence of capillary condensation in the pores of the adsorbent characteristic of cylinder-shaped pores, 'ink-bottle' pores or spheroidal cavities (95,158). If the deviations were downwards it would have meant that micropores or slit-shaped pores were present in the solid.

Deviations from linearity start at about a value of n* = 1.51 which corresponds to $P/P_o = 0.4$. This point belongs to the region where condensation of a liquid-like phase of adsorbate starts to occur in the mesopores.

The full type IV isotherms for the fresh Ni/Al_2O_3, reduced Ni_2/Al_2O_3, and γ-Al_2O_3 samples which were plotted in figure 5.3 are given in figures 5.5, 5.6 and 5.7.

From the inspection of the adsorption isotherm only it would appear as if they were type II isotherms, but when the adsorption-desorption curves are considered type IV are revealed. Following de

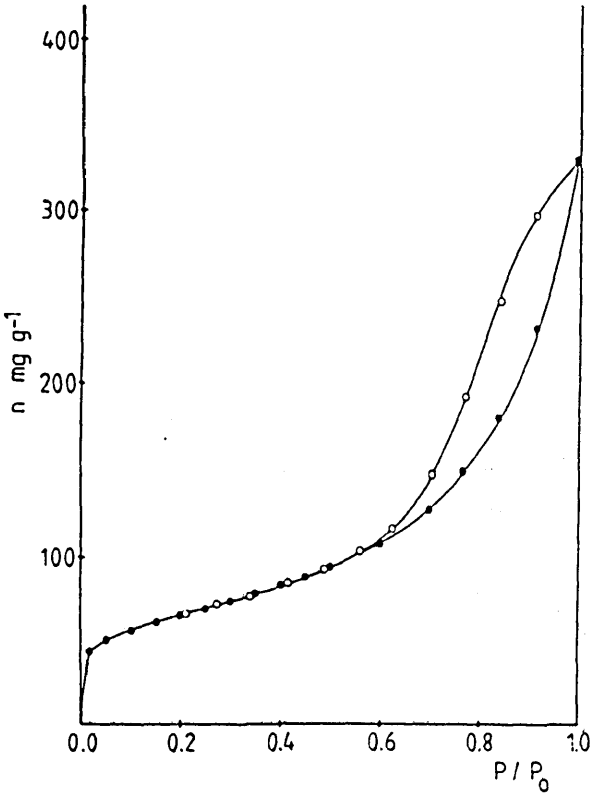

FIGURE 5.5

Nitrogen adsorption/desorption isotherm for fresh Ni/Al_2O_3.

Adsorption (●), desorption (O).

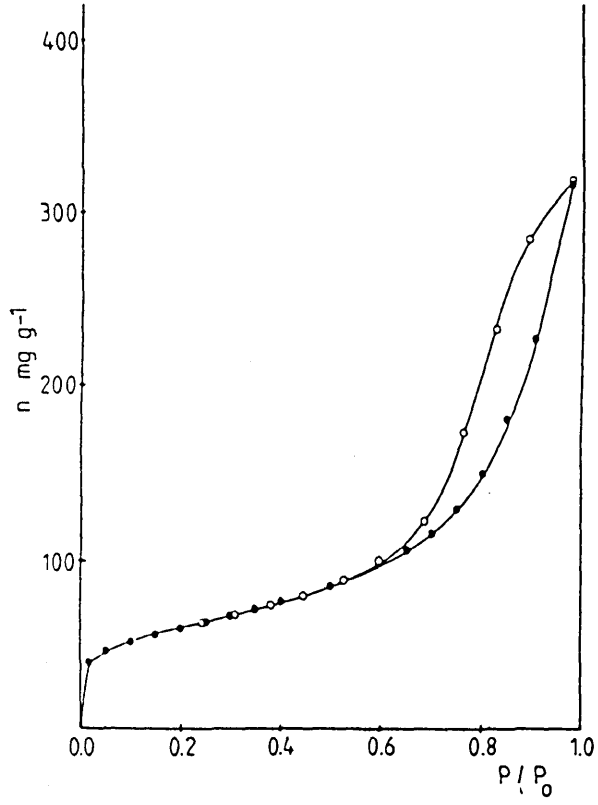

FIGURE 5.6

Nitrogen adsorption/desorption isotherm for reduced Ni/Al_2O_3.

Adsorption (●), desorption (O).

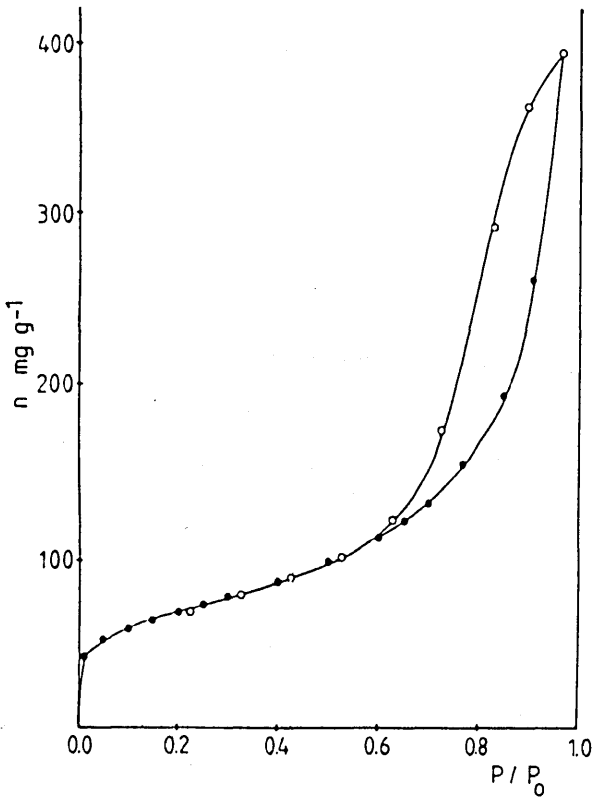

FIGURE 5.7

Nitrogen adsorption/desorption isotherm for γ-Al_2O_3.

Adsorption (●), desorption (O).

Boer's classification (103) the hysteresis loop is designated type A. This could represent a porous material with cylinder-shaped pores of rather constant cross section.

The mesopore volume Vp_G can be determined from the adsorption isotherm. It is usually taken at the point where the isotherm shows a defined plateau in the vicinity of $P/P_o = 1$ (95); at this point complete mesopore filling may be assumed. In the cases where the adsorption isotherms do not show this plateau but they are asymptotical near saturation point, the mesopore volume is thus assessed either by taking the upper closing point of the hysteresis loop, or if the hysteresis loop is not fully developed by following Gurtvisch's rule defining the Vp_G as the volume of adsorbate taken up at a relative pressure close to the saturation point, which may be $P/P_o = 0.95$, or $P/P_o = 0.98$ (95). The isotherms in figures 5.5 - 5.7 suggest the application of the Gurtvisch's rule at $P/P_o = 0.98$. The N_2 uptakes at this point are: 304 mg/g for fresh Ni/Al_2O_3, 317 mg/g for the reduced Ni/Al_2O_3, and 393 mg/g (at $P/P_o = 0.97$) for γ-Al_2O_3. Converted to liquid volumes result: 0.38 cm^3/g, 0.39 cm^3/g and 0.49 cm^3/g respectively, with an experimental uncertainty of ± 0.005 cm^3/g.

The application of this rule is rather arbitrary especially taking into account the shape of the adsorption isotherm. If, for instance, it had been decided to take the volumes at $P/P_o = 0.95$ they would have been: 0.33 cm^3/g, 0.34 cm^3/g and 0.44 cm^3/g respectively.

PSD calculations were made following the procedure of Orr and Dalla Valle (159) as outlined in Gregg and Sing (102). The procedure involves the use of the Kelvin equation (3.6):

$$\ln \frac{P}{P_o} = - \frac{2V_L \gamma}{RT} \frac{1}{r_k} \cos \phi$$

which relates the relative pressure P/P_o of condensed liquid to the radius of an open ended cylindrical capillary. Substituting the values of $\gamma = 8.72\ mNm^{-1}$; $V_L = 34.68\ cm^3\ mol^{-1}$, $\phi = 0$, and $T = 77.4K$ the equation is transformed to:

$$r_k(\text{Å}) = \frac{4.078}{\log(P_o/P)} \qquad (5.2)$$

The use of $\phi = 0$ implies that for cylindrical capillaries the meniscus is hemispherical.

As it stands the Kelvin equation relates the 'core' size to the relative pressure. To calculate the pore size it is necessary to know the thickness of the adsorbed film which varies according to the relative pressure.

From the several correlations (160-162) and experimental values (102,110) available it was decided to use the Halsey correlation (160) due to its simplicity, the accurate results obtained with it (108) and its general use in the literature:

$$t = \sigma \left[\frac{5}{\ln(P_o/P)}\right]^{1/3} \quad (\text{Å}) \qquad (5.3)$$

with a value of 3.54 Å for the effective cross-sectional diameter of N_2, σ, as recommended by de Boer (103), and used by Lippens et al. (163).

Calculation procedure

The calculations are based on an imaginary emptying of the pores by the stepwise lowering of the pressure from the point where the mesopore system is taken as completely filled, normally this is set at $P/P_o = 0.95$.

The calculation is as follows:

i) The desorption (or adsorption) process is divided into a number of standard steps either of relative pressure, or of pore radius. The use of relative pressure steps was chosen,

ii) the amount given up (or adsorbed) during each step is converted into a liquid volume δv_i using the N_2 liquid density,

iii) calculate the contribution of δv_f due to the thinning of the adsorbed film by: $\delta v_f = 0.1 \times \delta v_i \times \Sigma \delta A_p$

where $\Sigma \delta Ap$ is the accumulated surface area up to the step i-1. The equation is obtained assuming a model of pore shape, in this case a cylindrical pore,

iv) obtain the core volume δv_k associated with the mean core radius $\bar{r}_k$ by subtraction: $\delta v_k = \delta v_i - \delta v_f$, (5.4).

v) convert the core volume into the corresponding volume δv_p, and the core radius into the corresponding mean pore radius $\bar{r}_p$ with the aid of the relations:

$$r_p = r_k + t \qquad (5.5)$$

$$Q = \left(\frac{\bar{r}_{p_i}}{\bar{r}_{p_i} - t_i}\right)^2 \qquad (5.6)$$

and $$\delta v_p = Q\ \delta v_k \qquad (5.7)$$

vi) finally the area of the particular group of pores is calculated from the volume and the radius of the pore group using the geometry of the cylinder:

$$\delta A_p = 2\ \frac{\delta v_p}{\bar{r}_p} \qquad (5.8)$$

The total area of multilayer which is thinned down during any step, $\Sigma\ \delta A_p$, is obtained by summing the δA_p contributions in all the previous pore groups and the present one.

PSD's for fresh Ni/Al_2O_3, reduced Ni/Al_2O_3 and γ-Al_2O_3 using the desorption branch of the isotherm are shown in figure 5.8.

The plot shows that the pore volume distribution function $\delta v_p/\delta r_p$ peaks at $\bar{r}_p$ = 47Å for the reduced Ni/Al_2O_3 and Al_2O_3 samples, whereas for the fresh Ni/Al_2O_3 $\bar{r}_p$ = 38Å. The maximum value of the distribution of Al_2O_3 is higher than those of the two nickel/alumina determinations. The curve of the reduced Ni/Al_2O_3 is slightly displaced towards higher radius compared to that of fresh Ni/Al_2O_3.

It can also be noticed that the pore volume (area under the curve) of the alumina sample is larger than those of the two nickel/alumina samples. When the metal is loaded onto the support the pore volume is reduced; the contribution of certain pore sizes to the total pore volume is decreased by deposition of the metal in those pores which in extreme circumstances can be blocked. The pore volumes of the fresh

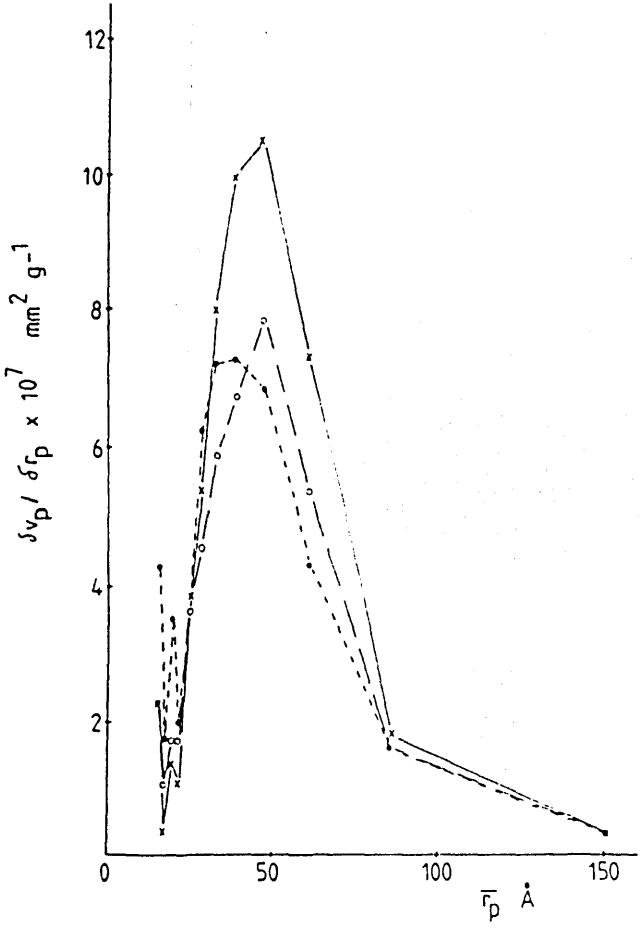

FIGURE 5.8

Pore size distribution from desorption isotherms. Fresh Ni/Al_2O_3 (●), reduced Ni/Al_2O_3 (O), γ-Al_2O_3 (x).

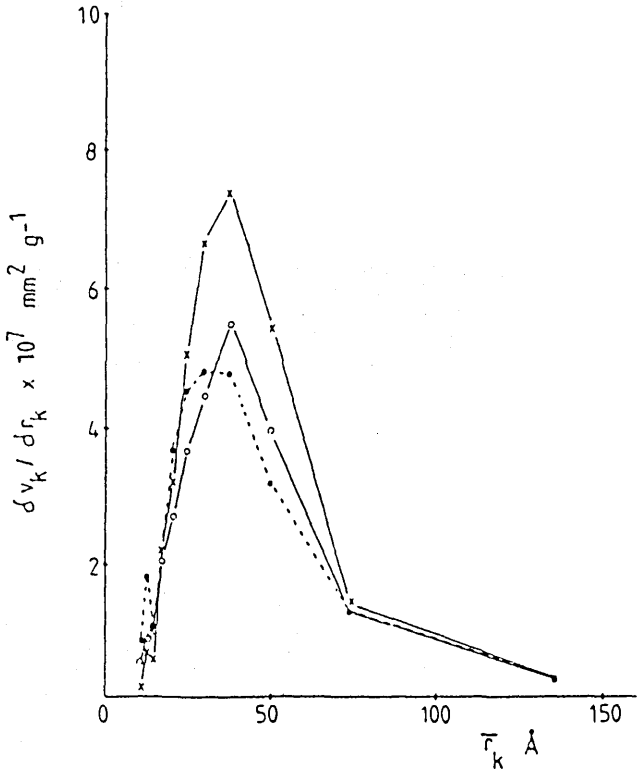

FIGURE 5.9

Core size distribution from desorption isotherms. Fresh Ni/Al_2O_3 (●), reduced Ni/Al_2O_3 (O), γ-Al_2O_3 (x).

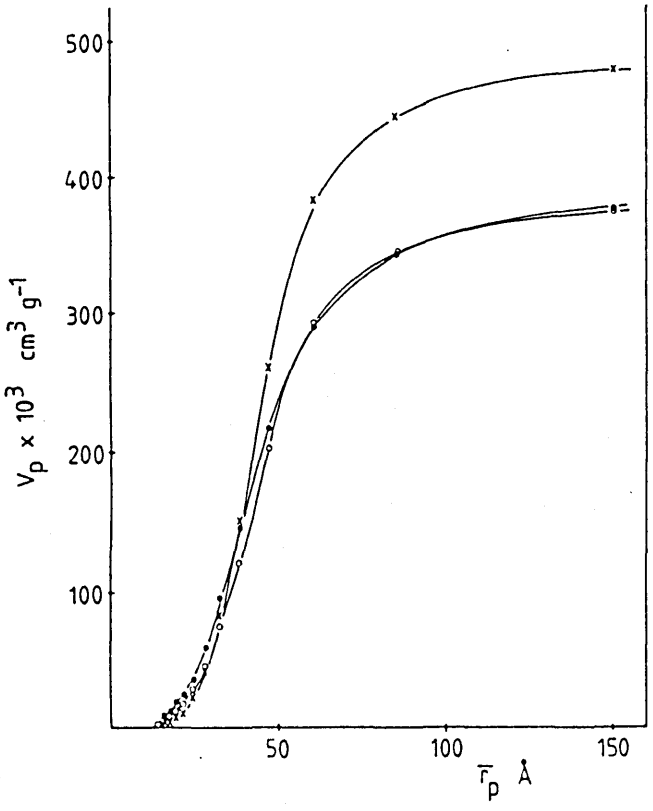

FIGURE 5.10

Cumulative pore volume distribution from desorption isotherms. Fresh Ni/Al_2O_3 (●), reduced Ni/Al_2O_3 (O), γ-Al_2O_3 (x).

and reduced Ni/Al_2O_3 catalysts appear to be the same, and it is shown to be comparing the values in Table 5.3. The PSD of the reduced catalyst is slightly shifted towards higher pore radius, a fact that could be caused by sintering of the metal particles during reduction; these particles would hinder the access to small-size pores.

Table 5.3 Summary of Results from PSD Calculations from the Desorption Branch

Sample	Peak $\bar{r}_p$ Å	$A_{p_{cum}}$ m^2g^{-1}	$V_{p_{cum}}$ cm^3g^{-1}	r_p (calculated) Å
Ni/Al_2O_3 (Fresh)	38	175	0.40	43
Ni/Al_2O_3 (Reduced)	47	165	0.39	46
γ-Al_2O_3	47	203	0.49	49

$A_{p_{cum}}$ is the cummulative surface area as obtained from the PSD calculations. Accuracy of $\pm$ $2m^2g^{-1}$

$V_{p_{cum}}$ is the cummulative pore volume of the sample, with an accuracy of ± 0.005 cm^3g^{-1}

r_p is the mean pore radius calculated by the equation $rp = 2\frac{V_p}{A_{BET}}$. The area used in this calculation was the BET surface area rather than $A_{p_{cum}}$, as it is recommended (84,95,102).

The importance of the thickness correction is obvious when the plots in Figure 5.8 are compared to those in Figure 5.9. In the latter the curves correspond to the distribution of core size $\frac{\delta v_k}{\delta r_k}$ obtained when the size is determined by the Kelvin equation only. Although the curves retain the same shape and general relations between them there is a general shift to smaller pore radius. The curves peak at lower maxima therefore the "core" volumes are smaller than the pore volumes. The peak radius is 37Å for the 3 samples although the fresh Ni/Al_2O_3 shows a plateau between 37Å and 29Å. Figure 5.10 shows the cumulative pore volume distribution for the three samples.

The previous calculations were carried out using the desorption branch of the isotherm. Many researchers however favour the use of the adsorption branch (85,95,104,164,165).

Pore size distributions were calculated using the adsorption branch and are shown in Figure 5.11. There are marked differences between these curves and those obtained from the desorption isotherm. The curves are broader, they seem to 'peak' at lower pore radius but the 'peaks' are less defined than those shown in Figure 5.8. Below 45Å the pore volume of the fresh Ni/Al_2O_3 is higher than those of the γ-Al_2O_3 and reduced Ni/Al_2O_3; they 'peak' at 16Å (fresh Ni/Al_2O_3 and γ-Al_2O_3) and 14Å (reduced Ni/Al_2O_3), values at which the use of the Kelvin equation does not seem fully justified (165).

In Figure 5.12 the cumulative pore distributions resulting from

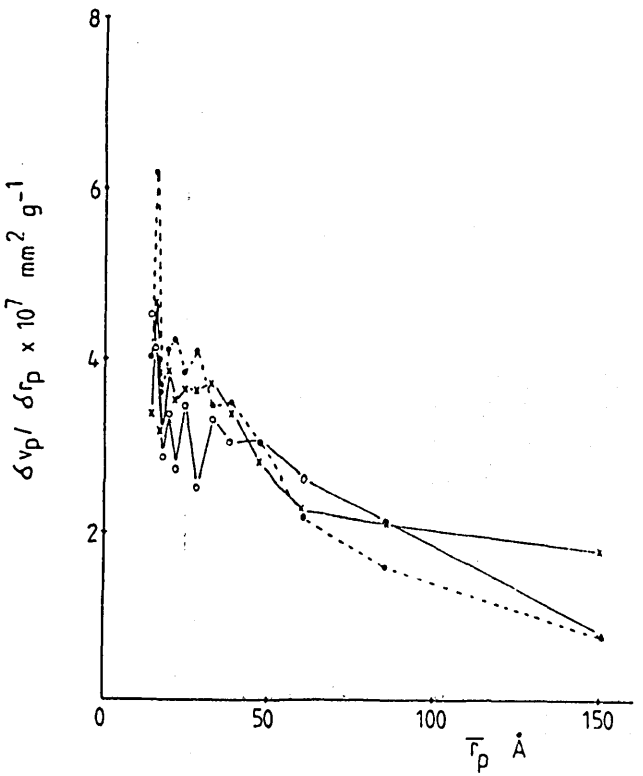

FIGURE 5.11

Pore size distribution from adsorption isotherms. Fresh Ni/Al_2O_3 (●), reduced Ni/Al_2O_3 (O), γ-Al_2O_3 (x).

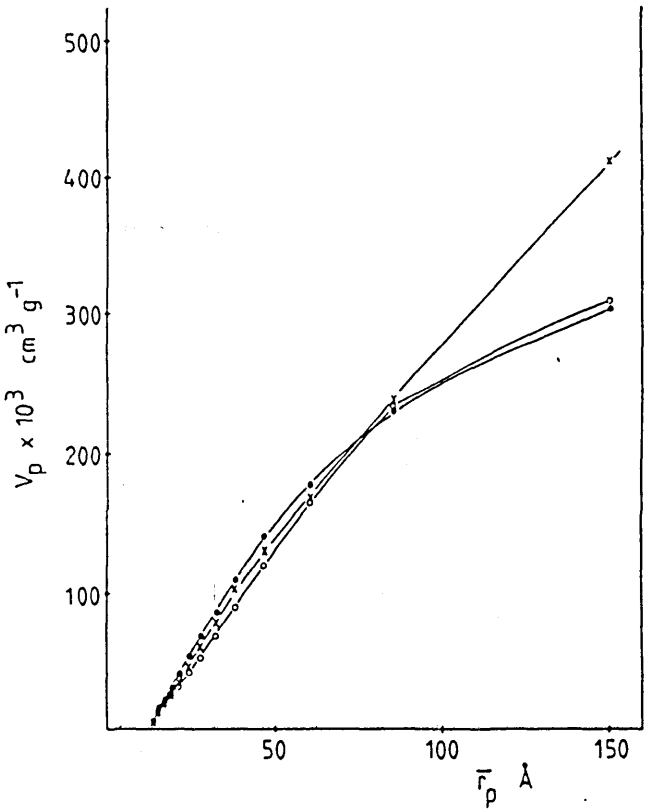

FIGURE 5.12

Cumulative pore volume distribution from adsorption isotherms. Fresh Ni/Al_2O_3 (●), reduced Ni/Al_2O_3 (O), γ-Al_2O_3 (x).

the use of the adsorption isotherm data are shown. The contribution to the pore volume of pores greater than 100Å is extremely high; this may be the cause of the low values of cumulative area. The results are summarized below.

Table 5.4 Results of PSD from the Adsorption Branch[a]

Sample	Peak $\bar{r}_p$ Å	$A_{p_{cum}}$ m^2g^{-1}	$V_{p_{cum}}$ cm^3g^{-1}	$\bar{r}_p$ calculated Å
Ni/Al_2O_3 (fresh)	16	140	0.38	41
Ni/Al_2O_3 (reduced)	14	132	0.37	44
γ-Al_2O_3	16	150	0.46	46

[a] $A_{p_{cum}}$ was determined with an accuracy of ±2.1 m^2g^{-1}; $V_{p_{cum}}$ is within ±0.006 cm^3g^{-1}.

It is noticeable the difference between the peak $\bar{r}_p$'s and the mean pore radius $\bar{r}_p$ calculated. As expected the cummulative areas are lower than those from the desorption isotherm; a trend followed by the pore volumes.

The calculation of the pore size distributions has been carried

out using certain assumptions regarding the model of pore, thickness correction and whether to use the adsorption or desorption branch of the isotherm.

For the pore model the simple cylindrical geometry was chosen. Among the factors that favour this selction are: the shape of the n-vs-n* plots in Figure 5.3 which indicate the presence of either cylindrical pores, "ink-bottle" pores or spheroidal cavities (95,158); simpler calculations than those of the packed-spheres model or "modelles" method which are rather cumbersome, predict similar PSD's and in the end produce no advantage (104,105).

The modified Halsey equation was employed for the evaluation of the thickness based on the study of Dollimore and Heal (108) who recommended either the Halsey equation or Shull's experimental values; the Halsey equation offers the advantage of fast calculations at any pressure ratio.

A more difficult matter to resolve is in the use of the adsorption or desorption branch of the isotherm. For a correct assessment of the pore distribution the whole set of data must be considered.

The results have shown that the distributions from the adsorption branch are broader than those from the desorption, and that the plots derived from the adsorption branch tend to peak at lower values of $\bar{r}_p$.

The adsorption-desorption isotherms suggest a type A hysteresis loop which according to deBoer may be caused by cylindrical pores. The n-vs-n* plots give upward deviations, and according to Lecloux (95) the desorption isotherm could give a better picture of the mesopore distribution. The values of the surface area and pore volume obtained

from the desorption branch, $A_{p_{cum}}$, $V_{p_{cum}}$, are in excellent agreement with those determined by the BET method A_{BET}, and the adsorption curve $-Vp_G-$. The results are unsatisfactory if the same comparisons are made using the estimates form the adsorption isotherm: the $A_{p_{cum}}$'s are smaller than the BET values for all 3 cases, so do the $V_{p_{cum}}$'s when compared to the V_{p_G}'s.

Everett (111) has argued that the reasonable agreement (20%) between mesopore areas derived by PSD's and surface areas using the BET equation may be due to some cancellation of the errors introduced rather than a true correspondence, and that desorption curves may be dominated by network effects which mask completely the true pore size distribution. Such effects can be identified by the study of hysteresis scanning curves, and if present the adsorption curve must be preferred.

However, considering the poor results obtained from the adsorption branch, and that the agreement found between the surface areas derived from measurements below the hysteresis region and those calculated from the PSD's using the desorption isotherm is good we can conclude that for the samples used in this study:

i) the pore size distributions are best described by the use of the desorption branch of the isotherm;

ii) the mesopore system is reasonably described by the cylindrical model;

iii) there is an excellent agreement between the surface areas determined by the BET method, the n* method and the PSD;

iv) the effect of metal content and reduction of the metallic

oxide precursor on the initial PSD of the support may be studied by the characterisation of the mesopore system through the N_2 adsorption-desorption isotherm.

5.3 Metal Area Determination

The determination of nickel metal areas is described in this section. The measurements were carried out using basically CO as titrant, but the potential use of N_2O was also investigated. In order to correctly evaluate the metal area of clean and sulphur-poisoned catalysts the effects of pressure, adsorption temperature, method of calculation of saturation coverage and sulphur presence were assessed.

5.3.1 Effect of pressure

Typical CO and N_2O adsorption curves can be seen in figures 5.13 to 5.16. Figures 5.13 and 5.14 show the adsorption of CO on NAT3 batch samples; in Figure 5.13 the adsorption was carried out at 77K, whereas in figure 5.14 the adsorption temperature was 195K. The chemisorption of N_2O at 195K and 273K is shown in figure 5.15 and figure 5.16 respectively for NAP samples. All the graphs show 3 curves that belong to the total (physical and chemical) adsorption, the physical adsorption and the difference of the two which corresponds to the chemisorption. It can be seen that for N_2O the adsorption uptakes are reported in mg/g instead of μmol/g. This is due to the fact that two species are responsible for the uptake: oxygen present as chemisorbed species and N_2O which is physically adsorbed. The only isotherm that can be converted to a μmol basis is the "difference" isotherm because this curve solely represents the amount chemisorbed.

Inspection of the curves reveals the extent of the pressure effect. When the physisorption is involved the amount of gas adsorbed

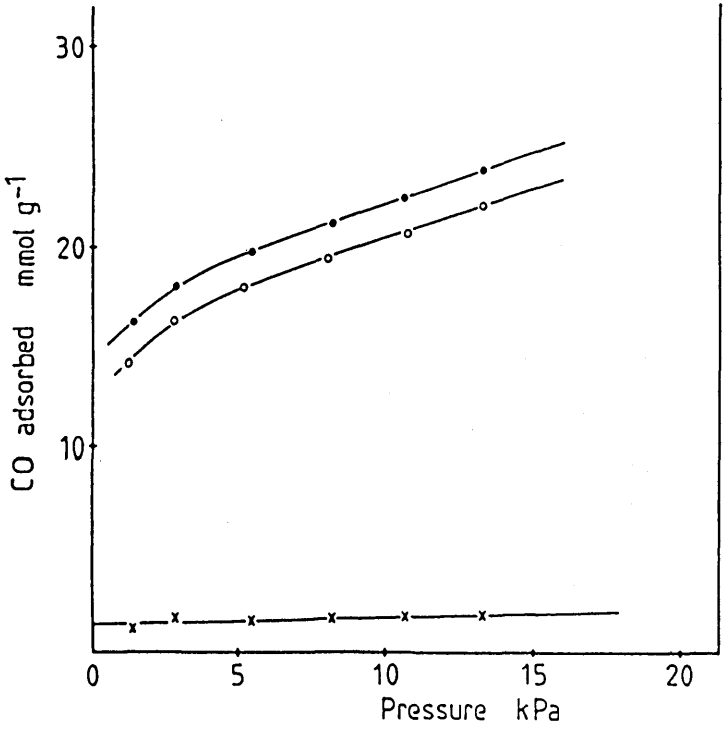

FIGURE 5.13

CO adsorption on Ni/Al_2O_3 (NAT3-3) at 77K. First isotherm (●), second isotherm (O), difference (x).

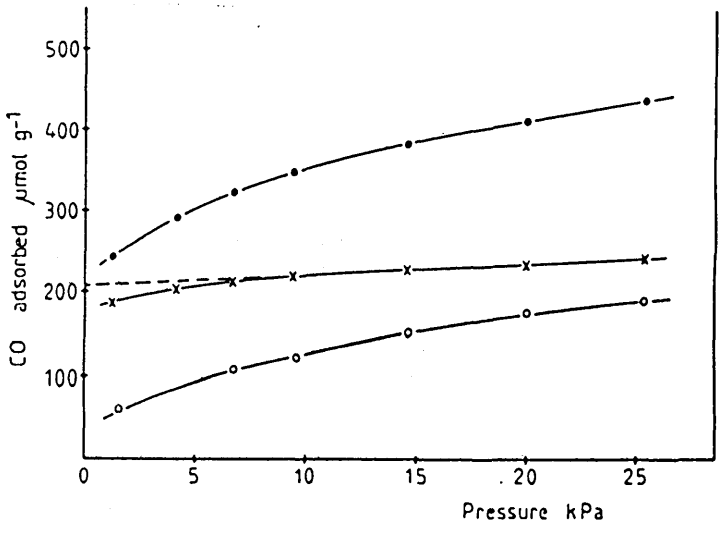

FIGURE 5.14

CO adsorption on Ni/Al_2O_3 (NAT3-38) at 195K. First isotherm (●), second isotherm (O), difference (x).

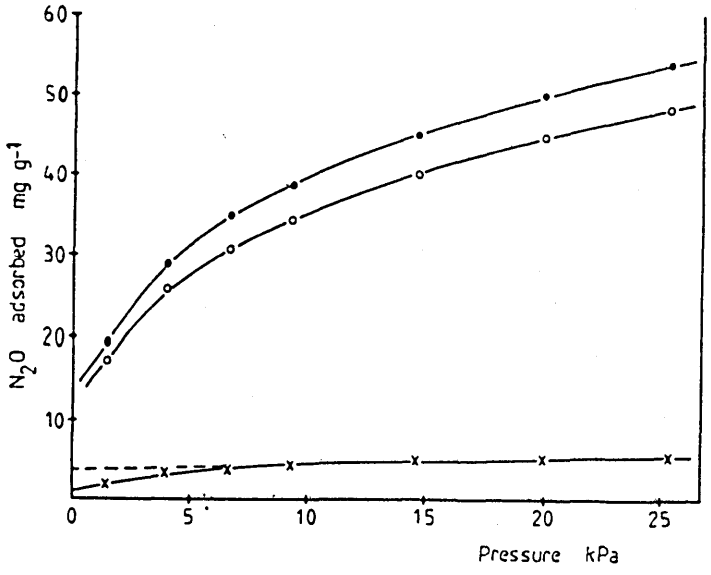

FIGURE 5.15

N_2O adsorption on Ni/Al_2O_3 (NAP-2) at 195K.
First isotherm (●), second isotherm (O), difference (x).

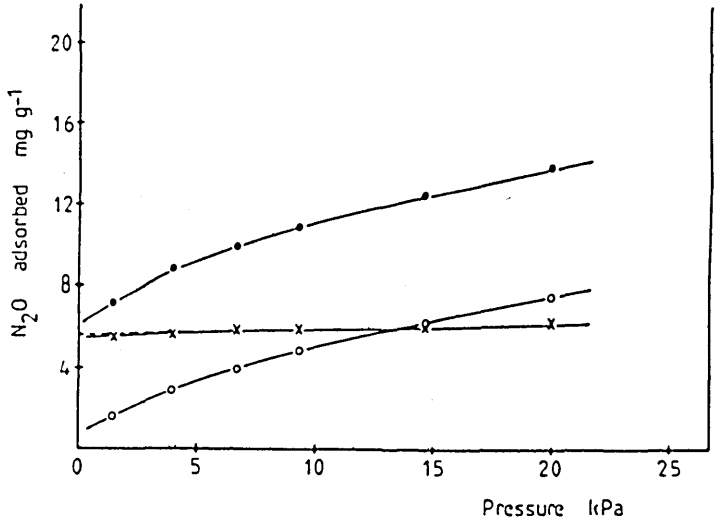

FIGURE 5.16

N_2O adsorption on Ni/Al_2O_3 (NAP-3) at 273K.
First isotherm (●), second isotherm (O), difference (x).

increases with pressure, as can be seen in the total and physical adsorption curves of each graph. The chemisorption curve is affected by the pressure but in a lesser degree; the effect being greater at pressure below 10kPa.

As described before in Chapter 3, one of the most common methods to determine the saturation coverage involves the extrapolation of the chemisorption isotherm to zero pressure and in that way eliminate any pressure effect; care has to be taken to identify the region from which the extrapolation is to be made. The results here shown suggest the extrapolation of the isotherm in the pressure region 10kPa-30kPa where it is linear and with almost zero slope. If lower values are taken the calculated intercept may be low and not represent the real saturation coverage.

It can also be said that methods in which the saturation coverage is determined by the adsorption uptake at 13.3kPa may give values in excess of saturation since the possibility of physical adsorption exists, unless the isotherm is independent of pressure.

In the case of CO adsorption the uptake increase as a function of pressure may involve not only physical adsorption but also the formation of more linear species which at high enough pressures may form carbonyl species as has been demonstrated by IR studies.

It seems that the extrapolation of the isotherm as outlined above represents the best estimate of the saturation coverage.

5.3.2 Effect of temperature

The adsorption of CO was studied at three different temperatures 77K, 195K, 273K; the N_2O adsorption was carried out at 195K and 273K only.

Typical CO adsorption at 77K is shown in Figure 5.13. The results at 195K are given in Figure 5.14, 5.17 and 5.18; whereas figures 5.19 and 5.20 show the adsorption at 273K. All these results were obtained for NAT3 samples. The adsorption of CO on NAP samples is given in figures 5.21 and 5.22 at temperatures of 195K and 273K.

It is demonstrated that as the temperature increases the physical adsorption decreases.

At 77K the adsorption uptakes are very high. They are about 5 times higher than the uptakes at 195K. The contribution of the CO physisorption is high (boiling point of CO: 81.5K). The amount of chemisorbed titrant which is determined by the subtraction of the second isotherm from the first (total) isotherm is very susceptible to errors since it involves the small difference between two large quantities. The use of this temperature for the chemisorption of CO is not recommended; in this case after few initial results it was abandoned.

The adsorption of CO at 273K on a freshly reduced NAT3 sample is shown in figure 5.19; after reduction treatment with H_2 at 773K for 8h the determination was repeated, the result is shown in figure 5.20. It can be noticed that physical adsorption is very small as shown by the second isotherm in both graphs. The reproducibility however is poor, while the first determination gave a saturation coverage of 102μmol/g, the second nearly doubled it. It should also be mentioned that during the intermediate evacuation between first and second isotherms the weight of the sample fell below the initial weight before adsorption, indication that the sample lost weight through nickel carbonyl formation. This is in accordance to results in the literature that

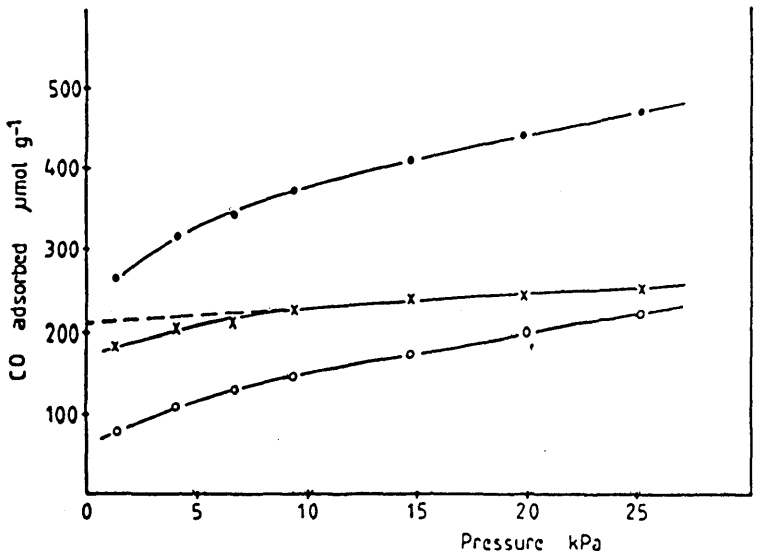

FIGURE 5.17

CO adsorption on Ni/Al_2O_3 (NAT3-53) at 195K.
First isotherm (●), second isotherm (O), difference (x).

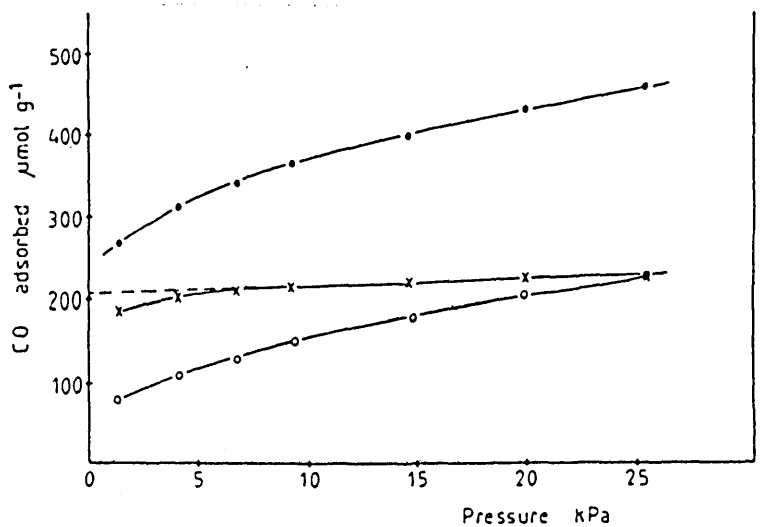

FIGURE 5.18

CO adsorption on Ni/Al_2O_3 (NAT3-54A) at 195K.
First isotherm (●), second isotherm (O), difference (x).

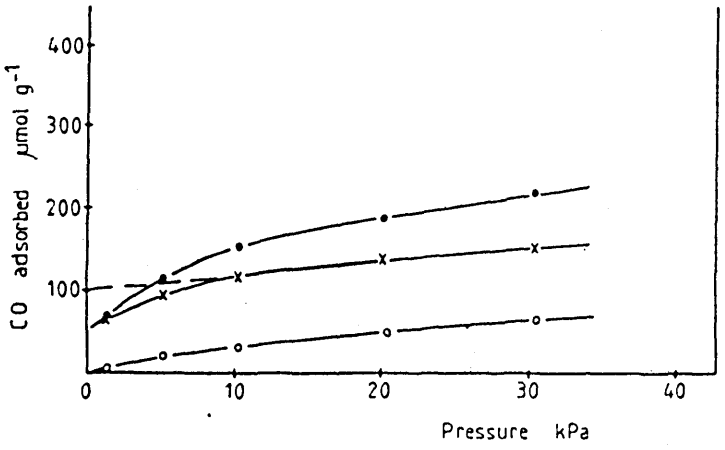

FIGURE 5.19

CO adsorption on Ni/Al_2O_3 (NAT3-6) at 273K.
First isotherm (●), second isotherm (O), difference (x).

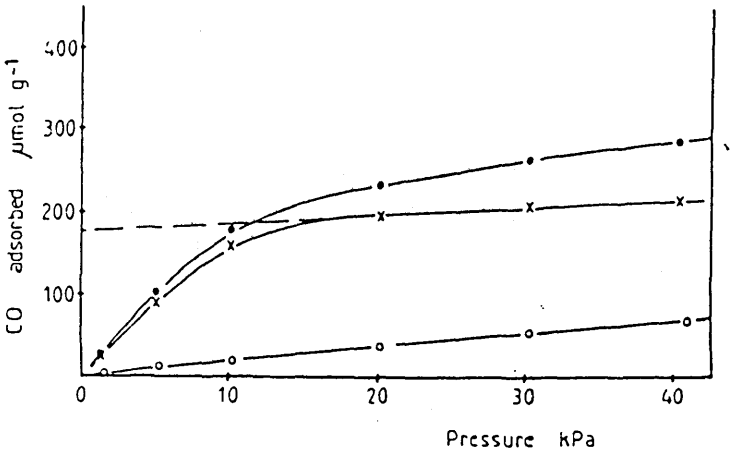

FIGURE 5.20

CO adsorption on Ni/Al_2O_3 (NAT3-6) at 273K.
First isotherm (●), second isotherm (O), difference (x).

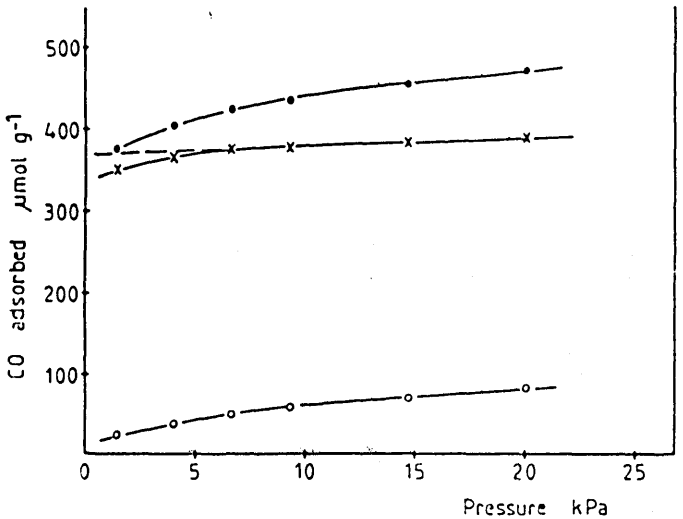

FIGURE 5.21

CO adsorption on Ni/Al_2O_3 (NAP-7) at 273K.
First isotherm (●), second isotherm (O), difference (x).

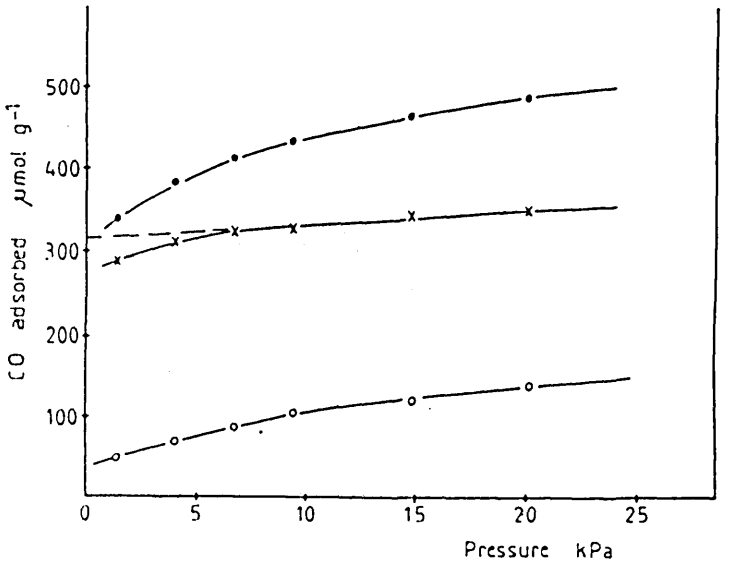

FIGURE 5.22

CO adsorption on Ni/Al_2O_3 (NAP-6) at 195K.
First isotherm (●), second isotherm (O), difference (x).

nickel carbonyl is formed at 273K (144).

The CO adsorption results on NAP samples at 273K were more reliable. Figure 5.21 shows that the total adsorption was high, and the physical adsorption contribution was small. The reproducibility was very good, with an error of 5% in the determinations. It is possible then that the method of catalyst preparation has an important role on the CO adsorption behaviour especially at temperatures where volatile products may be formed. Despite the low physisorption values, the fact that after following the same procedure disimilar results were obtained for the two sample batches (NAT3 and NAP), shows how unreliable the measurement of nickel area by CO adsorption at 273K is.

Adsorption results obtained at 195K are shown in Figures 5.14, 5.17 and 5.18 for NAT3 samples, those on NAP are shown in figure 5.22. Although the contribution of the weak adsorption is still high it does not reach the levels of the adsorption at 77K. The reproducibility was good; the error in the determination was less than 8%. During intermediate evacuation the weight loss was due to the physically adsorbed material only; there were no indications that volatile carbonyl compound was being formed, neither has it been reported in the literature at this temperature.

Comparing the adsorption on NAP samples at this temperature with that at 273K, the saturation coverage increases as the temperature is increased. This could mean that the percentage of linearly bonded CO has increased with temperature either replacing bridge bonded molecules or adsorbing on top of them forming sub-carbonyl species.

Bartholomew (119) has recommeded the use of 273K as the temperature of adsorption if CO is used based on the low physisorption

and the failure to detect $Ni(CO)_4$ in the vapour phase. Srinivasan and Krishnaswami (144) reported carbonyl presence at this temperature. Our results support the view that the nickel carbonyl may be formed at 273K and therefore must be avoided.

The adsorption at 195K offers the best compromise. It shows a high reversible contribution but on the other hand nickel carbonyl is not formed. Besides, the magnetization measurements of Primet (132) showed that as coverage increases the nature of the chemisorbed species is almost unchanged which results in a constant ratio of linear to bridge bonded species. Also at this temperature the results of several studies are in good agreement (119,125-128,132) with respect to the CO/Ni_s ratio of around 0.7-0.8 for samples with high nickel loading (~20wt%) and single crystal faces.

In view of these findings the temperature adopted as standard for the determination of Ni metal area by CO adsorption was 195K.

The N_2O results also show that as the temperature is increased the reversible adsorption uptake decreases. The data are presented in figures 5.15 and 5.16. The adsorption of N_2O at 195K has a similar behaviour to that of CO at 77K. The physisorption is very high (boiling point of N_2O: 185K), hence the irreversible adsorption can show high calculation errors. This is demonstrated; the error involved in the measurements at this temperature is of the order of 50%.

At 273K the reversible adsorption is lower although it is considerably high, the results however showed a good reproducibility with an error of 6%. The weight decrease during evacuation was equal to the physical adsorption at both temperatures.

The irreversible adsorption uptake increases with temperature. It

is possible that either the stoichiometry of the O-Ni bond changes or that at lower temperatures the number of nickel particles that have reacted with oxygen is smaller, as is the case with copper which shows an optimum temperature of adsorption at around 363K (138).

The use of N_2O adsorption at 273K is very reliable. The results are reproducible, the physical adsorption contribution despite being high can be accounted for and the errors that it introduces are low. Nevertheless it would be desirable to investigate the N_2O adsorption on Nickel at higher temperatures in order to find the optimum; optimum defined in terms of the lowest physisorption uptakes, the highest reproducibility of data and the avoiding of subsurface oxidation which is a latent complication.

5.3.3 Adsorption on the support

The adsorption of CO and N_2O on the γ-Al_2O_3 support was significant especially at low temperatures. The adsorption uptakes decreased with increasing temperature. The adsorption of CO on alumina at 195K and 273K is given in Figures 5.23 and 5.24. The amount of CO intrinsically adsorbed decreased as the temperature was increased from 17μmol/g at 195K to 4μmol/g at 273K.

The irreversibly adsorbed N_2O was higher at both temperatures than that of CO. Figure 5.25 and 5.26 show the adsorption on γ-Al_2O_3 at 195K and 273K. The total adsorption at 195K is very high and the error involved in the calculation of the N_2O held on the sample was high, about 16%. The reproducibility was much better at 273K, error of ~6%. As expected the total adsorption is still high, of the same order as that of the nickel alumina samples, but the amount physisorbed can be easily accounted for and the N_2O intrinsically held by the support is

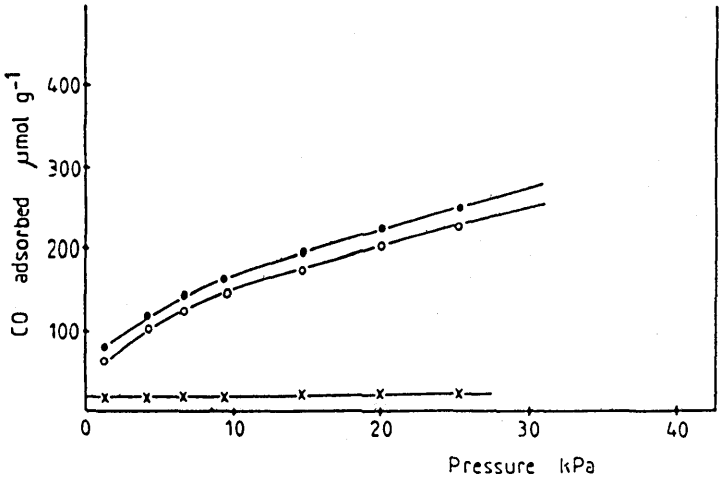

FIGURE 5.23

CO adsorption on γ-Al_2O_3 (A1-20) at 195K.
First isotherm (●), second isotherm (O), difference (x).

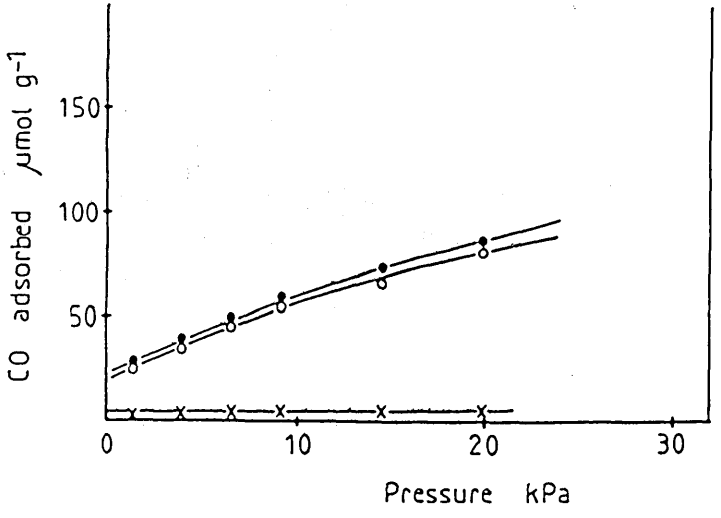

FIGURE 5.24

CO adsorption on γ-Al_2O_3 (A1-40) at 273K.
First isotherm (●), second isotherm (O), difference (x).

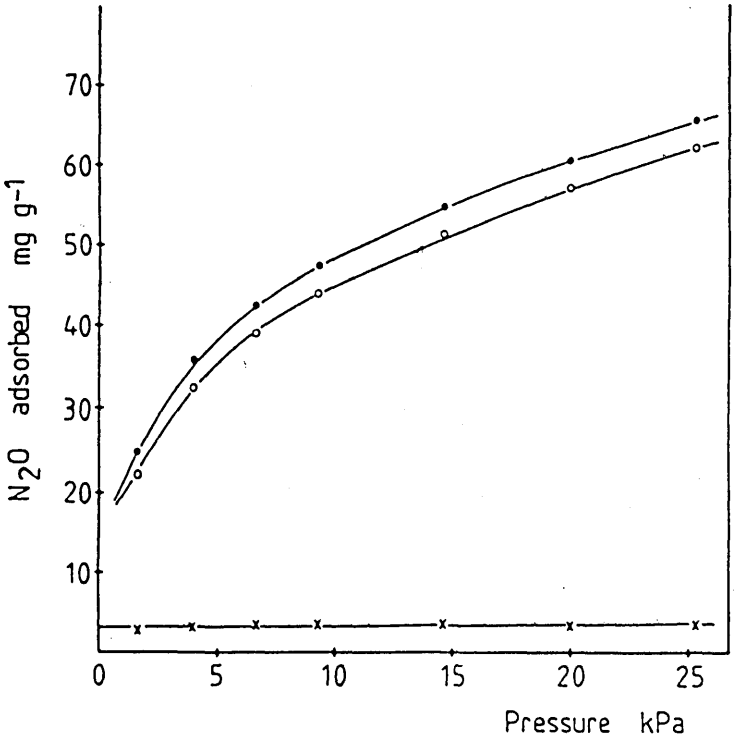

FIGURE 5.25

N_2O adsorption on γ-Al_2O_3 (A11-1) at 195K.
First isotherm (●), second isotherm (O), difference (x).

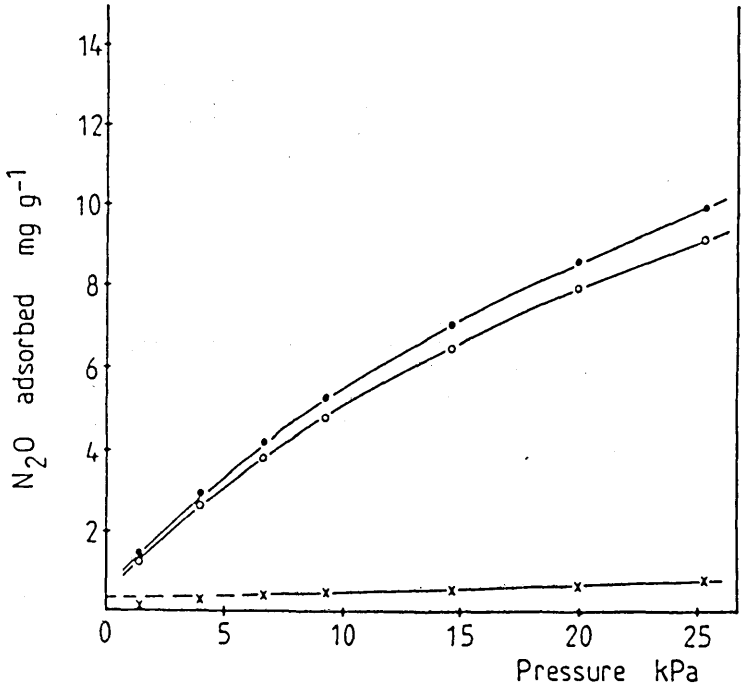

FIGURE 5.26

N_2O adsorption on γ-Al_2O_3 (A11-2) at 273K.
First isotherm (●), second isotherm (O), difference (x).

determined more accurately.

5.3.4 Method of saturation coverage determination

The survey of the literature on the monolayer coverage determination revealed the existence of several methods for the calculation of the saturation coverage.

It was found that for the calculation it is necessary to evaluate the chemical and physical adsorption on the metal as well as the contribution of the support.

It was shown that in the case where the isotherm is pressure dependent the extrapolation of the linear region to zero pressure gives the best estimate of the saturation coverage. This procedure was involved in the determination of the coverage, for which two methods of calculation were tested in order to find out how best the chemisorbed amount is evaluated.

The first method, method A, consisted of:

i) determination of the first, total isotherm which accounts for the physical and chemical adsorption on the catalyst as a function of pressure;

ii) the system was evacuated for 20 minutes at adsoprtion temperature and a second isotherm was obtained, this isotherm accounts for the weak adsorption on the catalyst;

iii) the difference of the two isotherms was obtained and plotted along with the other two as a function of pressure. This difference represents the material chemisorbed on the nickel and the support.

iv) The linear part of this chemisorption isotherm above 10kPa was extrapolated to zero pressure. The intercept to the ordinate axis gave the saturation coverage after correction for chemisorption on the

support, chemisorption which was determined following the same procedure.

The second method, method B, could be used as follows:

i) The 1st total isotherm is determined;

ii) the total isotherm is determined on an alumina sample.

iii) The difference of the two total isotherms is obtained and plotted;

iv) the linear part of the isotherm between 10kPa and 30kPa is extrapolated to zero pressure, the uptake at this pressure is corrected for chemisorption on the support as before.

A comparison of the results obtained for several samples with both methods was made and is given in Table 5.5 below. The results were obtained for the CO chemisorption.

Table 5.5 CO Chemisorption Uptakes Obtained by Methods A and B at 195K

Sample	CO Uptake Method A µmol/g	CO Uptake Method B µmol/g
NAT3-38	193	172
NAT3-49	183	178
NAT3-50A	213	233
NAT3-51	208	238
NAT3-53	196	195
NAT3-54A	192	190
NAT3-55B	198	224
NAT3-56	220	242
NAT3-57	200	212
NAT3-58	220	237
AVERAGE	202	212

It is noticeable that with method B the results are more scattered than with method A. For some samples the uptake determined by method B is smaller than with method A, but for the majority it is higher.

On average the results obtained by method B are higher than by method A, with an error of 12.5% compared to 7% in method A calculations.

It can be explained as follows:

i) In method A the difference of the 1st and 2nd isotherms subtract all the weak interactions between CO and Ni, and CO and the support. In the intermediate evacuation between isotherms all the reversible or weak bonds are removed from the total adsorption. During the second adsorption isotherm only those weak bonds are formed. The subtraction of the two isotherms gives the amount due to strong adsorption bonds, bridge and linear bonded species.

ii) Method B involves the difference of the total uptakes on the supported Ni catalyst and on the support. The adsorption on the support is basically physisorption. If at any pressure the adsorption involves the formation of Nickel subcarbonyl compounds, these modes of adsorption are not taken into account when the CO held in the support is subtracted.

If the isotherm depends strongly on pressure, the 2nd isotherm on the catalyst may be higher than the total (1st) isotherm on the support. Hence the resulting difference in method B is higher than in method A.

Values obtained with method A are more reliable and represent better estimates of the chemisorption of CO (113,119). This method must be preferred.

The results of the saturation coverages following method A are reported in table 5.6. This table contains the chemisorption uptakes of CO and N_2O at two temperatures and for the two catalysts used NAT3 and NAP.

Table 5.6 Chemisorption Uptakes of CO and N_2O

Sample	Adsorption Temperature K	CO Coverage µmol/g	N_2O Coverage* µmol/g
γ-Al_2O_3	195	17 ±2	90 ±14
γ-Al_2O_3	273	4 ±1	10 ±1
NAT3 (20% Ni/Al_2O_3)	195	204 ±15	-
NAP (20% Ni/Al_2O_3)	195	303 ±26	80 ±40
NAP (20% Ni/Al_2O_3)	273	356 ±13	176 ±12

* The coverage is given as µmol of oxygen per gram of catalyst since only oxygen is adsorbed

The adsorption amount on the support decreases as the temperature increases. The amount of CO irreversibly adsorbed is negligible at 273K compared to the adsorption on the nickel catalyst; even though is higher at 195K it does not represent a high contribution to that of the

nickel catalyst, and in some cases could be neglected (NAP samples). The N_2O however shows a very high uptake on the support at 195K, even higher than the chemisorption on the metal. The error in the calculation is about 16% for the adsorption on the support, and could reach 50% for the catalyst.

The adsorption of CO on the nickel catalyst exhibit an increase in the uptake as the temperature increases. The effect can be explained as an increase in the percentage of linear bonded species to that of the bridge bonded CO molecules. The ratio of the uptake at 273K to that at 195K is 1.17. This result agrees with some of the results of Bartholomew and Pannell (145) who observed an increase in the CO/Ni_s ratio with increasing the temperature from 195K to 294K. However the results of Primet et al (132) and some results published earlier by Bartholomew and Pannell (119) showed the opposite effect.

It is expected that as the temperature increases the number of linearly bonded CO molecules increases with a likely reduction of the bridge bonded species, and ultimately the formation of volatile nickel tetracarbonyl at high enough temperatures. Our results show this trend.

The metal area of the nickel catalysts can be calculated using the CO chemisorption uptakes.

Studies (125-128) have demonstrated that at 195K the saturation coverage corresponds to about $\theta = 0.7$ of a monolayer (with a monolayer defined as one CO molecule per nickel atom); this saturation coverage was determined to be 1.10×10^{19} CO molecules/m^2. Based on this value the areas obtained for the nickel catalysts are:

Sample	Area* m^2/g
NAT3 (20% Ni/Al_2O_3)	11.17 ± 0.82
NAP (20% Ni/Al_2O_3)	16.60 ± 1.42

* Based on the CO chemisorption at 195K.

As for the use of N_2O for the determination of nickel areas the results in table 5.6 show that there is a massive increase in the amount of N_2O chemisorbed on the nickel catalysts as the temperature increases. This effect may result from a change in the stoichiometry with temperature or from an increase in the number of occupied nickel sites as explained in the case of copper or both.

The saturation coverage of N_2O on copper involves a ratio of 2 Cu atoms per oxygen atom (138), whereas for silver the relation is 1:1 (139). Without changing the stoichiometry the coverage on Cu increases with increasing temperature, but above 373K subsurface oxidation may occur and bulk oxides can be formed. It is also possible that with increasing temperature the stoichiometry changes with an increasing reactivity of the metal particles. Unfortunately no evidence exists in the case of nickel, therefore all the conclusions will be based on the N_2O adsorption behaviour observed and its relation to that of CO.

The results show that the N_2O adsorption at 273K rather than at 195K should be preferred. The determination is more accurate, with

good reproducibility.

The ratio of chemisorption of N_2O at 273K to the chemisorption of CO at 195K is equal to 0.58 mol O_2/mol CO, or 1.16 O atom/CO molec, the latter being more significant because oxygen atoms rather than molecules are involved in the adsorption. The last result indicates that a ratio of 0.83 O atom/Ni atom exists at 273K which is equivalent to a stoichiometry of 1.21 Ni atom/O atom corresponding to a saturation coverage of 1.28×10^{19} Oxygen atoms/m^2.

The stoichiometry of 1.21 indicates that most of the oxygen atoms are linearly bonded to Ni atoms with a smaller percentage occupying 2 Ni atoms.

5.3.5 Effect of sulphur

The effect of the thiophene on the adsorption of CO on nickel catalysts was studied. It was carried out to assess the possibility of the determination of free nickel areas in sulphur-poisoned catalysts by CO adsorption. The experiments were performed on slightly-poisoned and heavily-poisoned Ni/Al_2O_3 samples. The results were as follows:

i) Slightly poisoned samples.

The results were obtained by adsorption of CO on samples poisoned during reduction by very small amounts of thiophene contained either in the feeding lines or in the reactor after a poisoning run.

Figures 5.27 and 5.28 show the adsorption of CO on slightly-poisoned samples of Ni/Al_2O_3 at 195K. The results presented in figure 5.27 correspond to a sample reduced with H_2 passing through the feeding line previously treated with a thiophene/H_2 stream. During the intermediate evacuation at 195K the sample lost more weight than it had taken up during adsorption, indication that Ni was being removed from

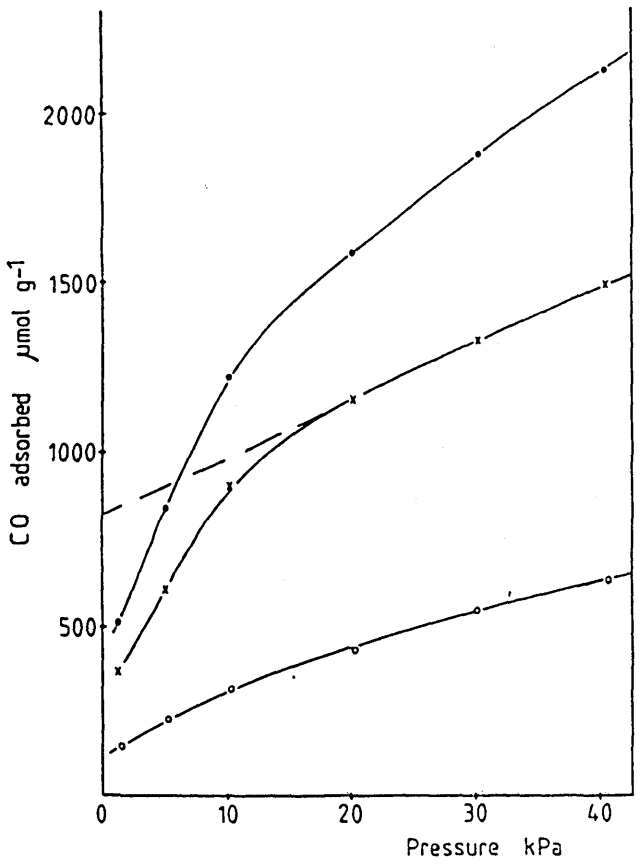

FIGURE 5.27

CO adsorption at 195K on a slightly poisoned Ni/Al_2O_3 (NAT3-11) sample. First isotherm (●), second isotherm (O), difference (x).

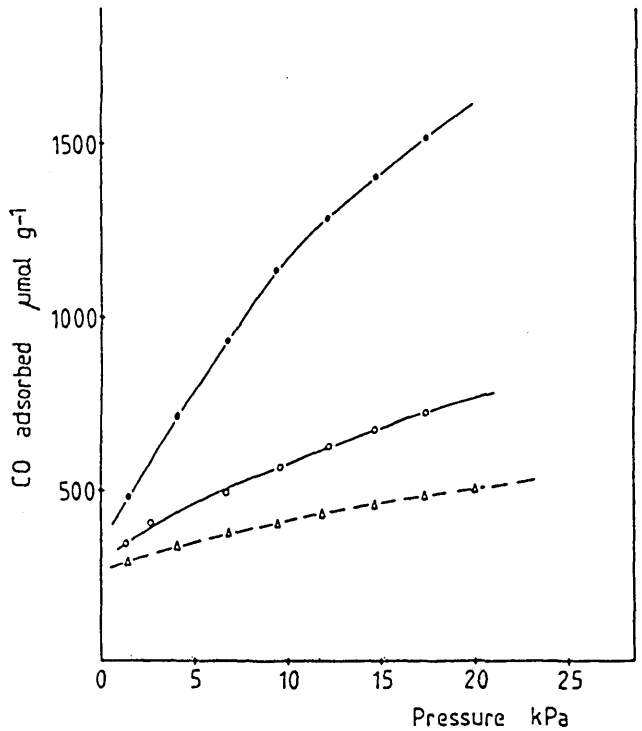

FIGURE 5.28

CO adsorption at 195K on two slightly poisoned Ni/Al_2O_3 samples: NAT3-18 (●), NAT3-24 (O), clean NAT3-25 (Δ) as comparison.

the catalyst at the adsorption temperature. The saturation coverage has a value of 830μmol/g, which is 4 times larger than that on clean samples. The total adsorption of CO on two slightly poisoned catalyst samples is compared to the adsorption on a clean sample in Figure 5.28.

It is clear that the adsorption uptake of CO on poisoned samples is higher than on clean samples, and that the uptake increases as the amount of sulphur in the sample increases. The sample NAT3 - 18 was treated during reduction with H_2 passing through the thiophene-containing feed lines, whereas the sample NAT3-24 was reduced with H_2 without cleaning the reactor after a poisoning experiment. The adsorption on clean NAT3-25 was used as reference. The thiophene content in the feeding lines was higher than the thiophene content in the dirty reactor, and it was reflected in the amount of CO adsorbed. At 15kPa the amount of CO adsorbed by NAT3-24 was 1.5 times that adsorbed by the clean sample NAT3-25; whereas on NAT3-18 it was 3 times as much as on NAT3-25. At pressures below 4kPa the adsorption uptake on poisoned samples took longer to reach equilibrium than on clean samples. As the CO pressure was increased the equilibration time was being reduced and at pressures of 10kPa and higher the time was the same as on clean samples. It should also be pointed out that the equilibration time was dependent on the amount of sulphur present on the sample, taking longer times with increasing amounts of sulphur. It was decided that subsequently the readings would be taken at the same times as employed on clean samples.

The increase in CO uptake with increasing sulphur content is in agreement with an increase in the percentage of linear bonded CO

molecules at the expense of bridge bonded species, and the formation of carbonyl compound. The four-fold increase in the CO uptake that was determined on the poisoned sample of figure 5.27 implies that the linear and bridge bonded species found on clean nickel samples are converted into subcarbonyl and carbonyl species when sulphur is present. The decrease in weight during intermediate evacuation to levels below the initial weight is an indication that the carbonyl species are removed from the surface with the consequent loss of nickel, in complete agreement with IR results (47,133,154,155). In fact cleaning of the balance after some CO adsorption experiments on poisoned samples revealed that nickel had been deposited on the light bulb of the balance.

Results of the CO adsorption on poisoned samples at 273K are presented in Figure 5.30. The sample was reduced with H_2 fed through the thiophene-treated tubing. In the first adsorption isotherm the uptake increases with increasing pressure, reaches a maximum, and after this point the weight decreases as the pressure is increased. The qualitative behaviour of the CO uptake with time is shown in figure 5.29. At 273K the weight uptake first increases, goes through a maximum and then decreases continuously, although the rate of weight loss decreases with time. This behaviour was observed in the entire pressure range used for the adsorption experiments. The weights reported in Figure 5.30 correspond to readings taken at the same periods as with the clean samples (40 min for the first adsorption point, 20 min for the others).

The results are consistent with the formation of nickel tetracarbonyl which is readily volatile at this temperature (the vapour

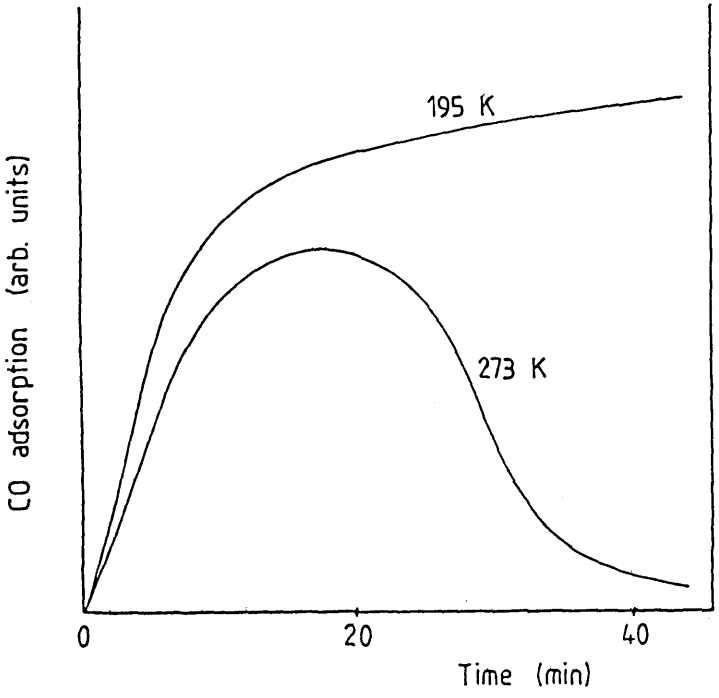

FIGURE 5.29

Qualitative diagram of the adsorption of CO on sulphur-poisoned nickel catalysts at pressures below 10 kPa.

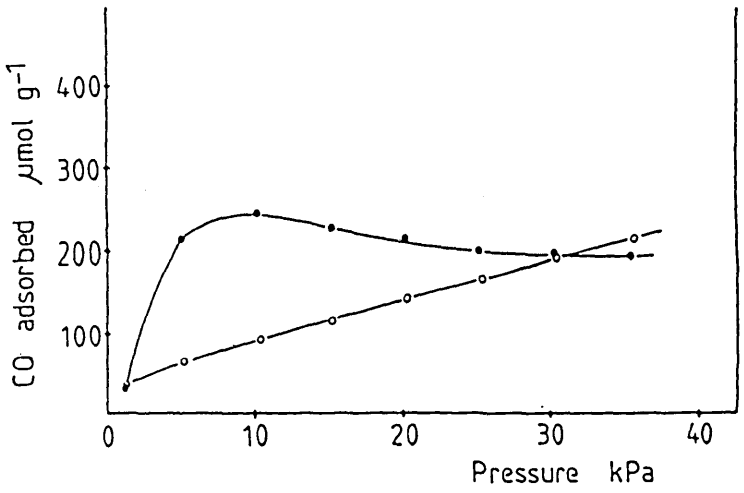

FIGURE 5.30

CO Adsorption at 273K on a slightly poisoned Ni/Al_2O_3 sample (NAT3-13). First isotherm (●), second isotherm (O), difference (x).

pressure of $Ni(CO)_4$ at 273K is 17.56kPa).

The adsorption behaviour can be described as a function of time as follows: at a given pressure CO is adsorbed on the catalyst surface and forms subcarbonyl and tetracarbonyl compounds ($Ni(CO)_x$, x = 2,3,4), the sample weight increases; as soon as the nickel tetracarbonyl is formed it starts to evaporate since there is no tetracarbonyl compound in the gas phase initially, and the sample weight decreases until the nickel tetracarbonyl on the catalyst is depleted or reaches equilibrium with its pressure in the gas, this can be seen in Figure 5.29.

As a function of pressure the adsorption is as follows: initially the CO is adsorbed and forms subcarbonyl and tetracarbonyl species; the tetracarbonyl evaporates and the subcarbonyl species remain on the catalyst. As the pressure is increased the subcarbonyl species are transformed into higher carbonyl compounds ($Ni(CO)_2 \xrightarrow{CO} Ni(CO)_3$; $Ni(CO)_3 \xrightarrow{CO} Ni(CO)_4$) resulting in the tetracarbonyl being transferred to the gas phase, the proportion of $Ni(CO)_3$ being increased and the sample weight increased; at high enough pressure as soon as the CO reaches the surface it is transformed to nickel tetracarbonyl so that the net effect is a weight loss due to nickel removal; this behaviour is shown in Figures 5.30 and 5.31.

The weakly adsorbed subcarbonyl species that remain on the catalyst are removed during the intermediate evacuation. The weight lost in this evacuation was observed to be higher than the weight gained due to adsorbed CO, therefore more nickel was removed during this process.

In the second adsorption isotherm the weight of the sample always

increased with time and pressure. The amount adsorbed in the second isotherm was higher than the amount adsorbed in the second isotherm of a sulphur-free nickel catalyst sample. This phenomenon was observed at both adsorption temperatures 195K and 273K. After the removal of the carbonyl species in the intermediate evacuation new nickel particles are exposed in the second isotherm. These new particles adsorb CO preferentially as linear species with possible formation of subcarbonyl compounds. Although the sulphur presence is still affecting the CO adsorption its effect appears to be less marked than in the first isotherm. Unfortunately this cannot be explained with the present results only and there is no relevant information available in the literature.

ii) Heavily poisoned samples.

The results described here correspond to the adsorption of CO on samples poisoned with thiophene at a concentration of 1000ppm at temperatures of 298K, 373K and 773K and on samples regenerated with H_2 at 873K after being heavily poisoned with thiophene.

Figure 5.31 shows the adsorption of CO at 273K on a sample poisoned at 373K. Only the total (first) isotherm is shown. The general features showed by the CO adsorption on slightly poisoned samples are also found here but with increased intensity:

a) at every point in the isotherm the weight increases with time, reaches a maximum and then decreases;

b) the points at low pressure do not attain equilibrium, but they are taken at the same time intervals used for the clean samples;

c) the isotherm reaches a maximum with pressure, later as the pressure is increased the weight decreases dramatically. For this

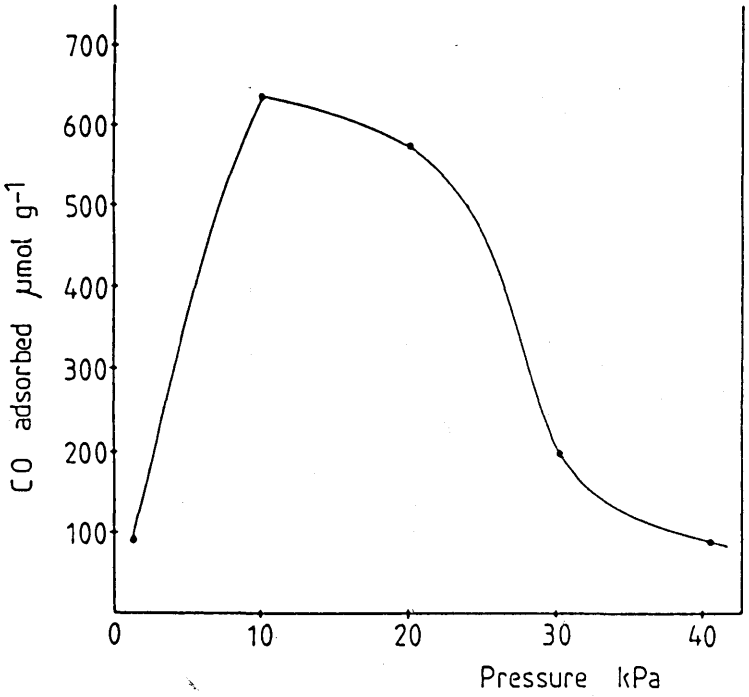

FIGURE 5.31

CO adsorption at 273K on a heavily poisoned Ni/Al_2O_3 sample (NAT3-10).

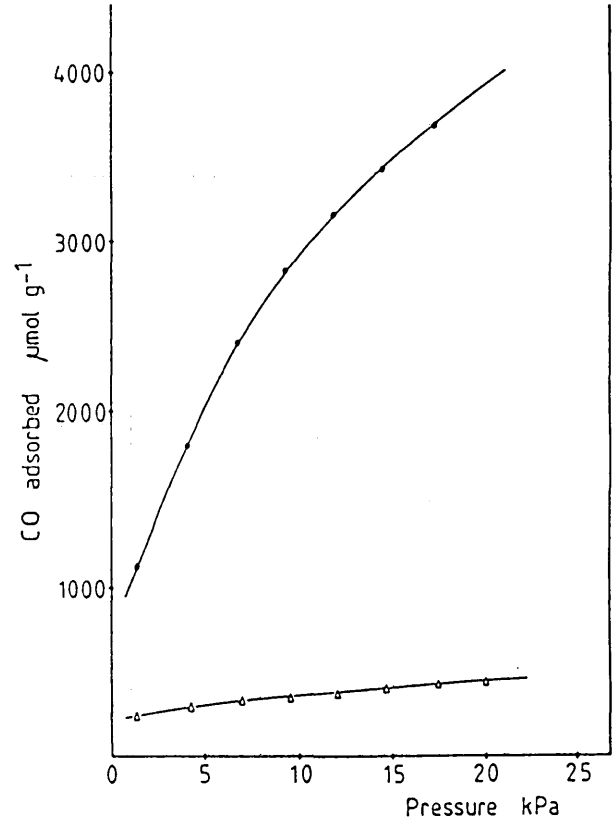

FIGURE 5.32

CO adsorption on a Ni/Al_2O_3 sample (NAT3-31) poisoned at 298K, 1000ppm thiophene (●); clean sample as reference (Δ).

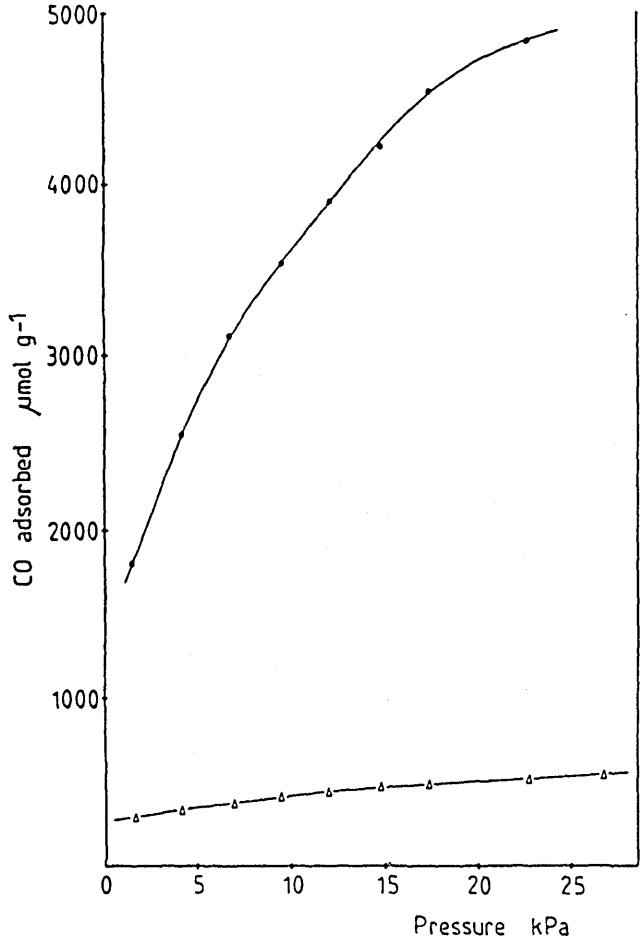

FIGURE 5.33

CO adsorption at 195K on a Ni/Al_2O_3 sample (NAT3-32) poisoned with 1000 ppm thiophene at 773K (●); clean sample as reference (Δ).

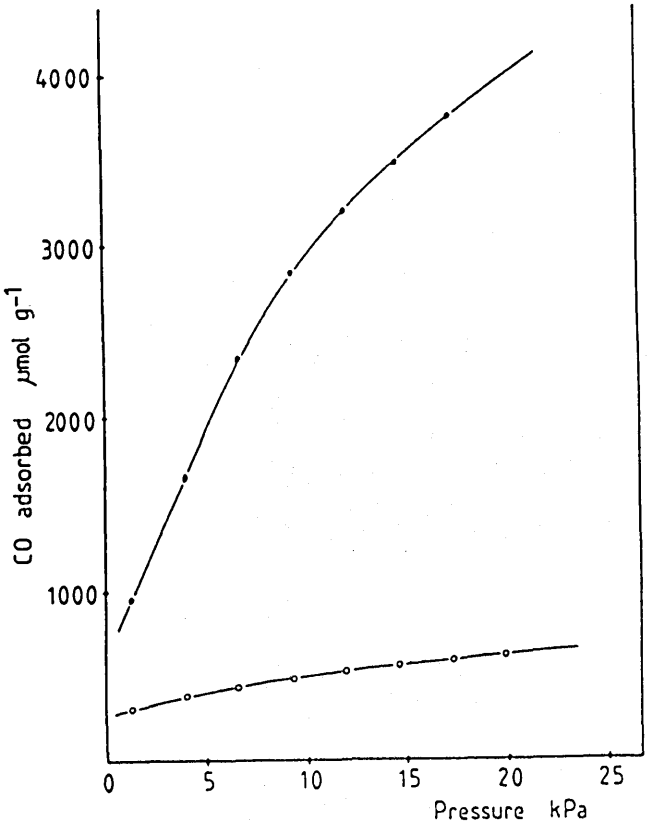

FIGURE 5.34

CO adsorption at 195K on a regenerated Ni/Al_2O_3 sample (NAT3-21) poisoned at 298K, 1000ppm thiophene (●); clean sample as reference (O).

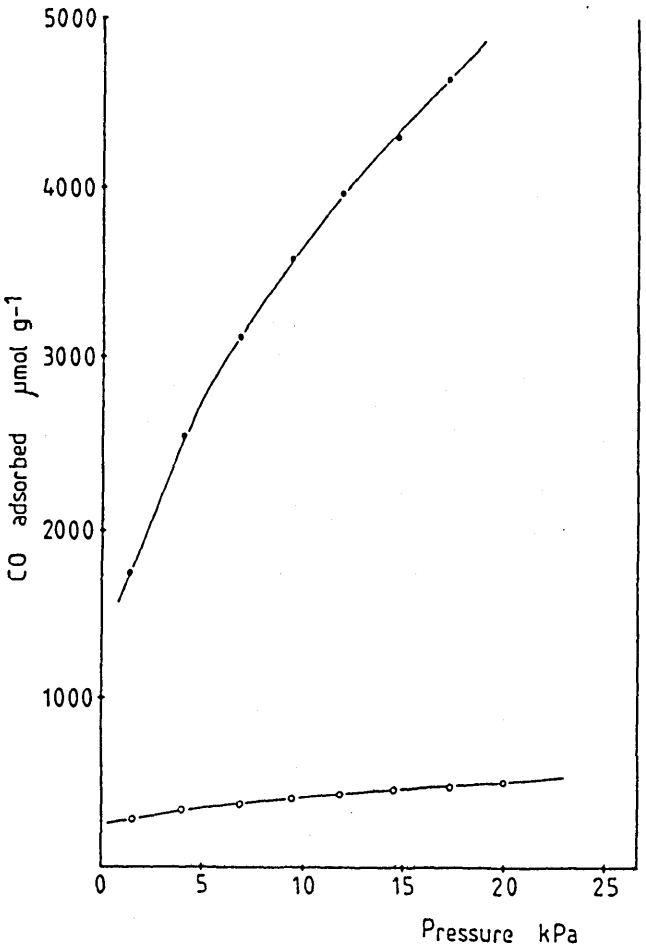

FIGURE 5.35

CO adsorption at 195K on a regenerated Ni/Al_2O_3 sample (NAT3-25) poisoned at 773K, 1000 ppm thiophene (●); clean sample as reference (O).

sample however the maximum is higher than for the slightly poisoned samples;

d) the weight of the sample falls below the initial weight during the evacuation between the 2 isotherms. In this case the loss in weight was so high that it was impossible to determine the second isotherm. The weight went below the limit of the microbalance and it could not be adjusted electrically. The weight loss amounted to about 40% of the nickel content of the sample.

To avoid this problem and the removal of volatile compounds from the sample during evacuation it was decided that only the total (1st) isotherm should be determined when using heavily poisoned samples.

The adsorption of CO at 195K on samples poisoned with thiophene at 298K and 773K is shown in Figure 5.32 and figure 5.33 respectively; whereas that on regenerated samples can be seen in Figures 5.34 and 5.35.

As with the slightly poisoned samples the adsorption on the heavily poisoned samples show that the weight increases with pressure, no maximum is found. The adsorption at low pressures ($P_{CO} < 10kPa$) does not attain equilibrium, therefore the uptake values were taken following the procedure described above.

In figures 5.32 to 5.35 the adsorption isotherms of the clean samples are shown as reference. At 15kPa the CO uptakes on poisoned and regenerated catalysts are about 7-9 times higher than the uptakes on the clean samples. Nevertheless small differences can be noticed between the adsorption on sulphur-poisoned samples; for instance it seems that the CO adsorption on the catalyst poisoned at 773K is higher than that on the sample poisoned at 298K. Comparing the plots of

figures 5.32 and 5.33 to those of figures 5.34 and 5.35 the adsorption on regenerated samples appears to be similar to that on the adsorption on their poisoned counterparts; poisoning was performed at the same temperatures for those samples reported in figures 5.32 and 5.34, and those in figures 5.33 and 5.35. If the CO uptake is related to the sulphur content then the sample poisoned at 773K has more sulphur than the one poisoned at 298K, and the regenerated samples seem to have the same content than the samples just poisoned.

The CO surface saturation coverage of sulphur-free Ni catalysts is equal to $\frac{CO}{Ni_s} = 0.7$ which corresponds to a stoichiometry of 1.41 Ni atoms per CO molecule; if the surface Ni atoms were converted to nickel tetracarbonyl it would be expected a 5 to 6 fold increase in the CO uptake. The 9-fold weight increase found experimentally implies that not only surface nickel particles are bonded to CO but also subsurface nickel atoms are involved in the tetracarbonyl formation. It is possible that at this temperature the CO-Ni interaction involved the formation of clusters of [CO-Ni] but no evidence exists to prove it.

iii) to test whether the thiophene presence affects the adsorption of CO on the support, the adsorption was carried out on an alumina sample poisoned at 298K. The same isotherm was found on the fresh and poisoned alumina samples, allowing for experimental errors. This is shown in figure 5.36. Hence thiophene had no effect on the CO uptake on alumina.

5.3.6 Discussion

The measurement of nickel metal areas by chemisorption of CO and N_2O has to be done carefully to obtain correct results and avoid

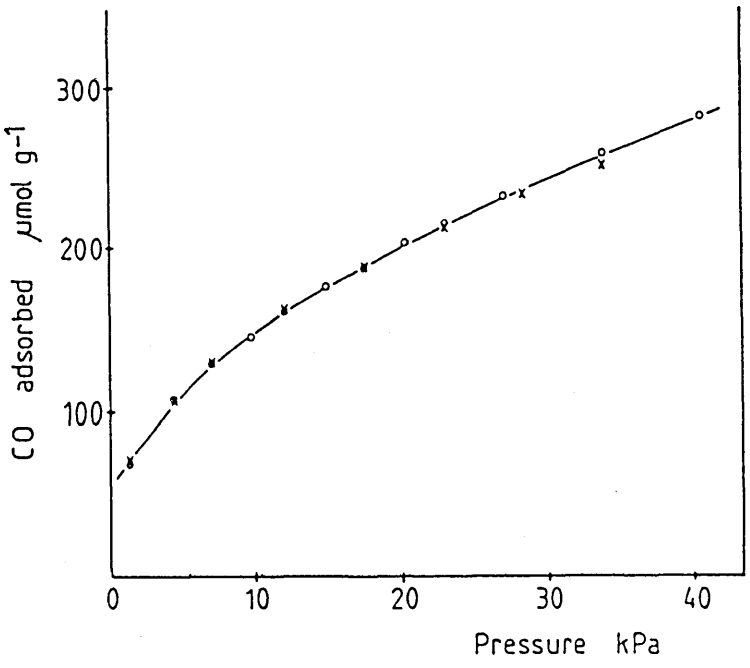

FIGURE 5.36

CO adsorption at 195K on thiophene-poisoned Al_2O_3
Poisoned sample (x), clean sample (O).

problems inherent to the complex gas-nickel interactions.

It has been demonstrated that the determinations are affected by the temperature of adsorption, the gas pressure and the method by which the saturation coverage is calculated.

Due to the complex nature of the CO-Ni and N_2O-Ni adsorptions the amount chemisorbed on the catalyst should be determined free of any physical or weak contribution. This is achieved by choosing an appropriate pressure range and a suitable temperature to work.

If the pressure at which the coverage is determined is low it may not represent the complete area available and the result may be low; on the other hand at too high pressures the risk of having adsorbed amounts in excess of monolayer is present. For CO it has been shown in IR studies that the increase in pressure increases the number of linear bonds with possible carbonyl formation, hence the pressure should be confined to regions at which that effect is less likely. In the case of N_2O very high pressures may promote the oxidation of nickel particles underneath the surface layer. The results reported here show that the best way to determine the saturation coverage is to extrapolate to zero pressure the chemisorption isotherm that results from the difference taken between a first total isotherm and a second isotherm which accounts for the weak adsorption species determined after 20 minutes of evacuation at the adsorption temperature. The extrapolation of the linear region between 10kPa and 30kPa eliminates any excess in the uptake which could be due to subcarbonyl species and assures that full coverage has been reached. Bartholomew (119) pointed out that the results obtained below 10kPa may be suspect of not having reached equilibrium, and they may be lower than the true value. If the

chemisorption isotherm is still pressure dependent the coverage determined at 13kPa, as used by some investigators (146,147), may be in excess of saturation therefore extrapolation represents the best way for calculating the saturation coverage. The favoured method of subtracting the two isotherms determined on the same sample takes into account all the species formed during adsorption and offers the best alternative for the metal area determination; it should be used in preference to the 2nd method, method B, which gives less accurate results and possibly with a different meaning since the adsorption of CO on the support cannot include the excess due to carbonyl formation, neither the possible sublayer oxidation of the catalysts when using N_2O.

The temperature of adsorption has also a strong effect on the behaviour of the isotherm and the coverage determined. Too low the temperature the physical adsorption becomes too high, whereas high temperatures may promote the formation of volatile nickel carbonyl or subsurface nickel oxidation.

The use of 77K for the adsorption of CO or 195K for the N_2O adsorption proved to be unsuitable. The physisorption is too high and the uptake is basically formed by physisorbed material; this material is also present in the second isotherm and the difference of the two isotherms gives inaccurate results due to the errors involved in the calculation procedure.

The determination of the nickel metal area by CO adsorption at 273K is unreliable. The results were mixed: successful for a sample batch, unsuccessful for another. In some samples nickel carbonyl was formed and the catalyst lost nickel during the intermediate evacuation.

In some others this effect was not observed, however the amount of CO adsorbed at saturation increased with increasing temperature from 195K to 273K. This effect can be explained by an increase in the number of linear bonded CO-Ni species as the temperature is increased, which at high enough temperatures ($T \geqslant 273K$) may form volatile nickel tetracarbonyl. The results published by Primet et al. (132) and some of the results by Pannell and Bartholomew (119) predict a decrease in the CO/Ni_s ratio as the temperature is increased from 195K to 294K which means that the number of bridge bonded (or multicentered) CO-Ni species increases with temperature with a corresponding decrease in the linear bonded species; if this is so it can not explain the fact that nickel tetracarbonyl which requires a high CO/Ni ratio (CO/Ni = 4) can be formed at room temperature but not at 195K. However some results published later by Pannell and Bartholomew (145) showed an increase in the CO/Ni_s ratio with increasing temperatures using samples with a similar nickel loading (2.3% Ni/Al_2O_3) as those used in the previous publication (3% Ni/Al_2O_3) (119). The results of Primet were obtained at several nickel loadings (4% - 16% Ni/SiO_2). It is clear that the subject is still unresolved, that more work is necessary to clarify it. Nevertheless on the basis of the results obtained by other techniques such as IR (130,133,157), LEED and AES (125-128) it would be expected that as the temperature increases the percentage of linear bonded CO-Ni species would increase, hence the CO/Ni_s ratio would be increased as well.

In any case, despite the low physical adsorption, it cannot be recommended to determine the nickel active area by CO adsorption at 273K due to the possible formation of volatile carbonyl compounds.

The CO adsorption at 195K provides the best determinations of nickel metal area, in terms of reproducibility, no complications of volatile compounds formation and good agreement among the results available in the literature. With both sets of samples used (NAT3 and NAP) the reproducibility was better than 8% in spite of the high amounts of physisorbed material. The adsorption results of Pannell and Bartholomew for supported catalysts with high nickel content (119) agree with the bond numbers obtained by Primet et al (132) at this temperature, and also with those reported for the adsorption of CO on well defined Ni crystal faces (125-128). At this temperature the saturation coverage of CO on nickel is equal to about 0.7-0.8 CO molecules per surface nickel site. Some material is adsorbed as linear species and some as bridged or multicentered species. Furthermore the saturation coverage was found to be constant irrespective of the crystal orientation (125-129). The formation of nickel tetracarbonyl was not detected, and it has not been reported in the literature either.

It can be conluded that the measurement of nickel areas of supported catalysts is recommended to be performed at 195K.

In the case of N_2O the use of 273K is preferred to 195K. The reproducibility is much better and the physisorption contribution is lower. The stoichiometry found in terms of the CO-Ni stoichiometry at 195K is equal to 1.21 which means that some nickel particles are bonded to one oxygen atom, whereas some others show a ratio of 2 Ni atoms per oxygen atom adsorbed.

It cannot be claimed yet that it is the optimum temperature for the measurement of nickel areas because the physical adsorption is high

and the stoichiometry is fractional between 1 and 2. However, based on the results obtained it could be said that this temperature - 273K - is suitable for the measurement of the active area of supported nickel catalysts.

It is recommended though to widen the temperature range in order to find a region at which the physisorption could be minimized, and the stoichiometry could be defined with 1:1 O/Ni relation. Care should be taken to avoid subsurface oxidation.

The measurement of free nickel areas of catalysts poisoned by sulphur is more difficult. It cannot be made through the adsorption of CO because of the nature of the CO-Ni interactions. It was found that irrespective of the temperature the CO uptake is increased in the presence of adsorbed sulphur compounds. Sulphur then behaves as a catalyst for the multilinear CO adsorption on nickel. The catalytic effect of sulphur was reported by Milliams et al. (152) who showed that nickel tetracarbonyl production is promoted if sulphur is present. The amount of CO adsorbed is to be increased in the presence of sulphur and Bartholomew and Pannell (145) observed this increase together with the tetracarbonyl formation. In contrast to these results Bourne et al (46) and Feng (153) reported that the increasing amounts of sulphur resulted in decreasing uptakes of CO; in this case sulphur poisons nickel sites and CO is adsorbed only on the free nickel available without any interaction with the sulphur, a behaviour which has also been found in the adsorption of CO on nickel at low pressure studied by LEED and AES (28) and magnetization measurements (38).

The results reported here agree with those of Bartholomew and Pannell (145); the effect of sulphur is to increase the CO uptake to

promote the formation of carbonyl compounds; these results are also supported by IR results which observed an increase in the number of linear bonded species and a reduction of the bridged or multicentered bonds (47,133,154,155).

At 273K the nickel tetracarbonyl is readily volatile, so that as soon as it is formed it is desorbed.

The increase in the CO uptake is directly dependent on the sulphur content; at higher sulphur content the CO uptake is higher. With heavily poisoned samples the CO uptake is about 9 times higher than the uptake on sulphur free samples which means that if nickel tetracarbonyl is formed then nickel particles below the surface layer are also bonded to CO in the presence of sulphur and form tetracarbonyl compound. Another possible explanation is that in the presence of sulphur the mobility of the nickel particles would increase and the formation of [CO-Ni] clusters would be promoted, but unfortunately this cannot be proved since there is no evidence available in the literature.

The results obtained on the alumina support poisoned with thiophene revealed that the uptake of CO is similar to the uptake on clean alumina samples and is not affected by the presence of sulphur.

It can be concluded that in the presence of sulphur the CO uptake is increased and it cannot be a measure of the free nickel area available. The search for a suitable titrant for the determination of nickel areas of poisoned catalysts has to be continued; the only gas available for this job presently is H_2, but it is too light to be used with confidence in gravimetric systems. N_2O appears to be a good alternative; it is decomposed by nickel and oxidizes the metal particles, it is less reactive than oxygen and there are temperature

regions at which subsurface oxidation does not occur. The results obtained at 273K are reproducible and accurate. It is recommended to study its adsorption on sulphur-poisoned catalysts. Unfortunately, this was not part of the present study.

Summary

In conclusion the following points can be drawn:

i) The Ni metal area of clean catalysts can be assessed by the adsorption of CO and N_2O. The measurement has to be performed carefully to overcome the drawbacks inherent to the determination.

ii) The chemisorption is affected by variations in temperature, pressure, time of equilibration and contaminants present on the surface. It was found that the best conditions for the determination using CO as titrant are: adsorption temperature 195K; evaluation of the saturation coverage from the extrapolation to zero pressure of the linear part of the chemisorption isotherm between 10kPa and 30kPa; an equilibration time of 40-45 minutes is needed for the first equilibrium point, then 20 minutes between readings are enough. Using N_2O the conditions are the same except the temperature which should be 273K.

iii) The best method for the evaluation of the saturation coverage involves the determination of two isotherms on the same sample with an intermediate evacuation of 20 minutes at the adsorption temperature.

iv) The metal area is calculated using the saturation coverage obtained from the isotherm and the saturation coverage per unit area of catalyst which has been determined to be 1.10×10^{19} CO mole/m^2. Based on this coverage and the CO/N_2O ratio the saturation coverage of N_2O per unit area at 273K was found to be 1.28×10^{19} Oxygen atoms/m^2 this is because only oxygen is chemically adsorbed onto the nickel sites.

v) The measurement of free nickel area of sulphur poisoned catalysts cannot be made by CO adsorption. Sulphur compounds catalyze the adsorption of CO and the formation of $Ni(CO)_4$. This compound is released to the gas phase at 273K. At 195K the amount of CO adsorbed on sulphided samples is about 9 times larger than on a clean catalyst; it is possible that CO reacts with more than one layer of Ni in the presence of sulphur. The adsorption of CO therefore is an excellent qualitative method to test the presence of sulphur on Ni catalysts.

vi) N_2O offers many advantages and it could be used to measure nickel areas of clean and sulphur poisoned catalysts. It is recommended to do a more extensive study of the adsorption of N_2O and test its suitability as a titrant for nickel on poisoned samples and develop the method.

CHAPTER 6

ADSORPTION AND REGENERATION STUDIES

The results of the experiments performed for the adsorption of thiophene and H_2S on Ni/Al_2O_3 and γ-Al_2O_3 are reported in this chapter. The analysis is divided into short and long term behaviour and the effects on the behaviour of temperature and concentration. The adsorption was carried out at temperatures between 298K and 773K, at concentrations of 100ppm and 1000ppm. Catalysts were regenerated and the extent of regeneration was measured by CO chemisorption and re-adsorption of thiophene at the same temperature as that of the first poisoning; in each case the short and long term behaviour are also noted and their variation with temperature and concentration reported. Finally the results of the elemental analysis of the sulphur and carbon content of several catalysts and electron microscopy results showing characteristics of the nickel/alumina samples are also given.

6.1 Adsorption of Thiophene on Ni/Al_2O_3 Samples

After reduction of the catalyst precursor to a Ni/Al_2O_3 sample and measurement of the metal area by CO adsorption the catalyst was treated at 773K for 10h with a hydrogen flow to remove the CO adsorbed on the surface. The catalyst was cooled down to the adsorption temperature and the adsorption performed. The adsorption behaviour showed different characteristics at short initial times and at long term; these are described and presented below.

6.1.1 Short term adsorption. Effect of temperature and concentration

The adsorption of thiophene on alumina-supported nickel catalysts was performed at temperatures of 298, 373, 573 and 773K, at concentrations of 100ppm and 1000ppm. Results corresponding to a concentration of 100ppm at the various temperatures are given in Figure 6.1 following the weight uptake as a function of time between 0 and 60 minutes.

Observing the plots in this figure it can be said that in general as the temperature increases the amount adsorbed decreases. The amount adsorbed at 298K is higher than that at 373K, this is higher than that at 573K and the lowest is the uptake at 773K.

Between 0 and 15 minutes the adsorption curve at 298K shows an increase in weight reaching a certain value and remaining there after about 5 min. Between 15 and 60 min the weight decreases slowly to about 90% of the maximum value reached previously.

At 373K the uptake increases continuously up to about 20 min, when it reaches a value that remains constant for the rest of the period being considered.

At 573K the adsorption uptake increases in a short initial time, and then has a small decrease and the weight remains constant for about 10-12min, after which it starts to increase slowly. This behaviour is also noticed in the adsorption at 773K but with bigger changes: the weight reaches a value of about 1.8mg/g in about 2 minutes and decreases to about 0.90mg/g in 5 min where remains constant for a short period, then starts to go upwards at a higher rate than at 573K.

The weight uptake behaviour at higher temperatures (573K-773K) corresponds to a process which may be visualized as follows: a strong

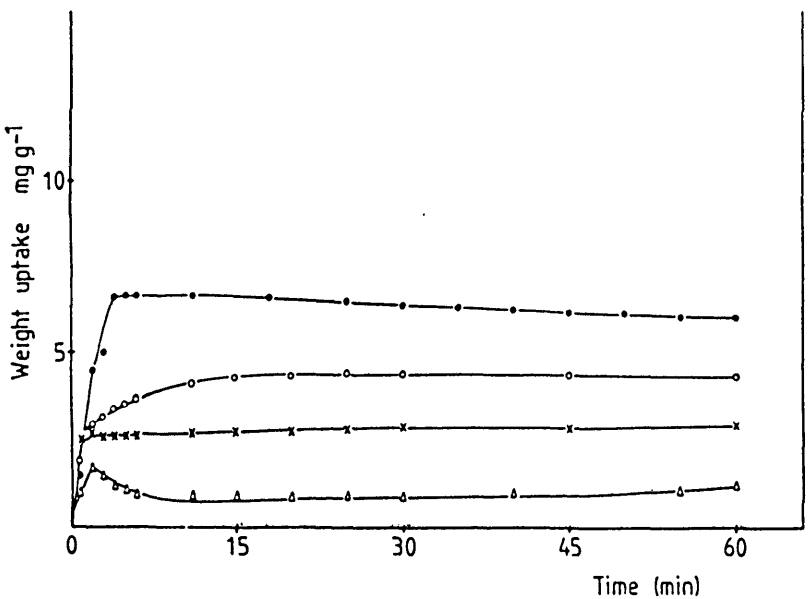

FIGURE 6.1

Adsorption of thiophene on Ni/Al_2O_3 at a concentration of 100 ppm. Short time behaviour. 298K (●), 373K (O), 573K (x), 773K (Δ).

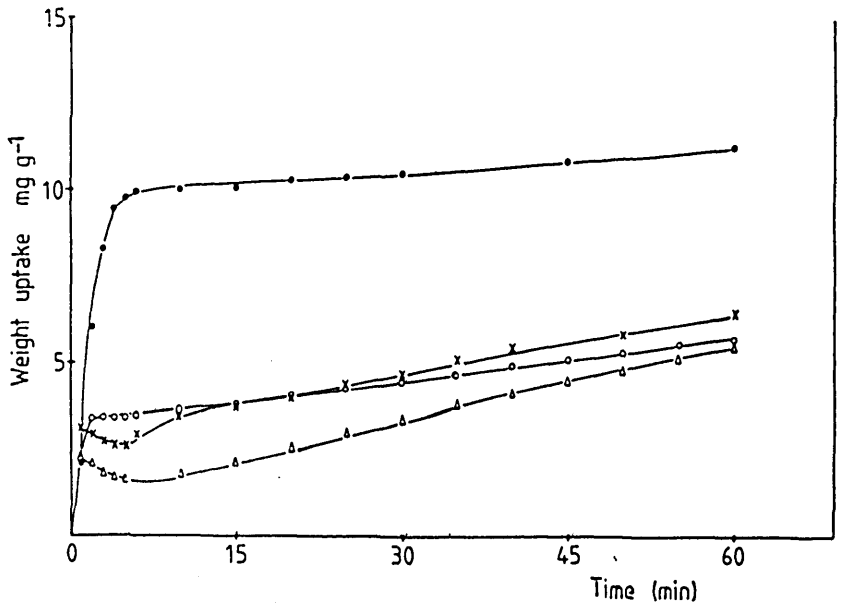

FIGURE 6.2

Adsorption of thiophene on Ni/Al_2O_3 at a concentration of 1000ppm. Short time behaviour. 298K (●), 373K (O), 573K (x), 773K (Δ).

adsorption of thiophene covering a fraction of the area available; once adsorbed thiophene undergoes decomposition and part of the molecule - mainly the hydrocarbon part - leaves the surface so that the weight decreases, reaching a point where an equilibrium between adsorption-reaction-desorption is established for a short time and the weight is constant.

As time passes the weight uptake increases due to either coverage of higher area or sulphur and carbon deposition in the area already covered by the thiophene both resulting in higher sulphur and carbon content, and reaching equilibrium at very long time (long term adsorption).

At room temperature the surface is readily saturated in a short time; the adsorption may be seen as a dissociative coverage of the nickel surface, the dissociation of the thiophene molecule would allow some material to be desorbed hence the weight would decrease as was the case of the high temperature behaviour.

These effects were not observed at 373K. The weight uptake rate is slower than at 298K, it increases monotonically and reaches a constant value. The possible reaction scheme mentioned above can be applied if the adsorption-desorption rates are equal in this period.

The fact that the weight decreases with increasing temperature at this concentration (100ppm) is a result of the adsorption being exothermic.

At low temperatures another possibility that has to be taken into account besides chemisorption is physical adsorption. The thiophene boiling point is 357.2K and the vapour pressure at 298K is 10.5kPa (79mmHg.).

The effect of the concentration on the short term adsorption can be found when comparing Figure 6.1 with Figure 6.2. In Figure 6.2 the plots give the adsorption uptake of thiophene at the same temperatures as in Figure 6.1 but at 1000ppm thiophene/H_2.

The 298K adsorption isotherm shows a fast adsorption attaining a constant value of 9.95mg/g in 6 min, where remains for about 5 minutes after which starts to increase its weight. In this case the decrease in weight shown by the 100ppm adsorption at the same temperture is not observed. This may be caused by both increased physisorbed amount, and little or no desorption of material from the surface prevented by the high thiophene concentration which causes a higher adsorption rate.

The thiophene coverage is higher at 1000ppm; the weight reached at the plateau between 6 and 10 minutes is about 50% higher than the weight reached in the same period by the sample poisoned at 100ppm and 298K shown in Figure 6.1

The observed slow increase in weight after 15 min may be due to an exchange of carbon with sulphur in which the hydrocarbon part of the thiophene molecule adsorbed on the catalyst is slowly exchanged with heavier sulphur atoms and the weight increases. This process, in agreement with Lyubarskii (45), should be faster at higher temperatures due to increased rate of adsorption and higher rate of thiophene decomposition. It will be described in more detail in the following section.

This behaviour is observed clearly on the other three isotherms of Figure 6.2; and indeed it can also be seen at 100ppm in Figure 6.1 but at a slower rate.

At 373K the sample reaches a constant weight in 2 min but after 4 min starts to increase slowly. At higher temperatures after an initial fast uptake the weight decreases and after a minimum it rises at a faster rate than at 100ppm, as it is observed comparing both isotherms at 573K and 773K in Figure 6.2 with those in Figure 6.1.

Another characteristic of the adsorption at 1000ppm is that the relative uptakes obtained as a function of temperature at 100ppm are not found at the higher concentration. The adsorption at 298K is still the highest, but the effect of temperature on the reaction rate is reflected in the adsorption isotherms at 1000ppm, the higher the temperature the higher the reaction rate; being the initial uptake similar for the three temperatures 383K, 573K and 773K, in 60 minutes the uptake at 573K is already higher than that at 373K and this is similar to that at 773K.

That the effect of temperature on the reaction rate is more noticeable at 1000ppm than at 100ppm might be an indication of a possible mass transfer limitation. Because the thiophene uptake appears to be controlled by the adsorption rate (48,51,53) and adsorption is fast at the beginning of the process as shown by the isotherm at 298K, the short term behaviour would possibly be more affected by mass transfer resistances than the long term behaviour. The kinetic results and the analysis of internal and external mass transfer resistances are given later in section 6.5. The long term behaviour is given in the next section.

6.1.2 Long term adsorption. Effect of temperature and concentration

During poisoning it was observed that the weight uptake continued increasing for long periods and therefore it was followed throughout.

The results presented in this section correspond to the adsorption of thiophene at times up to 20h. It is assumed that at this time the adsorption has reached equilibrium. It was observed though that in the cases where adsorption was still occuring variations in the ambient temperature caused spurious changes in weight; this effect was observed during daytime when the biggest variations in the laboratory temperature were recorded after approximately 20-22h the run had started. The effect is shown in Figure 6.3. After 20h the uptake rate increases, the weight reaches a maximum and then decreases. All the experimental conditions remained constant except the room temperature, which induced buoyancy effects in the balance and spurious weight changes. To avoid taking into account effects that do not correspond to a true adsorption behaviour it was decided to stop experiments after 20h when the variations in room temperature were smallest, this corresponded to overnight conditions.

In Figure 6.4 the plots correspond to adsorption isotherms at 100ppm. In the long term the relative uptakes seen in Figure 6.1 are not maintained; at 20h the uptake at 573K is the highest then in progressively lower order the uptakes at 298K, 373K and 773K.

After two hours when it reaches a minimum in weight the uptake at 298K increases and attains a nearly constant value after 16h. As the temperature goes up the weight uptake increases so that at long time the weight at 573K is higher than at 373K and continues increasing at a near constant rate higher than at 373K. At 773K after ½h the weight always goes up and reaches equilibrium in about 15h. The isotherms at 573K and 773K show the same pattern and seem to increase at the same rate for a long period. The adsorption seems to be occurring through a common mechanism.

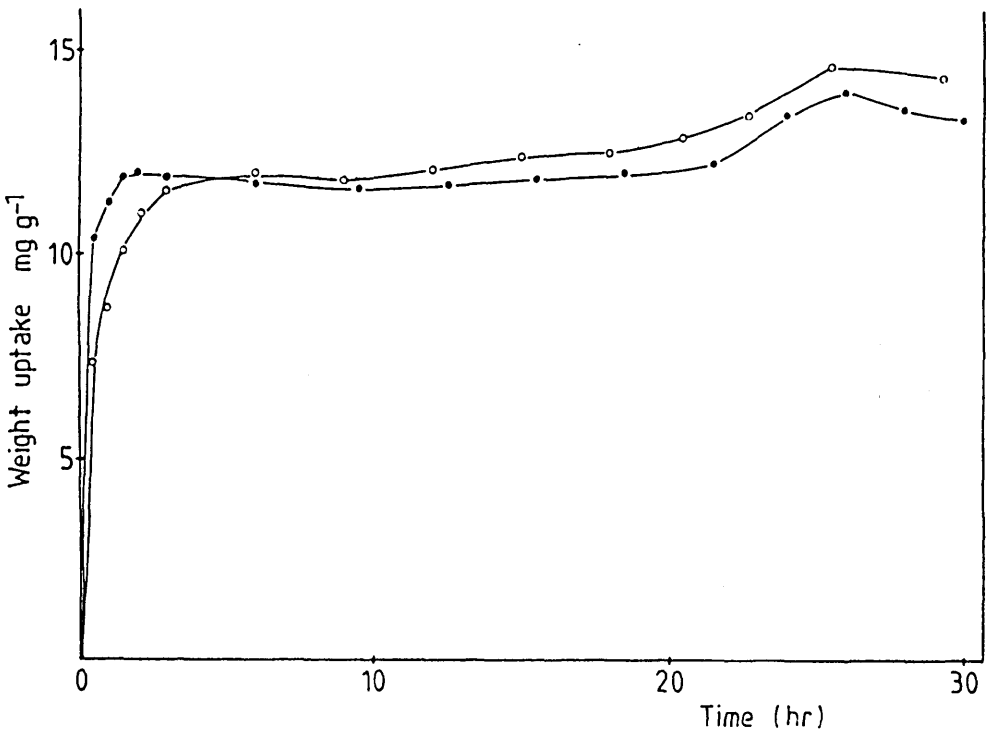

FIGURE 6.3

Effect of ambient conditions on the adsorption uptake after 20h. Adsorption of thiophene at 298K. NAT3-21 (●), NAT3-22 (O).

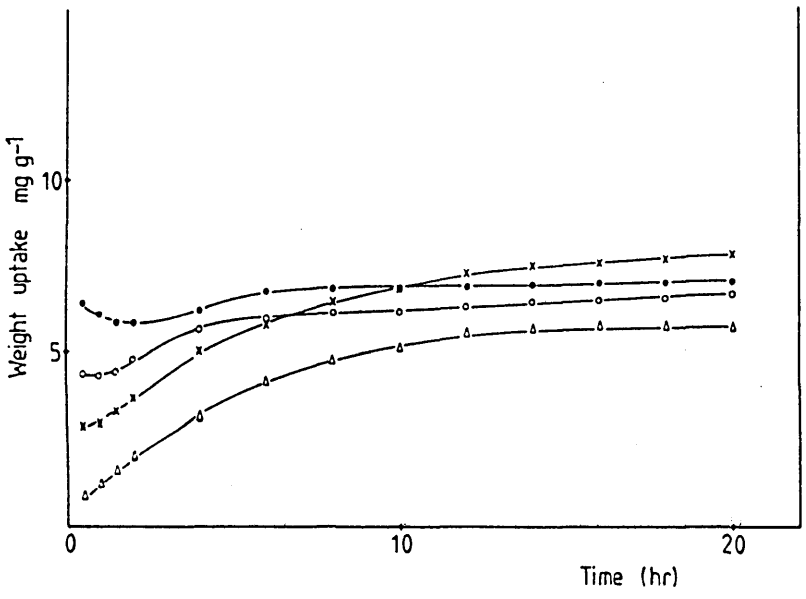

FIGURE 6.4

Long term adsorption of thiophene on Ni/Al_2O_3 at 100 ppm. 298K (●), 373K (O), 573K (x), 773K (Δ).

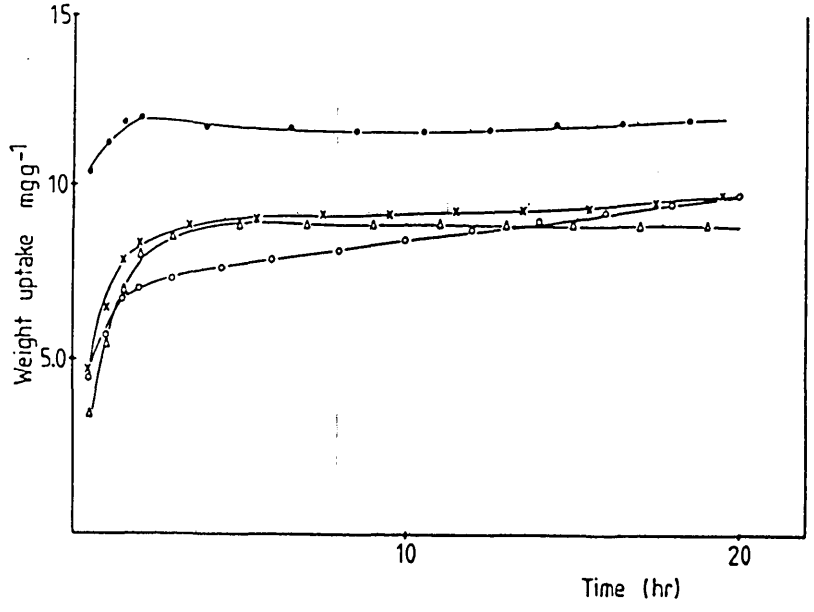

FIGURE 6.5

Long term adsorption of thiophene on Ni/Al_2O_3 at 1000 ppm. 298K (●), 373K (O), 573K (x), 773K (Δ).

Figure 6.5 shows the adsorption curves of thiophene on Ni/Al_2O_3 at a concentration of 1000ppm and several temperatures. The adsorption at 298K shows a maximum at 2h and then decreases slightly over a period of 10h after which it starts to increase again until it attains equilibrium.

At 373K the weight goes up monotonically, first at a high rate in the initial 3 hours, but at a lower rate between 3 and 20h.

The adsorption at 573K and 773K increased very fast in the first three hours, with a slower rate after this period; the 773K run reached equilibrium in 5h, whereas that at 573K was still continuing after 20h although at a very low rate. The run at 573K reaches 90% of its final weight in about 5h whereas in the same period the adsorption at 773K has already reached its final weight.

Comparing figures 6.4 and 6.5 the effect of concentration is easily seen:

i) at higher poison concentration the equilibrium (final) weights are higher;

ii) at higher concentration the adsorption rates are higher, reaching equilibrium at shorter times.

The results at 298K show a fast saturation at both concentrations, with possible reactions occurring at the surface and a very slow process occurring at long times which increases the weight of the sample. The secondary process of increasing weight after the initial adsorption is accelerated by increasing the temperature.

As mentioned before the behaviour of the adsorption isotherms suggest the following mechanism which was proposed by Lyubarskii et al. (45):

i) $C_4H_4S + 5\square \rightarrow C_4H_4S_{(a)}$

ii) $C_4H_4S_{(a)} + 2H_2 \rightarrow C_4H_8\ S_{(a)} + 4\square$

iii) $C_4H_8S_{(a)} + H_2 \rightarrow S_{(a)} + C_4H_{10}$

Step i) is the adsorption of thiophene on 5 vacant sites to give adsorbed thiophene. They (45) proposed that thiophene was adsorbed as a molecule and that in step ii) the adsorbed molecule would be attacked by H_2 to give a thiophane molecule adsorbed through the heteroatom. In step iii) the thiophane would be further hydrogenated yielding butane in the gas phase and the sulphur remaining on the catalyst surface.

Evidence obtained by IR results (48,53) clarifies the basic mechanism: the thiophene is dissociatively adsorbed; hence the hydrogen attack occurs on the adsorbed species yielding adsorbed sulphur and adsorbed C_4H_6 which is further attacked by H_2 to break the double bonds and form C_4H_{10} which is then desorbed.

Lyubarskii et al. (45) pointed out that the proposed mechanism was dependent on temperature. That is at room temperature thiophene would be found as adsorbed species only, as the temperature increases it is attacked by H_2 to form thiophane and finally butane at higher temperatures.

Table 6.1 shows the saturation uptakes on nickel/alumina catalysts as function of temperature and thiophene concentration. Also given are the metal surface area of each sample as CO coverage. The results are summarised in table 6.2 which gives the saturation uptake per nickel metal area.

Table 6.1 Saturation uptakes of thiophene on Ni/Al_2O_3.

Thiophene Concentration	Adsorption Temperature	Sample	Weight Uptake	CO Coverage
ppm	K		mg/g	μmol/g
100	298	NAT3-33	6.20	200
100	298	NAT3-56	7.00	220
100	373	NAT3-48	5.22	169
100	373	NAT3-51	6.60	208
100	373	NAT3-57	8.92	200
100	573	NAT3-49	6.79	183
100	573	NAT3-53	7.71	196
100	773	NAT3-35	6.00	198
100	773	NAT3-50A	5.73	213
1000	298	NAT3-21	12.01	229
1000	298	NAT3-22	12.47	243
1000	298	NAT3-31	8.40	153
1000	298	NAT3-55B	9.41	198
1000	373	NAT3-30	7.93	197
1000	373	NAT3-58	9.63	220
1000	573	NAT3-23	9.83	204
1000	573	NAT3-27	9.82	204
1000	573	NAT3-40	8.80	195
1000	773	NAT3-25	8.89	198
1000	773	NAT3-26	8.08	186
1000	773	NAT3-32	8.66	219
1000	773	NAT3-54A	7.51	192

Table 6.2 Saturation Uptakes of Thiophene on Ni/Al_2O_3 per unit metal area

Thiophene Concentration ppm / Temperature K	100	1000
	mg/m^2Ni	mg/m^2Ni
298	0.574 ± 0.01	0.942 ± 0.056
373	0.653 ± 0.141	0.767 ± 0.032
573	0.698 ± 0.02	0.861 ± 0.026
773	0.522 ± 0.031	0.698 ± 0.020

The data in Table 6.1 shows that the weight uptake at saturation is a function of the metal area available, so that the best comparison is obtained when the values per nickel area are taken as presented in Table 6.2. The results in Table 6.2 are plotted in Figure 6.6. This graph shows that at 100ppm the saturation uptake increases with increasing temperature from 298K to 573K, a further increase to 773K decreases the final weight. This behaviour is also observed at 1000ppm with the exception of the region 298K-373K which shows a decrease in weight with increasing temperature. Possibly the physisorption of thiophene at 298K is higher with 1000ppm than it is at 100ppm and that could explain the higher uptake obtained.

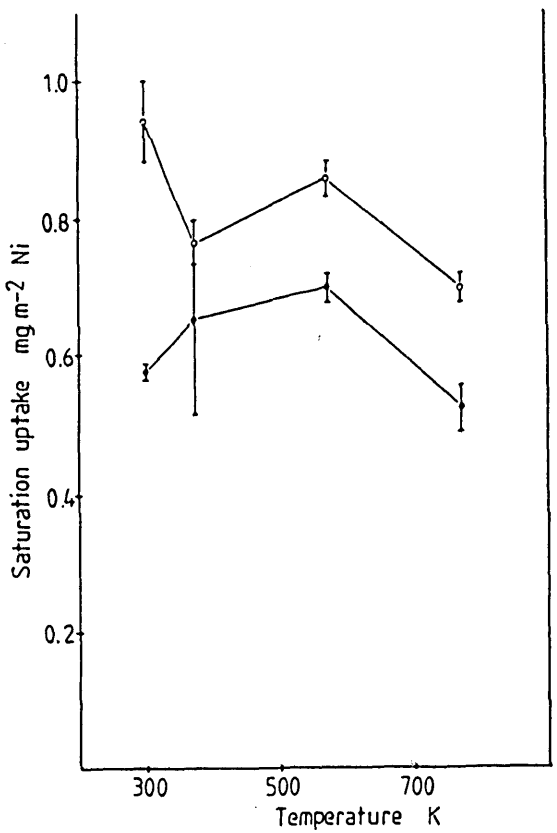

FIGURE 6.6

Effect of adsorption temperature on the thiophene saturation uptakes. 100 ppm (●), 1000 ppm (0).

If the mechanism of adsorption-reaction discussed before is valid the pattern shown in Figure 6.6 suggests that as the temperature is increased the sulphur coverage is increased up to a temperature whereby thermodynamic restrictions the weight has to decrease. It could be argued that the decrease in weight from 573K to 773K is due to carbon deposition on nickel sites therefore blocking the adsorption of the heavier sulphur atom; however it may be difficult to occur because of the hydrogen-rich atmosphere, the low temperature (773K), and the presence of sulphur (6,7,14). This is to be discussed later in section 6.8 after the elemental analysis results have been presented.

6.2 Adsorption of Thiophene on the Support

6.2.1 Short term behaviour. Effect of temperature and concentration

In Figure 6.7 the results for the adsorption of thiophene on γ-alumina in the first 60 minutes are plotted as function of temperature of adsorption at 100ppm.

The initial adsorption behaviour observed on the nickel catalysts is not present here except at 773K. At this temperature the weight increases to a maximum at 2 min and then starts to decrease. The experiment at 573K shows a small induction period after which the weight increases and attains a nearly constant value. An induction period is also observed at 373K after which the weight increases fast at the beginning and much slower after 6 minutes. In the experiment at 298K the weight starts to increase after 1 minute and goes up monotonically during the first hour. After a period of 60 minutes the relative adsorption uptakes are: the highest at 298K, then it is followed by the adsorption at 373K and finally the experiments at 573K and 773K show the same uptake.

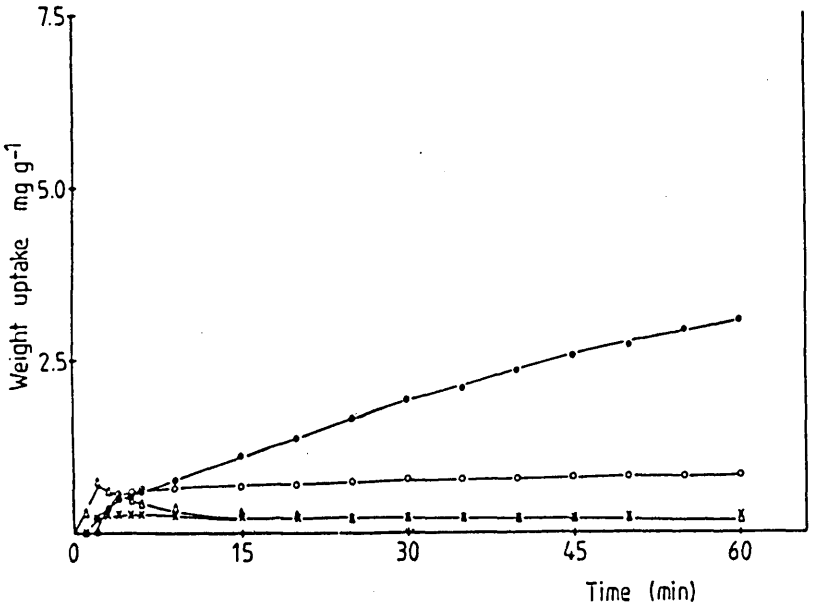

FIGURE 6.7

Adsorption of thiophene on γ-Al_2O_3 at 100 ppm.
Short time behaviour, 298K (●), 373K (O), 573K (x), 773K (Δ).

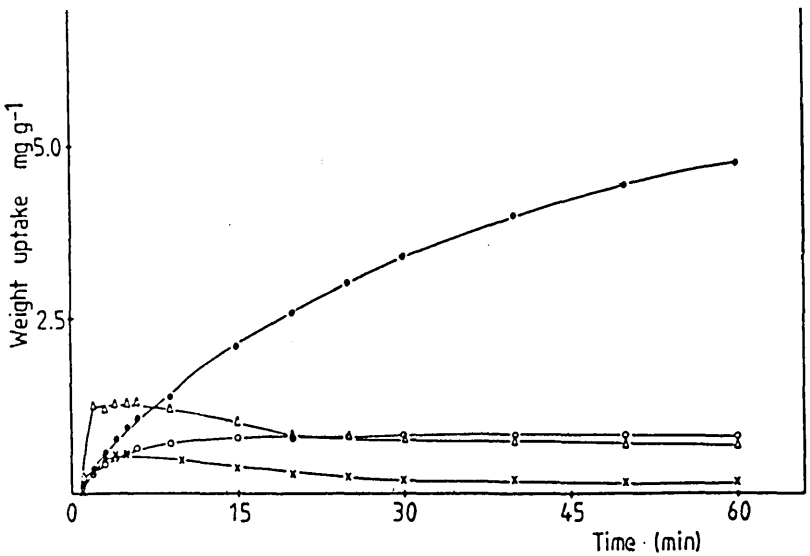

FIGURE 6.8

Adsorption of thiophene on γ-Al_2O_3 at 1000 ppm.
Short time behaviour. 298K (●), 373K (O), 573K (x), 773K (Δ).

The increase in weight at 298K could be due to physically asorbed thiophene; however the same effect is not observed on the nickel catalyst in which most of the weight is taken in the first 10 minutes. Nevertheless it has to be considered that the forces responsible for the physisorption of thiophene may be affected by the different surface characteristics of the Ni/Al_2O_3 and γ-Al_2O_3 samples. A second explanation could be that the thiophene is chemically adsorbed, it is an activated process and is controlled by the adsorption step with little effect of mass transfer resistances. If this explanation is true the adsorption would be affected by the temperature, whose effect would be first to increase the initial rate of adsorption and second to decrease the equilibrium amount adsorbed if the adsorption is exothermic.

The adsorption at 373K is faster than at 298K attains a nearly constant value in about 6 minutes and after this point it has a small increase in weight in a slow process.

As the temperature increases to 573K and 773K the adsorption rate increases and the induction period observed at 573K and lower temperatures is not seen at 773K. It is possible however that as the temperature is increased the thiophene reacts and decomposes so that the weight decreases in time; this is shown at 773K.

The effect of concentration can be observed comparing the adsorption at 100ppm in Figure 6.7 with the adsorption uptakes at 1000ppm shown in Figure 6.8.

The characteristics of the adsorption at 100ppm are observed at 1000ppm but in a greater extent. The adsorption seems to be faster and the weight uptake higher.

The adsorption at 298K and 1000ppm shows a higher weight uptake rate than at 100ppm and the amount adsorbed after 60 minutes is higher. Increasing the temperature to 373K decreases the amount adsorbed and after the initial faster period it increases at a slower rate between 10 and 60 min.

The adsorption isotherm at 573K shows a maximum uptake higher than at 100ppm; but the rate of weight decrease is more noticeable at 1000ppm.

The experiment performed at 773K shows that the adsorption is very fast, that it reaches a maximum uptake that remains nearly constant for a period of about 7 minutes and then decreases. It is noticeable that as with 100ppm, the initial uptake is higher at 773K than at 373K-573K hence the initial controlling process is accelerated by temperature; but the decomposiion (reaction-desorption) process is also accelerated by increasing the temperature. At high temperatures thiophene is adsorbed in the initial period, but then it reacts and decomposes and the products are desorbed into the gas phase, hence the weight decreases. The behaviour is consistent with the adsorption-reaction-desorption process and shows that very little amount remains on the alumina at equilibrium at high temperatures, this is clearly seen in the long term adsorption process, whose results are given in the next section.

6.2.2 Long term behaviour. Effect of temperature and concentration

As in the case of the nickel catalysts the samples of γ-Al_2O_3 support were subjected to poisoning for 20h time at which the system had reached equilibrium at all temperatures but 298K. Following the

same criteria as before with the nickel catalysts it was decided to stop the adsorption at 20h. Figures 6.9 and 6.10 show the long term weight uptakes for the support as function of temperature at thiophene concentrations of 100ppm and 1000ppm respectively.

A remarkable feature that is noticeable is the fact that the final adsorption (20^{th}h) at 298K is much higher at 100ppm than at 1000ppm, and the rate at which the weight is increased in the long-term is higher at 100ppm than at 1000ppm. The phenomenon was reproducible in both cases and can not be taken as fortituous.

It may be explained based on the results of Rochester and Terrell (48) and Curtis et al. (82) who found that thiophene undergoes polymerization reactions on acid catalysts. It would be expected that at 1000ppm the thiophene adsorbed would form a polymer aggregate of thiophene molecules and because of the higher physisorption it would form a layer which does not permit interaction of gaseous thiophene with the surface; at 100ppm it would be expected that with a lower physical adsorption that layer is not formed and thiophene may still be adsorbed (and possibly absorbed) in higher amounts (184). It has to be pointed out that IR results (43,48,80,81) support the view that on acidic supports the thiophene is adsorbed through the sulphur atom due to its electron-donor character hence it would be sitting perpendicular to the surface, whereas in the case of nickel catalysts the thiophene is believed to be mainly co-planar to the surface (45,61,63).

The amounts adsorbed at the end of the 20h experiments are given in Table 6.3. The values are given in mg/g of sample and correspond to the saturation amounts of thiophene adsorbed at temperatures between 373K-773K; at 298K they represent the final weights at 20h. In Table

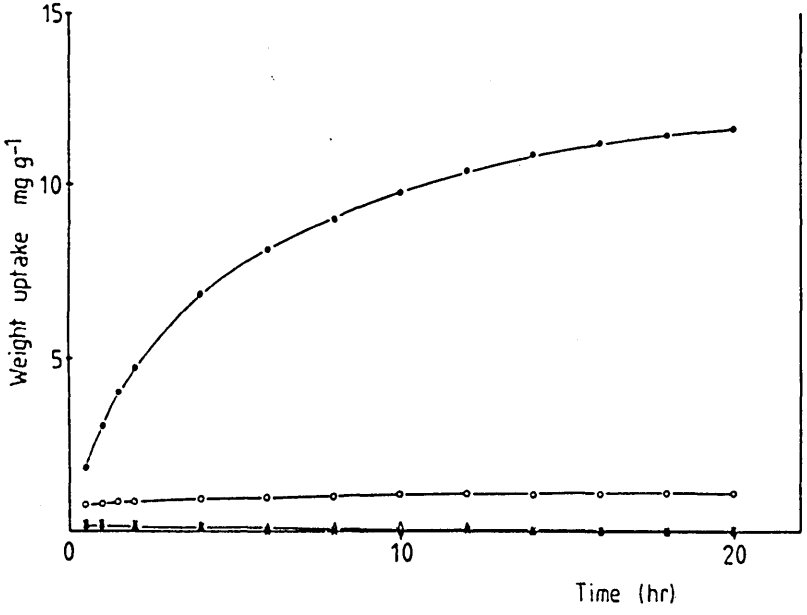

FIGURE 6.9

Long term adsorption of thiophene on γ-Al_2O_3 at 100 ppm. 298K (●), 373K (0), 573K (x), 773K (Δ).

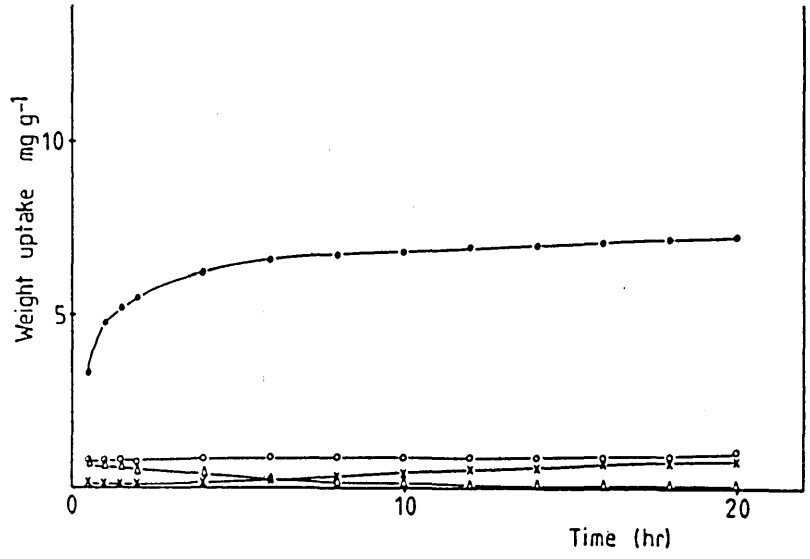

FIGURE 6.10

Long term adsorption of thiophene on γ-Al_2O_3 at 1000 ppm. 298K (●), 373K (0), 573K (x), 773K (Δ).

6.4 the saturation amounts are given in mg/m^2 of sample, in this case the total surface area of the support.

At 100ppm the results in Figure 6.9 show that at 298K the support is still increasing its weight after 20h.

After a period of 10h in which there was a small increase in weight the adsorption experiment at 373K reaches a constant uptake value. As the temperature is increased to 573K and 773K the weight uptake decreases from the initial uptake to a value of zero in about 12h and remains constant.

As the thiophene concentration is increased to 1000ppm the adsorption at 298K shows a faster adsorption rate during the first 4h, this rate decreases and seems to be slower than the adsorption at 100ppm in the period 5h-20h. At 20h the uptake is still increasing although at a slow rate.

The uptake at 373K reaches a constant value after 6h, but the adsorption at 573K after a period of constant weight starts to increase the uptake up to the 20^{th} hour. At 773K the uptake decreases from the intial uptake down to a constant value after 12h.

In both cases (100ppm and 1000ppm) as the temperature increases the final weight uptake decreases but there is a great difference between the uptakes at 298K and 373K and higher temperatures as can be seen in both figures 6.9 and 6.10.

Table 6.3 Amount adsorbed on γ-Al_2O_3 at saturation

Thiophene Concentration / Temperature K	100ppm mg/g	1000ppm mg/g
298	11.92 ± 0.40	7.14 ± 0.02
373	0.90 ± 0.30	0.90 ± 0.30
573	0.0	0.56 ± 0.20
773	0.0	0.10 ± 0.05

Table 6.4 Amount adsorbed at saturation on γ-Al_2O_3 per unit total area

Thiophene Concentration / Temperature K	100ppm $mg/m^2 \times 10^2$	1000ppm $mg/m^2 \times 10^2$
298	6.0 ± 0.2	3.6 ± 0.01
373	0.45 ± 0.15	0.45 ± 0.15
573	0.0	0.28 ± 0.10
773	0.0	0.05 ± 0.03

6.3 Adsorption of H_2S on Ni/Al_2O_3

Few experiments were performed using H_2S as poisoning agent. They were carried out using an H_2S/H_2 mixture of 2ppm concentration and an 8ppm H_2S/N_2 mixture. The studies were carried out at 373K and 773K. The results are shown in Figures 6.11 and 6.12. Figure 6.11 gives the short term adsorption. It can be seen that at 373K the adsorption is very fast, in 2 minutes the catalyst has reached its saturation uptake; there is a small decrease in weight in the following 30 minutes but it is very small indeed and remains at this value for the rest of the experiment as can be seen in Figure 6.12. The experiment at 773K shows a very fast uptake rate; the weight reaches a maximum in about 2 minutes and then decreases for the next 15min until it reaches a constant value where it remains. The experiment using 8ppm H_2S/N_2 shows that the adsorption uptake is slower but is monotonically increasing with a constant rate. The effect of H_2 presence is highly important and it is presumed that in the presence of N_2 there can be bulk sulphide formation at this H_2S concentration. Hence the weight uptake increases indefinitely probably until all nickel has been tranformed into nickel sulphide.

In figure 6.12 the long term adsorption in shown up to 20h. The experiments performed with the H_2S/H_2 mixture reached equilibrium during the first hour, but with H_2S/N_2 the nickel catalyst is still increasing its weight after 20h at a constant rate. In Table 6.5 the final uptakes obtained at 20h are given. These values are in mg per unit nickel area.

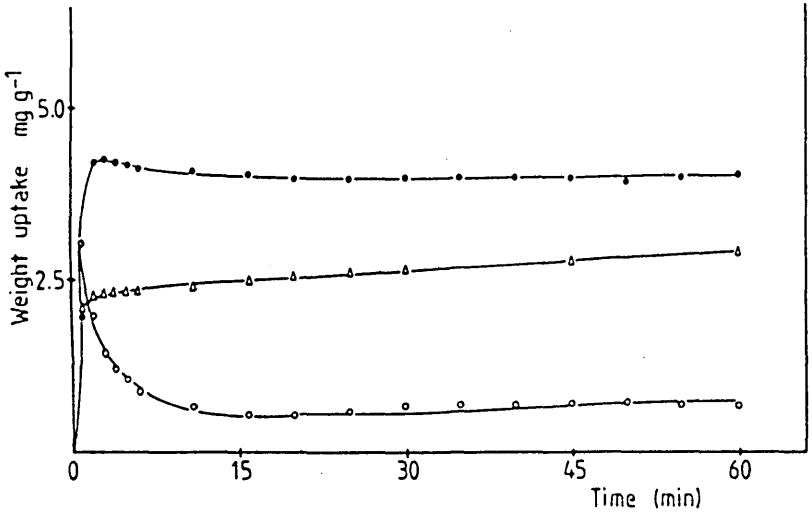

FIGURE 6.11

Adsorption of H_2S on Ni/Al_2O_3. Short time behaviour. 2ppm H_2S/H_2, 373K (●); 2ppm H_2S/H_2, 773K (O); 8ppm H_2S/N_2, 373K (Δ).

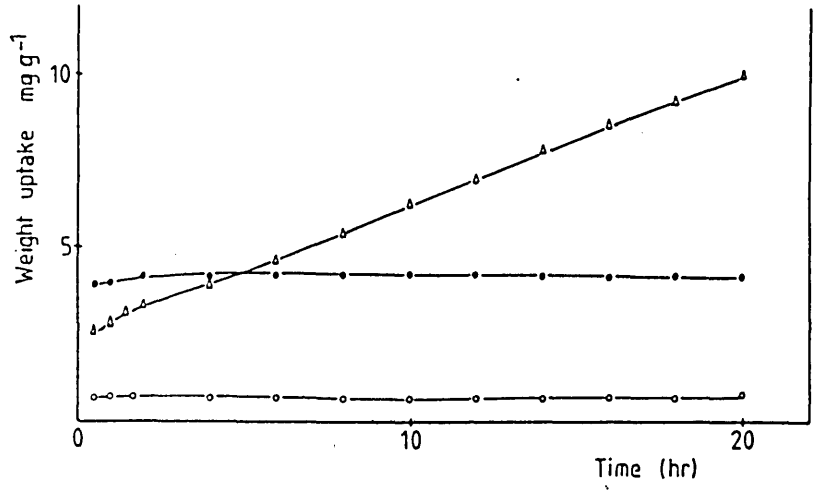

FIGURE 6.12

Long term adsorption of H_2S on Ni/Al_2O_3. 2ppm H_2S/H_2, 373K (●); 2ppm H_2S/H_2, 773K (O); 8ppm H_2S/N_2, 373K (Δ).

Table 6.5 H_2S uptakes on Ni/Al_2O_3 after 20h.

H_2S Concentration	2ppm H_2S/H_2	8ppm H_2S/N_2
Temperature K	mg/m^2Ni	mg/m^2Ni
373	0.30 ± 0.08	0.92
773	0.074 ± 0.01	-

The surface sulphur coverages, θ_s, that correspond to these uptakes are:

0.34 S atom/Ni atom (373K, 2ppm H_2S/H_2) and 0.09 (773K, 2ppm H_2S/H_2).

The sulphur coverage at 373K and 2ppm H_2S/H_2 suggests that H_2S occupies 3 nickel sites and this is in agreement with the results of Saleh et al. (36), but the coverage at 773K is very low compared to the values reported in the literature of 0.74-1.0 at this concentration (33,39). Our results are in agreement with the general view that θ_s decreases with increasing temperature at constant P_{H_2S}/P_{H_2} due to the exothermicity of the adsorption process; however at high temperatures (>673K) saturation sulphur coverages greater than 0.5 have been found (3,32,33,39) and explained considering that at these conditions hydrogen is not adsorbed and therefore there are more Ni sites which sulphur can occupy. Due to the few results obtained it is recommended to study in more detail the H_2S adsorption especially at temperatures

between 373K and 673K to try to identify the temperature region at which the increase in sulphur coverage occurs.

The weight uptake obtained using 8ppm H_2S/N_2 suggests that bulk sulphide is being formed and subsurface Ni layers are being attacked by sulphur since no saturation has been reached after 20h.

6.4 Regeneration of Catalysts

Attempts were made to regenerate the poisoned catalysts. The regeneration consisted on the treatment with H_2 at 873K for a minimum of 40h. The catalyst samples reached equilibrium weight at the end of the process and the weight lost during the treatment was recorded. The effectivity of the regeneration was tested by CO chemisorption to determine the "free" nickel area and by readsorption of thiophene at the temperature of the first adsorption. The results are given below.

6.4.1 Removal of adsorbed thiophene

The introduction of hydrogen for the regeneration treatment and the increase in temperature from the adsorption temperature to the standard regeneration temperature 873K led to the reduction of sample weight due to loss of material adsorbed during poisoning and the effect of buoyancy on the apparent weight of the sample. The overall loss in weight was recorded and the change in weight due to buoyancy was accounted for by measuring the weight loss of a nickel sample when the temperature was raised from the various adsorption temperatures to 873K with hydrogen flowing through. These measurements allowed us to calculate the net weight loss which presumably was due to the removal of thiophene or its component elements (C,S,H). These results are given in Table 6.6, where the overall and net weight losses are given, together with the percentage of material removed which is calculated by

the ratio of the net weight loss to the weight adsorbed during poisoning.

Table 6.6 Material removed during regeneration with H_2 at 873K

Sample	Adsorption Temperature K	Thiophene concentration ppm	Weight loss mg g^{-1}	Net loss mg g^{-1}	%Removal
NAT3-21	298	1000	42.8	8.70	72
NAT3-55B	298	1000	42.1	8.04	85
NAT3-58	373	1000	22.9	3.50	36
NAT3-25	773	1000	7.8	6.50	73
NAT3-56	298	100	39.6	5.52	79
NAT3-57	373	100	22.7	3.20	36
NAT3-50A	773	100	6.0	4.66	81

As mentioned above the weight loss is the total weight change observed from the start of the regeneration until it was finished and includes the weight change due to material desorbed plus the effect of buoyancy as the temperature was increased from the adsorption temperature to the standard regeneration temperature. A nickel catalyst sample - NAT3-22 - was used to determine the corrections due to buoyancy, the values obtained were reproducible with an accuracy of ±0.05 mg/g. Table 6.6 shows that the total weight loss decreases as the adsorption temperature is increased, and this is a direct effect of the weight change due to buoyancy which decreases as the initial temperature increases. The net loss however shows a minimum at the adsorption temperature of 373K; the fraction of the amount removed

seems to be constant at around 80% for catalysts poisoned at 298K and 773K but it has a sharp decrease to 36% for those poisoned at 373K.

A possible explanation for the behaviour observed lies in the type of compounds deposited on the catalyst during adsorption and the facility at which they can be removed.

During adsorption at 298K thiophene is adsorbed, it undergoes little decomposition and very little is desorbed. Increasing the temperature to 373K increases the adsorption rate and the rate at which thiophene reacts and decomposes, great part of the thiophene molecule is desorbed as hydrocarbon but it is expected that part remains on the catalyst. At 773K the percentage of hydrocarbons adsorbed is small but it is possible that carbon polymerises and forms deposits which sit on the catalytic surface.

During regeneration with H_2 carbon and sulphur are removed as the temperature is increased from the adsorption to the regeneration temperature (873K) (177). From 298K to 873K great amounts of sulphur and carbon are removed; however as the adsorption temperature is increased, it is more difficult to remove the adsorbed sulphur due to its high stability (3,32,33). Samples poisoned at 373K are expected to have less carbon (than at 298K) and the sulphur is retained by the nickel catalyst, hence the amount removed is smaller. The percentage of carbon adsorbed at 773K is high and it is possible to be removed by H_2 at 873K, resulting in high amounts of material removed.

It also has to be considered that the errors in the net loss calculation may be high due to the high buoyancy corrections involved.

Whether the values of percentage removal given in Table 6.6 represent the true percentage of regeneration has to be assessed, but

it is clear that the treatment is partially successful in removing material adsorbed on the catalysts.

6.4.2 CO Chemisorption on regenerated catalysts

The regeneration of a spent catalyst may be assessed in several ways. One of them consists in the measurement of the active metal area or free metal area after the treatment and its comparison with the initial area or with the area before regeneration.

CO chemisorption at 195K was used to try to assess the free nickel area after regeneration. Nickel catalysts poisoned at 298K and 773K with 1000ppm thiophene in hydrogen and regenerated at 873K with hydrogen were subjected to the CO chemisorption process. Figures 5.34 and 5.35 show the CO adsorption on regenerated nickel catalysts which were poisoned at 298K and 1000ppm and 773K and 1000ppm respectively.

The figures show the first, total, adsorption isotherms of the regenerated catalysts and the clean sulphur-free samples. Only the first isotherm was determined to avoid damage to the microbalance by the nickel tetracarbonyl removed during evacuation (see section 5.3.5).

It can be seen that the isotherms for the regenerated catalysts show a much higher uptake than the corresponding isotherms on the clean catalysts. As demonstrated in Chapter 5 this is explained by the presence of sulphur which promotes the formation of nickel tetracarbonyl so that the CO uptakes are larger than on clean samples. Sulphur, then is still present on the catalyst after the regeneration treatment.

Comparisons can be made between figures 5.34 and 5.35 with figures 5.32 and 5.33. The former are the CO isotherms on the regenerated catalysts, the latter show the CO adsorption on the poisoned samples.

Poisoning was carried out at 298K and 1000ppm for the samples shown in figures 5.32 and 5.34; and at 773K and 1000ppm for the other two.

It can be noticed that the regeneration process does not seem to remove sulphur from the samples; the uptake curves for the regenerated and poisoned samples appear to be very close at both poisoning temperatures (298K and 773K). It can also be said that the CO uptake on the samples poisoned at 298K seems to be lower than the uptake on the samples poisoned at 773K. In Table 6.7 the values of the CO uptake on regenerated and poisoned samples masured at a pressure of 15 kPa are given.

Table 6.7 Total CO uptake on poisoned and regnerated catalysts at 15 kPa, T_{ads} = 195K

Sample*	CO uptake clean $\mu molg^{-1}$	CO uptake regenerated $\mu molg^{-1}$	CO uptake poisoned $\mu molg^{-1}$	Ratio**
NAT3-21 (298K,1000ppm)	560	3530	-	6.3
NAT3-25 (773K,1000ppm)	470	4360	-	9.3
NAT3-31 (298K,1000ppm)	410	-	3490	8.5
NAT3-32 (773K,1000ppm)	470	-	4280	9.1

* Numbers in parenthesis give temperature of poisoning and thiophene concentration

** Ratio of the uptake on poisoned or regenerated sample to that on the clean.

The values in Table 6.7 show firstly that as the poisoning temperature is increased the CO uptake on the poisoned catalyst increases. Therefore, since more CO uptake means more sulphur as was shown in Chapter 5, it is expected that the amount of sulphur taken up by the catalysts be higher at the higher temperature. Secondly the regeneration process does not seem to have a great effect. The amount of CO adsorbed on samples poisoned at 773K and regenerated after poisoning at the same temperature is very similar and the ratios of the uptakes are very close. In the case of the samples poisoned at 298K and 1000ppm the CO uptakes on poisoned and regenerated samples are close but the ratio of the uptakes on the regenerated sample is lower than the ratio of the poisoned-only sample. This could mean that the amount of sulphur on the regenerated sample is lower than on the poisoned sample. It can be said then, that for catalysts poisoned at 298K the regeneration treatment is at least partially successful in removing sulphur. This is also supported by results from the elemental analysis (see section 6.6). The regeneration process appears to be unsuccessful for samples poisoned at 773K, 1000ppm which show similar ratios of CO uptakes for both poisoned and regenerated samples.

On the whole it seems that the regeneration process does not remove sulphur at the levels required for the re-use of the catalyts. However the measurement of the extent of regeneration by CO chemisorption does not appear to be satisfactory since it does not measure the free nickel area because it is dominated by the presence of sulphur which promotes nickel carbonyl formations and at most it can only give qualitative results.

6.4.3 Adsorption of thiophene on regenerated catalysts

Samples poisoned with sulphur compounds and regenerated at 873K with hydrogen were subjected to a second poisoning with thiophene. This adsorption was carried out at the same conditions used for the first poisoning. Following the trend used in previous sections the results are presented in short and long term adsorption patterns.

6.4.3.1 Short term adsorption - Effect of temperature and concentration

Ni/Al_2O_3 samples were poisoned at temperatures of 298K, 373K and 773K after being poisoned and regenerated with hydrogen. The results of the adsorption behaviour during the first 60 minutes using a thiophene concentration of 100ppm are shown in Figures 6.13 to 6.15. In Figure 6.13 the plots correspond to the adsorption at 298K and 100ppm. The adsorption uptake on the fresh catalyst is fast, reaches a maximum and decreases slightly in the rest of the period; in contrast the uptake on the regenerated catalyst is fast at the beginning with a rate similar to that of the fresh sample, the rate decreases slightly but the weight uptake increases during the 60 minute period. This behaviour is also observed at the adsorption temperature of 373K on the NAT3-57 catalyst of figure 6.14. On the clean sample the adsorption is fast, reaches a maximum weight and then the weight starts to decrease slowly for the following 55 minutes; on the regenerated catalyst the initial adsorption appears to be occurring at the same rate as on the clean sample, then it slows down slightly but the weight is still increasing and seems to attain an almost constant weight in about 40 minutes. At 773K and 100ppm the adsorption pattern appears to be the same on both clean and regenerated catalysts although the amount

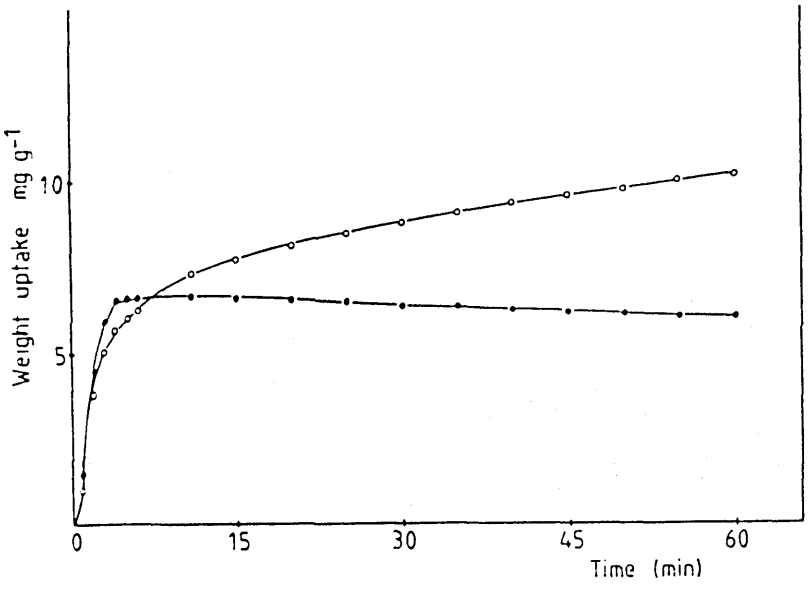

FIGURE 6.13

Adsorption of thiophene on Ni/Al_2O_3 at 298K, 100ppm. Short time behaviour. Clean catalyst (●), regenerated catalyst (0).

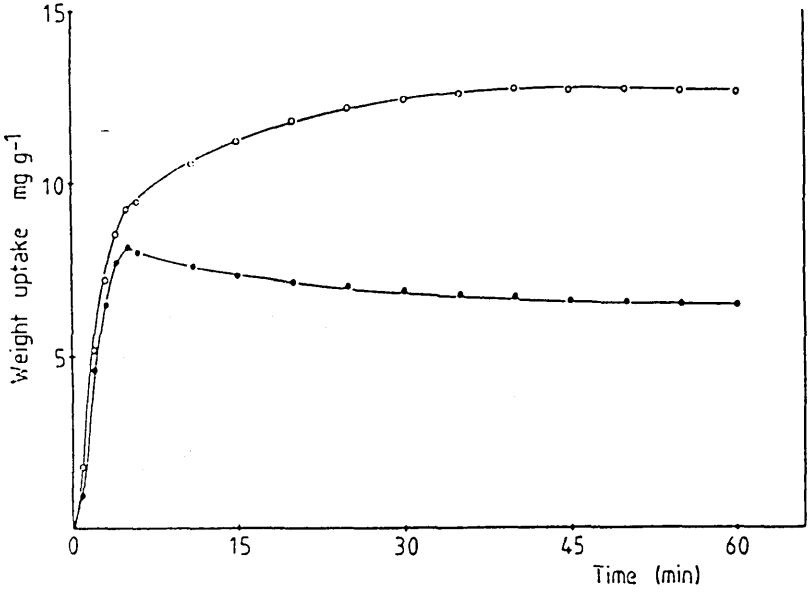

FIGURE 6.14

Adsorption of thiophene on Ni/Al_2O_3 at 373K, 100ppm. Short time behaviour. Clean catalyst (●), regenerated catalyst (0).

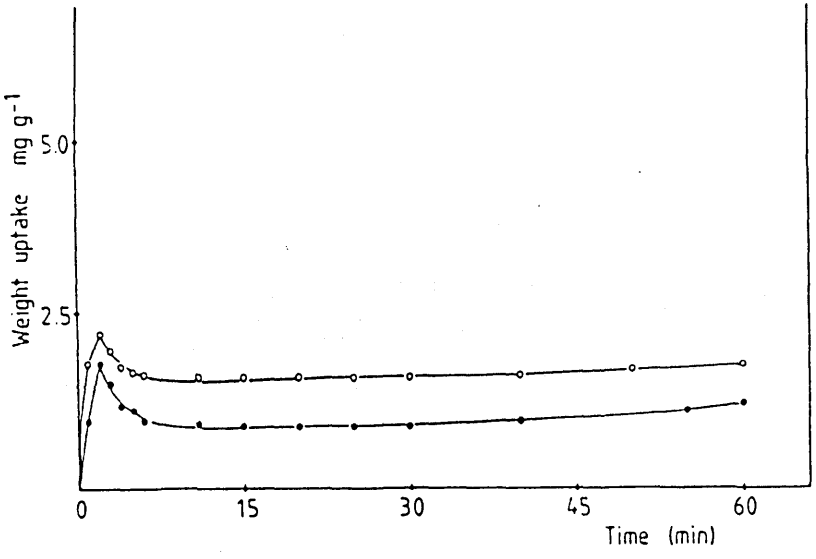

FIGURE 6.15

Adsorption of thiophene on Ni/Al_2O_3 at 773K, 100ppm. Short time behaviour. Clean catalyst (●), regenerated catalyst (O).

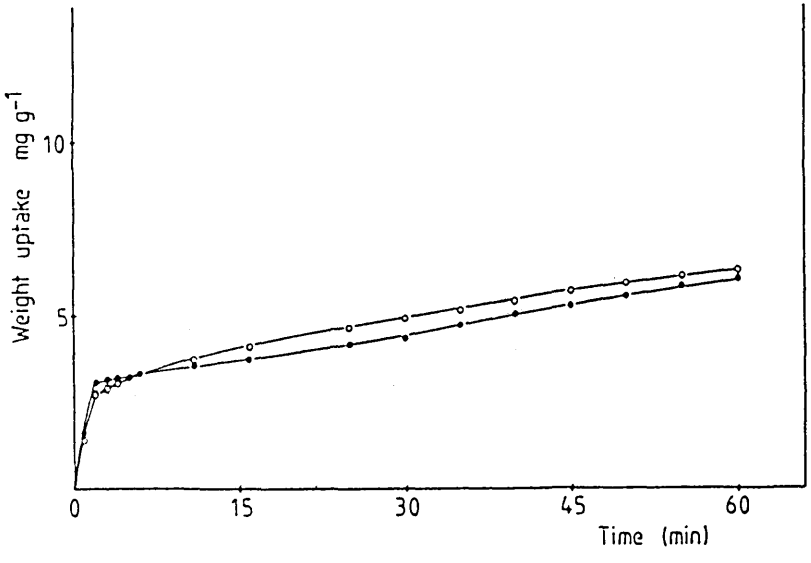

FIGURE 6.16

Adsorption of thiophene on Ni/Al_2O_3 at 298K, 1000ppm. Short time behaviour. Clean catalyst (●), regenerated catalyst (O).

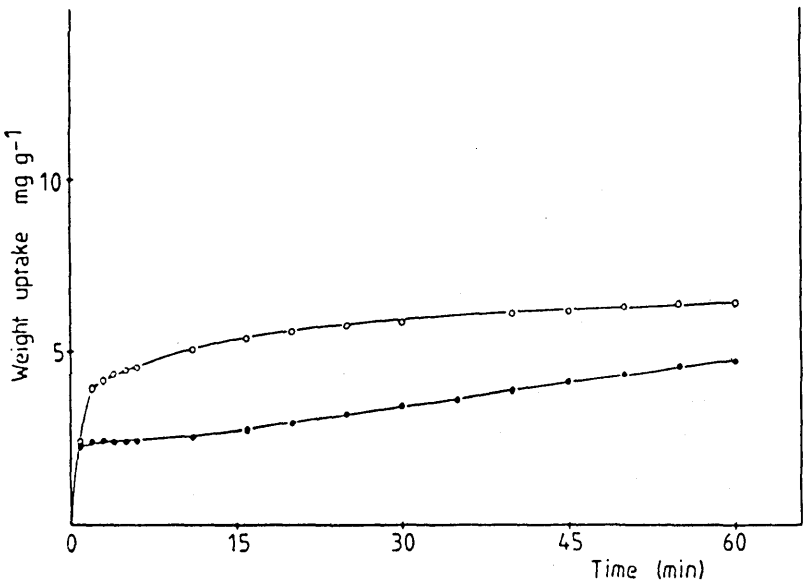

FIGURE 6.17

Adsorption of thiophene on Ni/Al_2O_3 at 373K, 1000ppm. Short time behaviour. Clean catalyst (●), regenerated catalyst (O).

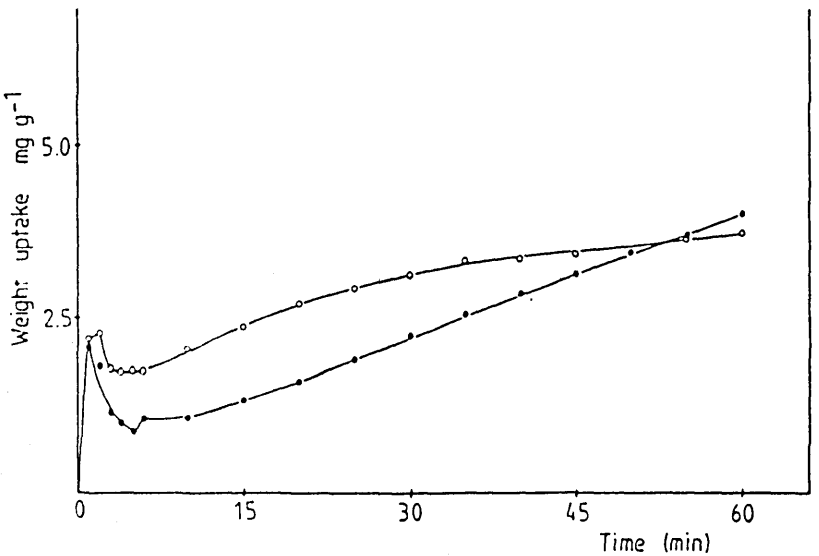

FIGURE 6.18

Adsorption of thiophene on Ni/Al_2O_3 at 773K, 1000ppm. Short time behaviour. Clean catalyst (●), regenerated catalyst (O).

adsorbed on the regenerated sample is higher as can be seen in Figure 6.15. The fast initial adsorption reaches a maximum in weight in 2 minutes and then decreases to a constant weight between the 12^{th} and 30^{th} minutes, after this the weight starts to increase slowly.

The results obtained at the same temperatures and at 1000ppm are shown in figures 6.16 to 6.18.

The adsorption of thiophene on Ni/Al_2O_3 at 298K and 1000ppm is shown in figure 6.16. There is an initial adsorption after which the weight increases at a near constant rate. The adsorption on the regenerated sample shows the same pattern and any variation could be attributed to experimental error. The weight uptakes on the clean and regenerated samples are very similar during the first 60 minutes, unlike the adsorption at 100ppm in which the adsorption uptake on the regenerated sample is higher than on the clean sample. This may indicate that the adsorption mechanism on clean and regenerated samples is the same at 1000ppm, but at 100ppm it is different. The differences observed with increasing thiophene concentration may be the result of the higher physical adsorption at the higher concentration and may be closely related to the behaviour observed on the γ-Al_2O_3 support.

The results shown in Figure 6.17 correspond to the experiment at 373K and 1000ppm. In this case the adsorption curve on the regenerated sample is always above the curve observed for the clean catalyst, and in this way is similar to the adsorption at 100ppm. On the clean catalyst a constant weight which lasts a few minutes is observed after the initial adsorption, then it is followed by a continuous increase in weight for the rest of the hour. On the regenerated catalyst the uptake is higher, and increases over the period at a near constant rate.

Increasing the adsorption temperature to 773K the adsorption behaviour of 1000ppm thiophene on the regenerated catalyst is similar to that on the fresh sample but the uptake is higher during the first 45 minutes as seen in Figure 6.18. The initial uptake on the fresh catalyst is high, then decreases sharply, reaches a minimum in 5 minutes and then increases in the following hour. The uptake on the regenerated catalyst is also high, but the decrease is smaller and the minimum weight is higher than that on the fresh catalyst, then the weight increases initially at the same rate as on the clean sample but decreasing later. At the end of the 60 minute period the uptake on the regenerated catalyst is lower than on the fresh sample.

Two other experiments were performed: nickel/alumina samples were poisoned with 2ppm H_2S/H_2 for 20h, after which they were regenerated with H_2 at 873K and re-poisoned with thiophene 100ppm. The experiments were carried out at 373K and 773K and the results in Figures 6.19 and 6.20 show the short term adsorption.

As can be seen in Figure 6.19 the thiophene adsorption isotherm at 373K on the regenerated catalyst has the same shape as those found for the thiophene adsorption on clean samples (Figure 6.1) and the uptake on regenerated catalysts previously poisoned with thiophene (Figure 6.14). The uptake values however fall between the uptakes on clean and regenerated samples. It appears then that the sulphur retained by the catalyst after regeneration affects the adsorption behaviour of the thiophene. Thiophene is adsorbed in greater extent on regenerated (poisoned previously with 2ppm H_2S/H_2) samples, but to lower amounts than on samples regenerated after being poisoned with 100ppm thiophene at the same temperature. It seems therefore that the adsorption uptake depends on the sulphur coverage since it is expected that the amount of

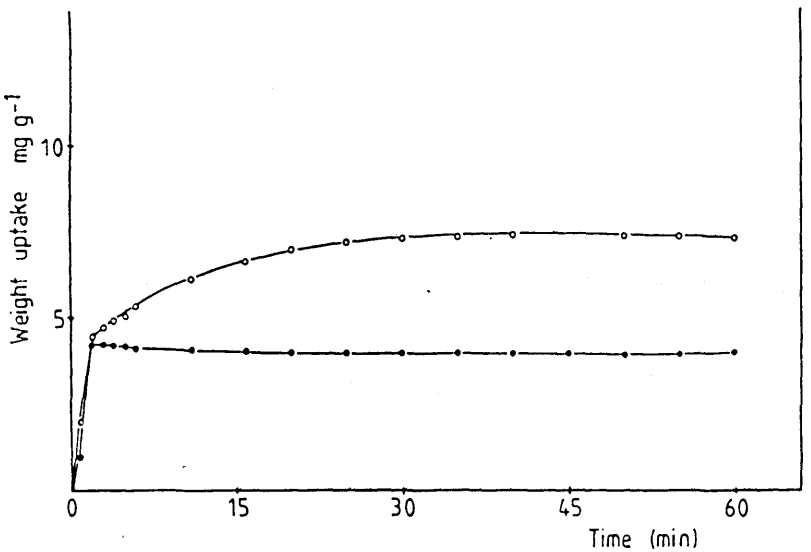

FIGURE 6.19

Adsorption on Ni/Al_2O_3 at 373K. Poisoning with 2ppm H_2S/H_2 clean catalyst (●); re-poisoning with 100ppm thiophene, regenerated catalyst (0). Short time behaviour

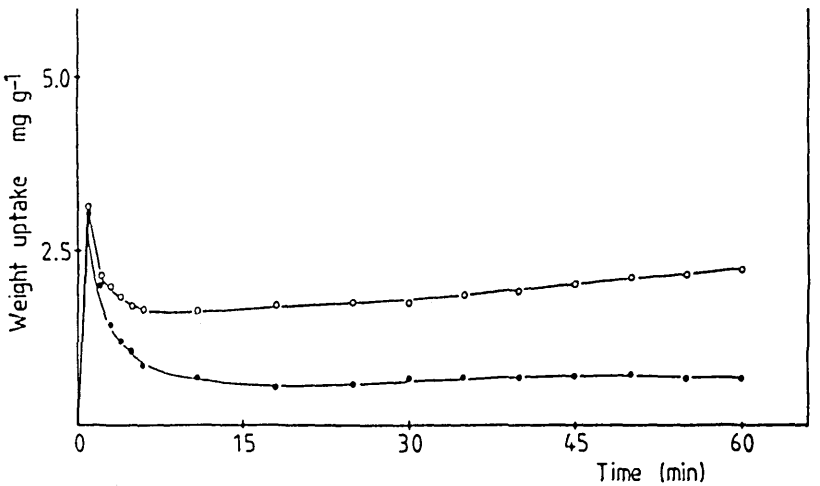

FIGURE 6.20

Adsorption on Ni/Al_2O_3 at 773K. Clean sample poisoned with 2ppm H_2S/H_2 (●), re-poisoning with 100ppm thiophene, regenerated catalyst (0). Short time behaviour.

sulphur adsorbed using 100ppm thiophene would be higher than with 2ppm H_2S/H_2.

The result of the adsorption of thiophene on regenerated Ni/Al_2O_3 at 773K is shown in Figure 6.20. The shape of the curve at the beginning of the adsorption is similar to the one observed on the regenerated sample (poisoned with 100ppm thiophene) as seen in Figure 6.15; but the increase in weight after the constant weight period is faster than on both the clean and regenerated samples.

6.4.3.2 Long term adsorption - Effect of temperature and concentration

As with the results reported in Section 6.1 the re-adsorption of thiophene on the regenerated samples was carried out for 20h. The results of the poisoning with 100ppm thiophene/H_2 are shown in Figure 6.21 for 298K, Figure 6.22 for 373K and Figure 6.23 for 773K; figures 6.24 to 6.26 give the results at the same temperatures but using 1000ppm.

The adsorption uptake on regenerated samples using 100ppm thiophene at 298K increases rapidly during the first two hours, then the rate decreases and the weight goes up very slowly. The uptake is higher than on the clean sample with a final weight which is almost double of the one found on the clean catalyst, and in the range of the uptakes using 1000ppm on fresh catalysts.

At 373K a similar situation occurs: the final weight is higher on the regenerated than on the clean catalyst. The slight weight increase observed on the fresh sample between 3 and 20 hours is lower on the regenerated sample for which the uptake increases in about 6% in that period, whereas it represents about 25% for the clean catalysts as can be seen in Figure 6.22.

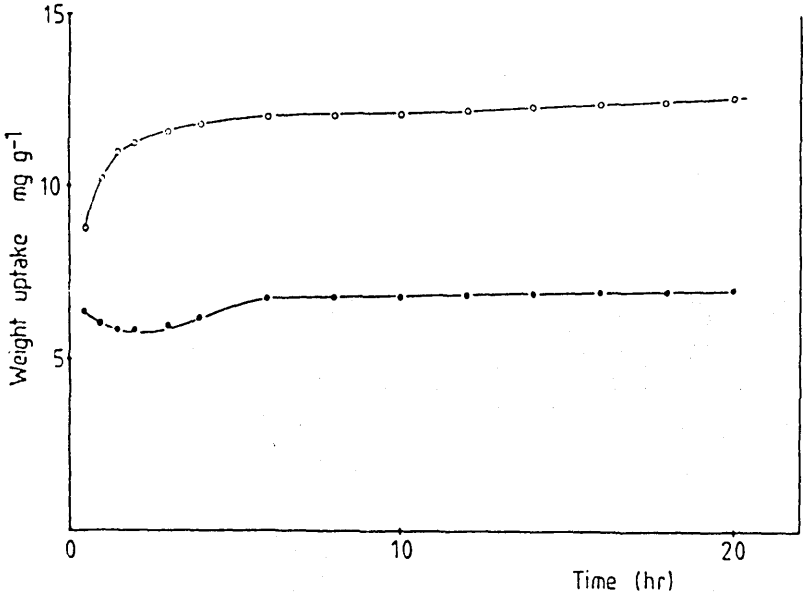

FIGUER 6.21

Long term adsorption of thiophene on Ni/Al_2O_3 at 298K, 100ppm. Clean catalyst (●), regenerated catalyst (O).

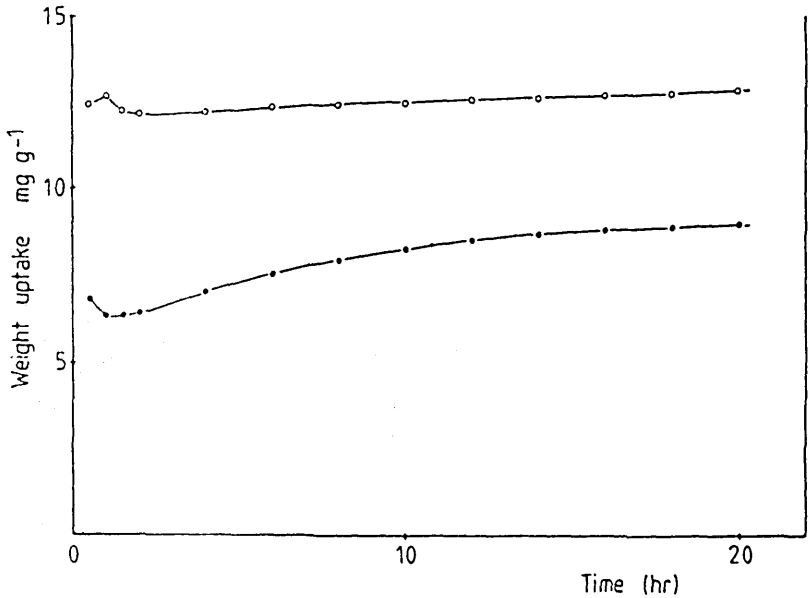

FIGURE 6.22

Long term adsorption of thiophene on Ni/Al_2O_3 at 373K, 100ppm. Clean catalyst (●), regenerated catalyst (O).

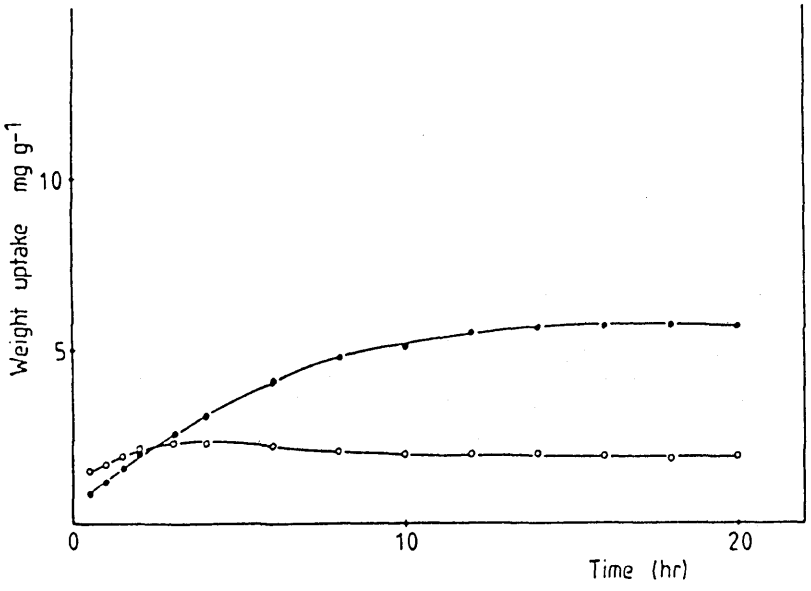

FIGURE 6.23

Long term adsorption of thiophene on Ni/Al_2O_3 at 773K, 100ppm. Clean catalyst (●), regenerated catalyst (O).

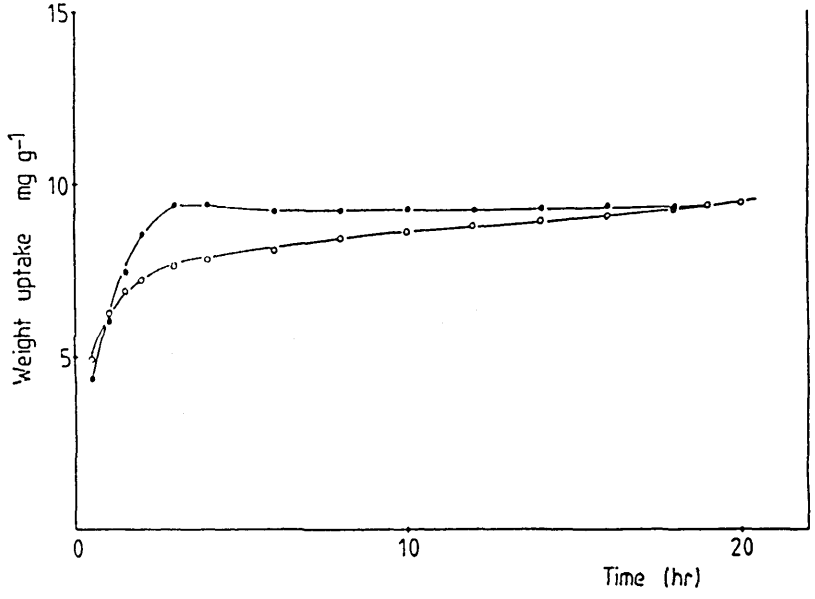

FIGURE 6.24

Long term adsorption of thiophene on Ni/Al_2O_3 at 298K, 1000ppm. Clean catalyst (●), regenerated catalyst (O).

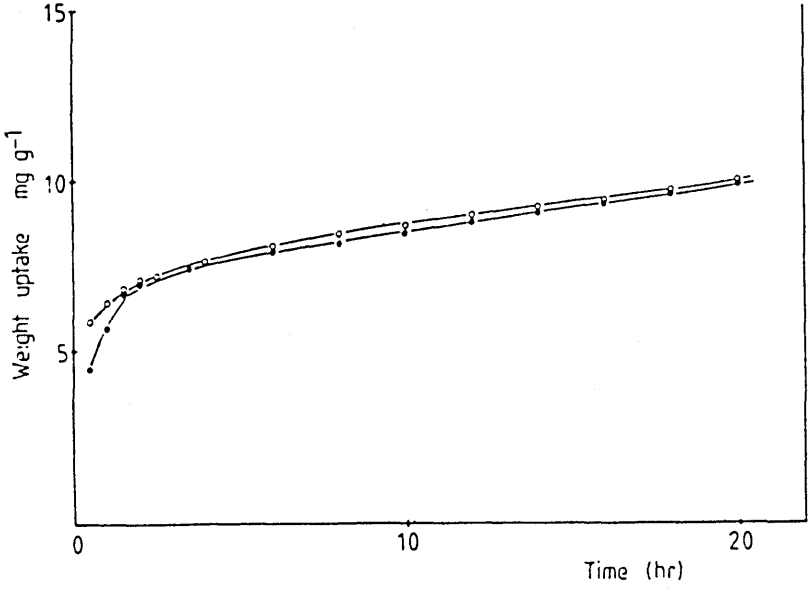

FIGURE 6.25

Long term adsorption of thiophene on Ni/Al_2O_3 at 373K, 1000ppm. Clean catalyst (●), regenerated catalyst (O).

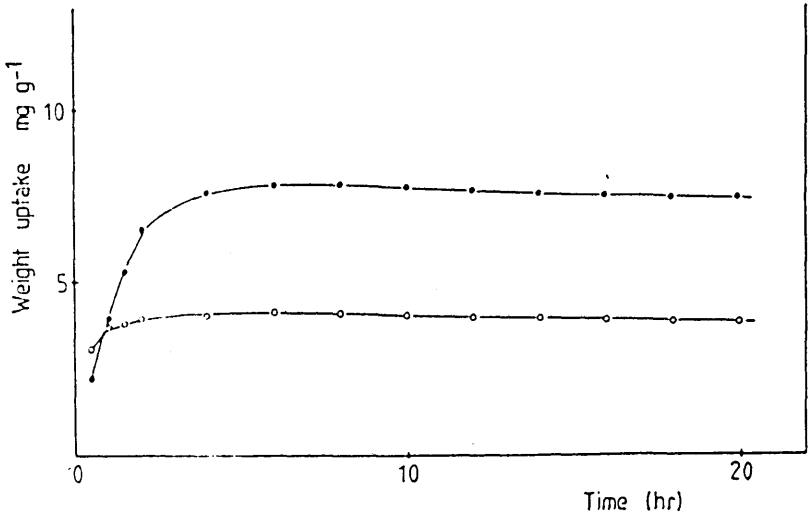

FIGURE 6.26

Long term adsorption of thiophene on Ni/Al_2O_3 at 773K, 1000ppm. Clean catalyst (●), regenerated catalyst (O).

The situation changes for the adsorption at 773K. Figure 6.23 shows that after being higher during the first 2 hours the weight uptake on the regenerated sample reaches a maximum in the 3rd hour and then decreases slightly, whereas the uptake on the fresh sample increases at a constant rate in the same period and reaches saturation with an equilibrium weight higher than on the regenerated sample. The final weight on the latter is about a third of the weight gained by the fresh catalyst.

With a concentration of 1000ppm the adsorption pattern of the regenerated sample is the same as that on the fresh catalyst at both 298K and 373K as can be seen in figures 6.24 and 6.25. At 298K the adsorption isotherm on the fresh catalyst reaches saturation in about five hours and remains there with little variation upwards, whereas the adsorption on the regenerated sample is slower and continues to increase at a slow rate for the rest of the period.

The adsorption at 373K and 1000ppm showed a higher uptake on the regenerated catalyst during the first hour; the rate, however, decreases and after the second hour the isotherms on both fresh and regenerated samples are the same.

Figure 6.26 shows that the adsorption behaviour at 773K and 1000ppm is similar to that observed at the same temperature at 100ppm; initially the adsorption on the regenerated sample has a higher uptake but its rate decreases fast and reaches saturation in 2 hours; after the first hour the uptake on the fresh catalyst is higher and its equilibrium weight is about twice as much as that on the regenerated catalyst. Table 6.8 contains the final weights observed on the fresh and regenerated catalysts at the end of the experiments.

The long term results of the experiments in which the catalyst was

poisoned with 2ppm H_2S/H_2, regenerated and poisoned with 100ppm thiophene/H_2 are shown in Figures 6.27 and 6.28. The adsorption of thiophene at 373K as given in Figure 6.28 shows that after a period of constant weight the uptake increases in a manner similar to that on fresh catalysts. The weight, however, falls between the weights observed for the thiophene adsorption on fresh and regenerated (thiophene-poisoned) catalysts as can be seen when comparing Figure 6.27 with Figure 6.22.

Figure 6.28 shows that the adsorption of thiophene on the regenerated (H_2S poisoned) catalyst at 773K follows the same pattern as that of the fresh samples. The uptake though seems to occur at a faster rate and the final uptake is slightly higher than on clean catalysts. The saturation uptakes are given in Table 6.9 below.

Table 6.8 Saturation Uptakes of Thiophene on Fresh and Regenerated Ni/Al_2O_3 Catalysts

Temperature K	Thiophene Concentration ppm			
	100		1000	
	Fresh Sample	Regenerated Sample	Fresh Sample	Regenerated Sample
	mg g^{-1}	mg g^{-1}	mg g^{-1}	mg g^{-1}
298	7.00	12.51	9.41	9.32
373	8.92	12.82	9.63	9.77
773	5.73	2.00	7.51	3.93

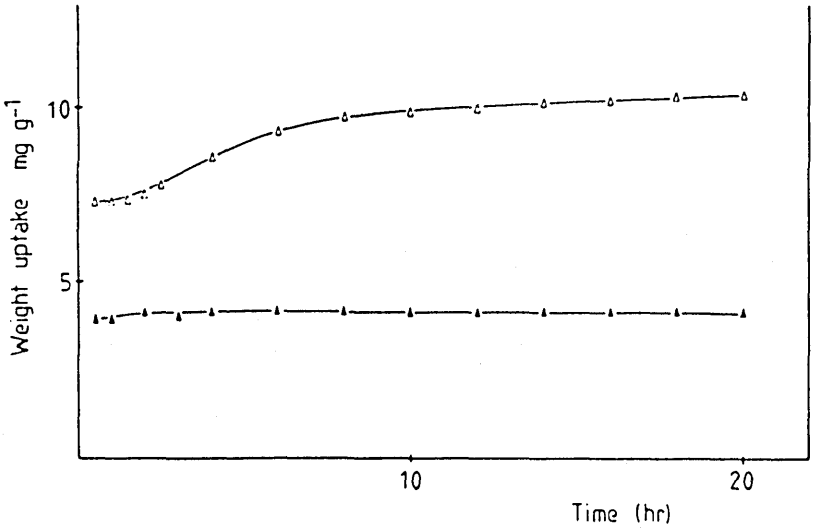

FIGURE 6.27

Long term adsorption on Ni/Al_2O_3 at 373K. Clean catalyst poisoned with 2ppm H_2S/H_2 (●), regenerated catalyst re-poisoned with 100ppm thiophene/H_2 (○).

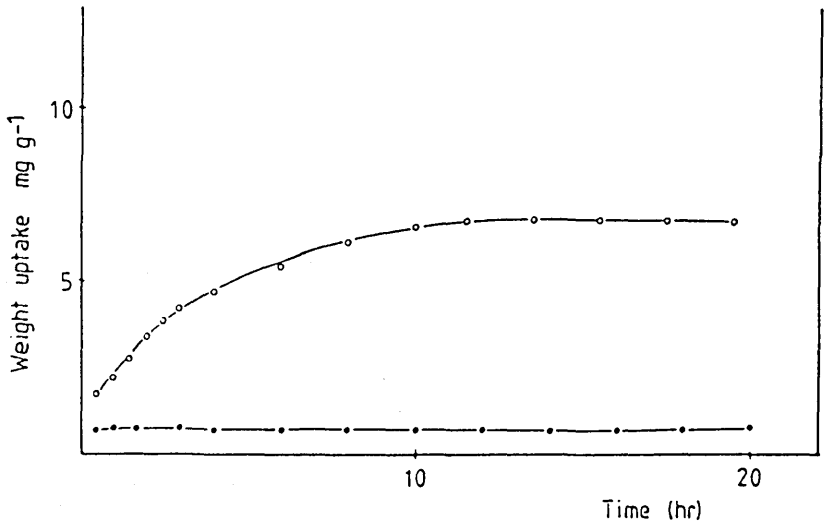

FIGURE 6.28

Long term adsorption on Ni/Al_2O_3 at 773K. Clean catalyst poisoned with 2ppm H_2S/H_2 (●), regenerated catalyst re-poisoned with 100ppm thiophene/H_2 (○).

Table 6.9 Saturation Uptakes of H_2S on Fresh Catalysts and Thiophene 100ppm on the Regenerated Samples

Temperature K	Fresh Sample mg g^{-1}	Regenerated Sample mg g^{-1}
373	4.20	10.40
773	0.80	6.85

The values in weight per area of metal surface are given in Tables 6.10 and 6.11 respectively.

Table 6.10 Saturation Uptakes per unit area of Thiophene on Fresh and Regenerated Ni/Al_2O_3 Catalysts.

Temperature K	Thiophene Concentration ppm			
	100		1000	
	Fresh Sample mg/m^2Ni	Regenerated Sample mg/m^2Ni	Fresh Sample mg/m^2Ni	Regenerated Sample mg/m^2Ni
298	0.58	1.04	0.87	0.86
373	0.81	1.17	0.80	0.81
773	0.49	0.17	0.37	0.37

Table 6.11 Saturation Uptakes per Unit Area of H_2S on Fresh Samples and Thiophene 100ppm on Regenerated Catalysts

Temperature K	Fresh Sample mg/m^2Ni	Regenerated Catalyst mg/m^2Ni
373	0.40	0.98
773	0.074	0.63

These tables show that with 100ppm thiophene/H_2 the adsorption uptake at saturation is higher on the regenerated sample at 298K and 373K whereas with 1000ppm the uptakes are similar; in both cases the adsorption at 773K results in lower uptakes on the regenerated samples. These results demonstrate firstly that the mechanism of thiophene adsorption on regenerated samples may be different from that on clean samples; secondly that the mechanism is affected by the thiophene concentration; and thirdly that as the temperature increases the mechanism may change.

With clean samples the basic mechanism proposed by Lyubarskii et al. (45) is followed. At room temperature thiophene is adsorbed dissociatively. A very small amount reacts slowly with hydrogen to form gaseous products and leaving sulphur adsorbed, but the major part of the material adsorbed remains on the surface. It is also expected that a physical adsorption contribution exists which would increase with an increase in the thiophene concentration; therefore the amount

adsorbed increases as the concentration increases.

Increasing the temperature increases the rate of thiophene adsorption and decomposition. The proportion of carbon atoms staying adsorbed on the surface decreases since the formation of gaseous hydrocarbons is faster; once the hydrocarbon part of thiophene is desorbed, more nickel sites are available to adsorb more thiophene which reacts yielding more hydrocarbons and adsorbed sulphur; in the long term it would be expected that the amount of sulphur per unit metal area would increase. The rate of this overall process is expected to increase as the thiophene concentration increases. This was observed (comparing Figures 6.4 with 6.5).

During regeneration with hydrogen at 873K thiophene or carbon atoms adsorbed react and decompose to give hydrocarbons; if sulphur is removed it is done in much smaller proportions and it is believed that the greater part is retained by the catalyst. At the end of the regeneration the catalyst has lost weight due to material desorbed, but it still contains sulphur and perhaps carbon. These elements are blocking possible adsorbing nickel sites so that the number of free nickel sites is smaller than on clean samples.

Since thiophene requires an ensemble of five nickel sites to be adsorbed co-planar to the surface it is possible that the fewer sites available induce adsorption through the sulphur atom and possibly through a carbon atom close to the sulphur; therefore thiophene would be in an upright position rather than parallel to the surface, in this case the amount of thiophene adsorbed at low temperatures would be higher than on clean catalysts. This effect has been observed during the poisoning at 298K and 373K with 100ppm thiophene, but not with 1000ppm. A possible explanation for this behaviour would have to

consider the amount of thiophene physisorbed, which is higher at 1000ppm. The chemically and physically adsorbed thiophene may polymerize forming a condensed layer on the catalyst surface at 1000ppm; whereas at 100ppm the concentration may be low enough to avoid polymer aggregation but instead the thiophene is adsorbed through the heteroatom forming a close-packed arrangement, which with less physisorbed material may allow the thiophene to reach the catalyst surface, and therefore the weight observed at 100ppm would be higher than with 1000ppm. This is a situation similar to that found for the adsorption of thiophene on the γ-alumina support; in this case the observed amount of thiophene being adsorbed with a concentration of 100ppm was higher than with 1000ppm. This behaviour was explained using the same argument and it is supported by the results of Rochester and Terrell (48), Curtis et al. (82) and Klosterman et al. (53).

At 773K the amount adsorbed at saturation on the regenerated sample is lower than on the clean sample at both thiophene concentrations. This suggest that the regeneration process removes part of the material adsorbed during poisoning allowing thiophene to re-adsorb and react. It is expected that thiophene adsorbs through the sulphur atom, perpendicular to the surface, because some surface nickel atoms are still blocked by sulphur adsorbed in the first poisoning which hinders the co-planar adsorption as was shown in the low temperature experiments. It would also be expected that the gaseous products formed during thiophene reaction are unsaturated rather than saturated hydrocarbons.

The results of the adsorption of thiophene on regenerated Ni catalysts poisoned previously with H_2S are in agreement with the

results on regenerated Ni catalysts previously poisoned with thiophene (Figures 6.27 and 6.28).

However the amount of thiophene adsorbed at both temperatures lies between that on fresh catalysts and regenerated (thiophene-poisoned) catalysts; this may be a result of the lower sulphur coverage attained with 2ppm H_2S/H_2 which would permit that some thiophene molecules are adsorbed co-planarly to the surface and some through the sulphur atom yielding in once case (373K) an adsorbed amount higher than that on clean catalysts, and at 773K higher amounts due to the increased sulphur uptake as thiophene is adsorbed through the sulphur atom, hence the hydrocarbon part of the molecule has less contact with the nickel and less carbon is deposited on the surface.

6.5 Kinetic Results

The adsorption results were adjusted to an empirical rate equation to determine an apparent rate constant and the possible controlling mechanisms during the adsorption process.

A power-law equation of the type proposed by Ritchie (166) was used. Ritchie stated that if θ is the fraction of surface sites occupied by the adsorbed gas, α the number of surface sites occupied by each molecule of adsorbed gas, and k the rate constant, the rate of adsorption can be described by the equation:

$$\frac{d\theta}{dt} = k\ (1-\theta)^{\alpha} \qquad (6.1)$$

assuming that the rate of adsorption depends only on the fraction of free sites.

Upon integration equation (6.1) gives:

$$(1-\theta)^{1-\alpha} = (\alpha-1)\ kt + 1 \quad \text{for } \alpha \neq 1 \qquad (6.2)$$

or

$$\theta = 1-e^{-kt} \qquad \text{for } \alpha = 1 \qquad (6.3)$$

with $\theta = 0$ at $t = 0$

Introducing the amount adsorbed n at time t equations 6.2 and 6.3 become:

$$\left(1 - \frac{n}{n_\infty}\right)^{1-\alpha} = (\alpha-1)\ kt + 1 \qquad (6.2a)$$

and

$$n = n_\infty(1-e^{-kt}) \qquad (6.3a)$$

where n_∞ is the amount adsorbed at infinite time (saturation 20h), and $\theta = \frac{n}{n_\infty}$.

The adsorption data was fitted to a linear form of equation 6.3a to find k, and it corresponded to the best fit since the use of eqn 6.2a for α=2,3 was not successful.

To continue with the manner the results were presented previously the analysis was divided in short and long term at the two concentrations used (100ppm and 1000ppm).

6.5.1 Short-term determinations

These determinations correspond to the adsorption observed until 60 minutes. First the calculation obtained with the uptakes at 100ppm are given, then those found at 1000ppm.

As was seen in section 6.1 the adsorption isotherms using a thiophene concentration of 100ppm that can be fitted to an equation of the form (6.1) are those obtained at 298K and 373K in which an increase in weight with time was observed; the adsorptions at 573K and 773 are more complex in the short term and cannot be treated with a simple equation as eqn. (6.1).

For the adsorption with 100ppm thiophene the values at 298K and 373K were plotted as $\ln(1-\frac{n}{n_\infty})$ vs. time as shown in Figure 6.29. It was observed that for the adsorption at 298K two slopes existed: one at very short times, $t \leq 4$min, and another at $4 \leq t \leq 15$min; at 373K only one region was observed at $t \leq 4$min, time after which the weight remained constant; on the regenerated samples however two regions were found at both temperatures.

At 1000ppm two regions were observed in the short time adsorption behaviour at 298K and 373K and only one at 573K and 773K. At the lower temperatures the two slopes were the initial at $1 \leq t \leq 4$min and the second at $15 \leq t \leq 60$min; whereas at the higher temperatures the rate constant was determined only at $15 \leq t \leq 60$min, this was due to the complex behaviour observed at $t \leq 15$min in which the weight first increased and then decreased . Figure 6.30 shows the plot of $\ln(1- n/n_\infty)$ vs. time for the adsorption at 1000ppm.

The values of the rate constants so determined are given below in Tables 6.12, 6.13 and 6.14.

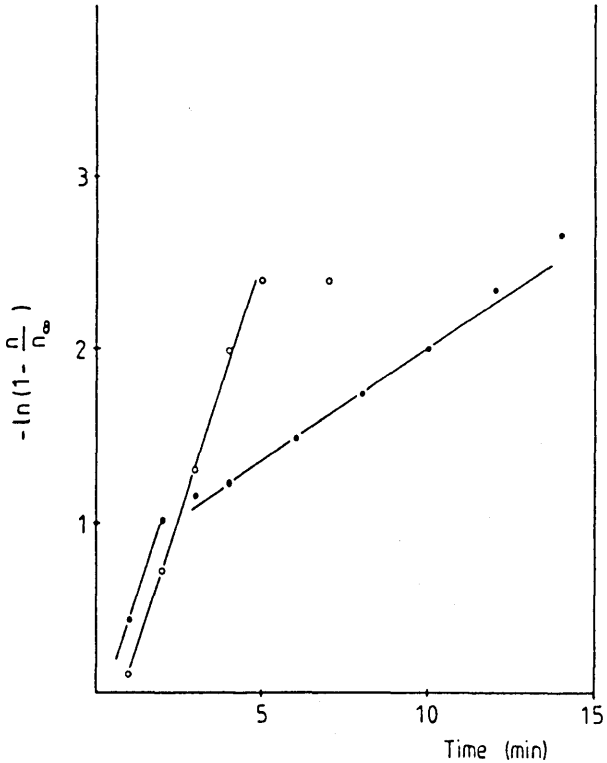

FIGURE 6.29

Plot of ln (1 - n/n_∞) vs time for the short term adsorption of thiophene (100ppm) on Ni/Al_2O_3. 298K (●), 373K (O).

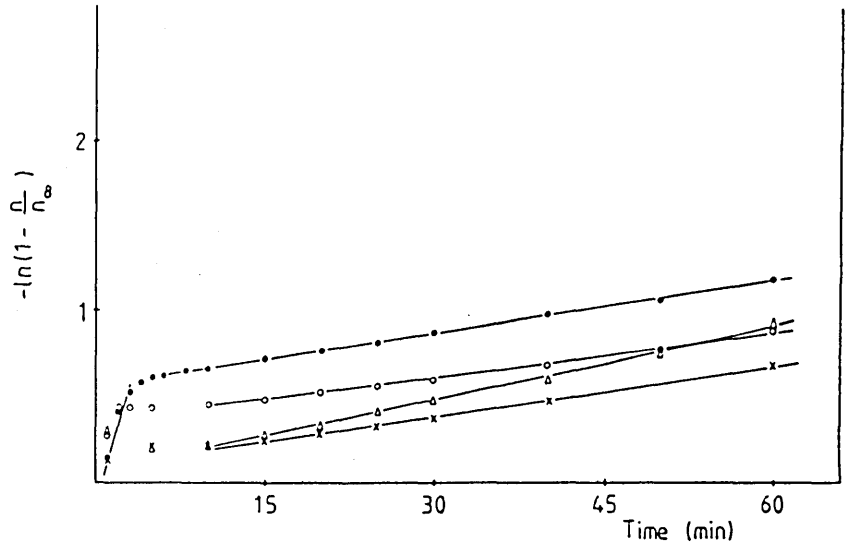

FIGURE 6.30

Plot of ln (1 - n/n_∞) vs time for the short term adsorption of thiophene (1000ppm) on Ni/Al_2O_3. 298K (●), 373K (O), 573K (x), 773K (Δ).

Table 6.12 Rate Constant Values for the Thiophene Adsorption. Short Term, 100ppm. Ni/Al_2O_3 Catalysts.

Temperature K	k, min^{-1} $1 \leq t \leq 4min$	k, min^{-1} $4 \leq t \leq 15min$
298	0.47 ± 0.11	0.11 ± 0.011
373	0.38 ± 0.17	-
298 (regenerated)	0.22	0.02
373 (regenerated)	0.31	0.08
373 (regenerated/ H_2S poisoned)	0.34	0.03

Table 6.13 Rate Constant Values for the Thiophene Adsorption. Short term, 1000ppm. Ni/Al_2O_3 Catalysts.

Temperature K	k, min^{-1} $1 \leq t \leq 4min$	k, min^{-1} $15 \leq t \leq 60min$
298	0.24 ± 0.04	0.011 ± 0.001
373	0.25 ± 0.08	0.009 ± 0.0003
573	-	0.012 ± 0.002
773	-	0.014 ± 0.001
773 (Regenerated)	-	0.045

Table 6.14 Rate Constant Values for the Adsorption of Thiophene on Al_2O_3. Short term, 298K.

Thiophene Concentration	k, min^{-1} $4<t<55min$
100ppm	0.005 ± 0.0003
1000ppm	0.018 ± 0.001

The values in Table 6.12 show that the initial adsorption is fast compared to the second process occurring at $4<t<15min$. That the initial adsorption at 298K is faster than at 373K and this could possibly mean that the adsorption mechanism or the adsorbed structure are different. The adsorption at 298K on the regenerated sample is slower as can be seen by the lower rate constants; at 373K the initial rates are the same on the fresh and regenerated samples although the second process not observed on the clean samples shows a small rate constant on the regenerated ones.

Increasing the concentration to 1000ppm the values reported in Table 6.13 show that the initial adsorptions at 298K and 373K have the same rate constant so do the adsorption isotherms in the second process occurring at $15<t<60min$ at all temperatures which suggest that a common mechanism is controlling the rate of adsorption: the process could be controlled by mass transfer, or could be deactivated. The rate of adsorption increases on the regenerated sample about 3 times at 773K; whereas at the lower temperatures the rate of adsorption on regenerated and clean samples is similar.

For the adsorption on alumina, the short term behaviour showed that only the uptake at 298K could be adjusted to the rate equation used and the results in Table 6.14 show that the adsorption is faster at 1000ppm than at 100ppm. Comparing the values of the rate constants on alumina with those on Ni/Al_2O_3 it can be seen that at 100ppm the rate constant on alumina is lower than on nickel catalysts, but at 1000ppm is higher than those obtained on clean nickel catalysts although in the same order of magnitude.

6.5.2 Long term determination

The results of the long term adsorption were adjusted to eqn. 6.3a and the rate constants calculated. At 100ppm the rate constants were calculated for the adsorption at 373K-773K on Ni catalysts as can be seen in Figure 6.31. The variation in the weight uptake at 298K was negligible in the long term and the rate could be taken as zero. Changes in weight were noticed at 1000ppm and 298K, thus the rate constant at this adsorption conditions are included along with those at 373K-773K and 1000ppm in Figure 6.32.

The results are given in Tables 6.15, 6.16 and 6.17 below. At 100ppm two regions were observed for the adsorption at 573K and 773K: one including most of the uptake and a second close to the saturation region; at 373K only one slope was obtained for the adsorption rate and this was close to the saturation region. If we define θ_T the coverage by thiophene (or thiophene products) as the ratio of weight uptake at any point to the uptake at saturation (or infinite time) so that $\theta_T = \frac{n_T}{n_{T_\infty}}$, then the regions involved in the calculations are $0.2 < \theta_T < 0.9$

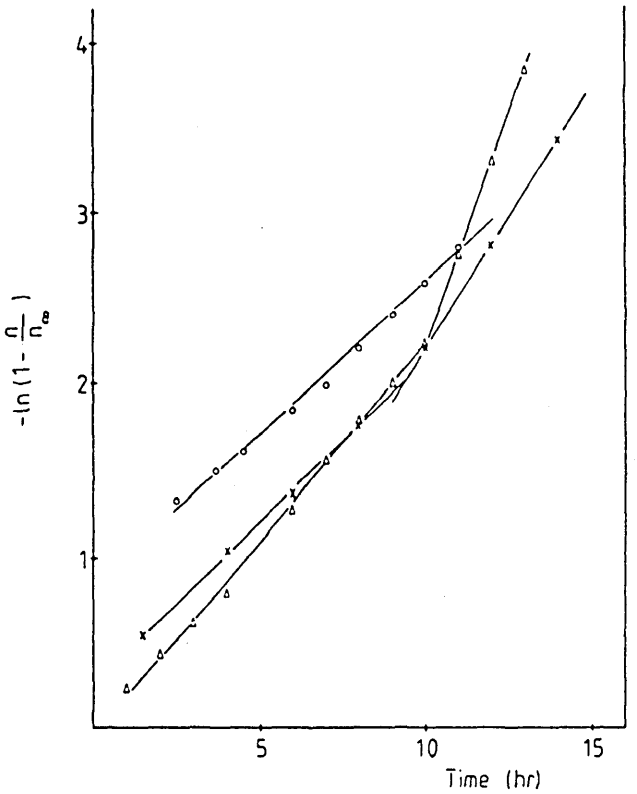

FIGURE 6.31

Plot of ln $(1 - n/n_{\infty})$ vs time for the long term adsorption of thiophene (100ppm) on Ni/Al_2O_3. 373K (O), 573K (x), 773K (Δ).

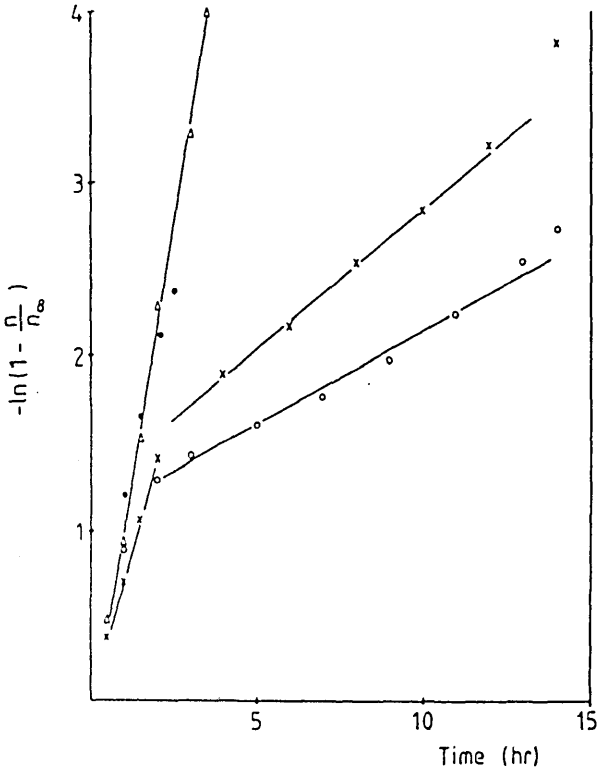

FIGURE 6.32

Plot of ln $(1 - n/n_{\infty})$ vs time for the long term adsorption of thiophene (1000ppm) on Ni/Al_2O_3. 298K (●), 373K (O), 573K (x), 773K (Δ).

for the first, and $0.9 \leq \theta_T \leq 0.98$ for the second in the 573K and 773K adsorptions; at 373K it is between $0.8 \leq \theta_T \leq 0.93$. As can be seen in Table 6.16 at 1000ppm the coverages involved are: $0.65 \leq \theta_T \leq 0.91$ at 298K; $0.8 \leq \theta_T \leq 0.94$ for 373K; $0.4 \leq \theta_{T_1} \leq 0.8$ and $0.85 \leq \theta_{T_2} \leq 0.95$ at 573K; and $0.4 \leq \theta_T \leq 0.95$ at 773K.

Table 6.15 Rate Constant Values for Adsorption of Thiophene on Ni/Al_2O_3. Long term determinations, C_T=100ppm

Temperature K	k x 10^3 min^{-1}	k x 10^3 min^{-1}
373	-	2.92 ± 0.08 ($0.8 \leq \theta_T \leq 0.93$)
573	3.42 ± 0.4 ($0.3 \leq \theta_T \leq 0.90$)	5.98 ± 1.1 ($0.90 \leq \theta_T \leq 0.97$)
773	3.70 ± 0.07 ($0.2 \leq \theta_T \leq 0.9$)	10.4 ± 2.1 ($0.90 \leq \theta_T \leq 0.98$)
373 (Regenerated)	-	1.933 ($0.95 \leq \theta \leq 0.98$)
773 (Regenerated)	13.97 ($0.65 \leq \theta_T \leq 0.86$)	-
373 (Regenerated/ H_2S poisoned)	-	3.850 ($0.73 \leq \theta_T \leq 0.93$)
773 (Regenerated/ H_2S poisoned)	3.93 ($0.25 \leq \theta_T \leq 0.84$)	8.93 ($0.90 \leq \theta_T \leq 0.97$)

Table 6.16 Rate Constant Values for the Adsorption of Thiophene on Ni/Al_2O_3. Long term determinations c_T=1000ppm

Temperature K	k x 10^3 min^{-1}	k x 10^3 min^{-1}
298	-	16.58 ± 5.8 ($0.65<\theta_T<0.90$)
373	-	1.92 ± 0.02 ($0.8<\theta_T<0.94$)
573	13.10 ± 1.58 ($0.4<\theta_T<0.8$)	2.67 ($0.85<\theta_T<0.95$)
773	22.77 ± 3.2 ($0.4<\theta_T<0.95$)	-
298 (Regenerated)	-	1.983 ($0.8<\theta_T<0.95$)
373 (Regenerated)	-	1.783 ($0.71<\theta_T<0.92$)

Table 6.17 Rate Constant Values for Adsorption of Thiophene on γ-Al_2O_3. Long term determinations, T = 298K

Thiophene Concentration ppm	k x 10^3 min^{-1}	k x 10^3 min^{-1}
100	2.52 ± 0.13 ($0.4<\theta_T<0.89$)	-
1000	4.83 ± 0.60 ($0.71<\theta_T<0.89$)	2.53 ± 0.02 ($0.90<\theta_T<0.95$)

From the results in Tables 6.15 and 6.16 it seems that the mechanisms controlling the weight uptake during the poisoning vary with temperature; and although the rate constants determined in the short term adsorption are similar, in the long term they change with temperature. At 298K the adsorption rate constant is the same from a coverage of 0.25 until near saturation. At 373K the constant decreases in the long term although the coverage involved is high and close to saturation; its value in the long term is lower than the value at 298K. From the adsorption isotherms given in Section 6.1 it appears that at 573K and 773K the process of adsorption is the same throughout great part of the coverage, and therefore offers the possibility of estimate the effect of temperature on the rate of adsorption through the calculation of a "temperature coefficient" or an apparent "activation energy". The calculation was performed following the Arrhenius law and the results are given in Table 6.18.

Table 6.18 Apparent Activation Energy for Adsorption of Thiophene in the range 573K-773K

Thiophene Concentration ppm	Ea, $Jmol^{-1}$ $0.3 \leq \theta_T \leq 0.9$	Ea, $Jmol^{-1}$ $0.90 \leq \theta_T \leq 0.97$
100	1475	10145
1000	10230	-

According to Table 6.18 the apparent activation energy varies with concentration. This and the low values obtained at 100ppm may indicate that the apparent rate of adsorption is masked by mass transfer

limitations or that a complex set of reactions is occurring, and it is affected by the gas phase composition. Further discussion is provided in Section 6.8.

6.5.3 Tests of interparticle and intraparticle transport limitations

Several of the above results appear anomalous, and the behaviour observed would suggest that certain mechanisms such as external or internal mass transfer resistances are controlling the adsorption process. Accordingly, the presence of concentration gradients has to be tested.

To test the absence of interphase concentration gradients in isothermal systems Butt and Weekman (167) suggested the criterion proposed by Carberry (168) should be observed for a first order reaction:

$$\frac{\eta k}{k_m a} < 0.1$$

where:

η: effectiveness factor due to pore diffusion ($\eta > 0.95$)

k: first order rate constant, s^{-1}

k_m: mass transfer coefficient between gas and particle, ms^{-1}

a: external surface to volume ratio of particle, m^{-1}

To estimate k_m one must know the Reynolds and Schmidt numbers. Considering flow around single particles:

$$Re_m = \frac{dpG}{\mu_m} \qquad Sc = \frac{\mu_m}{\rho_m D_{Tm}}$$

where:

dp: particle diameter, m^{-1}

G: mass velocity, kg s^{-1} m^{-2}

μ_m: viscosity of gas, kg s^{-1} m^{-1}

ρ_m: density of gas, kg m^{-3}

D_{Tm}: diffusivity coefficient of thiophene in the gas mixture, $m^2 s^{-1}$

For a thiophene concentration of 1000ppm in H_2 and with a total flow of 150ml/min (1 bar, 291K) we have:

$$G = 9.611 \times 10^{-4} \quad kg/s\ m^2$$

$$dp = 4 \times 10^{-4}\ m$$

The properties of the gas mixture were calculated following the procedures outlined in Reid et al. (169):

at T = 298K and p = 1 bar

$$\mu_m = 8.85 \times 10^{-6}\ kg/sm$$

$$\rho_m = 8.52 \times 10^{-2}\ kg/m^3$$

and using the Chapman-Enskog equation, the diffusivity is:

$$D_{T/H_2} = 4.12 \times 10^{-5}\ m^2/s$$

$$Sc = 2.52 \quad , \quad Re = 4.34 \times 10^{-2}$$

The low Re and the calculated Pe = Re Sc = 0.11 point to the 'creeping' flow situation, for which k_m is evaluated through the limiting value of the Nu_m =2 according to Sherwood et al. (170) therefore:

$$\frac{k_m\ dp}{D} = 2$$

$$k_m = \frac{2D}{dp}$$

$$km = 0.206\ m/s$$

At 298K the largest value of k obtained was at the initial adsorption: $k = 0.24\ min^{-1} = 4.0 \times 10^{-3}\ s^{-1}$

$$a = \frac{6}{dp} = \frac{6}{4x10^{-4}m} = 1.5 \times 10^{4}\ m^{-1}$$

assuming $\eta \rightarrow 1$

$$\frac{k}{k_m a} = \frac{4 \times 10^{-3}\ s^{-1}}{(0.206\ \frac{m}{s})\ (1.5 \times 10^{4} m^{-1})} = 1.29 \times 10^{-6} < 0.1$$

Therefore film diffusion is not controlling the rate of adsorption. Following the same procedure at 773K it is obtained:

$$k = 23 \times 10^{-3}\ min^{-1} = 3.83 \times 10^{-4}\ s^{-1}$$

$$k_m = 1.09\ m\ s^{-1}$$

$$\frac{k}{k_m a} = \frac{3.83 \times 10^{-4}}{(1.09)(1.5x10^{4})} = 2.34 \times 10^{-8} < 0.1$$

$\therefore$ External resistances are negligible.

For the intraparticle diffusion the Weisz and Prater criterion can be used to test the absence of concentration gradients in an isothermal spherical particle ($\eta > 0.95$) for a first order reaction (167,171,172):

$$\frac{r\, R_p^2}{C_o D_{eff}} < 1$$

Where:

r: observed reaction rate per unit particle volume, kg—mol s^{-1} m^{-3}

R_p: particle radius, m

C_o: concentration of reactant at surface,

D_{eff}: effective diffusivity, m^2 s^{-1}

To calculate the effective diffusivity the procedure outlined in Smith's book (185) was followed assuming a random pore model and a monodisperse catalyst:

$$D_{eff} = D_\mu \, \varepsilon_\mu^2$$

and

$$\frac{1}{D_\mu} = \frac{1}{D_{T/H_2}} + \frac{1}{D_k}$$

where:

D_{T/H_2}: bulk diffusivity of thiophene in H_2

D_k : Knudsen diffusivity of thiophene

ε_μ : catalyst void fraction.

The Chapman-Enskog equation was used to estimate D_{T/H_2}, and the equation obtained from the kinetic theory for D_K (185).

at 298K, 101kPa:

$$D_{T/H_2} = 4.12 \times 10^{-5} \ m^2/s$$

$$D_K = 9.236 \times 10^{-7} \ m^2/s$$

$$D_\mu = 9.04 \times 10^{-7} \ m^2/s$$

from the catalyst data (see Chapter 5) and Smith's book (185)

$$\varepsilon_\mu = 0.503$$

$$D_{eff} = 2.26 \times 10^{-7} \ m^2/s$$

Similarly

at 773K, 101kPa:

$$D_{T/H_2} = 2.173 \times 10^{-4} \ m^2/s$$

$$D_K = 1.487 \times 10^{-6} \ m^2/s$$

$$D_\mu = 1.48 \times 10^{-6} \ m^2/s$$

$$D_{eff} = 3.69 \times 10^{-7} \ m^2/s$$

The Weisz and Prater test was applied to four different situations:

i) 1000ppm, 298K initial uptake

ii) 1000ppm, 298K for $15 \leq t \leq 60$ min

iii) 100ppm, 773K long term uptake

iv) 1000ppm, 773K long term uptake

i) For 1000ppm, 298K Initial uptake:

The observed rate of adsorption, obtained from the slope of the adsorption isotherm is:

$$r = 3.75 \frac{mg}{g_{cat} min} = 6.25 \times 10^{-5} \frac{kg}{kg_{cat} s}$$

$$\rho_p: \text{ particle density} = 1.212 \times 10^3 \frac{kg}{m^3}$$

$$r = 6.25 \times 10^{-5} \frac{kg}{kg_{cat} s} \times 1.212 \times 10^3 \frac{kg_{cat}}{m^3} = 7.58 \times 10^{-2} \frac{kg}{sm^3}$$

$$R_p = 2 \times 10^{-4} \text{ m} \qquad R_p^2 = 4 \times 10^{-8} \text{ m}^2$$

$$C_o = 4.2 \times 10^{-5} \frac{kg \text{ mol}}{m^3} = 3.534 \times 10^{-3} \frac{kg}{m^3}$$

$$\frac{rR_p^2}{C_o D_{eff}} = \frac{\left(7.58 \times 10^{-2} \frac{kg}{sm^3}\right)\left(4 \times 10^{-8} \text{ m}^2\right)}{\left(3.534 \times 10^{-3} \frac{kg}{m^3}\right)\left(2.26 \times 10^{-7} \frac{m^2}{s}\right)} = 3.80 > 1.0$$

∴ There are diffusional resistances.

ii) 1000ppm, 298K $15 < t < 60$min

from the adsorption isotherm:

$$r = 5.6 \times 10^{-2} \text{ mg/g}_{cat} \text{ min} = 1.14 \times 10^{-3} \text{ kg/sm}^3$$

$$\frac{rR_p^2}{C_o D_{eff}} = \frac{(1.14\times10^{-3} \text{ kg/sm}^3)(4\times10^{-8}\text{m}^2)}{(3.534\times10^{-3}\text{kg/m}^3)(2.26\times10^{-7}\text{m}^2/\text{s})} = 0.06 < 1$$

∴ Diffusional resistances are negligible

iii) 100ppm, 773K long term uptake

from the adsorption isotherm:

$$r = 0.89 \frac{\text{mg}}{g_{cat}\text{h}} = 3.0\times10^{-4} \text{ kg/sm}^3$$

$$C_o = 4.2 \times 10^{-6} \frac{\text{kgmol}}{\text{m}^3} = 3.534 \times 10^{-4} \text{ kg/m}^3$$

$$\frac{rR_p^2}{C_o D_{eff}} = \frac{(3\times10^{-4}\text{kg/sm}^3)(4\times10^{-8}\text{m}^2)}{(3.53\times10^{-4}\text{kg/m}^3)(3.69\times10^{-7}\text{m}^2/\text{s})} = 0.09 < 1$$

iv) 1000ppm, 773K long term uptake

from the adsorption isotherm:

$$r = 5.94 \frac{\text{mg}}{g_{cat}\text{h}} = 2 \times 10^{-3} \text{ kg/sm}^3$$

$$\frac{rR_p^2}{C_o D_{eff}} = \frac{(2\times10^{-3})(4\times10^{-8})}{(3.534\times10^{-3})(3.69\times10^{-7})} = 0.06 < 1$$

These four cases illustrate the fact that after the initial uptake (at $t > 15$min) the intraparticle diffusional resistances are negligible. The rate of weight uptake is not controlled by internal diffusion, unless the intrinsic rate of adsorption is so fast that pore-mouth poisoning occurs. At very short times ($t < 4$min) however the criterion is not observed and $\frac{rR_p^2}{C_o D_{eff}} > 1$; it could be concluded that internal diffusion is important and that it may offer the greatest resistance. However under these conditions the limiting factor is the amount of thiophene being fed to the reactor rather than any transport process.

Calculations for other conditions showed that the comments above are observed for all the experiments: the apparent rate constants found for the long term adsorption, and for $t > 15$min, are not masked by diffusional limitations; and that the initial adsorption rate is limited by the amount of thiophene fed to the catalyst.

6.6 Elemental Analysis Results

The sulphur and carbon contents of the nickel catalysts obtained by means of elemental analysis are given in tables 6.19 and 6.20. The results show that the sulphur content increases with temperature and reaches a maximum at 573K decreasing to lower levels as the temperature is increased to 773K. This trend is observed at both concentrations employed: 100ppm and 1000ppm. The carbon content decreases with temperature although it has a near constant value between 373K and 573K at 100ppm. At 1000ppm the carbon content is nearly constant throughout the whole temperature range although it has a maximum at 373K. Figure 6.33 shows the sulphur and carbon contents and the S/C ratio for the samples poisoned at 100ppm. It can be seen that at this poison

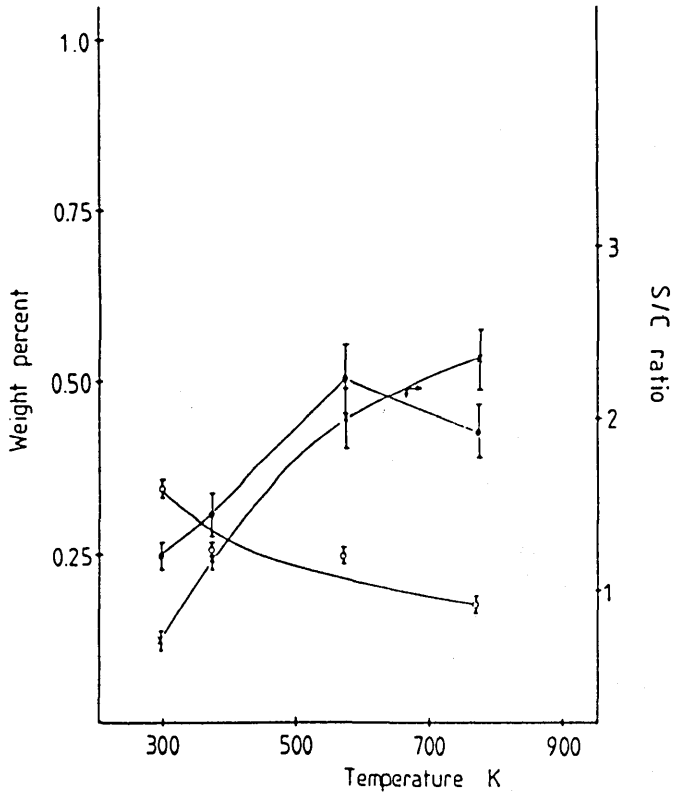

FIGURE 6.33

Sulphur and carbon contents of nickel catalysts poisoned with 100ppm thiophene/H_2. Sulphur (●), carbon (O), S/C ratio (x).

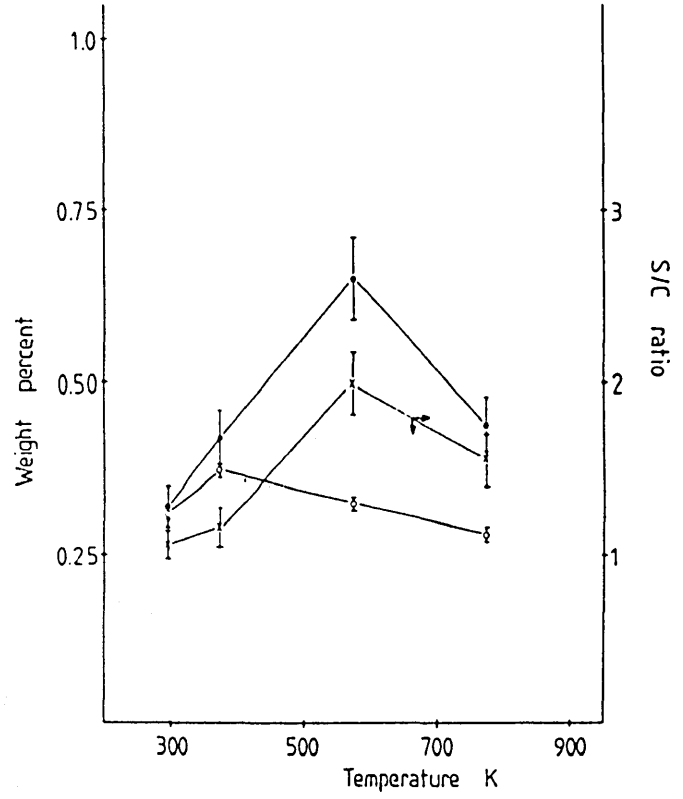

FIGURE 6.34

Sulphur and carbon contents of nickel catalysts poisoned with 1000ppm thiophene/H_2. Sulphur (●) carbon (O), S/C ratio (x).

Table 6.19 Sulphur and Carbon contents of the Poisoned Nickel Catalysts C_{THIO} = 100ppm

Temperature K	%S	%C	S/C Ratio
298	0.25 ± 0.03	0.35	0.71 ± 0.05
373	0.31 ± 0.03	0.26	1.17 ± 0.08
573	0.50 ± 0.05	0.25	2.0 ± 0.14
773	0.43 ± 0.04	0.18	2.36 ± 0.17
298R	0.30 ± 0.03	0.22	1.32 ± 0.10
373R	0.36 ± 0.04	0.30	1.20 ± 0.08
773R	0.58 ± 0.05	0.25	2.32 ± 0.08

R: These samples were poisoned, regenerated and poisoned again. The percentages reported were obtained after the 2nd poisoning.

Table 6.20 Sulphur and Carbon Contents of Poisoned Nickel Catalysts C_{THIO} = 1000ppm

Temperature K	%S	%C	S/C ratio
298	0.32 ± 0.03	0.31	1.06 ± 0.08
373	0.42 ± 0.04	0.37	1.16 ± 0.11
573	0.65 ± 0.06	0.33	1.99 ± 0.18
773	0.44 ± 0.04	0.28	1.55 ± 0.15
298R	0.40 ± 0.04	0.30	1.32 ± 0.14
373R	0.58 ± 0.08	0.27	2.10 ± 0.30
773R	0.62 ± 0.07	0.43	1.45 ± 0.15

R: These samples were poisoned, regenerated and poisoned again. The percentages reported were obtained after the 2nd poisoning.

concentration the S/C ratio increases with temperature. At 298K the ratio is only slightly higher than the corresponding to the thiophene molecule (S/C = 0.67) which suggest that at room temperature the amount of thiophene that is decomposed is very little, consequently the S/C ratio remains close to that of the thiophene. As the temperature increases the S/C ratio increases: thiophene reacts and the hydrocarbon part is removed; however even at 773K some carbon remains adsorbed.

With 1000ppm thiophene/H_2 the S/C ratio reaches a maximum at 573K, as shown in Figure 6.34, but it can be noticed that at 773K the S/C ratio is lower than that obtained at 100ppm. Carbon is less effectively removed at the higher thiophene concentration presumably due to the lower P_{H_2}/P_{Thio} value which may decrease the rate of hydrogenation of the ring therefore increasing coking at the higher temperature.

The samples that were poisoned twice with an intermediate regeneration show a higher amount of sulphur; however the amounts determined at the low temperatures (298K and 373K) are just slightly higher than those determined on samples poisoned once, and the sum of the sulphur and carbon contents does not correspond to the total amount adsorbed: differences of up to 50% between the total weight adsorbed and the sum of sulphur and carbon contents determined by elemental analysis were found (being higher the total weight uptake). It is possible that some material is lost during the termination of the experiment and the storage and transfer because some material may be physically adsorbed. The carbon content is similar to that of the samples poisoned once, especially at the low temperatures, which could mean that the carbon adsorbed in the poisoning is removed in great part

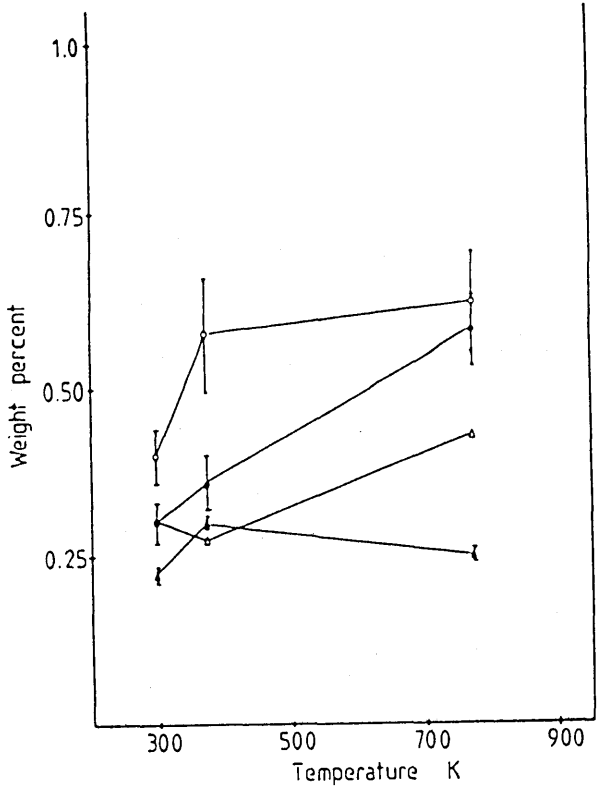

FIGURE 6.35

Sulphur and carbon contents of nickel catalysts poisoned, regenerated and re-poisoned. Sulphur (●,0), carbon (▲,Δ); 100ppm (●,▲); 1000ppm (0,Δ).

by the regeneration treatment. The sulphur content seems to be higher for the samples poisoned twice, especially at the high temperatures where it is clearly seen. Figure 6.35 shows the sulphur and carbon contents of the samples poisoned, regenerated and poisoned again at both concentrations (100ppm and 1000ppm).

The sulphur coverages calculated from the sulphur content and the nickel metal area are given in Tables 6.21 and 6.22. The values show that the minimum coverage suggests an arrangement of four nickel atoms per sulphur atom at 298K, whereas the maximum of 0.71 at 573K corresponds to a stoichiometry of Ni_3S_2. X-Ray diffraction analysis were carried out to determine the presence of bulk sulphides and they showed that they were not formed or that its concentration was too low to be detected. Hence ratio of 0.7 probably represents a surface sulphide compound.

Table 6.21 Sulphur Coverages calculated from the Sulphur Content C_{THIO} = 100ppm

Temperature K	$\frac{S_{atom}}{g_{cat}} \times 10^{19}$	$\frac{Ni_{atom}}{g_{cat}} \times 10^{20}$	$\theta_s = \frac{S_{atom}}{Ni_{atom}}$
298	4.71	1.686	0.28 ± 0.02
373	5.82	1.754	0.33 ± 0.03
573	9.47	1.652	0.57 ± 0.05
773	8.09	1.670	0.48 ± 0.04
298R	5.57	1.855	0.30 ± 0.03
373R	6.74	1.686	0.40 ± 0.04
773R	10.92	1.796	0.61 ± 0.05

R: These samples were poisoned-regenerated-poisoned.

Table 6.22 Sulphur Coverages calculated from the Sulphur Content C_{THIO} = 1000 ppm

Temperature K	$\frac{S_{atom}}{g_{cat}} \times 10^{19}$	$\frac{Ni_{atom}}{g_{cat}} \times 10^{20}$	$\theta_s = \frac{S_{atom}}{Ni_{atom}}$
298	6.17	1.855	0.33 ± 0.03
373	7.94	1.661	0.48 ± 0.05
573	12.20	1.720	0.71 ± 0.07
773	8.19	1.670	0.49 ± 0.05
298R	7.55	1.670	0.45 ± 0.04
373R	10.84	1.855	0.58 ± 0.08
773R	11.65	1.619	0.72 ± 0.08

R: These samples were poisoned-regenerated-poisoned.

In order to have a better idea of the processes occurring in the long term adsorption experiments were carried out in which the adsorption was stopped at about 50-70% of the final weight, and the samples were analysed to determine the sulphur and carbon contents. The results are presented in Table 6.23 below.

Table 6.23 Sulphur and Carbon contents of nickel catalysts poisoned at 50-70% of saturation

Temperature K	Thiophene Concentration ppm	%S	%C	S/C ratio
298	100	ND	0.22	-
373	100	ND	0.11	-
773	100	0.27	0.14	1.93
373	1000	ND	0.23	-

ND: non detected; the sulphur content was below 0.1% which was the detection limit.

Sulphur was detected only on the sample poisoned at 773K, its content was too low on the others to be detected. Carbon however is about 50% of the value determined at saturation at 298K and 373K. At 773K the carbon content is very close to the one found at saturation, the sulphur content is about 60% of the final value so that the S/C ratio is lower than that obtained when the adsorption is carried out to saturation.

6.7 Electron Microscopy Results

Several samples were observed by electron microscopy to find out whether the carbon could be identified as any of the structures reported in the literature for carbon formation. The results are given in figures 6.36 and 6.37 for some of the samples poisoned at the different temperatures. In Figure 6.36 the micrographs correspond to Ni/Al_2O_3 samples poisoned at 298K (6.36A&B), 373K (6.36C), and 573K (6.36D). In Figure 6.37 the results correspond to Ni/Al_2O_3 catalysts poisoned at 773K (6.37A), in 6.37B the catalyst was poisoned twice at 773K with intermediate regeneration; Al_2O_3 is shown in 6.37C and clean Ni/Al_2O_3 in 6.37D as comparison. Ni can be easily identified by the darker spots in the micrographs. It does not appear to be any difference between the poisoned samples and the clean catalyst. The regenerated sample seems to have incipient 'sausage' like structures close to nickel sites but these also appear in the Al_2O_3 micrograph; therefore it can not represent carbon deposition since the alumina sample was clean. It may have resulted during the grinding of the sample.

It can be concluded that at the thiophene concentrations and temperatures used in the poisoning experiments carbon does not form any

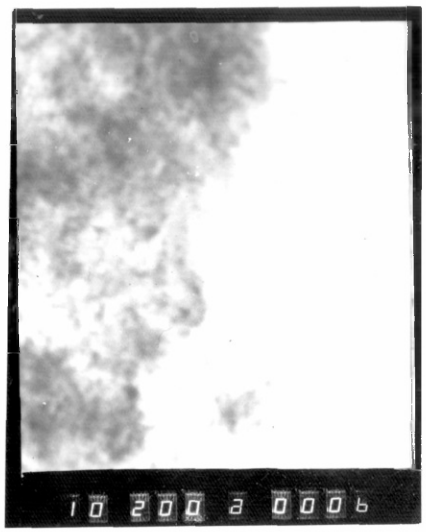

A: STEM X 200 000

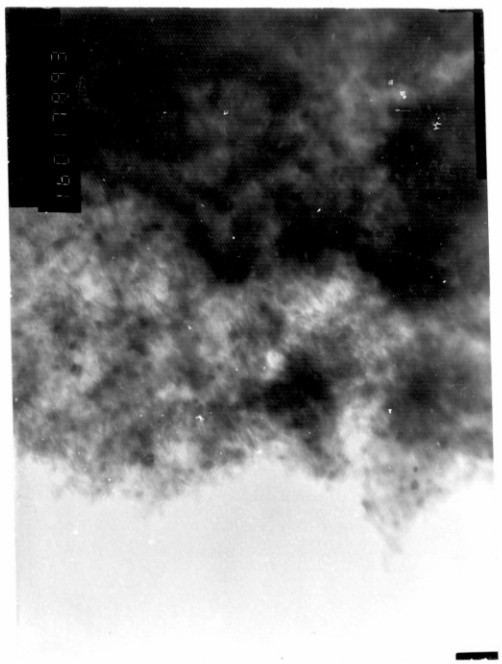

B: TEM X 160 000

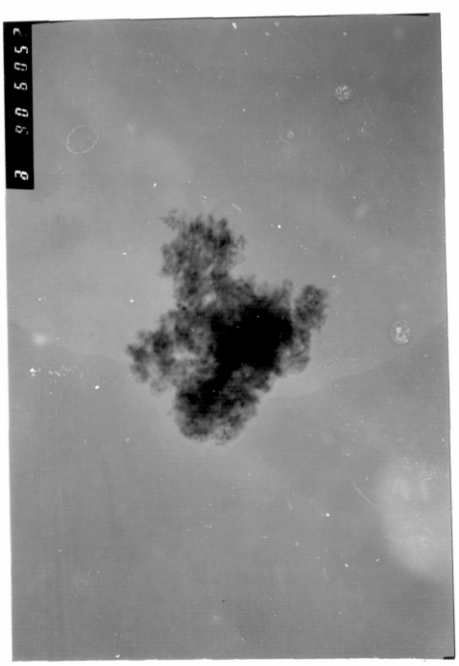

C: TEM X 90 000

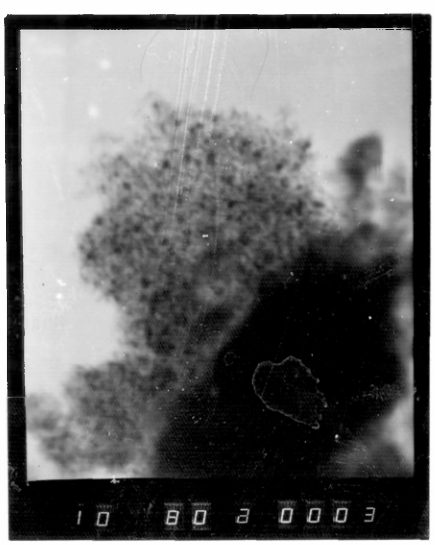

D: STEM X 80 000

FIGURE 6.36

Electron micrographs of poisoned Ni/Al_2O_3

Plate	Sample	Thiophene concentration ppm	Temperature of poisoning K
A	Ni/Al_2O_3	100	298
B	Ni/Al_2O_3	100	298
C	Ni/Al_2O_3	1000	373
D	Ni/Al_2O_3	100	573

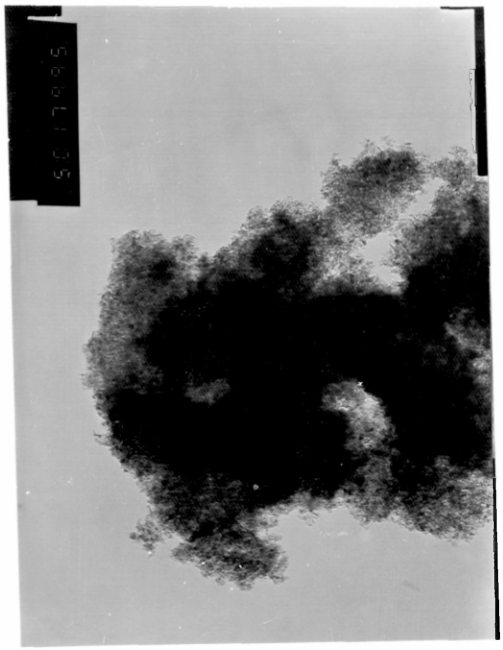

A: TEM X 50 000

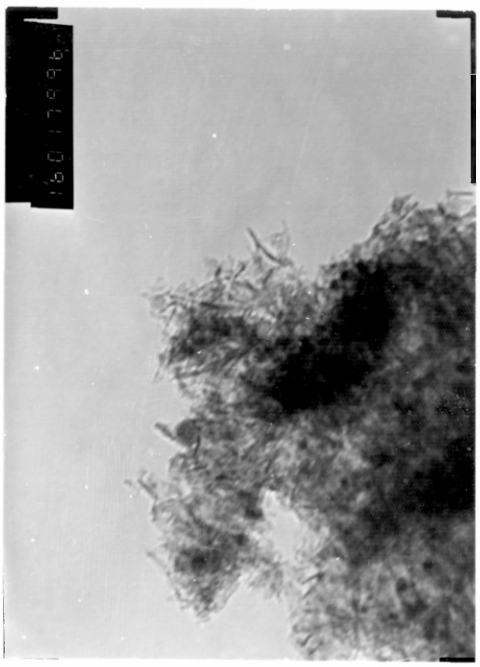

B: TEM X 160 000

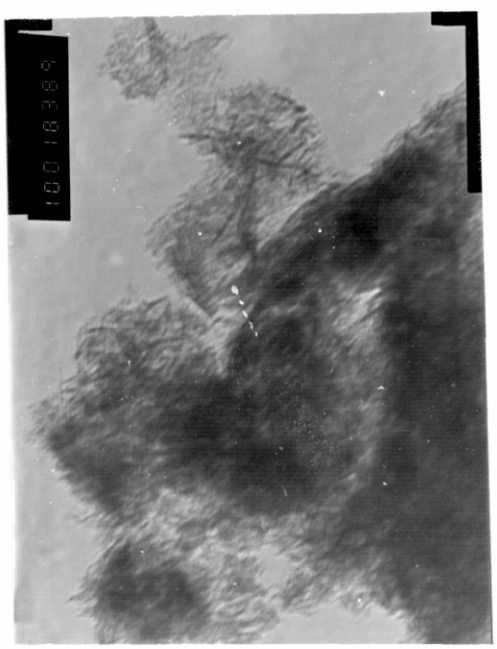

C: TEM X 100 000

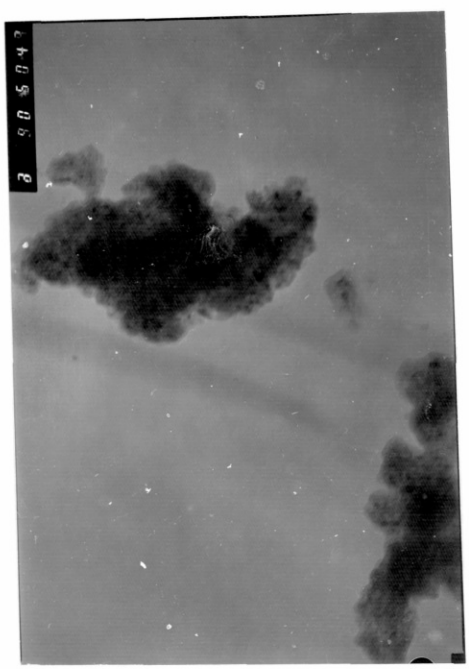

D: TEM X 90 000

FIGURE 6.37

Electron micrographs of Ni/Al_2O_3 and γ-Al_2O_3

Plate	Sample	Thiophene concentration ppm	Temperature of poisoning K
A	Ni/Al_2O_3	100	773
B	Ni/Al_2O_3	100(Regenerated)	773
C	Al_2O_3	Reduced-unpoisoned	-
D	Ni/Al_2O_3	Reduced-upoisoned	-

of the known structures identifying carbon deposition. This is explained by the low concentration of carbon adsorbed as determined by the elemental analysis; hence it would hardly be detected by the microscope. Carbon must them be adsorbed onto the nickel or possibly on the alumina.

6.8 Discussion

The strong adsorption of sulphur on nickel catalysts is a well-known fact. Results available in the literature (32-35) have shown that the adsorbed structure is very stable. The gas concentration necessary to completely deactivate nickel catalysts is very small (of the order of 10ppb) resulting in a saturation coverage of 0.5 S atoms per nickel atom (15,23); concentrations of the order of 10-25ppm produce higher coverages ($\theta_s \gtrsim 1$) with a possible surface reconstruction (32,39). Most of these studies have been carried out using H_2S as the poisoning agent and little information exists for the adsorption behaviour of other compounds.

The results obtained in this work for the adsorption of thiophene on a 20% Ni/Al_2O_3 catalyst have shown that the amount adsorbed is a function of temperature and gas composition.

The uptake behaviour observed as a function of time is as follows: thiophene is adsorbed fast, reaching a near constant uptake in few minutes. Then the thiophene reacts yielding gaseous products and producing free nickel sites where more thiophene can be adsorbed increasing the weight uptake. The rate at which the weight increases after the initial period is low at temperatures of 373K and lower, but increases with increasing temperature. As the concentration is

increased the rate of weight uptake increases as can be seen by inspection of Figures 6.1 to 6.5.

The amount of thiophene adsorbed by the alumina is negligible at temperatures in the range 573K-773K, but considerable at 373K and very high at room temperature. An unexpected feature found was the higher uptake on alumina at the lower thiophene concentration (100ppm) and the fact that the adsorption still continued after 20h, whereas at 1000ppm the sample had reached saturation. The possible explanation based on IR results (48,82) considers the formation of a polymer of thiophene molecules weakly adsorbed to the surface, this would be favoured at the higher concentration. Due to the acidic character of the support thiophene would be prefererably adsorbed through the sulphur atom, with a slow adsorption process (48). At the low concentration thiophene would stand perpendicular to the surface occupying less area and allowing more thiophene to be adsorbed and possible absorbed, whereas at the higher concentration the polymer formed would not allow more thiophene to be in contact with the surface.

On the Ni/Al_2O_3 catalyst the adsorption of thiophene at 298K shows that the adsorption is fast, reaching saturation in a short time. The presence of nickel promotes the adsorption of thiophene coplanar to the surface forming the polymer aggregate which prevents more thiophene to be adsorbed. The amount adsorbed however exceeds considerations that thiophene is adsorbed only parallel to the surface (45,46) since calculations show that if this is so the thiophene adsorbed (assuming a 5-site adsorption, an average nickel area of 11.17 m^2/g_{cat} and a close-packed (compressed) structure) is equal to 4.75 mg thiophene/g_{cat}.

Thiophene then is expected to be adsorbed as both parallel and perpendicular to the surface. It also has to be taken into account the possible physisorption of thiophene at the lower temperatures (T<373K) which increases as the concentration is increased.

As the temperature is increased the rate of thiophene reaction (decomposition) to sulphur (H_2S) and hydrocarbons increases being noticeable at 373K with a low increase in weight in the long term and more pronounced at higher temperatures.

The overall process and catalyst changes can be listed as follows according to Massoth and Kibby (173):

i) Adsorption of thiophene: irreversible and reversible.

ii) Thiophene decomposition: hydrocarbons production, hds reactions.

iii) H_2S adsorption (from thiophene decomposition).

iv) Adsorption of hydrocarbon products from thiophene decomposition.

v) Adsorption of coke.

It is clear that these steps occur as function of temperature such that at room temperature it is expected that most of the weight uptake is due to adsorbed thiophene and as the temperature increases steps (ii) to (v) occur.

This scheme also points out that:

a) as the temperature increases the "nature" of the carbon remaining on the catalyst changes; and

b) that as the temperatures increases the ratio of the sulphur to carbon contents changes, and is expected to increase with a maximum at an intermediate temperature and high coke

formation at higher temperatures.

Point (a) is intuitively expected but it is difficult to prove at least at the concentrations used and the high hydrogen to thiophene pressure ratio. Electron microscopy analysis of catalyst samples did not reveal any carbon formation even after the regeneration treatment at 873K. Due to the conditions used it is possible that the carbon deposited at the higher temperatures may be a polymer that forms an encasulating film on nickel particles (6), the transformation of this polymer into more inactive carbon forms such as the pyrolitic carbon is effected only at high temperatures ($>$873K).

The results of the elemental analysis showed that carbon was present on the catalyst after the poisoning was carried out. That carbon content has a near constant value although it decreases slightly with temperature, this latter effect is more noticeable at the lower thiophene concentration and it is thought to be the result of the high hydrogen to thiophene pressure ratio which permits that carbon be removed through reaction with H_2. It seems to be the case also at 1000ppm but the carbon content has a more constant value (Tables 6.19 and 6.20).

Point (b) is proved by the elemental analysis which showed that the S/C ratio increases with temperature. At 100ppm the increase is monotonic with the higher ratio at 773K, but at 1000ppm the ratio has a maximum at 573K. This is due to removal of carbon more effectively at 100ppm than at 1000ppm, a fact which is closely related to the hydrogen partial pressure and the thiophene concentration. In both cases (100 and 1000ppm) the sulphur content has a maximum at 573K, and this together with the S/C ratio depends on the processes occurring which

are discussed below.

The presence on the catalyst of thiophene irreversibly and reversibly adsorbed can occur at low temperatures only. The reversible adsorption may occur considering that at 298K the thiophene vapour pressure is 10.5kPa (79mmHg). The sum of the sulphur and carbon contents determined for the samples poisoned at 298K was not equal to the total amount adsorbed, some material presumably physisorbed, was lost (desorbed) during storage and handling.

Thiophene decomposition occurs increasing the temperature which results in hydrocarbon and H_2S products that can be adsorbed (steps (ii) to (iv)) or released to the gas phase. Most of the hydrocarbon is desorbed but H_2S remains adsorbed on the catalyst. The elemental analysis results show that the increase in weight at the high temperatures (573K and 773K) is basically an increase in the sulphur content with little or no increase in the carbon content. The long term increase in weight represents sulphidation of the nickel.

Step (v) is assumed to occur at the higher temperatures (773K and possibly 573K). This coke may have been formed in the early stages of the process through polymerization of the adsorbed hydrocarbons however, as said before, it is difficult to differenciate the coke from other adsorbed hydrocarbons (173).

Upon regeneration, the nickel catalysts re-adsorb thiophene. The adsorption behaviour varies with concentration and appears to be similar to the adsorption on the alumina support. At the lower concentration the amount of thiophene adsorbed at temperatures $\leq$373K is higher than on the fresh catalyst. This is explained by an enhanced

adsorption through the heteroatom rather than coplanar to the surface. This preferred adsorbed state allows further adsorption of thiophene. This behaviour seems to be caused by the presence of sulphur which would hinder the adsorption parallel to the surface and promote adsorption perpendicular to the surface. In the case of the higher concentration the fact that the behaviour is similar for both clean and regenerated catalysts suggests that in both cases parallel and perpendicular adsorbed species exist and in both cases the thiophenic polymer is formed.

Increasing the temperature to 773K brings the decomposition of thiophene. The sulphiding process occurs at a higher rate than on clean catalysts but at both concentrations the amount adsorbed at saturation is less than that on clean samples. If on clean samples the thiophene is adsorbed preferably coplanar to the surface, the higher uptake rate on the regenerated samples suggests that thiophene would be preferably adsorbed through the sulphur atom on sulphur-poisoned nickel catalysts. Support for this view is given by the adsorption of thiophene on the regenerated sample pre-poisoned with 2ppm H_2S/H_2: this catalyst adsorbed more material than the clean samples and at a faster rate; a result that can be correlated to the slight amount of sulphur present on the catalyst which would hinder adsorption through the ring and promote that through the sulphur.

The sulphur content of the re-poisoned catalysts increases with temperature. The amount of sulphur determined on the catalysts re-poisoned at low temperatures (<373K) is just slightly higher than that found on samples poisoned once only. This is presumably due to the removal of thiophene during regeneration and material desorbed

during handling of samples. On the samples poisoned at 773K the sulphur is also slightly higher than the corresponding to samples poisoned only once, however the amount determined agrees with the total sulphur that should be present since the weight uptake in the second adsorption was lower than on the first. This suggests that during regeneration little or no sulphur is removed.

The amount of carbon found on the samples poisoned twice is similar to that on samples poisoned once, although greater differences are found at the higher temperature at 1000ppm. At the lower concentration carbon shows a maximum at 373K, but is close to that found on poisoned-once samples; at 1000ppm the carbon content determined after the second poisoning is significantly higher than that after the first poisoning, carbon then is not removed during regeneration or its deposition is increased during the second adsorption by the presence of sulphur. Perhaps both situations occur: carbon is not completely removed by the regeneration treatment; and also coke formation is increased by sulphur due to the presence of olefinic products which polymerise easier on nickel catalysts than parafinic compounds (6,7). Bourne et al. (46) reported that the initial conversion of thiophene on nickel products gave butane as product until the activity decreased at a sulphur coverage of ~0.30 (θ_s), at this point butenes started to appear although at very low concentration. Then sulphur presence on the nickel surface reduces activity and promotes olefin production.

An interesting point to note is that with 100ppm thiophene/H_2 the sulphur coverage θ_s (S atom per surface nickel atom) has a maximum value of 0.5; a value that is lower than the one it would be found if H_2S/H_2 of similar concentration wa used: in this case it would be

expected that $\theta_s > 1$ (3,32,35). Even at 1000ppm the θ_s=0.71 suggests a stoichiometry of the type Ni_3S_2; but the failure to detect this compound by x-ray diffraction suggests that there is little sulphur attack in depth, bulk compounds are not formed at this concentration and sulphur remains on the surface with a possible surface reconstruction. Presumably a higher concentration is needed to obtain sulphidation in depth as was reported by Bourne et al. (46) to occur.

Regarding the kinetics the first order rate equation used proved to be suitable to fit the data, especially at the higher temperatures. This type of equation has been successful for the fitting of adsorption data of H_2S on platinum catalysts (174) and several other systems (166). Equations of other orders were not successful. In system such as deactivation by coke Froment and co workers (175,176) have reported that the best fit is obtained by an equation of the form:

$$\frac{dC_c}{dt} = r_o \exp(-k_c C_c)$$

where r_o and k_c are constants at defined experimental conditions, and C_c is the amount of coke deposited. An equation of this type however does not predict saturation at infinite times, a feature which is found experimentally hence it was discarded.

The apparent rate constants k determined using equation 6.1 for α=1 confirm the qualitative assessment carried out on the adsorption uptake graphs. After the initial uptake period the k values show that the rate of adsorption (or sulphidation) increases with concentration and temperature. The adsorption rate is higher on regenerated samples, especially at higher temperatures where equilibrium adsorption is

reached faster than on clean samples. Several regions may exist: in the long term one found over a great part of the thiophene uptake and a second near saturation (θ_T>0.8). Presumably this could represent a change in the controlling process, however care should be taken not to make statements a priori because of the complexity of the adsorption and reaction processes.

In the initial adsorption the rate constants decrease as the temperature is increased from 298K to 373K at 100ppm, and remain constant at 1000ppm. Little significance should be attached to these values because at this stage the uptake is controlled by the amount of thiophene being fed to the reactor. Nevertheless the rate at which the adsorption occurs is high, suggesting a high initial sticking coefficient, and that it may be difficult then for the adsorption to be the rate controlling process on clean sulphur-free nickel catalysts.

On alumina however the results strongly suggest that the controlling process is the adsorption step: there is a small induction time, the induction time decreases as the concentration is increased, the uptake rate increases with increasing concentration, and is slower than the rate on Ni/Al_2O_3 samples. This is in complete agreement with IR results (48).

The apparent activation energies determined for the uptake rate at T>573K are dependent on thiophene concentration: at 100ppm the Ea is much lower than at 1000ppm over most of the thiophene coverage. A second activation energy was found at 100ppm for the adsorption near saturation, with a value similar to that obtained at 1000ppm. It could be argued that it is proof that the process is controlled by mass transfer limitations, however the analysis of the inter- and intraparticle transport revealed that these were absent in the regions

under consideration. However it is believed that more experimental evidence is necessary to sustain the last paragraph because, as was pointed out by Froment and Bischoff (171) in the cases where the reaction rate is strongly inhibited by adsorption of products, in which a Langmuir-Hinshelwood type expression is found, the Weisz-Prater criterion may give misleading results.

The external mass transfer criterion proposed by Carberry (168) was easily satisfied and it may be considered with confidence that the weight uptake rate is not limited by external transport.

Two possible explanations can be given for the dependence upon concentration of the apparent activation energy:

a) The fact that the Ea at high coverage (θ_T) at 100ppm is similar to the Ea at 1000ppm, but much lower at low coverage suggests that the controlling mechanism changes. At low coverage and low concentration thiophene adsorbs preferably coplanar to the surface, decomposes through hydrogenation of the ring and sulphur is adsorbed. As the coverage increases geometric requirements limit the reaction until a certain sulphur content at which thiophene is adsorbed through the sulphur and is decomposed with production of olefins. This adsorption mode is faster and the limiting process becomes the hydrogenolisis of the thiophene. At 1000ppm the higher concentartion and the higher uptake observed initially promotes higher contribution of the heteratom adsorption mode and the rate limiting step becomes from the beginning the hydrogenolisis of thiophene.

b) The thiophene reaction brings about two processes: adsorption of sulphur and carbon deposition. At 100ppm the carbon deposited is low because of the high H_2/thiophene ratio which allows hydrogenation

of adsorbed carbon. As the thiophene concentration is increased and the H_2/thiophene ratio decreases the rate of carbon deposition increases and therefore the observed weight uptake is a combination of sulphidation and carbon deposition which may be more activated than the sulphidation alone.

In order to discriminate between these two possible explanations more experiments are necessary and recommended. However with the amount of data available and discussed the second explanation seems to be more credible and is favoured.

The apparent activation energy of 10.2 kJ/mol is very close to the one determined from Richardson's data (51): 10.8 kJ/mol, but is higher than the one reported by Weng et al. (52): 4.5 kJ/mol. The latter result however was obtained at temperatures of 338K-448K whereas Richardson's were obtained between 473K-673K, therefore the activation energies belong to different rate limiting steps since thiophene decomposition is higher at the higher temperature region. Richardson concluded that the controlling mechanism in the region 473K-673K was the adsorption of thiophene in agreement with the mechanism favoured by Bourne et al. (46). Whether it is a 5-site or 1-site adsorption it is not specified, although Bourne suggested that the 5-site mechanism is occuring. The 5-site adsorption however fails to explain the high sulphur coverage at temperatures above 373K, since it is expected to cover a maximum of 20% of available nickel sites. Equation 6.1 used to fit the adsorption data with α=1, suggests a one-point adsorption for thiophene, but it may just be fortituous, and a more detailed analysis of the mechanism is necessary as well as further experimentation.

In summary the adsorption and reaction of thiophene can be described with the help of the results given here and in the literature

(43-71,175) as follows:

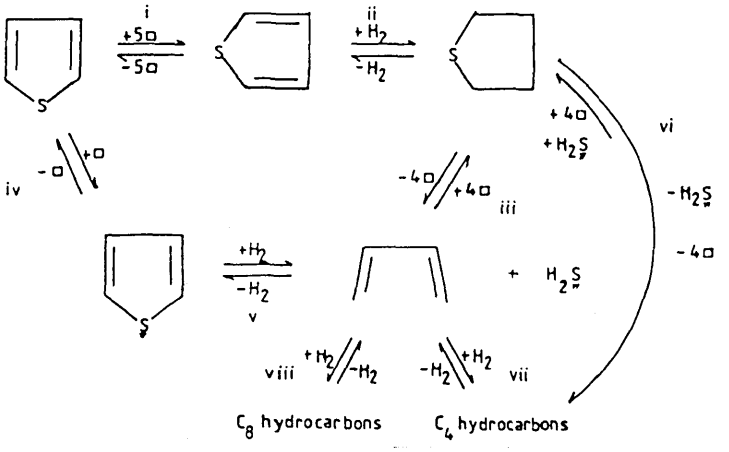

Route: i-ii-vi is favoured on clean nickel catalysts

Route: i-ii-iii$\begin{matrix}\nearrow vii \\ \searrow viii\end{matrix}$ is present on slightly poisoned catalysts.

Route: iv-v-$\begin{matrix}\nearrow vii \\ \searrow viii\end{matrix}$ is favoured on poisoned catalysts but is present on clean catalysts at high thiophene concentrations.

At low temperaturs the extent of hydrogenolysis is low, but thiophene may be hydrogenated. At higher temperatures (> 373K) the ring is broken and hydrocarbons are formed more extensively.

It has to be pointed out that in order to characterise each step and determine the rate limiting step more research is necessary. It is recommended to span the range of the variables studied (temperature and concentration), check the validity of the mass transport limitation tests varying the flow rate and particles size, and measure the product distribution.

The experiments carried out with H_2S showed that the adsorption is fast, with a very high sticking probability in good agreement with results in the literature (3,15). The sulphur coverage obtained suggests a mechanism in which 3 nickel atoms are occupied by one H_2S

molecule at 373K in good agreement with the result of Saleh et al (36) and considering the variation in coverage found experimentally it also covers a possible 4Ni atom for H_2S molecule mechanism as proposed by Den Besten and Selwood (37). The results then confirm the general view that at low concentrations of H_2S/H_2 mixtures, the adsorption is dissociative. The results obtained at higher temperature (773K) however do not agree with the coverages reported in literature of $\theta_s > 0.5$ (3,32,34,39). The obtained coverage of 0.09 is much lower and cannot be reconciled with the published data. The trend however of decreasing coverage with increasing temperature agrees with an exothermic adsorption process.

A very interesting result obtained was that of the adsorption of H_2S from an 8ppm H_2S/N_2 mixture. The sulphur coverage after 20 h was >1.0 and the adsorption uptake was still increasing at constant rate. Two factors contribued to this: the concentration of H_2S (8ppm) and most important the fact that the diluent was N_2. At 723K and 8ppm H_2S/H_2 a sulphur coverage $\theta_s=0.86$ was reported by Oliphant et al (32) whereas using 25ppm H_2S/H_2 the coverage was 1.08 for a 3% Ni/Al_2O_3 and 1.14 for Ni powder; since it has been claimed that at temperatures of 373K or below Hydrogen from the H_2S dissociation remains adsorbed the coverage is expected to be lower than 0.5. However the resulting coverage is higher than those reported by Oliphant et al (32) and Rostrup-Nielsen (39) therefore the important factor is N_2. Equations 2.1 and 2.2 have shown that the equilibrium of the sulphur adsorption is governed by the P_{H_2S}/P_{H_2} ratio. In the absence of H_2 in the gas phase the equilibrium is favoured towards the metal sulphide and therefore the amount of H_2S adsorbed should be higher. As a result it

is expected to form bulk sulphides with strong sulphidation in depth. The process in this case should be controlled by the H_2S diffusion through the nickel layers.

Another major subject involved in this work was the regeneration of the poisoned catalysts by reduction with H_2 at 873K. The studies show that the regeneration is partially successful. The results showed that the H_2 treatment removes part of the material adsorbed. The percentage of material removal is high; however it may not represent the real amount of material removed because of the possible errors involved in the large corrections in weight that were carried out due to buoyancy. Nevertheless the elemental analysis demonstrated that material was removed since the sum of carbon and sulphur content was not equal to the amounts adsorbed in the two poisonings.

The H_2 treatment of samples poisoned at 298K removed great part of the amount adsorbed. Carbon is believed to be completely removed but not sulphur, part of which remains adsorbed. As the temperature is increased the amount of sulphur retained by the catalyst increases, which is a direct consequence of the reactions that thiophene undergoes. The samples poisoned at 773K release little or no sulphur during the regeneration treatment; the carbon contained is believed to be removed in great percentage but not completely as shown by the carbon content determined after the second poisoning: the percentage is higher than the corresponding amount adsorbed during poisoning (see Tables 6.19 and 6.20 and Figures 6.23 and 6.26).

In support of this statements are the CO chemisorption experiments. The amount of CO adsorbed on regenerated samples was of

the same order of magnitude as that on poisoned catalysts. However samples poisoned at 298K showed higher CO uptake than their corresponding regenerated samples. Since the amount of CO adsorbed increases with the sulphur content it can be concluded that upon regeneration the amount of sulphur decreases. For the samples poisoned at 773K the amount of CO chemisorbed on poisoned and regenerated samples was very similar, therefore there was little difference in the sulphur content of both samples. This result is in agreement with the result of Oliphant et al (32) who could only remove about 5-10% of the sulphur adsorbed at 725K after a period of 2-3 days with flowing H_2.

Richardson reported that regenerated thiophene-poisoned nickel beds do not retain their ability to adsorb thiophene (51). Our results show that after regeneration the nickel catalysts do adsorb thiophene even at 773K. At low temperatures and concentrations ($T<373K$, $C_T=100ppm$) the amount of thiophene adsorbed after regeneration was higher than on clean nickel samples which suggests that the remaining sulphur affects the way thiophene is adsorbed. At higher temperatures nickel catalysts can be resulphided after regeneration at a rate higher than on clean samples which then again is presumably due to adsorption through the heteratom rather than co-planar to the surface, a consequence of the sulphur presence. It remains to be seen if catalytic activity is recovered, and it is recommended to carry out activity tests to measure the extent of the regeneration. The differences with Richardson's data may lie in stronger sulphidation of the catalyst bed due to the higher thiophene concentration employed (0.5-2.6 mole%), even so if the magnetic properties of the nickel

catalyst were restored it would be expected that they could re-adsorb thiophene as was the case with H_2S. These results cast some doubts on the ability of the magnetic methods to represent the true chemical state of nickel particles and the detection of chemical changes.

Based on the system of reactions occurring during TPD/TPR of adsorbed thiophene proposed by Ramachandran and Massoth (177) and our results it can be proposed that during regeneration with H_2 the following occurs:

$$C_4H_4S_{(a)} \xrightarrow[\text{Temp}]{H_2} C_4H_4S + C_4H_8 + S(a) + \text{polymer/coke} \quad \text{(I)}$$

$$\text{(polymer/Coke)} \xrightarrow[\text{Temp}]{H_2} C_4H_4S + C_4H_8 + H_2S \quad \text{(II)}$$

Reaction (I) is assumed to occur at low temperatures ($T < 450K$) duing the period of increasing temperature in H_2 stream from 298K (or 373K) to 873K, obviously C_4H_4S and C_4H_8 are released in the lower region ($T < 400K$) and the polymer/coke is formed. This polymer may contain S which is released at higher temperatures as H_2S, or as C_4H_4S. The samples poisoned at higher temperatures ($T \geq 573K$) do not contain $C_4H_4S_{(a)}$ as such but $S_{(a)}$ and the polymer/coke which undergoes decomposition during regeneration. The formation of C_4H_4S in step (II) from the catalysts poisoned at high temperatures may not occur, but the

formation of hydrocarbons and H_2S is quite feasible.

The partial success of the regeneration with H_2 and the failure to remove sulphur adsorbed at high temperatures point to the search and use of other regenerative agents. Oxygen is not convenient as has been found out and reported (9,47,74-77). Steam seems to be more suitable (78) and it is recommended as a good alternative to be tested.

Summary

The results obtained can be summarised as follows:

i) Thiophene is dissociatively adsorbed on clean nickel catalysts. The mode of adsorption appears to be composed of co-planar to the surface and through the heteroatom. The amount adsorbed increases with concentration. As the temperature is increased thiophene undergoes decomposition into hydrocarbons and H_2S. Sulphur remains adsorbed on the surface with part of the hydrocarbons. At low temperatures thiophene polymerises forming a layer over the catalyst surface. At high enough temperatures (773K) coke may be formed through polymerisation of adsorbed carbon, however it is difficult to distinguish between coke and adsorbed hydrocarbons.

ii) The increase in weight uptake over long periods is due to an increase in the sulphur content of the nickel catalysts (sulphidation process). The rate at which this process occurs increases with temperature, but it is affected by the thiophene concentration. At high concentrations (1000ppm) the activation energy was determined to be 10.2 kJ/mole, but at 100ppm a value of 1.5 kJ/mole was obtained. Internal and external mass transfer limitations seem to be absent during the period at which the activation energy was determined. Possible explanations are given in terms of differences in the mode of

adsorption and competing sulphidation and carbon formation processes. However it is necessary to continue the investigation to discriminate between the two, and to find out the rate limiting step.

iii) The adsorption of thiophene on alumina is significant at low temperatures but negligible at high temperatures. At 298K the amount of thiophene adsorbed on Al_2O_3 was found to be higher at 100ppm than at 1000ppm, although the rate of weight uptake increased with concentration. The reason appears to be that thiophene is adsorbed through the sulphur atom and at 1000ppm it forms a polymer-like aggregate, whereas at 100ppm the concentration is low for the polymer to form at the same rate and allows that more thiophene be adsorbed perpendicularly, and possibly absorbed.

iv) It is possible to partially regenerate thiophene-poisoned nickel catalysts by H_2 treatment at 873K. The process removes carbon but very little of sulphur. The regenerated samples adsorb thiophene on a second adsorption experiment. The amount adsorbed is concentration and temperature dependent. At low concentration and T<373K the amount of thiophene adsorbed is higher on the regenerated than on the clean catalyst. This is assumed to be the effect of the sulphur remaining which 'promotes' adsorption through the sulphur atom. At higher concentrations the amount is the same on both fresh and regenerated catalysts, supporting the view of formation of the polymer. At higher temperatures thiophene is adsorbed to a lower extent on regenerated samples. This suggests that the adsorption occurs on clean nickel sites through the sulphur atom.

It is recommended to continue the efforts of regeneration using steam which presumably is more effective in removing adsorbed sulphur.

CHAPTER 7

CONCLUSIONS AND RECOMMENDATIONS

This study has dealt with the poisoning of nickel catalysts by sulphur compounds. The work involved the study of the adsorption behaviour of thiophene and H_2S on 20% Ni/Al_2O_3 samples, the regeneration of the poisoned catalysts, and the design and construction of a high pressure system. The catalyst was characterised by measuring the total surface area, the pore size distribution and the metal area available. The studies were performed in a gravimetric system where it was possible to perform a set of experiments which involved the characterisation, poisoning, regeneration and re-poisoning of the catalyst samples. The conclusions derived from this work and some suggestions for future work are given below.

7.1 Conclusions

Regarding the catalyst characterisation the following conclusions can be drawn:

i) The total area of the catalyst can be determined by the BET equation, the n* method or from the PSD. The easiest way of doing it is through the BET equation; care should be taken however for the interpretation of the values of C_{BET} obtained which can show a great dispersion and are subjected to large errors. The n* method can be used to find the region to which the C_{BET} belongs. This method is also suitable to analyse the type of pores present in the catalyst.

ii) The pore size distribution of the samples used can be

determined by using the N_2 desorption isotherm assuming that the pores are cylindrical. This conclusion was arrived at after the excellent agreement obtained between the total areas calculated by BET, n* method, and PSD. The distribution from the adsorption isotherm was broader, and the areas were lower than those from the BET equation and n* method.

iii) The metal areas of clean nickel catalysts can be determined by titration with CO at 195K. Temperatures of 273K or higher are not recommended due to the possible formation of nickel tetracarbonyl which is readily volatile and leads to the loss of nickel from the catalyst. At temperatures lower than 195K the physisorption contribution is too high and could lead to large errors. The monolayer coverage can be calculated by the extrapolation to zero pressure of the linear region of the curve obtained from the difference of a first (total) adsorption isotherm and a second isotherm determined after 20 min of evacuation at the adsorption temperature at the end of the first isotherm.

iv) N_2O was tested as a titrant for the determination of Ni metal areas. The best measurements were obtained at 273K. The determination is reliable and accurate. Lower temperatures are not suitable due to the high physical adsorption contribution. Higher temperatures were not tried although at temperatures > 373K there is the possibility of sublayer attack by the oxygen from the N_2O.

v) The determination of free nickel area of sulphur-poisoned catalysts is very difficult. It cannot be effected by CO adsorption because sulphur catalyzes the formation of nickel tetracarbonyl. The amount of CO adsorbed at 195K by the sulphur-poisoned catalysts is

higher than that by the clean catalysts, and increases with increasing sulphur content. At 273K the nickel tetracarbonyl is readily volatile and evaporates as soon as it is formed. Other gases must be tried to measure free nickel area of poisoned catalysts. N_2O, known to react with metal sites, could be a possible titrant that should be tried.

As for the adsorption of sulphur compounds and regeneration of the poisoned catalysts the results have shown that:

i) Thiophene is dissociatively adsorbed on the Ni/Al_2O_3 catalysts. Thiophene appears to adsorb both co-planar to the surface and perpendicular through the sulphur atom; the relative amounts of these two adsorption modes seem to vary with poison concentration, adsorption temperature and sulphur content of the catalyst. The total amount adsorbed is a function of concentration and temperature. As the concentration increases the amount adsorbed increases. At low temperatures (<373K) thiophene polymerises forming a layer on the catalyst surface; as the temperature increases thiophene undergoes decomposition producing gaseous products and sulphur adsorbed onto the nickel. An increase in weight is observed over long periods; this corresponds to an increase in sulphur content. This process occurs at a rate which appears to increase with temperature.

ii) Kinetic studies showed that the initial adsorption is controlled by the thiophene availability (amount of thiophene being fed) although the adsorption is fast. In the long term the rate of weight uptake increases with temperature and concentration. An apparent activation energy determined for the sulphidation process in the temperature region 573K-773K was found to be concentration dependent. This may be explained by differences in the adsorption mode

or by competing sulphidation and carbon formation processes.

iii) H_2S (from 2ppm H_2S/H_2) is adsorbed very fast onto nickel catalysts. It is dissociatively adsorbed and occupies 3 nickel sites per sulphur atom at 373K. The sulphur coverage decreases with increasing temperature. With a 8ppm H_2S/N_2 gas the catalyst does not reach saturation in 20h at 373K, it is presumed that sulphidation in depth occurs due to the presence of N_2 which changes the P_{H_2S}/P_{H_2} ratio and therefore the thermodynamic equilibrium, resulting in the formation of bulk sulphides.

iv) Alumina support adsorbs thiophene significantly at low temperatures (<373K) but the amount is negligible at high temperatures. At 298K the amount adsorbed after 20h is higher with 100ppm thiophene/H_2 than with 1000ppm due to the favoured perpendicular adsorption of thiophene which occupies less area than the coplanar structure therefore allowing more thiophene to be adsorbed, and because at the higher concentration thiophene polymerisation occurs forming a layer that does not permit more adsorption.

v) The regeneration with H_2 of catalysts poisoned by thiophene is partially successful. During the process some material (mostly hydrocarbons and carbon) is removed but some sulphur remains adsorbed. The regenerated samples are able to re-adsorb thiophene. At 100ppm and temperatures <373K the amount of thiophene adsorbed is higher on regenerated samples than on clean catalysts. This is presumably due to the sulphur presence which promotes perpendicular adsorption. At 1000ppm the amount adsorbed is the same on both clean and regenerated

samples, suggesting the formation of a polymer aggregate on the catalytic surface. At higher temperatures the amount adsorbed at saturation on regenerated samples is lower than on fresh catalysts. This result suggests that thiophene is adsorbed on clean nickel sites through the sulphur atom, reacts yielding gaseous products and sulphur which remains adsorbed on the nickel sites.

7.2 Suggestions for Further Work

During the course of this work results have been obtained providing some insight into the complicated adsorption process of sulphur-containing molecules on nickel catalysts. However some aspects remain to be studied and hence some suggestions into the possible further work are enlisted:

i) It is recommended to continue the efforts to find a suitable titrant of free nickel sites on sulphur poisoned nickel catalysts. N_2O appears to offer several advantages and it is suggested to study its adsorption on clean and sulphur-treated nickel catalysts in more detail.

ii) It is recommended to expand the range of the poisoning variables studied (to higher temperatures and lower concentrations) and to find a method to determine the gaseous products formed as the catalyst increases its weight.

iii) It would be desirable to determine the kinetics of the poisoning process (by thiophene) in a suitable experimental system at conditions where internal and external mass transfer resistances were experimentally demonstrated to be absent. This together with the products distribution mentioned above would provide a stronger basis for the determination of an adsorption mechanism.

iv) The use of a different regenerating agent is recommended. Based on the results reported in the literature steam seems to be a good alternative to H_2.

v) The study of the H_2S adsorption in the temperature range 373K-773K is recommended. Results at this conditions using low H_2S/H_2 concentrations are lacking; they are needed to observe the conditions at which the adsorption stoichiometry changes and the sulphur coverage increases.

vi) It is suggested to carry out experiments at higher pressures in the HP system. These have to be done once the reactor has been covered internally by an inert material to avoid the adsorption-desorption of sulphur onto the walls. At present these effects are masking the results.

REFERENCES

1. P.J. Denny, D.A. Whan, in Catalysis. Specialist Periodical Reports (C.Kemball, D.A. Dowden, Eds) The Chemical Society London. V.2, 46 (1978).

2. E.B. Maxted - Adv. Catalysis, 3, 129 (1951)

3. C.H. Bartholomew, P.K. Agrawal, J.R. Katzer, Adv. Catal., 31, 135 (1982).

4. R.A. Dalla Betta, A.G. Piken, M. Shelef, J.Catal., 40, 173 (1975).

5. J.R. Rostrup-Nielsen, K. Pedersen, J.Catal., 59, 395 (1979)

6. J.R. Rostrup-Nielsen, in Progress in Catalyst Deactivation (J.L. Figueiredo Ed.) p.127 Martinus Nijhoff Pub. London (1982).

7. J.R. Rostrup-Nielsen, in Progress in Catalyst Deactivation (J.L. Figueiredo Ed.) p.209 Martinus Nijhoff Pub. London (1982).

8. R.W. Fowler Jr., C.H. Bartholomew, I&E.C. Prod. Res. Dev. 18, 339 (1979).

9. C.H. Bartholomew, G.D. Weatherbee, G.A. Jarvi, J.Catal., 60, 257 (1979).

10. D.C. Gardner, C.H. Bartholomew, I & E.C. Prod. Res. Dev. 20, 80 (1981).

11. E.J. Erekson, C.H. Bartholomew, Applied Catal., 5, 323 (1983)

12. P.W. Wentrcek, B.J. Wood, H. Wise, J.Catal., 43 363 (1976)

13. P.W. Wentrcek, J.G. McCarty, C.M. Ablow, H. Wise, J.Catal., 61, 232 (1980).

14. P.K. Agrawal, W.D. Fitzharris, J.R. Katzer, in Catalyst Deactivation (B. Delmon, G.F. Froment Eds.) p.179 Elsevier Pub. Co. Amsterdam (1980).

15. W.D. Fitzharris, J.R. Katzer, W.H. Manogue, J.Catal., 76, 369 (1982).

16. J.G. McCarty, H. Wise, J.Catal., 57, 406 (1979).

17. J.R. Rostrup-Nielsen, J.Catal., 27, 343 (1972).

18. S. Morita, L. Kato, T. Inoue, J.Chem. Soc. Japan, Ind. Chem. Sec. 66, 1671 (1963), as cited in reference (19).

19. S. Morita, T. Inoue, Int. Chem. Eng. 5, 180 (1965)

20. G.W. Bridger, G.C. Chinchen in Catalyst Handbook, Wolfe, London (1970).

21. J.R. Rostrup-Nielsen, J.Catal., 31, 173 (1973).

22. T. Rosenqvist, J. Iron and Steel Inst. 176, 37 (1954)

23. M. Perdereau, J. Oudar, Surf. Sci. 20, 80 (1970).

24. J. Benard, Catal. Rev., 3, 93 (1969).

25. J.J. McCarroll, T. Edmonds, R.C. Pitkethly, Nature 223, 1260 (1969).

26. T. Edmonds, J.J. McCarroll, R.C. Pitkethly, J.Vac. Sci Tech., 8, 68 (1971).

27. J.E. Demuth, D.W. Jepsen, P.M. Marcus, Phys. Rev. Let., 32, 1182 (1974).

28. W. Erley, H. Wagner, J. Catal., 53, 287 (1978).

29. G.B. Fisher, Surf. Sci., 62, 31 (1977).

30. J. Oudar, Catal. Rev. Sci. & Eng., 22, 171 (1980).

31. O. Kubaschewsky, E.L. Evans, C.B. Alcock, Metallurgical Thermochemistry, Pergamon Oxford (1967).

32. J.L. Oliphant, R.W. Fowler, R.B. Pannell, C.H. Bartholomew, Jo. Catal., 51, 229 (1978).

33. J.G. McCarty, H. Wise, J. Chem. Phys. 72, 6332 (1980).

34. I. Alstrup, J.R. Rostrup-Nielsen, S. Roen, Applied Catal., 1, 303 (1981).

35. C.H. Bartholomew, J.R. Katzer, in Catalyst Deactivation (B. Delmon, G.F. Froment Eds.) p.375 Elsevier Pub. Co. Amsterdam (1980).

36. J.M. Saleh, C. Kemball, M.W. Roberts, Trans. Faraday Soc., 57, 1771 (1961).

37. I.E. Den Besten, P.W. Selwood, J.Catal., 1, 93 (1962).

38. C.F. Ng, G.A. Martin, J.Catal., 54, 384 (1978).

39. J.R. Rostrup-Nielsen, J.Catal., 11, 220 (1968).

40. D.O. Hayward, B.M.W. Trapnell, Chemisorption, 2nd. Ed. Butterworths, London (1964).

41. S.P. Weeks, E.W. Plummer, Chem. Phys. Let., 48, 601 (1977).

42. A. Rudajevova, V. Pour, A. Regner, Collec. Czech. Chem. Commun., 38, 2566 (1973).

43. G. Blyholder, D. Bowen, J.Phys. Chem., 66, 1288 (1962).

44. J.M. Saleh, M.W. Roberts, C. Kemball, Trans. Faraday Soc., 58, 1642 (1962).

45. G.D. Lyubarskii, L.B. Avdeeva, N.V. Kul'kova, Kinetics & Katal., 3, 102 (1962).

46. K.H. Bourne, P.D. Holmes, R.C. Pitkethly, 3rd Int. Congr. in Catal., Amsterdam (1964), (W.M. Sachtler, G.C.A. Schuit, P. Zwietering Eds.), North Holland, 2, 1400 (1965).

47. L.D. Neff, S.C. Kitching, J. Phys. Chem. 78, 1648 (1974)

48. C.H. Rochester, R.J. Terrel, J. Chem. Soc. Farady Trans. I, 73, 596 (1977).

49. A. Koppova, V. Zapletal, V. Ruzicka, J. Soukup, Coll. Czech. Chem. Commun., 38, 2472 (1973).

50. D.G. Holah, I.M. Hoodless, A.N. Hughes, L. Sedor, J. Catal., 60, 148 (1979).

51. J.T. Richardson, J. Catal., 21, 130 (1971).

52. H.S. Weng, G. Eigenberger, J.B. Butt, Chem. Eng. Sci., 30, 1341 (1975).

53. K. Klostermann, H. Hobert, J. Catal., 63, 355 (1980).

54. P.G. Menon, J. Prasad, Proc. 6th Int. Congr. Catal. 1976 (G.C. Bond, P.B. Wells, F.C. Tompkins Eds.) p. 1061. The Chemical Society London. (1976).

55. G. Del Angel, B. Coq, F. Figueras, S. Fuentes, R. Gomez, Actas 8^0 Simp. Iberoamericano de Catal. Huelva Espana, 1, 180 (1982).

56. R.W. Coughlin, A. Hasan, K. Kawakami, J. Catal., 88, 163 (1984).

57. L. Gonzalez-Tejuca, K. Aka, S. Namba, J. Turkevich, J. Phys. Chem., 81, 1399 (1977).

58. J. Barbier, P. Marecot, L. Tifouti, M. Guenin, Actas 9^0 Simp. Iberomaericano de Catal. Lisboa, Portugal, 1, 540 (1984).

59. O. Weiser, S. Landa, Sulphide Catalysts. Their properties and applications. Pergamon, Oxford (1973).

60. P.C.H. Mitchell, in Catalysis. Specialist Periodical Reports. (C. Kemball Ed.) The chemical Society, London. V. 1, 204 (1977).

61. P.C.H. Mitchell, in Catalysis. Specialist Periodical Reports. (C. Kemball, D.A. Dowden Eds.) The Chemical Society London. V. 4, 175 (1981).

62. B.C. Gates, J.R. Katzer, G.C.A. Schuit, Chemistry of Catalytic Processes. McGraw-Hill. London (1979).

63. M. Zdrazil, Applied Catal., 4, 107 (1982).

64. M.L. Vrinat, Applied Catal., 6, 137 (1983).

65. M. Zdrazil, Collec. Czech. Chem. Commun., 42, 1484 (1977).

66. D. Dollimore, A. Galwey, G. Rickett, J. Chim. Phys. 72, 1059 (1975).

67. C.N. Satterfield, G.W. Roberts, A.I.Ch.E. Journal 14, 159 (1968).

68. F.E. Massoth, J. Catal., 47, 316 (1977).

69. J. Hernandez, Ph.D. Thesis, University of Bath, Bath U.K. (1983).

70. S. Morooka, C.E. Hamrin, Chem. Eng. Sci., 32, 125 (1977).

71. Y. Kawaguchi, I.G. Dalla Lana, F.D. Otto, Canad. J. Chem. Eng. 56, 65 (1978).

72. G.D. Blyholder, G.W. Cagle, Environ. Sci. Tech., 5, 158 (1971).

73. H. H. Dobashi, U.S. Patent 4 065 484 (1977).

74. P.H. Holloway, J.B. Hudson, Surf. Sci., 33, 56 (1972).

75. H. Windawi, J.R. Katzer, J.Vac. Sci. Technol., 16, 497 (1979).

76. A.R. Chughtal, J.R. Riter Jr., J. Phys. Chem. 83, 2771 (1979).

77. S.A. Colby, M.Ch.E. Thesis, University of Delaware, Newark Delaware (1977).

78. J.R. Rostrup-Nielsen, J.Catal., 21, 171 (1971).

79. A.J. de Rosset, C.G. Finstrom, C.J. Adams, J. Catal., 1, 235 (1962).

80. R.W. Glass, R.A. Ross, J. Phys. Chem., 77, 2576 (1973).

81. R.W. Glass, R.A. Ross, J. Phys. Chem., 77, 2571 (1973).

82. R.F. Curtis, D.M. Jones, G. Ferguson, D.W. Hawley, J.G. Sime, K.K. Cheung, G. Germain, Chem. Commun., 165 (1969).

83. S.J. Gregg, K.S.W. Sing, Adsorption, Surface Area and Porosity. Academic Press. London (1967).

84. J.R. Anderson, Structure of Metallic Catalysts. Academic Press London (1975).

85. B. Innes, in Experimental Methods in Catalytic Research (R.B. Anderson Ed.) p.44, Academic Press London (1968).

86. E.V. Ballou, O.K. Dvolin, Anal. Chem., 32, 532 (1960).

87. E.V. Ballou, R.T. Barth, Adv. in Chem. Series, 33, 133 (1961).

88. R. Haul, G. Durbgen, Chem. Ing. Techn., 32, 349 (1960).

89. D.A. Cadenhead, N.J. Wagner, in Experimental Methods in Catalytic Research Vol. II. (R.B. Anderson, P.T. Dawson Eds.) p. 223, Academic Press London (1976).

90. L. Cahn, H.R. Schultz, Vacuum Microbalance Techn., 3, 29 (1963).

91. A.W. Czanderna, J.M. Honig, J. Phys. Chem., 63, 620 (1959).

92. A.W. Czanderna, S.P. Wolsky, in Microweighing in Vacuum and Controlled Environments (A.W. Czanderna, S.P. Wolsky Eds.) Elsevier, Amserdam, Oxford (1980).

93. F.M. Nelson, F.T. Eggerston, Anal. Chem., 30, 1387 (1958).

94. K.R. Lange, J. Coll. Sci, 18, 65 (1963).

95. A.J. Lecloux, in Catalysis, Science and Technology. Vol. 2 (J.R. Anderson, M. Boudart Eds.) Springer Verlag, Berlin, New York (1981).

96. K.S.W. Sing, in Characterisation of Catalysts. (J.M. Thomas, R.M. Lambert Eds.) J. Wiley. Chichester (1980).

97. S. Brunauer, L.S. Deming, W.S. Deming, E. Teller, J.Am.Chem. Soc., 62, 1723 (1940).

98. J.H. de Boer, B.G. Linsen, Th. van der Plas, G.J. Zondervan, J. Catal., 4, 649 (1965).

99. E. Robens, in Microweighing in Vacuum and Controlled Environments (A.N. Czanderna, S.P. Wolsky Eds.) p.127 Elsevier, Amsterdam, Oxford (1980).

100. K.S.W. Sing, Chem. Ind. (London) 1520 (1968).

101. A. Lecloux, J.P. Pirard, J. Colloid Int. Sci., 70, 265 (1979).

102. S.J. Gregg, K.S.W. Sing, Adsorption, Surface Area and Porosity. 2nd Ed. Academic Press London (1982).

103. J.H. de Boer, in The Structure and Properties of Porous Materials (D.H. Everett, F.S. Stone Eds.) p.68 Butterworths, London (1958).

104. D.C. Havard, R. Wilson, J. Colloid Int. Sci., 57, 276 (1976).

105. D. Dollimore, G.R. Heal, J. Colloid Int. Sci., 42, 233 (1973).

106. S. Brunauer, R. Mikhail, E.E. Bodor, J. Colloid Int. Sci., 24, 451 (1967).

107. J.P. Irving, J.B. Butt, J. Appl. Chem., 15, 139 (1965).

108. D. Dollimore, G.R. Heal, J. Colloid Int. Sci., 33, 508 (1970).

109. A. Wheeler, Catalysis, Reinhold, New York, 2, 115 (1955).

110. C.G. Shull, J. Amer. Chem. Soc., 70, 1405 (1948).

111. D.H. Everett, in Characterisation of Porous Solids (S.J. Gregg, K.S.W. Sing, H.F. Stoeckli Eds.) p.229 Soc. Chem. Ind. London (1979).

112. R.J. Farrauto, A.I.Ch.E. Symp. Ser. No. 143, 70, 9 (1974).

113. R.B. Pannell, K.S. Chung, C.H. Bartholomew, J. Catal., 46, 340 (1977).

114. E. Cremer, H. Huber, Angew Chem., 73, 461 (1965).

115. C.S. Brooks, G.L.M. Christopher, J.Catal., 10, 211 (1968).

116. J. Freel, S.D. Robertson, R.B. Anderson, J. Catal., 18, 243 (1970).

117. P. Mars, J.J.F. Scholten, P. Zwietering, Actes Congr. Int. Catal. 2nd 1960, 1, 1245 (1961).

118. C.H. Bartholomew, R.J. Farrauto, J. Catal., 45, 41 (1976).

119. C.H. Bartholomew, R.B. Pannell, J. Catal., 65, 390 (1980).

120. D.G. Mustard, C.H. Bartholomew, J. Catal., 67, 186 (1981).

121. G. Lohrengel, M. Baerns, Applied Catal., 1, 3 (1981).

122. P.H. Emmett, N. Skau, J. Amer. Chem. Soc., 65, 1029 (1943).

123. R.J. Kokes, P.H. Emmett, J. Amer. Chem. Soc., 82, 1037 (1960).

124. G.C.A. Schuit, L.L. van Reijen, Advan. Catal., 10, 242 (1958).

125. K. Klier, A.C. Zettlemoyer, H. Leiheidser Jr., J. Chem. Phys., 52, 589 (1970).

126. J.C. Tracy, J. Chem. Phys., 56, 2736 (1972).

127. H.H. Madden, J. Kuppers, G. Ertl, J. Chem. Phys., 58, 3401 (1973).

128. H. Conrad, G. Ertl, J. Kuppers, E.E. Latta, Surf. Sci., 57, 475 (1976).

129. R.P. Eischens, S.A. Francis, W.A. Pliskin, J. Phys. Chem., 60, 194 (1956).

130. J.T. Yates, C.W. Garland, J. Phys. Chem., 65, 617 (1961).

131. G.J. Blyholder, J. Phys. Chem., 68, 2772 (1964).

132. M. Primet, J.A. Dalmon, G.A. Martin, J. Catal., 46, 25 (1977).

133. C.H. Rochester, R.J. Terrell, J. Chem. Soc. Faraday Trans. I., 73, 609 (1977).

134. A.I. Kreindel, V.S. Sobolevskii, E.Z. Golosman, V.I. Yakerson, Kinetics and Katal., 15, 355 (1974).

135. J. Muller, J. Catal., 6, 50 (1966).

136. J. Muller, V. Pour, A. Regner, J. Catal., 11, 326 (1968).

137. L. Spenadel, M. Boudart, J. Phys. Chem., 64, 204 (1960).

138. J.J.F. Scholten, J.A. Konvalinka, Trans. Faraday Soc., 65, 2465 (1969).

139. J.J.F. Scholten, J.A. Konvalinka, F.W. Beekman, J.Catal., 28, 209 (1973).

140. J.W. Evans, M.S. Wainwright, A.J. Bridgewater, D.J. Young, Applied Catal., 7, 75 (1983).

141. M.W. Roberts, K.W. Sykes, Trans. Faraday Soc., 54, 548 (1958).

142. S.E. Wanke, N.A. Dougharty, J. Catal., 24, 367 (1972).

143. T.R. Hughes, R.J. Houston, R.P. Sieg, I.E.C. Proc. Des. Dev., 1, 96 (1962).

144. V. Srinivasan, K.R. Krishnaswami, Current Sci., 25, 328 (1956).

145. C.H. Bartholomew, R.B. Pannell, Applied Catal., 2, 39 (1982).

146. J.H. Sinfelt, D.J.C. Yates, J. Catal., 8, 82 (1967).

147. D.J.C. Yates, J.H. Sinfelt, J. Catal., 8, 348 (1967).

148. J.E. Benson, M. Boudart, J.Catal., 4, 704 (1965).

149. S. Parkash, Canad. J. Chem. Eng., 60, 23 (1982).

150. K.D. Rendulic, A. Winkler, Surf. Sci., 74, 318 (1978).

151. R.S. Bordoli, J.C. Vickerman, J. Wolstenholme, Surf. Sci., 85, 244 (1979).

152. D.E. Milliams, J. Pritchard, K.W. Sykes, 6th Int. Congr. Catal., London Paper A32 p. 417 (1976).

153. Y.J. Feng, Internal Report. Dept. Of Chemical Eng. Imperial College, London (1981).

154. C.W. Garland, J. Phys. Chem., 63, 1423 (1959).

155. R.T. Rewick, H. WIse, J. Phys. Chem., 82, 751 (1978).

156. H. Pichler, Adv. Catal., 4, 326 (1952).

157. R. Van Hardeveld, F. Hartog, Adv. Catal., 22, 75 (1972).

158. B.C. Lippens, J.H. de Boer, J. Catal., 4, 319 (1965).

159. [illegible] alle, in Fine Particle Measurements, p. 271 McMillan, New York (1959).

160. G. Halsey, J. Chem. Phys., 16, 931 (1948).

161. R.W. Cranston, F.A. Inkley, Adv. Catal., 9, 143 (1957).

162. J.O. Mingle, J.M. Smith, Chem. Eng. Sci., 16, 31 (1960).

163. B.C. Lippens, B.G. Linsen, J.H. de Boer, J. Catal., 3, 32 (1964).

164. J.H. de Boer, A. van den Heuvel, B.G. Linsen, J. Catal., 3, 268 (1964).

165. M.R. Harris, Chem. and Ind. (London) 6, 268 (1965).

166. A.G. Ritchie, J. Chem. Soc. Faraday Trans. I., 73, 1650 (1977).

167. J.B. Butt, V.W. Weekman Jr., A.I.Ch.E. Symp. Ser. No. 143, 70, 27 (1974).

168. J.J. Carberry, A.I.Ch.E. Journal 7, 350 (1961).

169. R.C. Reid, J.M. Prausnitz, T.K. Sherwood, The Properties of gases and liquids, 3rd Ed. McGraw Hill New York (1977).

170. T.K. Sherwood, R.L. Pigford, C.R. Wilke, Mass Transfer, McGraw Hill London (1975).

171. G.F. Froment, K.B. Bischoff, Chemical Reactor Analysis and Design. J. Wiley, New York (1979).

172. D.E. Mears, I.E.C. Proc. Des. Dev., 10, 541 (1971).

173. F.E. Massoth, C.L. Kibby, J. Catal., 47, 300 (1977).

174. C.R. Apesteguia, J.F. Plaza de los Reyes, T.F. Garetto, J.M. Parera, Applied Catal., 4, 5 (1982).

175. R.P. de Pauw, G.F. Froment, Chem. Eng. Sci., 30, 789 (1975).

176. F.J. Dumez, G.F. Froment, I.E.C. Proc. Des. Dev., 15, 291 (1976).

177. R. Ramachandran, F.E. Massoth, Canad. J. Chem. Eng., 60, 17 (1982).

178. L.F.G. de Sousa Lobo, Ph.D. Thesis, Imperial College, University of London, London. (1971).

179. J.L.C. Figueiredo, Ph.D. Thesis, Imperial College, University of London, London (1975).

180. L.E. Brownell, E.H. Young. Process Equipment Design. John Wiley New York (1959).

181. Metals Handbook, 8th Edn. American Society for Metals. Vol. 1 (1976).

182. C.N. Satterfield, Heterogeneous Catalysis in Practice. McGraw Hill p. 82 (1980).

183. R.L. Moss, in Experimental Methods in Catalytic Research V.2 (R.B. Anderson, P.T. Dawson Eds.) p. 43 Academic Press, London (1976).

184. D.A. Dowden, Personal Communication (1984).

185. J.H. Smith, Chemical Engineering Kinetics, 3rd Ed. McGraw Hill London (1981).

186. ASME Boiler and Pressure Vessel Code, Section VIII, Rules for Construction of Unfired Pressure Vessels, Am. Soc. Mech. Engr. (1956).

187. D.W. Goodman, M. Kiskinova, Surf. Sci., 105, L265 (1981).

A P P E N D I C E S

A.1 High Pressure Reactor Design

The design of the high pressure reactor involved the selection of suitable materials to withstand the poisoning atmosphere, the maximum operating pressure and temperature conditions, and be able to sustain a vacuum of 1.3×10^{-2} Pa (10^{-4} torr).

The maximum operating conditions were set at:

Pressure: 30 bar

Temperature: 1073K

The construction material should have good strength properties at high temperatures, and resistance to oxidation, carbonization and corrosive atmospheres. Nickel alloys have these characteristics and among them Inconel 600 and Incoloy 800 offer all of them, with the 800 showing better strength at higher temperatures.

The reactor diameter and wall thickness were selected from considerations of available sizes, reactor configuration and bursting pressure. The reactor should have two concentric tubes, with the sample hanging in the centre of the inner tube. Enough space should be available for the sample basket and the configuration should allow a thermocouple to be placed near the sample in the annulus between the two tubes.

The reactor length was designed so that the working temperature of the top flanges should be around 673K when the reactor temperature was 1073K. The temperature profile along the reactor was calculated assuming only heat conduction and neglecting radiation to the atmosphere. It was found that 15cm were required from the top of the furnace to the flanges for the temperature to decrease to 673K. It is obvious that this distance is overestimated since the heat loss by

radiation is high and was not taken into account, and it was proved to be so experimentally: the flange temperatures were below 673K when the catalyst temperature was 1073K.

The chosen material of construction was Incolloy 800. From the tube sizes available in the market two were selected to calculate the maximum allowable pressure at operating conditions:

Material	Nominal Size (in)	Schedule	ID (mm)	Wall thickness (mm)	P_{allow} (bar)
Incoloy 800	1	80	24.3	4.55	52.7
Incoloy 800	1¼	80	32.46	4.85	43.7

The maximum allowable pressure (P_{allow}) was calculated using the modified membrane equation:

$$P = \frac{fEt}{R+0.6t}$$

Where: P: maximum allowable pressure, Nm^{-2}

f: maximum allowable stress, Nm^{-2}

E: welded joint efficiency (=1)

R: inside radius, m

t: thickness of shell, m.

at T = 1073K $f = 1.724 \times 10^{7}\ Nm^{-2}$ (=2500psi)

From these data 1¼" Schedule 80 Incoloy 800 tube was selected.

The design of the top and bottom flanges was done according to Brownell and Young (180). The material was Inconel 600 due to its availability in the market. The thicknesses of the flanges were calculated from:

Top flange (Integral flange):

$$t_T = 0.72 \sqrt{MoY/B\ f_{all}}$$

Bottom flange (blind flange):

$$t_b = d\sqrt{C(p/f)}$$

Where:

t: thickness of flange, m

Mo: total moment acting upon the flange, N m

Y: factor, from fig. 12.22 (Brownell and Young) (180)

B: inside diameter of flange, m

f_{all}: maximum allowable flange stress, Nm^{-2}

d: diameter, m

C: constant from appendix H, reference 180

p: design pressure, Nm^{-2}

f: maximum allowable stress, Nm^{-2}

Mo was calculated following the procedure outlined in Brownell and Young (180) and was equal to: 2.386×10^2Nm(=2111.7 in-pound).

$B = 3.246 \times 10^2 M$

$Y = 3.6$

$f_{all} = 1.379 \times 10^8\ Nm^{-2}$ (ref.181).

$d=B=3.246 \times 10^{-2} m$

$c= 0.5$

$P= 3 \times 10^{6}\ Nm^{-2}$

$f= 1.379 \times 10^{7}\ Nm^{-2}$ (=2000 psi) (ref.181)

$$t_T = 9.97 \times 10^{-3}\ m\ (=10mm)$$

$$t_b = 1.07 \times 10^{-2}\ m\ (=10.7mm)$$

As a safety factor the flange thicknesses were 1.5 times the calculated values

$$t_T = 15mm$$

$$t_b = 15mm$$

The top flanges configuration is shown in Figure 4.4 (Chapter 4).

The reactor shell is threaded into the inferior top flange (t_T=15mm) and welded. This flange contains a slot into which the soft copper gasket sits, and also holds the inner tube (Incoloy 800) by a tapered flange threaded to this tube. The reactor is tightened to the superior top flange (t_T=15mm) by means of 8 stainless steel bolts (diameter = 6.3mm) equally spaced.

The bottom flange is threaded 8mm into the reactor shell and welded as seen in Figure 4.3.

In summary:

Reactor: Incoloy 800 Schedule 80

Nominal size: 1½ in

External diameter = 42.2mm

thickness = 4.85mm

length = 450mm

Inner tube: Incoloy 800 Schedule 10

Nominal size: ½ inch

External diameter = 21.3mm

thickness = 2.11mm

length = 435mm

Bottom flange: Inconel 600

Size: 42.2mm

Thickness: 15mm: 8mm threaded and welded.

Top flanges: Inconel 600

Inferior flange: thickness: 15mm

External diameter: 75mm

Superior flange: thickness: 15mm

External diameter: 75mm

Gasket: soft copper

Internal diameter: 36mm

width: 3mm

Bolts: 8 bolts stainless steel 316

Nominal size ¼ in (6.3mm).

A.2 Tests of high pressure system

The high pressure system was first pressure tested with helium at twice the maximum operating pressure and room temperature. The pressure was maintained at 60 bar for 48h without leaks.

The adsorption of H_2S on Ni/Al_2O_3 was attempted but the results were not satisfactory.

Several experiments were carried out using 2ppm H_2S/H_2 at several pressures and 373K. No increase in weight was noticed in any of the runs. With a 8ppm H_2S/N_2 mixture the weight increased immediately, reached a constant weight and then decreased slightly as can be seen in figure A-1. The final weight obtained after 4h is lower than those observed in the experiments performed in the atmospheric pressure (glass) system with both gas mixtures (2ppm H_2S/H_2, 8ppm H_2S/N_2).

It can be said that:

i) the buoyancy is affecting the results since no weight increase was observed using 2ppm H_2S/H_2, and

ii) the sulphur which is adsorbed on the reactor walls may be desorbed during the catalyst reduction and be adsorbed onto the Ni catalyst effectively poisoning it.

It is recommended then to study the effect of buoyancy in more detail, and to cover the reactor walls with an inert material which does not adsorb sulphur and therefore eliminate unwanted poisoning.

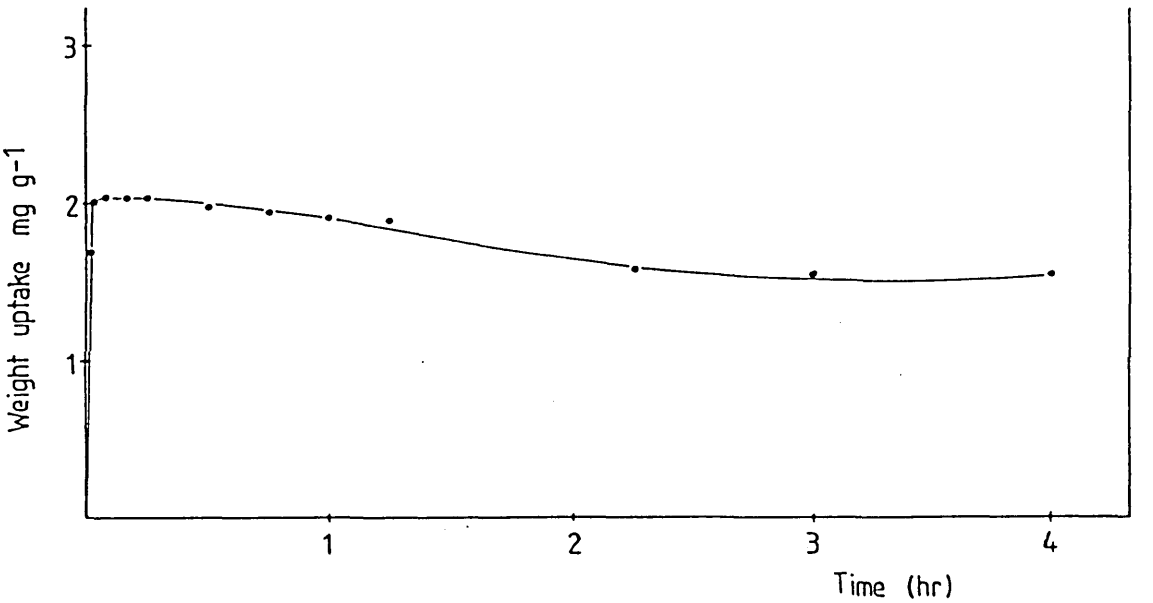

FIGURE A.1

Adsorption of H_2S on Ni/Al_2O_3 in the High Pressure System. 8ppm H_2S/N_2, 373K, 1.1 bar.

A.3 Comments on the microbalance operation

Microbalances are very delicate apparatus to operate and some comments are in order:

i) the capacity of the CI microbalance (1g) and the weight lost during reduction restricted the sample weight to between 0.1-0.2g if reasonable accuracy was required (±5μg);

ii) thermomolecular flow during total and metal area determinations was avoided by measuring the adsorption uptakes at or above 1.33kPa (10torr);

iii) buoyancy corrections were negligible for the total and metal area determinations due to the high surface area samples employed. However buoyancy effects were appreciable during the long term adsorption of thiophene and produced spurious weight increases. The buoyancy was found to be affected by changes in the room temperature during daytime;

iv) convection currents were of no importance at atmospheric pressure, however very strong effects were observed in the high pressure system at pressures above 1 bar, this is explained in more detail below;

v) the most frequently found trouble was static electricity. It was observed after loading a new sample and was created by friction while assembling the reactor, or if the reactor was wiped out after cleaning with dilute HNO_3 and isopropanol. It was avoided by leaving the reactor parts to dry after washing with isopropanol and doing a careful assembly.

vi) at the start of the poisoning experiments as the thiophene/H_2 mixture was fed to the reactor an immediate small increase in weight

was noticed, this corresponded to the force exerted by the flow on the basket. At the end of the adsorption as the poisoning stream was cut off the sample weight decreased a similar amount to that at the beginning. This spurious weight could be accounted for and was subtracted from the weight uptake due to adsorption.

vii) the operation of the high pressure system was more complex than the atmospheric pressure system. Buoyancy effects were more noticeable due to the larger volume of the reactor and the greater effect the temperature had on it. Convection currents were developed at high pressures ($p > 1$ bar) and/or high temperatures ($T > 373K$) and were especially affected by the interaction of the magnetic forces of the nickel catalyst and the furnace heating current, the presence of a hot spot in the furnace which created temperature gradients along the reactor, and the density of the gas used.

Static electricity was generated due to friction between the long silica wire and the small hole on the top flange through which it passed. The friction was caused by poor alignment of the reactor and the convection currents. A qualitative diagram of these two effects on the weight is shown in Figure A.2

Convective currents were diminished to a great extent by the inclusion of baffles to dampen the upward flow, by identification of the furnace hot spot and placing it at the level of the catalyst sample; by changing the temperature control from a Eurotherm automatic controller to a Variac to eliminate periodic induction of magnetic forces, and by using low density gases (H_2, He).

Buoyancy could not be eliminated since it is inherent to the system due to the large volume of the reactor. It is believed that

buoyancy affected the results of the H_2S adsorption tests at high pressure, and it is recommended that detailed studies be carried out by future workers so that the magnitude of the effect can be determined.

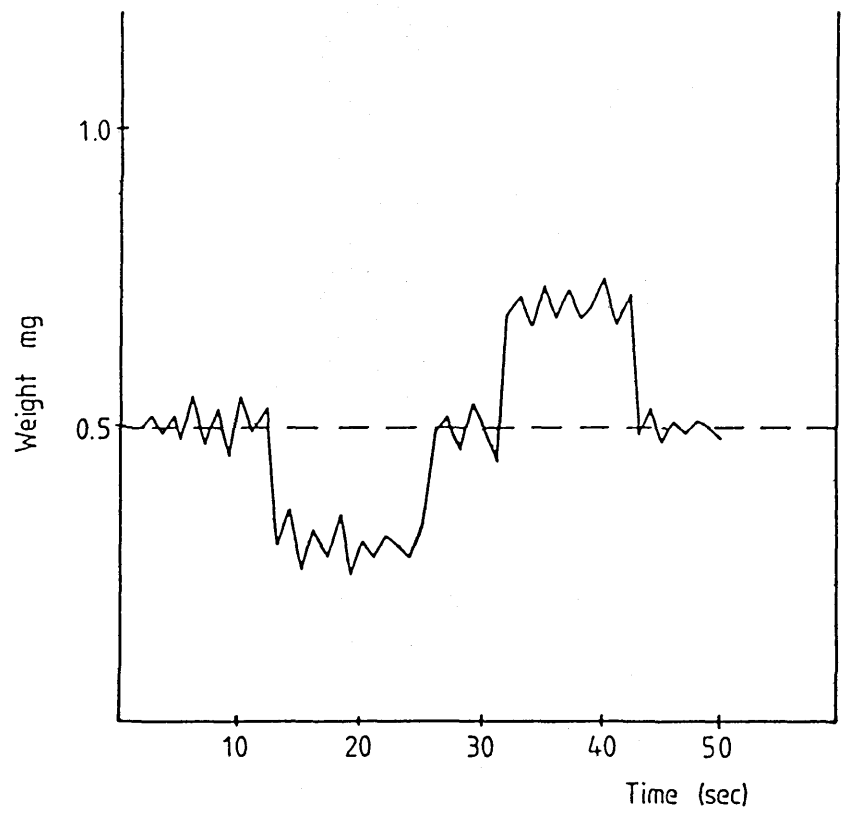

FIGURE A.2

Effect of static electricity and convective currents on the sample weight.

B.1 N_2 Adsorption Raw Data

Representative Nitrogen adsorption-desorption data are given in this appendix for γ-Al_2O_3, fresh Ni/Al_2O_3 and reduced Ni/Al_2O_3. These data were used to calculate total areas by the BET equation, n* method and for the pore size distribution.

For γ-Al_2O_3. Sample Weight: 0.1375g Po = 76 cm Hg

Adsorption		Desorption	
Pressure (cm Hg)	Amount adsorbed (mg)	Pressure (Cm Hg)	Amount adsorbed (mg)
1.05	5.95	9.80	8.40
3.80	7.32	17.30	9.68
7.70	8.27	24.80	10.97
11.45	8.96	32.35	12.36
15.25	9.58	40.05	14.12
19.00	10.19	47.75	17.02
22.80	10.82	55.20	23.92
30.35	12.12	62.95	40.02
38.00	13.66	68.10	49.82
45.80	15.69	73.60	54.12
49.80	16.99		
53.35	18.49		
58.55	21.49		
64.60	26.59		
69.05	35.69		

Sample: Fresh Ni/Al_2O_3 Weight: 0.1398g (oxide form) Po: 76cm Hg

Adsorption		Desorption	
Pressure (cm Hg)	Amount Adsorbed (mg)	Pressure (cm Hg)	Amount Adsorbed (mg)
1.40	5.83	6.00	7.15
3.95	6.76	11.00	8.02
7.70	7.50	16.00	8.79
11.55	8.13	20.85	9.52
15.30	8.67	25.85	10.28
19.00	9.22	31.60	11.27
22.80	9.80	36.95	12.30
26.60	10.41	42.50	13.78
30.50	11.05	47.50	15.58
34.20	11.75	53.50	19.48
37.95	12.53	58.80	25.48
45.60	14.32	63.90	32.78
53.10	16.92	69.40	39.38
58.40	19.72	75.60	43.28
63.80	23.82		
69.50	30.62		
76.10	43.52		

Sample: Reduced Ni/Al_2O_3 Weight: 0.1398g (oxide form) Po=76cmHg

Adsorption		Desorption	
Pressure (cm Hg)	Amount Adsorbed (mg)	Pressure (cm Hg)	Amount Adsorbed (mg)
1.25	5.28	8.50	6.92
3.85	6.15	13.45	7.66
7.75	6.88	18.50	8.35
11.40	7.42	23.55	9.04
15.25	7.94	28.95	9.82
18.95	8.43	33.95	10.62
22.75	8.95	40.00	11.82
26.55	9.49	45.65	13.32
30.55	10.10	52.20	16.32
37.95	11.34	58.15	22.92
45.55	13.06	62.95	30.92
49.65	14.26	67.90	37.82
53.35	15.46	74.50	42.32
57.20	17.26		
61.00	19.96		
64.95	23.96		
68.95	30.06		
74.55	41.96		

B.2 PSD Calculations

This appendix shows some of the results that were obtained for the pore size distribution of γ-Al_2O_3, fresh Ni/Al_2O_3 and reduced Ni/Al_2O_3. The calculations presented here were obtained using the desorption branch of the N_2 isotherm values given in appendix B.1, following the Orr and Dalla Valle method as given in Gregg and Sing (102).

In Tables B.1 to B.3 columns (1) and (2) are values taken from the plot of the adsorption-desorption isotherm at convenient intervals of P/P_o.

Column (3) shows the "core" radius calculated from the Kelvin equation:

$$r_k = \frac{4.078}{\log(P_o/P)} \qquad (\text{Å})$$

Column (4) gives the thickness of the adsorbed layer, t, calculated from the Halsey equation:

$$t = 3.54 \left\{ \frac{5}{\ln(P_o/P)} \right\}^{1/3}$$

Column (5) shows the pore radius obtained from $r_p = r_k + t$.

The mean values of r_p and r_k are shown in columns 6 and 7; and columns 8 and 9 give the diminution in film thickness (Δt) and decrease in pore radius (δr_p) respectively as the pressure decreases.

Column (10) gives the correction factor Q calculated by:

$$Q = \left(\frac{\bar{r}_{pi}}{\bar{r}_{pi} - t_i}\right)^2$$

Column (11) shows the amount adsorbed in terms of liquid volume, from column (2).

Column (12) shows the volume desorbed as the pressure decreased, obtained from column (11).

In column (13) is given the volume desorbed from the film on the walls during the desorption step. It is calculated by:

$$\delta v_f = 0.1 \times \Delta t \; \Sigma\delta A_p = [0.1 \times (8)(17)]$$

$\Sigma\delta A_p$ is the value taken from the previous row. The first value is zero.

Column (14) represents the decrease of capillary-condensed material (core volume), obtained by: $\delta V_k = \delta V - \delta V_f = [(12)-(13)]$.

The volume of the pore is calculated by $\delta V_p = \delta V_k \times Q = [(14)x(10)]$ and is given in Column (15). The area of the pore walls corresponding to the decreasing volumes δV_p are given in column (16) and are calculated by the expression $\delta A_p = 20 \times \delta V_p / \bar{r}_p = 20 \times [(15)/(6)]$, assuming pores of cylindrical geometry.

The values in Column (17) are obtained by the addition of all the preceding rows of column (16).

Column (18) is obtained by the ratio of columns (15)/(9); and column (19) is consequently calculated by the ratio of δV_k in column (14) and the appropriate δr_k obtained from column (3).

The addition of all the values of column (15) gives the total pore volume of the sample in question.

Table B.1 PSD Calculations for γ-Al_2O_3 Using Desorption Branch

(1)	(2)	(3)	(4)	(5)	(6)	(7)	(8)	(9)	(10)
P/P_o	n	r_k	t	r_p	$\bar{r}_p$	$\bar{r}_k$	Δt	δr_p	Q
	mg/g	Å	Å	Å	Å	Å	Å	Å	
0.968	393.6	288.72	18.96	307.68					
					253.51	235.89	2.66	108.33	1.142
0.95	386.18	183.06	16.3	199.35					
					150.6	136.06	3.48	97.4	1.195
0.90	363.64	89.12	12.82	101.9					
					85.39	73.45	1.72	33.02	1.321
0.85	326.18	57.78	11.1	68.88					
					60.49	49.94	1.10	16.78	1.435
0.80	255.42	42.1	10	52.1					
					46.96	37.37	0.83	10.29	1.544
0.75	194.76	32.64	9.17	41.81					
					38.34	29.49	0.63	6.94	1.655
0.70	155.42	26.33	8.54	34.87					
					32.35	24.07	0.52	5.05	1.768
0.65	130.91	21.8	8.02	29.82					
					27.9	20.09	0.42	3.84	1.889
0.60	116.36	18.38	7.6	25.98					
					24.4	17.05	0.41	3.08	2.01
0.55	105.53	15.71	7.19	22.9					
					21.65	14.63	0.35	2.5	2.137
0.50	99.06	13.55	6.89	20.4					
					19.35	12.66	0.31	2.10	2.278
0.45	93.16	11.76	6.53	18.3					
					17.39	11.01	0.30	1.82	2.428
0.40	88.15	10.25	6.23	16.48					
					15.69	9.6	0.27	1.58	2.60
0.35	82.69	8.94	5.96	14.9					
					14.20	8.37	0.27	1.40	2.784
0.30	78.18	7.8	5.69	13.5					

Table B.1 Continuation

(11)	(12)	(13)	(14)	(15)	(16)	(17)	(18)	(19)
V	δV	δV_f	δV_k	δV_p	δA_p	$\Sigma\delta A_p$	$\frac{\delta V_p}{\delta r_p}$	$\frac{\delta V_k}{\delta r_k}$
mm^3/g	mm^3/g	mm^3/g	mm^3/g	mm^3/g	m^2/g	m^2/g	$\frac{10^7 mm^2}{g}$	$\frac{10^7 mm^2}{g}$
487.13								
	9.18	0	9.18	10.484	0.827	0.827	0.10	0.09
477.95								
	27.9	0.288	27.61	33.0	4.38	5.21	0.34	0.29
450.05								
	46.73	0.90	45.47	60.07	14.07	19.28	1.82	1.45
403.68								
	87.57	2.12	85.45	122.62	40.54	59.82	7.31	5.45
316.11								
	75.10	4.97	70.13	108.29	46.12	105.94	10.52	7.41
241.04								
	48.69	6.67	42.02	69.54	36.27	142.21	10.02	6.66
192.35								
	30.33	7.40	22.93	40.55	25.07	167.28	8.03	5.06
162.02								
	18.01	7.03	10.98	20.75	14.87	182.15	5.40	3.21
144.01								
	13.40	7.47	5.93	11.92	9.77	191.92	3.87	2.22
130.61								
	8.01	6.72	1.29	2.76	2.55	194.47	1.10	0.60
122.60								
	7.3	6.03	1.27	2.90	2.99	197.46	1.38	0.71
115.3								
	6.2	5.92	0.28	0.67	0.77	198.23	0.37	0.19
109.10								
	6.76	5.35	1.41	3.66	4.67	202.9	2.32	1.08
102.34								
	5.58	5.48	0.10	0.28	0.40	203.3	0.20	0.09
96.76								

$$\Sigma\delta V_p = 487.5 \ \frac{mm^3}{g}$$

Table B.2 PSD Calculations for fresh Ni/Al_2O_3 (oxide form)

Using Desorption Branch

(1)	(2)	(3)	(4)	(5)	(6)	(7)	(8)	(9)	(10)
P/P_o	n	r_k	t	r_p	$\bar{r}_p$	$\bar{r}_k$	Δt	δr_p	Q
	mg/g	Å	Å	Å	Å	Å	Å	Å	
0.995	326.46	1873.3	35.4	1908.7					
					1054	1028	19.1	1709.4	1.032
0.95	311.91	183.06	16.3	199.35					
					150.6	136.06	3.48	97.4	1.195
0.90	289.28	89.12	12.82	101.9					
					85.39	73.45	1.72	33.02	1.321
0.85	255.56	57.78	11.1	68.88					
					60.49	49.94	1.10	16.78	1.435
0.80	213.09	42.1	10	52.1					
					46.96	37.37	0.83	10.29	1.544
0.75	173.49	32.64	9.17	41.81					
					38.34	29.49	0.63	6.94	1.655
0.70	145.20	26.33	8.54	34.87					
					32.35	24.07	0.52	5.05	1.768
0.65	124.46	21.80	8.02	29.82					
					27.9	20.09	0.42	3.84	1.889
0.60	110.13	18.38	7.60	25.98					
					24.4	17.05	0.41	3.08	2.01
0.55	101.08	15.71	7.19	22.9					
					21.65	14.63	0.35	2.5	2.137
0.50	95.04	13.55	6.84	20.4					
					19.35	12.66	0.31	2.10	2.278
0.45	88.63	11.76	6.53	18.3					
					17.39	11.01	0.30	1.82	2.428
0.40	83.73	10.25	6.23	16.48					
					15.69	9.6	0.27	1.58	2.60
0.35	78.07	8.94	5.96	14.9					
					14.20	8.37	0.27	1.40	2.784
0.30	73.54	7.8	5.69	13.5					

Table B.2 Continuation

(11)	(12)	(13)	(14)	(15)	(16)	(17)	(18)	(19)
V	δV	δV_f	δV_k	δV_p	δA_p	$\Sigma\delta A_p$	$\frac{\delta V_p}{\delta r_p}$	$\frac{\delta V_k}{\delta r_k}$
mm^3/g	mm^3/g	mm^3/g	mm^3/g	mm^3/g	m^2/g	m^2/g	$\frac{10^7 mm^2}{g}$	$\frac{10^7 mm^2}{g}$
404.04								
	18.02	0	18.02	18.60	0.35	0.35	0.01	0.01
386.02								
	28.01	0.12	27.89	33.33	4.43	4.78	0.34	0.30
358.01								
	41.72	0.82	40.90	54.03	12.65	17.43	1.64	1.31
316.29								
	52.56	1.92	50.64	72.67	24.03	41.46	4.33	3.23
263.73								
	49.01	3.44	45.57	70.36	29.97	71.43	6.84	4.82
214.72								
	35.01	4.50	30.51	50.49	26.34	97.77	7.28	4.84
179.71								
	25.67	5.08	20.59	36.40	22.50	120.27	7.21	4.55
154.04								
	17.74	5.05	12.69	23.97	17.18	137.45	6.24	3.71
136.30								
	11.20	5.64	5.56	11.18	9.17	146.62	3.63	2.08
125.10								
	7.47	5.13	2.34	5.00	4.62	151.24	2.0	1.08
117.63								
	7.94	4.69	3.25	7.41	7.66	158.90	3.53	1.82
109.69								
	6.07	4.77	1.30	3.16	3.64	162.54	1.74	0.86
103.62								
	7.00	4.39	2.61	6.79	8.65	171.19	4.30	1.99
96.62								
	5.60	4.62	0.98	2.72	3.83	175.02	1.94	0.86
91.02								

$$\overline{\Sigma\delta V_p} = 396.1 \ \frac{mm^3}{g}$$

Table B.3 PSD Calculations for Reduced Ni/Al_2O_3 Using Desorption Branch

(1)	(2)	(3)	(4)	(5)	(6)	(7)	(8)	(9)	(10)
P/P_o	n	r_k	t	r_p	$\bar{r}_p$	$\bar{r}_k$	Δt	δr_p	Q
	mg/g	Å	Å	Å	Å	Å	Å	Å	
0.98	319.22	464.8	22.23	487					
					343.2	323.9	5.93	287.7	1.102
0.95	307.38	183	16.3	199.3					
					150.6	136.06	3.48	97.4	1.195
0.90	287.39	89.12	12.82	101.9					
					85.39	73.45	1.72	33.02	1.321
0.85	254.58	57.78	11.1	68.88					
					60.49	49.94	1.10	16.78	1.435
0.80	202.53	42.1	10	52.1					
					46.96	37.37	0.83	10.29	1.544
0.75	157.05	32.64	9.17	41.81					
					38.34	29.49	0.63	6.94	1.655
0.70	130.12	26.33	8.54	34.87					
					32.35	24.07	0.52	5.05	1.768
0.65	112.17	21.8	8.02	29.82					
					27.9	20.09	0.42	3.84	1.889
0.60	100.47	18.38	7.6	25.98					
					24.4	17.05	0.41	3.08	2.01
0.55	91.42	15.71	7.19	22.9					
					21.65	14.63	0.35	2.5	2.137
0.50	85.61	13.55	6.84	20.4					
					19.35	12.66	0.31	2.10	2.278
0.45	80.56	11.76	6.53	18.3					
					17.39	11.01	0.30	1.82	2.428
0.40	76.18	10.25	6.23	16.48					
					15.69	9.6	0.27	1.58	2.60
0.35	71.66	8.94	5.96	14.9					
					14.20	8.37	0.27	1.40	2.784
0.30	67.13	7.8	5.69	13.5					

Table B.3 Continuation

(11)	(12)	(13)	(14)	(15)	(16)	(17)	(18)	(19)
V	δV	δV_f	δV_k	δV_p	δA_p	$\Sigma\delta A_p$	$\frac{\delta V_p}{\delta r_p}$	$\frac{\delta V_k}{\delta r_k}$
mm^3/g	mm^3/g	mm^3/g	mm^3/g	mm^3/g	m^2/g	m^2/g	$\frac{10^7 mm^2}{g}$	$\frac{10^7 mm^2}{g}$
395.08								
	14.66	0	14.66	16.15	0.94	0.94	0.06	0.05
380.42								
	24.74	0.33	24.41	29.17	3.87	4.81	0.30	0.26
355.68								
	40.61	0.83	39.78	52.55	12.31	17.12	1.59	1.27
315.07								
	64.41	1.88	62.53	89.73	29.67	46.79	5.35	3.99
250.66								
	56.30	3.88	52.42	80.93	34.47	81.26	7.86	5.54
194.36								
	33.32	5.12	28.20	46.67	24.35	105.61	6.72	4.47
161.04								
	22.22	5.49	16.73	29.58	18.28	123.89	5.86	3.69
138.82								
	14.47	5.20	9.27	17.50	12.55	136.44	4.56	2.71
124.35								
	11.20	5.59	5.61	11.27	9.24	145.68	3.66	2.10
113.15								
	7.19	5.10	2.09	4.47	4.13	149.81	1.79	0.97
105.96								
	6.26	4.64	1.62	3.68	3.80	153.61	1.75	0.91
99.70								
	5.41	4.61	0.80	1.95	2.24	155.85	1.07	0.53
94.29								
	5.60	4.21	1.39	3.62	4.61	160.46	2.29	1.06
88.69								
	5.60	4.33	1.27	3.53	4.97	165.43	2.52	1.11
83.09								

$$\Sigma\delta V_p = 390.8 \ \frac{mm^3}{g}$$

B.3 CO and N_2O Adsorption Data

Typical data obtained in the CO and N_2O chemisorption for nickel area measurements are given in this appendix.

B.3.1 CO Adsorption Data

For Ni/Al_2O_3 samples

Sample NAT3-40 T_{ads} = 195K

First Isotherm		Second Isotherm	
Pressure (cmHg)	CO Adsorbed µmol/g	Pressure (cmHg)	CO Adsorbed µmol/g
1.20	267	1.30	81
3.20	311	3.20	110
5.30	346	5.15	131
7.15	374	7.20	145
10.90	411	11.00	170
15.10	445	15.00	197
19.15	477	19.00	217

Sample NAT3-54A T_{ads} = 195K

First Isotherm		Second Isotherm	
Pressure (cmHg)	CO Adsorbed (µmol/g)	Pressure (cm/Hg)	CO Adsorbed (µmol/g)
1.05	268	1.00	80
3.05	313	3.10	112
5.05	343	5.10	132
6.95	366	7.10	153
10.95	402	11.10	181
14.95	433	14.90	206
19.00	462	19.05	232

Sample NAT3-57 T_{ads} = 195K

First Isotherm

Pressure (cmHg)	CO Adsorbed (μmol/g)
1.00	280
3.15	322
5.00	363
7.00	395
11.05	437
14.95	470
19.00	501

Second Isotherm

Pressure (cmHg)	CO Adsorbed (μmol/g)
1.10	87
3.10	120
5.00	143
7.10	165
11.10	195
15.05	221
19.00	246

Sample NAP-6 T_{ads} = 195K

First Isotherm

Pressure (cmHg)	CO Adsorbed (μmol/g)
1.10	333
3.05	364
5.05	388
7.00	413
11.05	435
15.00	461

Second Isotherm

Pressure (cmHg)	CO Adsorbed (μmol/g)
1.10	43
3.05	68
5.05	86
7.05	103
11.05	125
15.00	141

Sample NAP-7 T_{ads} = 273K

First Isotherm

Pressure (cmHg)	CO Adsorbed (μmol/g)
1.05	359
3.00	386
5.00	412
7.00	426
11.00	440
15.00	454

Second Isotherm

Pressure (cmHg)	CO Adsorbed (μmol/g)
1.10	27
3.00	40
5.00	51
7.45	64
11.00	77
15.00	90

For heavily poisoned Ni/Al_2O_3 Catalysts:

Sample NAT3-31 T_{ads} = 195K

Poisoning conditions: 1000ppm Thiophene/H_2, 298K

First Isotherm on clean sample		First Isotherm on poisoned sample	
Pressure (cmHg)	CO Adsorbed (μmol/g)	Pressure (cmHg)	CO Adsorbed (μmol/g)
1.00	239	1.05	1131
3.15	292	3.05	1811
5.20	324	5.10	2412
7.10	352	7.00	2833
9.00	377	8.95	3168
11.00	402	10.95	3445
13.10	424	13.00	3695
15.00	442		

Sample NAT3-32 T_{ads} = 195K

Poisoning conditions: 1000ppm Thiophene/H_2, 773K

First Isotherm on clean sample		First Isotherm on poisoned sample	
Pressure (cmHg)	CO Adsorbed (μmol/g)	Pressure (cmHg)	CO Adsorbed (μmol/g)
1.25	295	1.10	1805
3.10	337	3.05	2550
5.20	375	5.00	3121
7.05	409	7.10	3545
8.95	437	9.00	3900
11.05	462	11.05	4222
12.95	484	13.00	4547
16.95	518	16.95	4841

For γ-Al_2O_3

Sample Al-20 T_{ads} = 195K

First Isotherm

Pressure (cmHg)	CO Adsorbed (μmol/g)
1.00	83
3.10	121
5.05	145
7.05	165
11.00	197
15.00	224
19.05	248

Second Isotherm

Pressure (cmHg)	CO Adsorbed (μmol/g)
1.05	67
3.15	105
5.05	126
7.20	148
11.00	176
15.00	202
19.00	225

Sample Al-40 T_{ads} = 273K

First Isotherm

Pressure (cmHg)	CO Adsorbed (μmol/g)
1.15	28
3.05	40
5.05	50
7.00	60
11.00	73
15.00	87

Second Isotherm

Pressure (cmHg)	CO Adsorbed (μmol/g)
1.10	26
3.05	37
5.10	46
7.00	56
11.00	68
14.95	82

B.3.2 N_2O Adsorption Data

For Ni/Al_2O_3 samples:

Sample NAP-2 T_{ads} = 195K

First Isotherm

Pressure (cmHg)	N_2O Adsorbed (mg/g)
1.10	19.7
3.05	29.3
5.05	34.9
7.05	39.0
11.05	45.2
15.05	49.9
19.05	54.05

Second Isotherm

Pressure (cmHg)	N_2O Adsorbed (mg/g)
1.10	17.6
3.05	25.9
5.00	31.1
7.05	34.7
11.05	40.2
15.00	44.8
19.00	48.5

Sample NAP-3 T_{ads} = 273K

First Isotherm

Pressure (cmHg)	N_2O Adsorbed (mg/g)
1.10	7.2
3.00	8.8
5.05	10.0
7.00	11.0
11.00	12.6
15.00	14.0

Second Isotherm

Pressure (cmHg)	N_2O Adsorbed (mg/g)
1.10	1.7
3.00	3.0
5.05	4.1
7.00	4.9
11.00	6.4
15.00	7.7

For γ-Al_2O_3 Samples

Sample All-1 T_{ads} = 195K

First Isotherm

Pressure (cmHg)	N_2O Adsorbed (mg/g)
1.20	24.9
3.10	35.9
5.05	42.6
7.05	47.5
11.05	55.0
15.05	60.7
19.00	65.7

Second Isotherm

Pressure (cmHg)	N_2O Adsorbed (mg/g)
1.20	22.1
3.10	32.5
5.10	39.2
7.05	44.0
11.05	51.5
15.05	57.3
19.05	62.3

Sample All-2 T_{ads} = 273K

First Isotherm

Pressure (cmHg)	N_2O Adsorbed (mg/g)
1.10	1.47
3.00	3.01
5.00	4.26
7.00	5.33
11.00	7.09
15.00	8.67
19.00	10.07

Second Isotherm

Pressure (cmHg)	N_2O Adsorbed (mg/g)
1.10	1.32
3.00	2.72
5.00	3.86
7.00	4.81
11.00	6.54
15.00	8.00
18.95	9.26

C.1 Thiophene Adsorption Data

This appendix enlists typical thiophene adsorption data on nickel catalysts and alumina support. The data correspond to the samples shown in Sections 6.1 and 6.2.

C.1.1 Ni/Al_2O_3 (NAT3) Catalysts

Table C.1 Adsorption Values of Thiophene on Ni/Al_2O_3. Gas Concentration: 100ppm. The adsorption Temperature is given below the sample number

Time	NAT3-56 (298K)	NAT3-51 (373K)	NAT3-53 (573K)	NAT3-50A (773K)
min	mg/g	mg/g	mg/g	mg/g
1	1.50	1.95	2.59	0.98
2	4.49	3.00	2.75	1.77
3	5.99	3.21	2.67	1.51
4	6.62	3.48	2.67	1.21
5	6.66	3.60	2.67	1.13
10	6.66	4.07	2.75	0.94
15	6.62	4.26	2.78	0.91
20	6.54	4.34	2.82	0.91
25	6.50	4.38	2.86	0.91
30	6.38	4.38	2.90	0.91
40	6.26	4.38	2.93	0.98
50	6.14	-	-	-
60	6.06	4.34	2.95	1.24
90	5.87	4.46	3.32	1.66
120	5.87	4.81	3.70	2.04
240	6.18	5.67	5.00	3.17
360	6.73	5.94	5.76	4.15
480	6.80	6.13	6.40	4.79
600	6.83	6.14	6.86	5.12
720	6.86	6.32	7.24	5.52
840	6.90	6.42	7.46	5.68
960	6.97	6.46	7.56	5.73
1080	6.98	6.57	7.68	5.73
1200	7.00	6.68	7.80	5.71

Table C.2 Adsorption Values of Thiophene on Ni/Al_2O_3. Gas Concentration: 1000ppm. The adsorption temperature is given below the sample number.

Time	NAT3-21 (298K)	NAT3-58 (373K)	NAT3-27 (573K)	NAT3-25 (773K)
min	mg/g	mg/g	mg/g	mg/g
1	2.15	2.31	3.14	2.37
2	6.05	3.47	2.98	2.12
3	8.28	3.47	2.73	1.84
4	9.44	3.47	2.64	1.71
5	9.78	3.47	2.64	1.67
10	9.98	3.62	3.47	1.79
15	10.07	3.78	3.72	2.20
20	10.23	4.00	3.97	2.57
25	10.36	4.24	4.38	3.02
30	10.44	4.47	4.71	3.43
40	10.75	4.90	5.45	4.12
50	-	5.32	5.87	4.81
60	11.27	5.70	6.45	5.46
90	11.89	6.71	7.85	6.97
120	12.01	7.02	8.35	7.99
240	11.89	7.52	8.90	8.81
360	11.73	7.89	-	8.89
390	11.70	-	9.12	-
480	-	8.16	-	8.89
510	11.60	-	9.20	-
600	-	8.46	-	8.89
630	11.60	-	9.25	-
720	-	8.74	-	8.85
750	11.68	-	9.31	-
840	-	9.01	-	8.85
870	11.85	-	9.35	-
960	-	9.32	-	8.85
990	11.93	-	9.53	-
1080	-	9.56	-	8.85
1110	12.01	-	9.74	-
1170	12.01	-	9.83	-
1200	-	9.82	-	8.85

C.1.2 γ-Al_2O_3 (Al) Samples.

Table C.3 Adsorption Values of Thiophene on γ-Al_2O_3. Gas Concentration: 100ppm. The Adsorption Temperature is given below the sample number.

Time	Al-23 (298K)	Al-26 (373K)	Al-22 (573K)	Al-24 (773K)
min	mg/g	mg/g	mg/g	mg/g
1	0.0	0.0	0.0	0.29
2	0.22	0.0	0.23	0.79
3	0.37	0.29	0.27	0.61
4	0.48	0.57	0.27	0.54
5	0.51	0.61	0.27	0.47
10	0.84	0.65	0.23	0.36
15	1.13	0.68	0.23	0.29
20	1.39	0.72	0.19	0.25
25	1.64	0.75	0.19	0.22
30	1.90	0.79	0.19	0.22
40	2.34	0.79	0.19	0.22
50	2.70	0.82	0.23	0.22
60	3.07	0.86	0.27	0.22
90	4.02	0.90	0.23	-
120	4.75	0.90	0.19	0.18
240	6.87	0.97	0.11	0.14
360	8.11	1.00	0.00	0.07
480	9.00	1.04	0.0	0.17
600	9.77	1.08	0.0	0.11
720	10.36	1.11	0.0	0.04
840	10.85	1.13	0.0	0.0
960	11.20	1.13	0.0	0.0
1080	11.45	1.13	0.0	0.0
1200	11.63	1.15	0.0	0.0

Table C.4 Adsorption Values of Thiophene on γ-Al_2O_3. Gas Concentration: 1000ppm. The Adsorption Temperature is given below the sample number.

Time	Al-7 (298K)	Al-10 (373K)	Al-8 (573K)	Al-9 (773K)
min	mg/g	mg/g	mg/g	mg/g
1	0.12	0.0	0.0	0.24
2	0.36	0.28	0.32	1.29
3	0.60	0.44	0.53	1.25
4	0.80	0.53	0.57	1.33
5	0.97	0.61	0.57	1.33
10	1.57	0.77	0.49	1.17
15	2.09	0.81	0.36	1.05
20	2.57	0.81	0.28	0.88
25	3.01	0.85	0.24	0.84
30	3.38	0.85	0.20	0.80
40	3.98	0.85	0.20	0.76
50	4.42	0.85	0.16	0.72
60	4.74	0.85	0.16	0.72
90	5.23	0.85	0.12	0.64
120	5.51	0.81	0.12	0.56
240	6.19	0.85	0.16	0.44
360	6.55	0.89	0.19	0.28
480	6.71	0.89	0.36	0.21
600	6.79	0.89	0.43	0.15
720	6.95	0.89	0.53	0.10
840	7.03	0.89	0.57	0.10
960	7.11	0.89	0.70	0.08
1080	7.20	0.89	0.70	0.08
1200	7.20	1.10	0.79	0.08